Early diagenesis of phosphorus in continental margin sediments

Promotor: dr. L. Lijklema, hoogleraar in het waterkwaliteitsbeheer

Co-promotor: dr. ir. W. van Raaphorst, senior onderzoeker bij het
                 Nederlands Instituut voor Onderzoek der Zee

Early diagenesis of phosphorus in continental margin sediments

Caroline P. Slomp

Stellingen bij het proefschrift

Early diagenesis of phosphorus in continental margin sediments

1. In tegenstelling tot wat Caraco et al. (1990) beweren is opgelost fosfaat in de meeste mariene sedimenten geen conservatieve tracer van benthische decompositie.

(Caraco et al., 1990, Biogeochemistry 9: 277-290; dit proefschrift)

2. De fosfaatconcentratie in poriewater dat opgelost ijzer bevat kan ernstig worden onderschat wanneer voorafgaande aan de bepaling het poriewater niet wordt aangezuurd.

(Bray et al., 1974, Science 180: 1362-1364; dit proefschrift)

3. Wanneer de binding van fosfaat aan ijzeroxiden in 'gekoppelde' diagenetische modellen òf alleen wordt beschreven als een instantane evenwichtsreactie òf in het geheel niet wordt opgenomen, kan de sedimentaire fosfaatcyclus met deze modellen niet goed beschreven worden.

(Rabouille and Gaillard, 1991, Geochimica et Cosmochimica Acta 55: 2511-2525; Boudreau, 1996, Computers and Geosciences 2: 479-496; dit proefschrift)

4. Zolang nieuwe veldstudies steeds leiden tot een belangrijke herziening van het mondiale budget voor fosfaat in de oceaan, blijft het onderzoek aan fosfaat in mariene sedimenten belangwekkend en vernieuwend, terwijl aan de gevonden budgetten niet veel waarde gehecht hoeft te worden.

(Ruttenberg, 1993, Chemical Geology 107: 405-409; Howarth et al., 1995, p323-346. In: Phosphorus in the global environment, H. Tiessen, ed. Wiley, New York. Filippelli and Delaney, 1996, Geochimica et Cosmochimica Acta 60: 1479-1495; Wheat et al., 1996, Geochimica et Cosmochimica Acta 60: 3593-3608)

5. Het gebruik van de term *rate* (snelheid) om een hoeveelheid toegevoegde stof per gewichts- of oppervlakte-eenheid aan te duiden is onjuist omdat de dimensie tijd ontbreekt.

(bijvoorbeeld Gilpatrick, 1969, Phytopathology 59: 973-978; Zakaria et al., 1980, Phytopathology 70: 495-499; Tsutsuki and Ponnamperuma, 1987, Soil Science and Plant Nutrition 33: 13-33)

6. De gewoonte om in Amerikaanse speelfilms over de middelbare school de rollen van tieners door volwassenen te laten vervullen wijst op huiver voor een directe confrontatie met de adolescentie.

7. Bestuurlijke helderheid neemt toe wanneer de overheid in plaats van een Brede Maatschappelijke Discussie voortaan een erkend Orakel van Delphi raadpleegt.

8. Gedoogbeleid dwingt jongeren met een gezonde hang naar ongeaccepteerd gedrag tot extremiteiten.

9. De oudste, met lens op lichtgevoelige laag vastgelegde, dus fotografische opname, dateert van omstreeks 1500, toont het gelaat van Leonardo da Vinci en staat bekend als de Lijkwade van Turijn.

10. Indien de overtuiging heerst dat morele beginselen in eerste en laatste instantie door de mens worden bepaald, verliezen in een democratie de mensenrechten hun universele geldigheid.

Wageningen, 6 juni 1997   Caroline P. Slomp

Contents

Chapter 1

Introduction

GENERAL BACKGROUND

Although continental margin environments occupy only a minor portion of the surface area of the oceans (~8.6%; Jørgensen, 1983), their importance for oceanic element cycles is large. An estimated 18 to 33% of the total oceanic primary production takes place in these relatively shallow areas (Wollast, 1991). Whereas, in the rest of the oceans, the produced organic material is almost completely remineralized in the water column, 10-50% reaches the sea floor in continental margin environments (Jørgensen, 1983). A part of this organic matter is buried definitely. The major part is decomposed, however, giving rise to a multitude of biogeochemical transformations in the sediment. In combination with physical processes, these transformations bring about major changes in sediments during burial. When these changes occur within several hundred meters below the sediment-water interface, they are collectively referred to as early diagenesis (Berner, 1980).

Phosphorus (P) is an essential nutrient for the growth of marine phytoplankton. The availability of P for uptake by phytoplankton in continental margin environments depends on, firstly, the inflow of reactive P (i.e. potentially bioavailable P) from rivers and neighbouring oceanic waters and, secondly, the return to the overlying water of dissolved P, following deposition and decomposition of organic compounds. Since an enhanced supply of P is one of the causes of eutrophication in coastal areas (Nixon, 1995), it is important to understand the role of sediments as a source and sink for P in these environments on time scales of days to years. Results from field studies suggest that the efficiency of continental margin sediments in returning the P deposited on the sediment to the overlying water is very site-specific. Estimates range from nearly 100% regeneration within a single year for estuarine sediments (e.g. Caraco et al., 1990) to values of 12-66% (Balzer, 1984; Klump and Martens, 1987; Martens, 1993; Jensen et al., 1995) for coastal environments. Less is known about the regeneration of P in sediments in offshore areas. The data that are available suggest that substantial temporary retention of P can occur (Van Raaphorst et al., 1990; Nedwell et al., 1993).

Because certain marine organisms, e.g. cyanobacteria, are able to fix atmospheric N, it has been argued that P is the limiting nutrient for global marine productivity on geological time scales (Holland, 1978; Broecker and Peng, 1982; Howarth et al., 1995). If this is so, changes in the global ocean burial flux of P can affect organic carbon burial and atmospheric CO_2 and O_2 concentrations (Holland, 1978; Broecker, 1982; Broecker and Peng, 1982; Van Cappellen and Ingall, 1994 and 1996). Quantification of the modern

global ocean burial flux of P and the burial flux in the geological past will improve our understanding of the global oceanic P cycle and the interaction with other element cycles. This requires information on rates of sediment accumulation and on changes of the concentration of reactive sediment P with depth for a variety of sedimentary environments on continental margins and in the deep-sea, including both upwelling and non-upwelling areas. Current estimates of modern global reactive P burial (Ruttenberg, 1993; Van Cappellen and Ingall, 1994; Filippelli and Delaney, 1996) are based on a limited data set and should be considered tentative. These studies all recognize continental margins as the most important sites for burial of reactive P.

Continental margin sediments clearly can play an important role as a source or sink for P on short and long time scales. This makes it important to understand the controls on P release and retention, or in other words, to understand the early diagenesis of P in continental margin sediments. In the following two sections, I will give a concise description of the sedimentary P cycle and will briefly introduce the topics that are addressed in this thesis.

THE PHOSPHORUS CYCLE IN MARINE SEDIMENTS

A schematic overview of the sedimentary P cycle in marine sediments is presented in Figure 1. There are three main forms of reactive sediment P: (1) organic P, (2) Fe-bound P and (3) authigenic P. In the pH range normal for seawater, dissolved P is mainly present as HPO_4^{2-} (Kester and Pytkowicz, 1967).

Organic P is the principal carrier of reactive P to sediments (Berner et al., 1993). Following deposition, a part of the organic matter decomposes, resulting in a release of HPO_4^{2-} to the pore water. In the oxidized sediment zone, this HPO_4^{2-} is generally sorbed to Fe oxides (e.g. Krom and Berner, 1980; Sundby et al., 1992; Jensen et al., 1995; Van Raaphorst and Kloosterhuis, 1994). The sorption process often results in a buffering of pore water HPO_4^{2-} concentrations to low values in this zone (Froelich, 1988), thus allowing only limited diffusive transport to the overlying water. Storage of P in bacterial cells, resulting in the formation of organic P, may also remove some HPO_4^{2-} in the oxidized sediment zone (Gächter et al., 1988; Ingall et al., 1993). The quantitative role of this redox-dependent bacterial uptake is still uncertain. In the reduced sediment zone, HPO_4^{2-} is not only released from organic matter but also from Fe oxides upon their dissolution. In this part of the sediment, dissolved HPO_4^{2-} concentrations can become high enough for authigenic mineral formation to occur (e.g. Van Cappellen and Berner, 1988). When the oxidized surface layer is thin or absent, the HPO_4^{2-} released from organic matter and from Fe oxides can escape to the overlying water (Balzer, 1984; Sundby et al., 1986; Ingall and Jahnke, 1994). In this
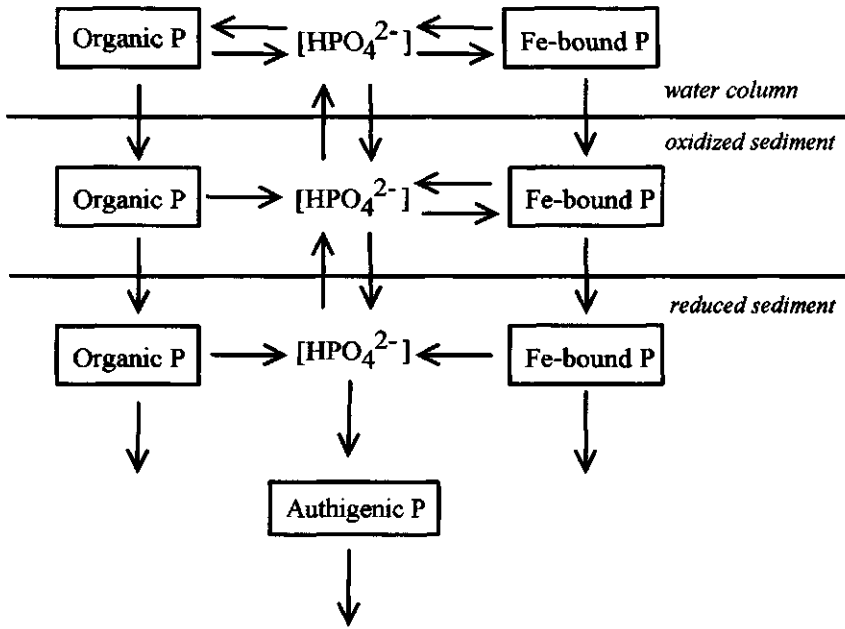
Fig. 1. A schematic representation of the P cycle in marine sediments. Note that in this view biogenic Ca-P, detrital Ca-P, CaCO₃-P and clay-bound P are assumed to be unimportant sources or sinks of reactive P.

case, pore water HPO_4^{2-} concentrations in the reduced zone may not become high enough to create conditions of supersaturation with respect to authigenic P minerals.

Oxidized surface sediment does not always act as a 'trap' for P, however. There are three reasons for this. First, release of dissolved HPO_4^{2-} from organic matter may occur so near the sediment-water interface and may be so rapid that not all the HPO_4^{2-} can be sorbed by Fe oxides (e.g. Martens et al., 1978). Second, sediment irrigation by benthic organisms may result in direct, non-local HPO_4^{2-} transport of deeper pore waters to the overlying water (e.g. Aller and Yingst, 1985). Third, desorption of P from Fe oxides near the sediment-water interface may support a flux to the overlying water, even when HPO_4^{2-} concentrations in the oxidized sediment are low (Schink and Guinasso, 1978; Van Raaphorst et al., 1988; Van Raaphorst and Kloosterhuis, 1994). This flux can only be maintained as long as there is a sufficient supply of desorbable Fe-bound P to the sediment near the sediment-water interface and as long as the HPO_4^{2-} concentration in the overlying water remains relatively low.

All three forms of reactive sediment P, i.e. organic P, Fe-bound P and authigenic P (Fig. 1), can act as a long-term sink of P in sediments (Berner et al., 1993; Ruttenberg and

Berner, 1993). The organic P which is buried may be present in phosphate esters and phosphonate compounds (Ingall et al., 1990; Berner et al., 1993). Fe oxides can act as a permanent sink for P since they can persist below the oxidized zone (e.g. Van Cappellen and Wang, 1996). Very little is known about the mineral forms of the Fe oxides responsible for the binding of P in marine sediments. Results from sequential extraction procedures suggest that they may be largely of a poorly crystalline nature (Jensen and Thamdrup, 1993; Jensen et al., 1995). Carbonate fluorapatite (CFA), the principal component of phosphorite deposits formed in upwelling areas (e.g. Jahnke et al., 1983; Froelich et al., 1988; Schuffert et al., 1994), is probably also the most important authigenic P mineral in non-upwelling, rapidly accumulating, terrigenous continental shelf sediments (Ruttenberg and Berner, 1993), continental rise sediments (Lucotte et al., 1994) and deep-sea sediments (Filippelli and Delaney, 1996). For a more extensive overview of the P cycle in marine sediments, the reader is referred to the reviews of Krajweski et al. (1994) and Howarth et al. (1995).

OUTLINE OF THIS THESIS

This thesis concentrates on the relatively short-term processes controlling sediment P release and retention in temperate, non-upwelling continental margin environments. The research comprised laboratory, field and modelling work and was carried out within the framework of three larger projects: (1) A meso/boxcosm project that focused on the benthic reponse of marine sandy sediments to eutrophication; (2) The BELS project (BEnthic Links and Sinks in North Sea Nutrient Cycling), that aimed at the elucidation of the role of sediments in the nutrient dynamics of the North Sea; (3) The OMEX project (Ocean Margin EXchange), an EU-funded program which is directed towards an understanding of fluxes of particles and organic carbon from the continental shelf to the deep-sea.

The deposition and decomposition of organic matter is the driving force for most early diagenetic processes in sediments. This makes research on the effect of organic matter deposition on sediment P dynamics a logical starting point. The effect of single and repeated organic matter deposition and macrofauna on sediment-water exchange and retention of P in Fe oxide-poor sediments is addressed in Chapter 2. This study was carried out in experimental marine sediment systems ('boxcosms'), to allow a better control of the added amounts of organic matter than would be possible under *in-situ* conditions.

Sorption of P to Fe oxides is the most important short-term process responsible for the retention of P in sediments. Very little is known about the nature of the Fe oxides in marine sediments, however. In the study presented in chapter 3, the Fe oxides in four sediments from contrasting sedimentary environments in the North Sea were characterized and their role for the binding of P was evaluated. Since direct determination with conventional techniques is not possible, a combination of X-ray powder diffraction measurements

(DXRD) and extraction procedures was used. The role of Fe-bound P as a temporary and permanent sink for P in these sediments is discussed.

Fe oxides loose their ability to sorb additional P upon their burial into the sediment zone where neither O_2 nor NO_3^- are present. In chapter 4, the seasonal and spatial differences in the sediment redox conditions in 4 types of sedimentary environments in the North Sea are described. Using a steady-state diagenetic model for the Mn and Fe cycle, the potential role of Mn and Fe oxides as redox intermediates in organic C oxidation in several of these sediments is evaluated.

In chapter 5, the role of sorption in sediment-water exchange of HPO_4^{2-} at the North Sea locations of chapter 4 is discussed. Furthermore, it is assessed whether both enhanced retention and release of HPO_4^{2-} due to sorption can be described with a diagenetic model for the sedimentary P cycle that includes simultaneous equilibrium and first-order kinetic HPO_4^{2-} sorption.

In chapter 6, the hypothesis is tested whether Fe-bound P plays a key role in authigenic CFA formation at two locations on a North Atlantic continental platform. Results from selective extraction procedures are combined with pore water data to determine whether CFA is forming in these sediments. A diagenetic model for the sedimentary P cycle is developed and applied to facilitate the interpretation of the observed depth profiles.

REFERENCES

Aller, R.C. and Y. Yingst, 1985. Effects of the marine deposit feeders *Heteromastus filiformis* (Polychaeta), *Macoma balthica* (Bivalvia), and *Tellina texana* (Bivalvia) on averaged sedimentary solute transport, reaction rates and microbial distributions. J. Mar. Res. 43: 615-645.

Balzer, W., 1984. Organic matter degradation and biogenic element cycling in a nearshore sediment (Kiel Bight). Limnol. Oceanogr. 29: 1231-1246.

Berner, R.A., 1980. Early diagenesis: A theoretical approach. Princeton University Press, Princeton, 241p.

Berner, R.A., K.C. Ruttenberg, E.D. Ingall, and J.-L. Rao, 1993. The nature of phosphorus burial in modern marine sediments In: R. Wollast, F.T. Mackenzie and L. Chou, eds. Interactions of C, N, P, and S Biogeochemical Cycles and Global Change, Springer-Verlag, NATO ASI Series Vol. 14, 521p.

Broecker, W.S., 1982. Ocean chemistry during glacial time. Geochim. Cosmochim. Acta 46: 1689-1705.

Broecker, W.S. and T.-H. Peng, 1982. Tracers in the sea. Eldigio Press, Palisades. 690p.

Caraco, N.F., J.J. Cole and G.E. Likens, 1990. A comparison of phosphorus immobilization in sediments of freshwater and coastal marine systems. Biogeochemistry 9: 277-290.

Filippelli, G.N. and M.L. Delaney, 1996. Phosphorus geochemistry of equatorial Pacific sediments. Geochim. Cosmochim. Acta 60: 1479-1495.

Froelich, P.N., M.L. Bender, N.A. Luedtke, G.R. Heath and T. DeVries, 1982. The marine phosphorus cycle. Am. J. Sci. 282: 474-511.

Froelich, P.N., 1988. Kinetic control of dissolved phosphate in natural rivers and estuaries: a primer on the phosphate buffer mechanism. Limnol. Oceanogr.33: 649-668.

Froelich, P.N., M.A. Arthur, W.C. Burnett, M. Deakin, V. Hensley, R. Jahnke, L. Kaul, K.-H. Kim, K. Roe, A. Soutar and C. Vathakanon, 1988. Early diagenesis of organic matter in Peru continental margin sediments: phosphorite precipitation. Mar. Geol. 80: 309-343.

Gächter, R., J.S. Meyer and A. Mares, 1988. Contribution of bacteria to release and fixation of phosphorus in lake sediments. Limnol. Oceanogr. 33: 1542-1558

Holland, H.D., 1978. The chemistry of the atmosphere and the oceans. Wiley, New York.

Howarth, R.W., H. Jensen, R. Marino and H. Postma, 1995. Transport to and processing of phosphorus in near-shore and oceanic waters. p323-346. In: Phosphorus in the global environment, H. Tiessen, ed., John Wiley, SCOPE 54, 462p.

Ingall, E.D., Schroeder, P.A. and R.A. Berner, 1990. The nature of organic phosphorus in marine sediments: New insights from 31P-NMR. Geochim. Cosmochim. Acta 54: 373-386.

Ingall, E.D., R.M. Bustin and P. Van Cappellen, 1993. Influence of water column anoxia on the burial and preservation of carbon and phosphorus in marine shales. Geochim. Cosmochim. Acta 57: 303-316.

Ingall, E.D. and R.A. Jahnke, 1994. Evidence for enhanced phosphorus regeneration from marine sediments overlain by oxygen-depleted waters. Geochim. Cosmochim. Acta 58: 2571-2575.

Jahnke, R.A., S.R. Emerson, K.K. Roe and W.C. Burnett, 1983. The present day formation of apatite in Mexican continental margin sediments. Geochim. Cosmochim. Acta 47: 259-266.

Jensen, H.S. and B. Thamdrup, 1993. Iron-bound phosphorus in marine sediments as measured by the bicarbonate-dithionite extraction. Hydrobiologia, 253, 47-59.

Jensen, H.S., P.B. Mortensen, F.Ø. Andersen, E. Rasmussen and A. Jensen, 1995. Phosphorus cycling in a coastal marine sediment, Aarhus Bay, Denmark. Limnol. Oceanogr. 40: 908-917.

Jørgensen, B.B., 1983. Processes at the sediment-water interface. In: The major biogeochemical cycles and their interactions. B. Bolin and R.B. Cook, eds. John Wiley, Chichester. p477-515.

Kester, D.R. and R.M. Pytkowicz, 1967. Determination of the apparent dissociation constants of phosphoric acid in sea water. Limnol. Oceanogr. 12: 243-252.

Klump, J.V. and C.S. Martens, 1987. Biogeochemical cycling in an organic-rich coastal marine basin. 5. Sedimentary nitrogen and phosphorus budgets based upon mass balances and the stoichiometry of nutrient regeneration. Geochim. Cosmochim. Acta 51: 1161-1173.

Krajweski, K.P., P. Van Cappellen, J. Trichet, O. Kuhn, J. Lucas, A. Martín-Algarra, L. Prévôt, V.C. Tewari, L. Gaspar, R.I. Knight and M. Lamboy, 1994. Biological processes and apatite formation in sedimentary environments. Eclogae geol. Helv. 87: 701-745.

Krom, M.D. and R.A. Berner, 1980. Adsorption of phosphate in anoxic marine sediments. Limnol. Oceanogr. 25: 797-806.

Lucotte, M., A. Mucci, C. Hillaire-Marcel and S. Tran, 1994. Early diagenetic processes in deep Labrador Sea sediments: reactive and nonreactive iron and phosphorus. Can. J. Earth Sci. 31: 14-27.

Martens, C.S., R.A. Berner and J.K. Rosenfeld, 1978. Interstitial water chemistry of anoxic Long Island Sound sediments. 2. Nutrient regeneration and phosphate removal. Limnol. Oceanogr. 23: 605-617.

Martens, C.S., 1993. Recycling efficiencies of organic carbon, nitrogen, phosphorus and reduced sulfur in rapidly depositing coastal sediments. p379-400. In: Wollast, R., F.T. Mackenzie and L. Chou, eds. Interactions of C, N, P and S Biogeochemical Cycles and Global Change. Springer.

Nedwell, D.B., R.J. Parkes, A.C. Upton and D.J. Assinder (1993) Seasonal fluxes across the sediment-water interface and processes within sediments. Phil. Trans. R. Soc. Lond. A. 343: 519-529.

Nixon, S.W., 1995. Coastal marine eutrophication: a definition, social causes and future concerns. Ophelia 41:199-219.

Schuffert, J.D., R.A. Jahnke, M. Kastner, J. Leather, A. Sturz and M.R. Wing, 1994. Rates of formation of modern phosphorite off western Mexico. Geochim. Cosmochim. Acta 58: 5001-5010.

Ruttenberg, K.C., 1993. Reassessment of the oceanic residence time of phosphorus. Chem. Geol. 107: 405-409.

Ruttenberg, K.C. and R.A. Berner, 1993. Authigenic apatite formation and burial in sediments from non-upwelling, continental margin environments. Geochim. Cosmochim. Acta 57: 991-1007.

Schink, D.R. and N.L. Guinasso, 1978. Redistribution of dissolved and adsorbed materials in abyssal marine sediments undergoing biological stirring. Am. J. Sci. 278: 687-702.

Sundby, B., L.G. Anderson, P.O.J. Hall, A. Iverfeldt, M.M. Rutgers van der Loeff, S.F.G. Westerlund, 1986. The effect of oxygen on release and uptake of cobalt, manganese, iron and phosphate at the sediment-water interface. Geochim. Cosmochim. Acta 50: 1281-1288.

Sundby, B., C. Gobeil, N. Silverberg and A. Mucci, 1992. The phosphorus cycle in coastal marine sediments. Limnol. Oceanogr. 37: 1129-1145.

Van Cappellen, P. and R.A. Berner, 1988. A mathematical model for the early diagenesis of phosphorus and fluorine in marine sediments: apatite precipitation. Am. J. Sci. 288: 289-333.

Van Cappellen, P. and E.D. Ingall, 1994. Benthic phosphorus regeneration, net primary production, and ocean anoxia: a model of the coupled marine biogeochemical cycles of carbon and phosphorus. Paleoceanography 9: 677-692.

Van Cappellen, P. and E.D. Ingall, 1996. Redox stabilization of the atmosphere and oceans by phosphorus-limited marine productivity. Science 271: 493-496.

Van Cappellen, P. and Y. Wang, 1996. Cycling of iron and manganese in surface sediments: a general theory for the coupled transport and reaction of carbon, oxygen, nitrogen, sulfur, iron, and manganese. Am. J. Sci. 296: 197-243.

Van Raaphorst W., P. Ruardij and A.G. Brinkman, 1988. The assessment of benthic phosphorus regeneration in an estuarine ecosystem model. Neth. J. Sea Res. 22: 23-36.

Van Raaphorst, W., H.T. Kloosterhuis, A. Cramer and K.J.M. Bakker, 1990. Nutrient early diagenesis in the sandy sediments of the Doggerbank area, North Sea: pore water results. Neth. J. Sea Res. 26: 25-52.

Van Raaphorst, W. and H.T. Kloosterhuis, 1994. Phosphate sorption in superficial intertidal sediments. Mar. Chem. 48: 1-16.

Wollast, R., 1991. The coastal organic carbon cycle: Fluxes, sources and sinks. p365-382. In: Mantoura, R.F.C., J.M. Martin, R. Wollast, eds. Ocean margin processes in global change, Dahlem Workshop reports. Wiley Interscience, Chichester.

Chapter 2

The effect of deposition of organic matter on phosphorus dynamics in experimental marine sediment systems[*]

ABSTRACT

The effect of deposition of organic matter on phosphorus dynamics in sandy marine sediments was evaluated using experimental systems (boxcosms) and three different strategies: (1) no supply (2) one single addition (3) weekly additions of a suspension of algal cells (*Phaeocystis spec.*). Macrofauna (3 species, 6 individuals of each) were added to half of the boxes. Both in the case of the single and weekly additions a clear effect of increased organic matter loading on phosphorus dynamics was found. Following the organic matter addition, porewater phosphate concentrations in the upper sediment layer increased, phosphate release rates from the sediment increased by a factor 3-5 and in the boxes to which a single addition was applied NaOH-extractable phosphorus increased substantially. The increase in phosphate release rates from the sediment was attributed to mineralization of the added material and to direct release from the algal cells. No clear effect of the presence of macrofauna on sediment-water exchange of phosphate could be discovered. The macrofauna were very effective at reworking the sediment, however, as illustrated by the organic carbon profiles. It is hypothesized that the sediment-water exchange rates of phosphate were regulated by the layer of algal material which was present on the sediment surface in the fed boxes. In the boxes to which the single addition was applied porewater phosphate concentrations were lower and NaOH-extractable phosphorus was higher in the presence of macrofauna, suggesting that macrofauna can stimulate phosphate binding in the sediment.

INTRODUCTION

Benthic phosphorus regeneration may strongly influence water column chemistry in shallow marine systems (e.g. Balzer, 1984; Callender & Hammond, 1982; Fisher et al., 1982; Hopkinson, 1987; Klump & Martens, 1981 & 1987; Rutgers van der Loeff, 1980). Therefore, the role of sediments in phosphorus recycling and eutrophication of these systems (e.g. the North Sea, Brockman et al., 1988 & 1990) is of major importance, even when phosphorus does not limit primary production (Peeters & Peperzak, 1990; Riegman et al., 1990).

Phosphorus cycling has mostly been studied in organic-rich, high porosity, fine-grained sediments (e.g. Froelich et al., 1988; Klump & Martens, 1981 & 1987; Krom & Berner, 1980 & 1981; Martens et al., 1978). Much less information is available on organic-poor, low porosity, sandy sediments (e.g. Hopkinson, 1987; Rutgers van der Loeff, 1980; Van

Raaphorst et al., 1990) which can be found in a major part of the North Sea (Eisma, 1990). In view of the general concern about increased eutrophication of the North Sea (Postma, 1985), presumably resulting in increased algal blooms (Cadée, 1990) and oxygen deficiency in certain areas (Westernhagen et al., 1986), it is important to obtain more quantitative information on the processes controlling phosphorus dynamics in sandy sediments.

Early diagenesis in marine sediments largely depends on the supply of organic carbon (Berner, 1980; Billen et al., 1990; Klump & Martens, 1987). Although a significant correlation between the amount of fine particles and of organic matter in sediments can often be found (Creutzberg et al., 1984; Billen et al., 1990) deposition of organic matter is not limited to fine-grained sediments. Jenness & Duineveld (1985) have shown that considerable amounts of phytoplanktonic material can be - at least temporarily - buried in sandy sediments down to a depth of 5 cm following deposition in periods of slack tidal current.

Binding of phosphorus in the sediment may cause a time lag between organic matter mineralization in the sediment and actual regeneration of phosphorus to the water column. Sorption to iron and aluminum oxides and precipitation processes (Lijklema, 1977; Martens et al., 1978; Froelich, 1988; Froelich et al., 1982) may substantially reduce regeneration to the overlying water. Furthermore, uptake of phosphorus by microorganisms, not only from the organic substrate but also from the porewater, may play an important role. This latter process obviously depends on the quality (e.g. C:P ratio) of the available organic matter (Billen et al., 1990; Gächter et al., 1988 & 1992). Under anoxic conditions, chemically bound phosphorus may be released due to reduction of iron oxides (Mortimer, 1941). According to Gächter et al. (1988) polyphosphates which have accumulated in bacterial cells during oxic conditions may then be released as well.

The presence of macrofauna can stimulate mineralization of organic matter and uptake of phosphorus by microorganisms through reworking of the sediment. Furthermore, sediment-water exchange rates of phosphorus can be enhanced, mostly due to bioirrigation activity (e.g. Aller, 1982; Hüttel, 1990; Hylleberg & Hendriksen, 1982; Yingst & Rhoads, 1980).

In this study, the effect of deposition of organic matter on phosphorus dynamics in a sandy marine sediment is evaluated. Furthermore, the role of macrofauna is discussed. To allow control of the added amounts of organic matter, experimental sediment systems were used. These were modified from the boxcosms described previously by Van Raaphorst et al. (1992). This research was part of a larger study on North Sea sediment eutrophication of which further results will be published elsewhere.

MATERIALS AND METHODS

Boxcosms. Sediment with a median grain size of 125-160 μm and a content of particles <50μm of ca. 2-5% was obtained from a station in the southern North Sea (Zeegat van Texel: 52°53'N, 4°34'E; depth: 17m). The sediment was stored in large covered containers at outdoor (winter) temperatures for ca. 4 months. Before use, the sediment was sieved (<0.5 cm) and homogenized in a cement mill. The boxcosm experiments were performed in 26 cylindrical polypropylene boxes with an inner diameter and height of 30 and 35 cm, respectively. The boxes were filled with sediment up to 10 cm from the rim, resulting in a sediment depth of 25 cm in each box. Incorporation of air bubbles while filling the boxes was avoided as much as possible by adding seawater simultaneously. The thin layer (ca. 5 mm) of fine particles which subsequently developed on top of the sediment was carefully removed.

The boxes were distributed over 2 separate basins, in order to be able to maintain the 'starved' and 'fed' boxcosms spatially apart thus avoiding mutual contamination. No communication existed between the boxes. To each box ca. 10 cm of overlying water was added, which was continuously replaced by filtered (over sand beds, grainsize 1-1.4 mm), aged (for several weeks in 2 large containers) North Sea water of constant salinity (29‰), an average dissolved organic carbon (DOC) content of 2.1 ± 0.4 mg l^{-1} and the following average (n = 16) nutrient concentrations: PO_4 = 2.7 ± 0.9 μmol l^{-1}; $NO_3 + NO_2$ = 54.3 ± 7.9 μmol l^{-1}; Si = 17.2 ± 3.3 μmol l^{-1}. The NH_4 concentration in the inflow was ca. 1.0 μ mol l^{-1} at the beginning, increased to ca. 7 μmol l^{-1} at day 14 and subsequently decreased to values < 0.8 μmol l^{-1} remaining at this level from day 24 onwards. The DOC present in the inflow water probably consisted of refractory components (Laane, 1980). The inflow rate of 10.4 ml min^{-1} resulted in a residence time of the overlying water of ca. 11 hours. Outflow took place by overflow over the rim of the boxes into the basin. Constant bubbling of air was performed to keep the water column in the boxes well-mixed and saturated with respect to oxygen. The boxcosms were kept in the dark at a temperature of 11.8 ± 0.5 °C.

One week after installation each box was supplied with micro- and meiofauna through a 250 ml sediment sample consisting of the 2.5 cm surface layer of freshly collected boxcores. Two weeks later three species of macrofauna (*Tellina fabula, Nephtys hombergii, Echinocardium cordatum*; 6 of each, resulting in a total density of 255 ind. per m^2) were added to 13 of the boxes. Dead individuals visible at the sediment surface were replaced on a weekly basis.

Three different strategies were used to study organic matter deposition: (1) no supply ('starved'; 8 boxes), (2) one single addition ('fed'; 10 boxes), (3) weekly additions ('fed'; 8 boxes). The organic matter consisted of a suspension of *Phaeocystis spec.*, a common alga

in coastal areas of the North Sea (e.g. Cadée, 1990; Lancelot et al., 1987), which was collected in the Schulpengat south-west of Texel with 50 µm plankton nets during the spring bloom. The material was homogenized by stirring with a paddle in large containers, divided into equal portions and subsequently stored at -20°C until use (ca. 4 weeks for the first addition). 16 days after the introduction of the macrofauna and 37 days after the installation of the boxes the first portion of (thawed) organic matter was added (day 0). The organic matter supply to the boxcosms resulted in loadings of ca. 8 g C m^{-2} and 6.3 mmol P m^{-2} for the weekly additions (during 19 weeks, resulting in a total of 152 g C m^{-2} and 120 mmol P m^{-2}), and 24 g C m^{-2} and 19 mmol P m^{-2} for the single additions. The amount of carbon supplied with the single addition is approximately equivalent to the annual metabolic loss of sandy North Sea sediments as estimated by De Wilde et al. (1984) and Cramer (1991). Although the water circulation was stopped for 24 h following each addition not all of the algal material settled on the sediment surface within this period, resulting in a loss of organic matter due to outflow from the boxes. This especially was a problem in the boxcosms to which the single addition of organic matter was applied. Therefore, the actual carbon loading in these boxes was somewhat lower than 24 g C m^{-2}. At each sampling event either intact boxes were used for the measurements (sediment-water exchange rates, oxygen uptake rates and penetration depth) or boxes were 'sacrificed' (porewater, sediment composition).

Sediment-water exchange rates. Sediment-water exchange rates of phosphate were measured in single boxes which were temporarily disconnected from the water supply. 500 ml of the overlying water was carefully removed and stored in a jar. At fixed time intervals 25 ml of sample was taken both from the overlying water and from the jar. The samples were filtered (0.45 µm cellulose acetate) and analyzed for phosphate. At the end of each experiment - which never took more than 8 hours - the water supply was reconnected.

The fluxes were calculated from the concentration change in time in the overlying water of the boxcosm corrected for the removal or production of phosphate in the jar and the decreasing depth of the overlying water due to sampling:

$$\frac{dC_O}{dt} = \frac{J}{h} - R \tag{1}$$

where

C_O = concentration of the overlying water (mol m^{-3});

t = time (s);

J = sediment-water exchange rate (mol m^{-2} s^{-1});

h = the depth of the overlying water which decreases in time due to sampling (m);

R   =   change of the phosphate concentration in the overlying water (mol m^{-3} s^{-1}) due to production/removal in the water column (jars).

Oxygen uptake and penetration. Benthic oxygen uptake was measured using the method described by Cramer (1990). The boxcosms were covered with a Plexiglas lid in which a stirring device, O_2 electrodes (YSI 5739) and a temperature electrode were fitted. Oxygen uptake was calculated from the change in the oxygen concentration in the chamber during incubation. Oxygen concentrations in the pore water were measured with an O_2 micro-electrode (Helder & Bakker, 1985) at 0.2 mm depth intervals using a micromanipulator. The oxygen penetration depth is defined as the depth at which zero oxygen concentrations or constant and low readings were obtained.

Porewater. The boxcosms were sampled with acrylic liners (i.d. 5.2 cm, length 30 cm) which were sliced into 5, 10 and 20 mm segments (depending on sediment depth). Interstitial water was obtained by squeezing under N_2 pressure using Reeburgh-type squeezers (Reeburgh, 1967) fitted with 0.45 µm cellulose-acetate filters. In all cases segments of three cores were pooled.

Sediment composition. The boxcosms were sampled with PVC tubes (i.d. 4.5 cm) and sliced into segments of 5, 10, 20 and 40 mm (depending on sediment depth). Three cores were pooled each time. Organic-C contents were measured on a Carlo Erba NA 1500-2 elemental analyzer following the procedure of Verardo et al. (1990).

The phosphorus speciation was determined using the sequential extraction scheme described by Hieltjes & Lijklema (1980). 50 mg of wet sediment was extracted sequentially with (1) 2 x 50 ml of 1 M NH_4Cl, pH = 7, (2 x 2 hours), (2) 50 ml of 0.1 M NaOH (17 hours) and (3) 50 ml of 0.5 M HCl (24 hours). These fractions presumably represent (1) loosely bound and exchangeable P, (2) P sorbed on surfaces of iron and aluminum oxides and (3) P occluded in iron and aluminum oxides and calcium bound P, respectively. NaOH may also solubilize some organic P (Levesque & Schnitzer, 1966). A shaking table was used for continuous agitation of the suspensions. After each extraction step the suspensions were filtered (0.45 µm cellulose-acetate), the filtrate was stored at -20°C until analysis and the filter with the sediment was added to the next extraction solution in the sequential procedure. The organic carbon content and phosphorus speciation were only determined for the sediments of the starved boxes and those that were fed once.

Easily exchangeable Fe and Mn was determined through an extraction with 0.1 M HCl (suprapur). It was assumed that most of the reactive iron and manganese oxides were

released by this method. 0.1 gr of dried (60°C) and homogenized (through grinding in an agate mortar) sediment was leached with 50 ml of HCl for 18 hours, followed by filtration over a pre-acid cleaned 0.45 μm cellulose nitrate filter (Duinker et al., 1974).

Analytical procedures. Phosphate concentrations (analytical precision $\pm$ 0.03 μmol l^{-1} at a concentration of 1 μmol l^{-1}) were determined on a Technicon AA II autoanalyzer (fluxes, porewater) and on a Shimadzu Double beam Spectrophotometer UV-150-02 (sediment phosphorus) following the method of Strickland and Parsons (1972). The Fe and Mn content of the HCl-leachate was determined with a Perkin Elmer 5100 PC Atomic Absorption Spectrophotometer using the standard addition method for calibration (analytical precision for Fe and Mn: $\pm$ 1 μmol l^{-1} and $\pm$ 0.5 μmol l^{-1} at a concentration of 18 μmol l^{-1}).

RESULTS

Sediment-water exchange rates. Fig. 1 shows the concentration change with time in the overlying water of the weekly fed boxcosms with macrofauna and in the jars on day -8 (no jar measurement), 2, 4 and 102. Calculated phosphate release rates from such data (assuming a linear relationship between the phosphate concentration and time) are given in Fig. 2. Error bars indicate the standard error of the calculated flux. Deviations from a straight line, as found, for example, on day 4 (Fig. 1), resulted in large standard errors for the estimated fluxes due to the small number of samples (n = 4-7). Phosphate release rates were generally low in the starved boxcosms with the exception of the high initial release rates in the boxes with macrofauna. Following deposition of organic matter (day 0) an increase in phosphate release rates from the sediment was found within 4 days in the case of the single additions, followed by a period of very low phosphate release from day 10 (with macrofauna) or 15 (without macrofauna) onwards. The interpretation of the results for the weekly fed boxes is hampered by the limited amount of measurements and the large errors in the estimated fluxes. From Fig. 2 it can be observed, however, that phosphate release rates increased within 2 days after the first organic matter addition in the boxes with macrofauna and within 4 days after the second addition in the boxes without macrofauna. The maximum phosphate release rates were 2-3 times higher in the boxes fed only once compared to the weekly fed ones. Apart from a slightly higher maximum phosphate release rate in the presence of macrofauna in the boxes which were fed once, no clear effect of the presence of macrofauna on the phosphate fluxes was observed.

The phosphate concentration in the overlying water was generally higher than in the inflow water, particularly in the fed boxcosms. In the case of the single addition, the

phosphate concentration in the overlying water increased from ca. 3 to ca. 10 μmol l^{-1} immediately following the food supply. This was followed by a decrease to 2-3 μmol l^{-1} within 2 days. The same pattern was observed in the case of the weekly additions, corresponding values being ca. 3, 6 and 3-4 μmol l^{-1}, respectively.

Porewater profiles. In the starved boxcosms the porewater concentration of phosphate (Fig. 3) slowly decreased in time, to a concentration of less than 5 μmol l^{-1} in the upper sediment layer both with and without macrofauna. When the boxcosms were fed only once an immediate increase of the porewater phosphate concentration was found (>20 μmol l^{-1}) in the upper 30-40 mm of the sediment, followed by a rapid decrease, especially in the presence of macrofauna (Fig. 3b). In the case of weekly additions of organic matter only a minor increase (Fig. 3b, with macrofauna) or even a decrease (Fig. 3a, without macrofauna) of the phosphate concentration in the porewater of the upper sediment layer could be detected following the addition of organic matter. Both in the presence and absence of macrofauna the phosphate concentration subsequently decreased rapidly, even though organic matter additions continued. In all boxes the porewater phosphate concentrations measured in the upper 5 mm were higher than those of the overlying water.

The porewater phosphate concentration declined in all of the boxes during the course of the experiments, apart from the initial increase in the fed boxcosms. The phosphate concentrations found at the start of the measurements, however, were very high: 15-25 μ mol l^{-1}. Presumably phosphate was released from the sediment during the period prior to the first measurements either due to mineralisation of organic matter and/or due to desorption from binding sites.

Oxygen uptake. Deposition of organic matter caused the benthic oxygen uptake to increase substantially (Fig. 4a). After a single organic matter addition oxygen uptake increased to ca. 20 and 30 mmol O_2 m^{-2} d^{-1} in the boxes with and without macrofauna, respectively. Oxygen uptake rates subsequently decreased to ca. 10 mmol O_2 m^{-2} d^{-1} within 30 days, slightly higher than the original rates (ca. 8 mmol O_2 m^{-2} d^{-1}). In the case of weekly supply, rates increased from approximately 10 to a maximum of 40 mmol O_2 m^{-2} d^{-1}. After an initial almost linear increase the oxygen uptake rates seemed to stabilize around 30-35 mmol O_2 m^{-2} d^{-1}. No clear effect of the presence of macrofauna on oxygen uptake could be discovered in the fed boxcosms.

Oxygen penetration. The addition of organic matter generally caused the oxygen penetration depth to decrease (Fig. 4b). Especially the single addition had a very clear effect
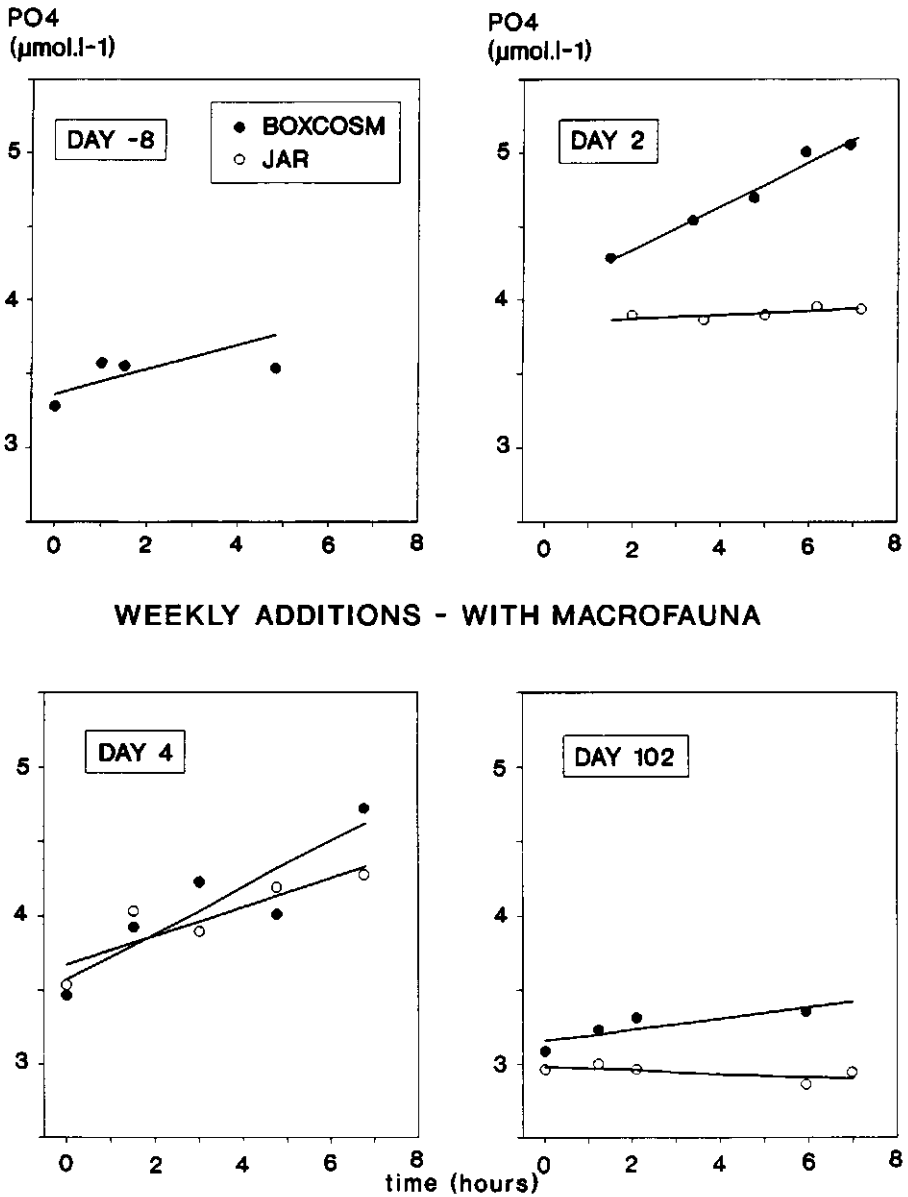
Fig. 1. Change in the phosphate concentration (μmol l^{-1}) with time in the overlying water of weekly fed boxcosms with macrofauna and the matching jars during fluxexperiments on day -8, 2, 4 and 102. Solid lines were obtained through linear regression.
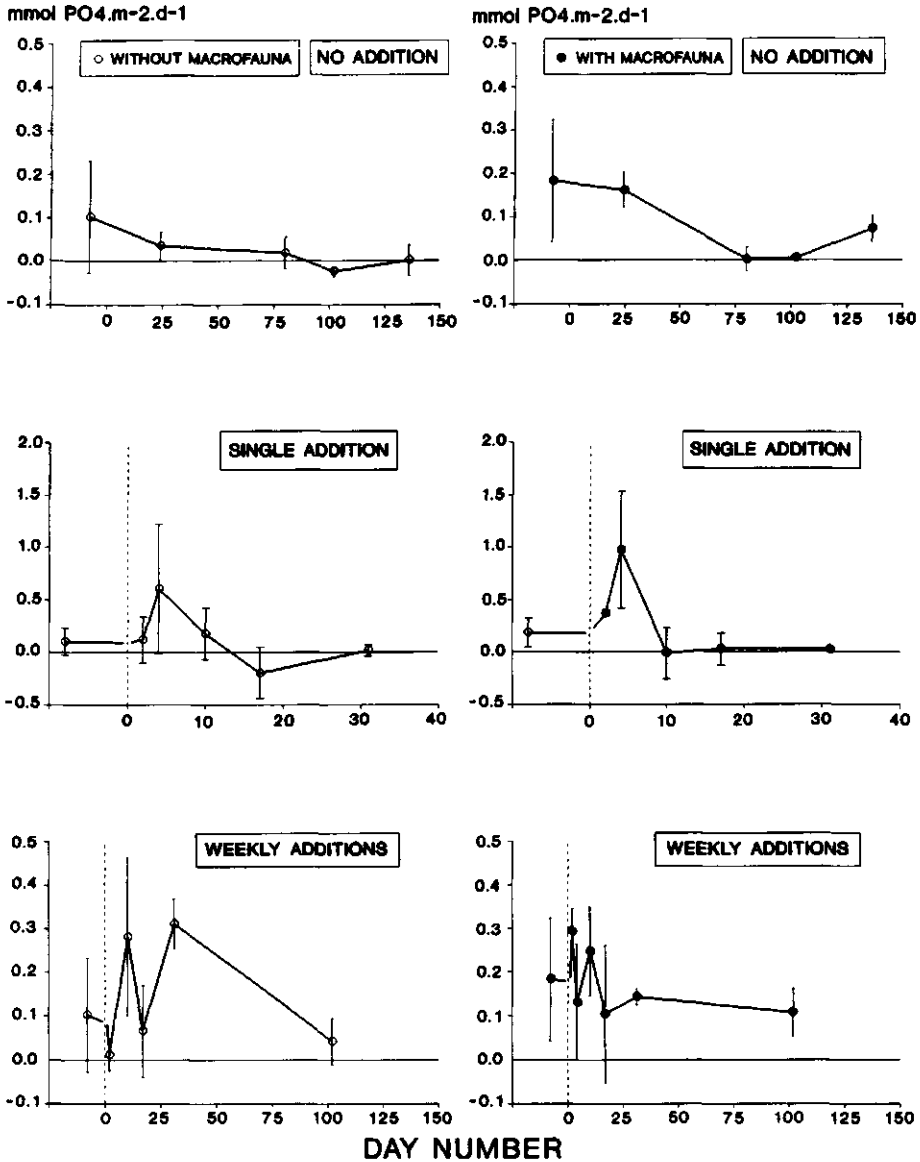
Fig. 2. Sediment-water exchange rates of PO_4 (mmol m^{-2} d^{-1}) measured in the boxcosms. Error bars indicate the standard error of the estimated flux. Note the different scales in the plots for the single and weekly additions.
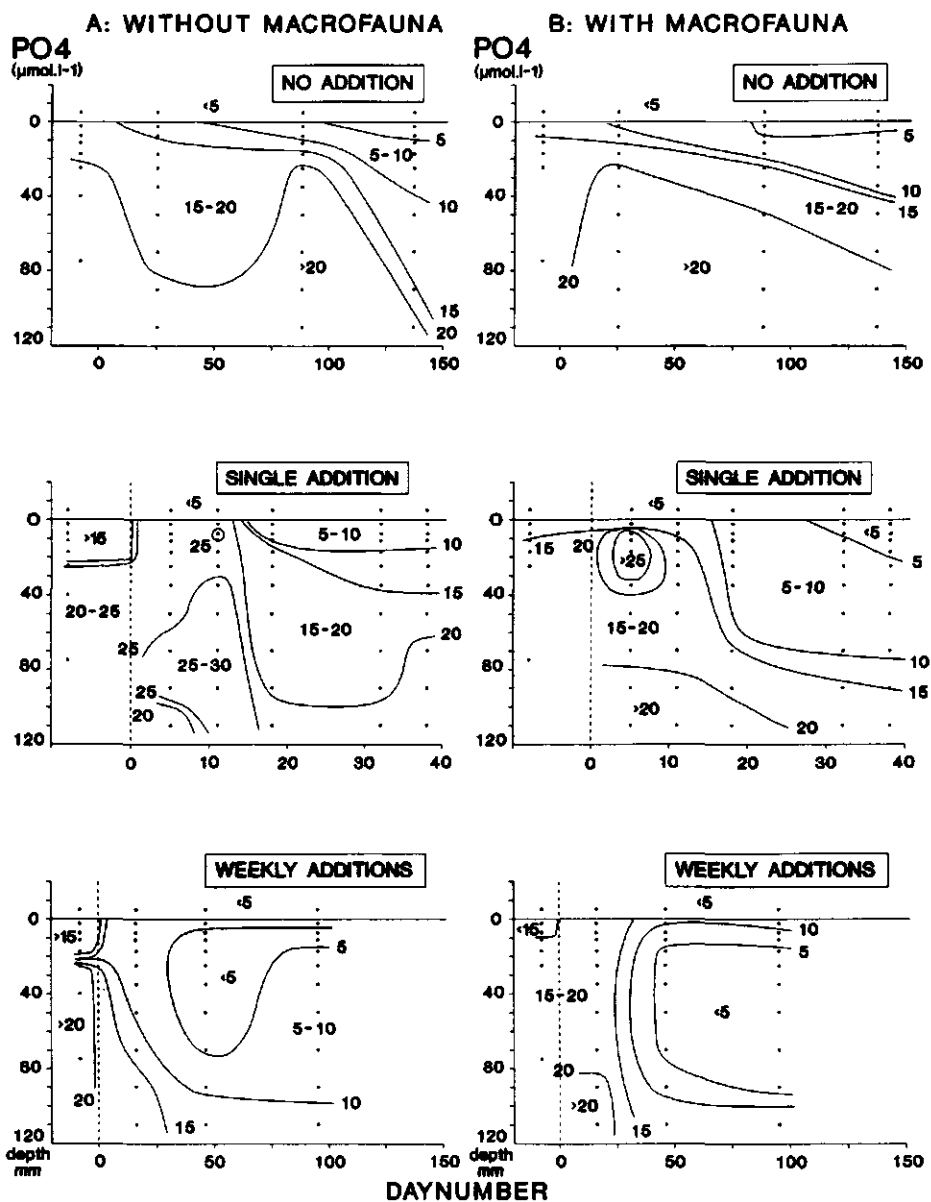
Fig. 3. PO$_4$ concentrations (μmol l^{-1}) in the porewater of the boxcosm sediment a. without macrofauna b. with macrofauna.

on the oxygen penetration depth both in the boxes with and without macrofauna. In these boxes oxygen penetration gradually decreased to depths < 1 mm 10 days after the addition, and subsequently increased again to ca. 5-15 mm. In the weekly fed boxcosms with macrofauna oxygen penetration depths decreased from ca. 30 to 2 mm during the experiment. In the weekly fed boxes without macrofauna large oscillations in the oxygen penetration depth were found, but overall, a decrease from 20 mm to 4 mm was observed. The oxygen penetration depth in the fed boxcosms with macrofauna was generally smaller than in the boxcosms without macrofauna (Wilcoxon's test; $n = 21$; $p < 0.05$).

Sediment composition. In the boxcosms to which no organic matter was added the carbon content remained very low, ranging from 0.01 to 0.03% (Fig. 5). After a single addition of organic matter the carbon content rapidly rose to 0.04-0.09% in the upper sediment layer, both with (Fig. 5b) and without macrofauna (Fig. 5a). When organic matter was added weekly and macrofauna were present, this increase of the carbon content was not limited to the upper sediment layer but extended down to 50 mm in the boxcosms, indicating substantial sediment mixing.

The leachable Fe- and Mn-contents of the sediment were very low: 0.03-0.04% (5.4-7.2 μmol Fe g^{-1}) and 0.002% (0.4 μmol Mn g^{-1}), respectively. NH_4Cl-, NaOH- and HCl-extractable phosphorus amounted to 0.01-0.03, 0.02-0.05 and 0.05-0.11 μmol P g^{-1} sediment, respectively. The phosphorus contents were lower than those found at a comparable sandy station in the North Sea where values of 0.05, 0.25 and 2.2 μmol P g^{-1} were found for the NH_4Cl, NaOH and HCl fraction, respectively (unpublished results). The low values found here can probably be explained by the removal of a part of the fine sediment fraction after filling of the boxes. No clear reaction to the single addition of organic matter could be discovered in the NH_4Cl and HCl fractions. Only NaOH-extractable phosphorus showed a clear reponse (Fig. 6) with the largest increase occurring in the presence of macrofauna.

DISCUSSION

Effect of organic matter additions. Both in the case of the single and weekly additions a clear effect of increased organic matter loading on phosphorus dynamics was found. Following deposition of organic matter, porewater phosphorus concentrations in the upper sediment layer increased, phosphate release rates showed a 3-5 fold increase and NaOH-extractable phosphorus increased substantially in the boxes to which a single addition was applied. Furthermore, oxygen uptake rates showed an immediate response. In the case of

A: O$_2$ UPTAKE

B: O$_2$ PENETRATION

mmol O2.m−2.d−1   NO ADDITION

depth mm   NO ADDITION

SINGLE ADDITION

SINGLE ADDITION

WEEKLY ADDITIONS   o WITHOUT MACROFAUNA   • WITH MACROFAUNA

WEEKLY ADDITIONS   o WITHOUT MACROFAUNA   • WITH MACROFAUNA

DAY NUMBER
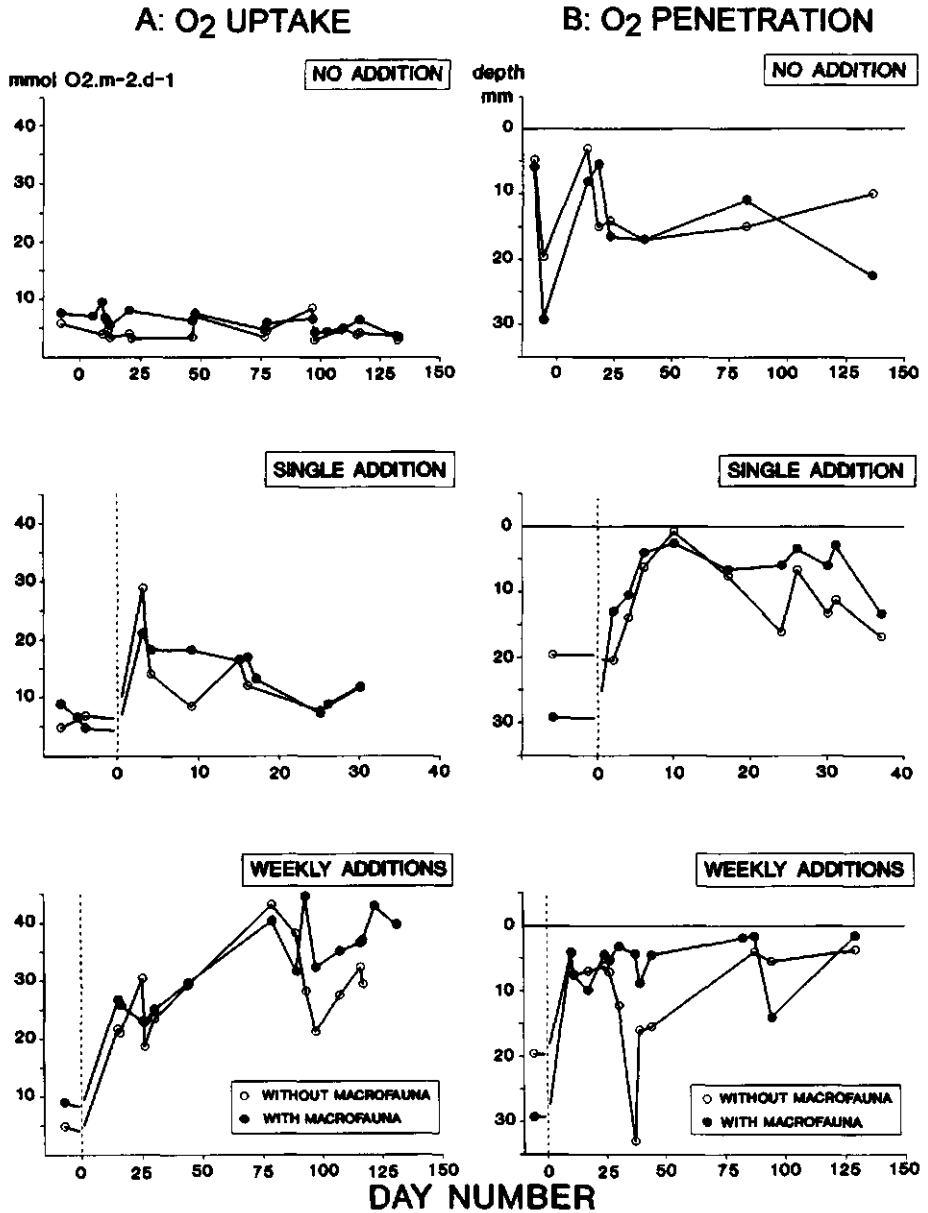
Fig. 4. a. Oxygen uptake rates (mmol O$_2$ m^{-2} d^{-1}) b. Oxygen penetration depths (mm) in the boxcosms.
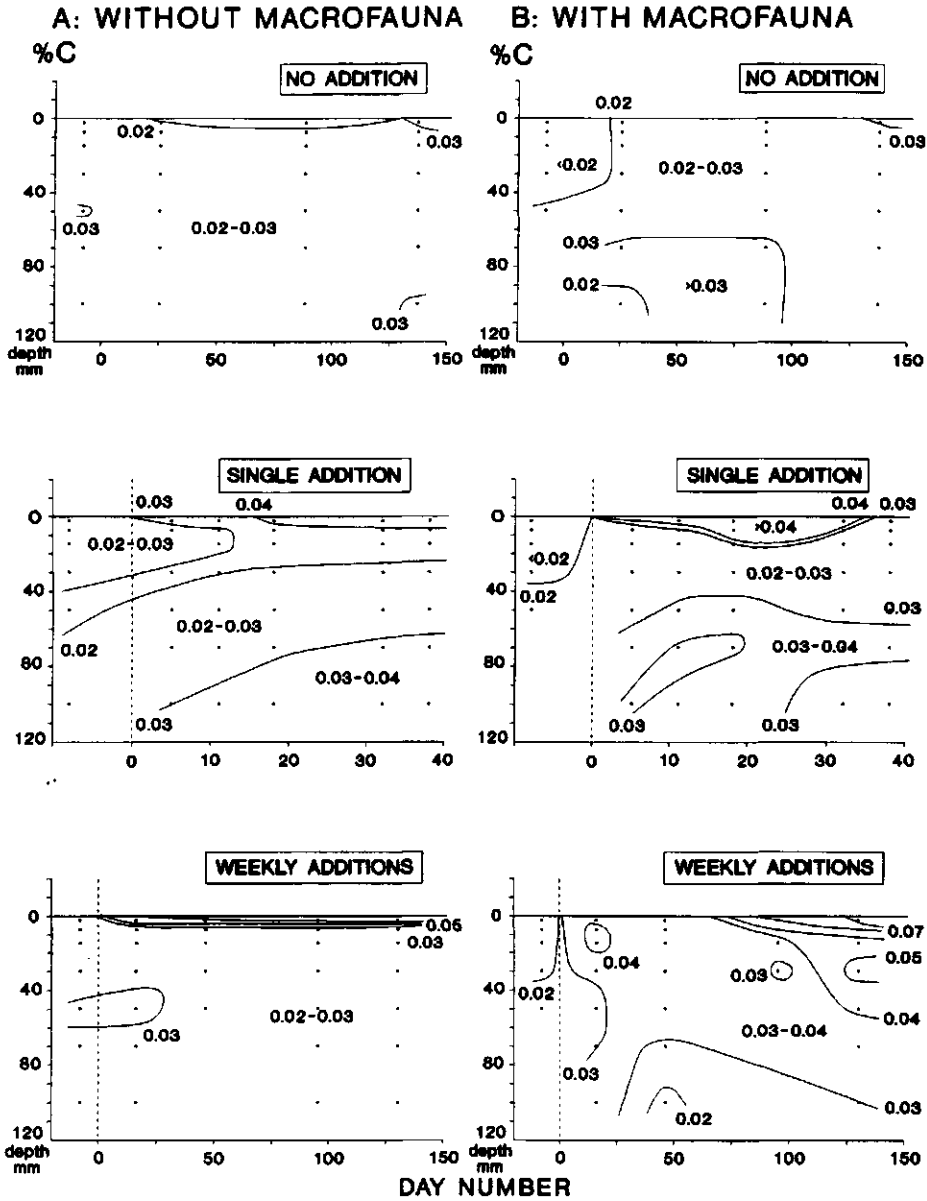
Figure 5. Organic carbon content (%C) of the sediment in the boxcosms a. without macrofauna b. with macrofauna.
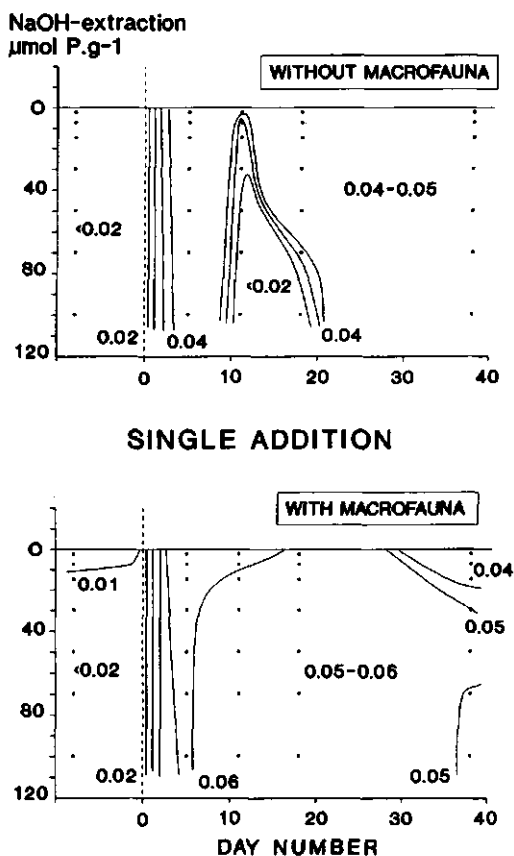
Figure 6. NaOH-extractable phosphorus (μmol P gr^{-1} sediment) in the sediment from the boxcosms which were fed once.

the single additions of organic matter this was accompanied by a rapid initial decrease of the oxygen penetration depth.

Previous field research on organic matter deposition on sediments has shown a rapid response of benthic microbial activity (Graf, 1982 & 1989; Meyer-Reil, 1983; Jensen et al., 1990) following deposition of a phytoplankton spring bloom. During laboratory experiments similar to ours but using intact cores from the field, Graf (1987) found a maximum oxygen uptake 3 days after the addition of algal matter. In experimental microcosms, Kelly & Nixon (1984) observed a time lag of 2-20 hours between an organic matter addition and maximum ammonium release rates. Enoksson (1987) found maximum oxygen uptake and phosphate release rates ca. 6 days following an organic matter addition

in the form of algal material. The results of our experiments are in accordance with these observations: following the single addition of organic material a large increase in oxygen uptake and phosphate release rates occurred within 2 and 4 days, respectively. Due to the relatively large intervals between sampling events it is impossible to say when the maxima occurred exactly.

When studying phosphorus dynamics it is of major importance to know what mechanism is controlling whether phosphorus is being released or bound in the sediment. The mechanisms involved can be of a chemical (adsorption/desorption and precipitation/dissolution) or biological nature (uptake or release by bacteria, excretion by macrofauna) or a combination of both (e.g. anoxic conditions mediated by bacteria resulting in release of sorbed phosphorus from iron oxides).

In the starved boxcosms a relatively large release of phosphorus, especially in the presence of macrofauna, was observed compared to the corresponding oxygen uptake. The average O_2-uptake/P-release atomic ratio in the starved boxes was low, ca. 55, indicating that oxic mineralization was not the dominating process. Excretion by macrofauna (Nixon et al., 1980) may explain part of these results. Initial porewater concentrations in the sediment were high and only gradually decreased, supporting the observed phosphorus release during almost the entire length of the experiment.

Following the addition of organic matter increased phosphate release occurred in the fed boxcosms. This can be attributed to (1) mineralization of the added organic matter, (2) release from iron oxides upon their reduction and (3) direct release from algal cells due to cell lysis.

In the same set-up, Van Duyl et al. (1992) measured increased bacterial numbers (from ca. 0.5 to 1.5 x 10^9 bacteria cm^{-3}) and bacterial production rates (from ca. 7 to 140 mg C m^{-2} d^{-1}; methyl-^{3}H-thymidine incorporation method) on day 5 compared to day -4 in the 0-3 mm sediment layer of the boxes which were fed once. In combination with the higher oxygen uptake rates from day 2 onwards, this indicates the potential importance of oxic mineralization for the phosphate fluxes.

If reduction of iron oxides controls the phosphate release, a decrease in the oxygen penetration depth would be expected during this period. Fig. 4b shows that oxygen penetration decreased to depths < 1 mm on day 10 in the case of the single additions. Although sulfate reduction may have taken place in locally reduced spots, diagenesis probably did not proceed beyond nitrate reduction as nitrate was generally still present in the porewater (not shown). Furthermore, only a relatively small amount of phosphorus was present in the NaOH-extractable phosphorus fraction at the start of the experiment and this fraction was found to increase from ca. 0.02 to 0.05 μmol P g^{-1} during the period of

maximum phosphate release. Apparently, the adsorption capacity of the sediment was not eliminated, making a chemical control of the increased phosphate release improbable.

Preferential P-release due to cell lysis is known to occur rapidly on death of algal cells (Balzer, 1984; Garber, 1984; Krom & Berner, 1981) and certainly may have occurred in the *Phaeocystis* suspensions.

In the boxes to which a single addition was applied the sediment-water exchange rates of phosphate were very low from day 10-15 onwards, coinciding with a gradual decrease in the oxygen uptake rate. When the organic matter was applied weekly, however, substantial phosphate release continued to occur. Furthermore, the oxygen uptake rates roughly stabilized and further depletion of the porewater did not occur. It is unlikely that a steady state situation was reached, however, as the sediment organic carbon content still continued to increase.

A tentative budget for the fate of the phosphorus added to the boxcosms through the organic matter additions is presented in Table 1. As the various input and output terms could not be quantified accurately, a great deal of assumptions were necessary. Each output/storage term in Table 1 is the highest value of the estimates with and without macrofauna. A loss of 20% of the added organic matter due to outflow over the rim was assumed for both feeding regimes. The release of phosphate from the sediment was estimated from the area under the curves in Fig. 2. The amount of added phosphorus which was bound in sediment organic matter and in the NaOH-extractable fraction of the sediment was calculated from Fig. 5 and 6 (assuming a sediment density of 2.65 g cm^{-3}, an average porosity of 0.40, a sediment depth of 10 cm and a C:P ratio for the organic matter of 106; Redfield et al., 1963). An estimate of the amount of phosphorus bound in bacteria was obtained from the increase in bacterial biomass in the weekly fed boxes with macrofauna integrated over 63 mm depth during 130 days (2.4 g C m^{-2}; Van Duyl et al., 1992) assuming a C:P weight ratio of 20 for the bacteria (Gächter et al., 1992). Ca. 40-60% of the phosphorus added through the organic matter is not accounted for in Table 1. Neither the phosphorus bound in bacteria in the case of the single additions nor the NaOH-extractable phosphorus in the sediment of the weekly fed boxes can account for this difference.

During the experiment total rates of oxygen uptake amounted to ca. 0.26 and 3.3 mol O_2 m^{-2} (calculated from the area under the curve in Fig. 4 and corrected for the uptake in the starved boxes) in the boxes with single and weekly additions, respectively. This corresponds to a carbon respiration of ca. 18-36% of the added material for both treatments when assuming a respiration quotient of 0.85 (Hargrave, 1973) and a loss due to outflow of 20%. These results suggest that for both feeding regimes a major part of the added organic matter was not mineralized during the experiment. This is in accordance with the fact that a

Table 1. A tentative budget for the fate of the phosphorus added to the fed boxcosms (in mmol P m^{-2}). n.d. = not determined.

	Single addition (mmol P m^{-2})	Weekly addition (mmol P m^{-2})
Input	+15	+95
Output/storage		
P flux	-4	-29
Organic P	-0.2	-3
NaOH-P	-5	n.d.
Bacterial P	n.d.	-4
Unaccounted for	+5.8 (39%)	+59 (62%)

layer of algal material was present on the sediment surface in most of the fed boxes during the entire experiment.

Effect of macrofauna. The macrofauna added to the boxcosms consisted of sub-surface and surface deposit feeders generally found in sandy sediments in the North Sea (Creutzberg et al., 1984). Apart from the sessile bivalve *Tellina*, of which up to 5 individuals per boxcosm had to be replaced during the experiment, the macrofauna generally had a low mortality and were very effective at reworking the sediment, as illustrated by the organic carbon profiles. Only *Echinocardium* reached high growth rates (Duineveld, pers. comm.). In some of the sampled boxes, however, the macrofauna (*Echinocardium* in particular) were completely inactive. Further details on the macrofauna in this study will be published elsewhere.

Previous research has shown that macrofauna can directly increase sediment-water exchange rates of oxygen and nutrients due to bioirrigation activity (Aller & Yingst, 1985; Hylleberg & Hendriksen, 1980; Kristensen & Blackburn, 1987) and indirectly due to the fact that macrofaunal feeding and burrowing can stimulate microbial activity in the sediment (Aller, 1982; Aller & Yingst, 1985; Kristensen & Blackburn, 1987; Yingst & Rhoads, 1980). Both in the case of the weekly and single additions of organic matter no clear effect of the presence of macrofauna on sediment-water exchange of phosphate and oxygen uptake rates could be discovered. The role of the burrowers *Echinocardium* and *Nephtys* was most likely limited to reworking of the sediment. Therefore, only indirect effects of macrofauna on solute transport would be expected.

The increase in substrate availability (higher organic carbon contents) at greater depths probably resulted in increased mineralization (Van Duyl et al., 1992) below the uppermost sediment layer explaining the smaller oxygen penetration depth in the presence of macrofauna. The increase of oxic mineralization below the upper sediment layer was

apparently too small to have a substantial effect on the total oxygen uptake rates. The organic carbon profiles show that mixing of the food into the sediment took several weeks, thus causing a major portion to remain at the sediment surface. In any case, this holds for the most labile, freshly deposited material in the weekly fed boxcosms. Consequently, most of the organic matter mineralization probably took place in the algal layer on the sediment surface and the processes in this layer most likely determined the phosphate and oxygen fluxes. Apparently, the processes in this layer were not substantially affected by the presence of macrofauna.

In the weekly fed boxes with macrofauna higher phosphate concentrations were observed in the upper cm's of the sediment in the second half of the experiment, corresponding to the higher organic carbon contents in these boxes. In the case of the single additions this was not observed, probably because time was too short to mix a substantial amount of carbon deeper into the sediment. In these boxes porewater phosphate concentrations were lower and NaOH-extractable phosphorus was higher in the presence of macrofauna. This suggests that macrofauna can stimulate phosphate binding in the sediment.

CONCLUSIONS

The results demonstrate that deposition of substantial amounts of organic matter on iron oxide poor sandy marine sediments enhances the sediment-water exchange of phosphate. This enhanced phosphate release is due to mineralization of the organic material and due to direct release of phosphate from algal cells. When the algal material largely remains at the sediment-water interface, this organic layer may regulate the sediment-water exchange of phosphate. The presence of burrowing macrofauna may stimulate phosphate binding in the sediment.

REFERENCES

Aller, R.C., 1982. The effects of macrobenthos on chemical properties of marine sediment and overlying water. p53-102. In: P.L. McCall & M.J.S. Tevesz, eds. Animal-sediment relations. Plenum publishing corporation. New York.

Aller, R.C. & J.Y. Yingst, 1985. Effect of the marine deposit-feeders *Heteromastus filiformis* (Polychaeta) *Macoma balthica* (Bivalvia) and *Tellina texana* (Bivalvia) on averaged sedimentary solute transport, reaction rates and microbial distributions. J. Mar. Res. 43: 615-645.

Balzer, W., 1984. Organic matter degradation and biogenic element cycling in a nearshore sediment (Kiel Bight). Limnol. Oceanogr. 29: 1231-1246.

Berner, R.A., 1980. Early diagenesis. A theoretical approach. Princeton University Press. Princeton. 241p.

Billen, G., C. Joiris, L. Meyer-Reil & H. Lindeboom, 1990. Role of bacteria in the North Sea Ecosystem. Neth. J. Sea Res. 26: 265-293.

Brockmann U.H., G. Billen & W.W.C. Gieskes, 1988. North Sea nutrients and eutrophication. p348-383. In: W. Salomons, B.L. Bayne, E.K. Duursma & U. Förstner, eds. Pollution of the North Sea. An assessment. Springer Verlag, Berlin.

Brockmann U.H., R.W.P.M. Laane & H. Postma, 1990. Cycling of nutrient elements in the North Sea. Neth. J. Sea. Res. 26: 239-264.

Cadée, G.C., 1990. Increased bloom. Nature. 346: 418.

Callender, E. & D.E. Hammond, 1982. Nutrient exchange across the sediment-water interface in the Potomac river estuary. Est.. Coast. Mar. Sci. 15: 395-413.

Cramer, A., 1990. Seasonal variation in the benthic metabolic activity in a frontal system in the North Sea. p54-76. In: M. Barnes & R.N. Gibson, eds. Trophic relationships in the marine environment. Proc. 24th Europ. Mar. Biol. Symp. Aberdeen. Univ. Press.

Cramer, A., 1991. Benthic metabolic activity at frontal systems in the North Sea. Ph.D.-thesis. University of Amsterdam, The Netherlands. 93p.

Creutzberg F., P. Wapenaar, G. Duineveld & N. Lopez Lopez, 1984. Distribution and density of the benthic fauna in the southern North Sea in relation to bottom characteristics and hydrographic conditions. Rapp. P. v. Réun. Cons. int. Explor. Mer. 183: 101-110.

De Wilde, P.A.W.J., E.M. Berghuis & A. Kok, 1984. Structure and energy demand of the benthic community of the Oyster Ground, Central North Sea. Neth. J. Sea Res. 18: 143-159.

Duinker, J.C., G.T.M. Van Eck & R.F. Nolting, 1974. On the behaviour of copper, zinc, iron and manganese and evidence for mobilization processes in the Dutch Wadden Sea. Neth. J. Sea Res. 8: 214-239.

Enoksson, V., 1987. Nitrogen flux between sediment and water and its regulatory factors in coastal areas. Ph.D.-thesis. Department of Marine Microbiology. University of Göteborg, Sweden.

Eisma, D., 1990. Transport and deposition of suspended matter in the North Sea and the relation to coastal siltation, pollution and bottom fauna distribution. Rev. Aq. Sci. 3: 181-216.

Fisher, T.R., P.R. Carlson & R.T. Barber, 1982. Sediment nutrient regeneration in three North Carolina estuaries. Est. Coast. Shelf Sci. 14: 101-116.

Froelich, P.N., M.L. Bender, N.A. Luedtke, G.R. Heath & T. DeVries, 1982. The marine phosphorus cycle. Am. J. Sci. 282: 474-511.

Froelich, P.N., 1988. Kinetic control of dissolved phosphate in natural rivers and estuaries: a primer on the phosphate buffer mechanism. Limnol. Oceanogr. 33: 649-668.

Froelich, P.N., M.A. Arthur, W.C. Burnett, M. Deakin, V. Hensley, R. Jahnke, L. Kaul, K.H. Kim, K. Roe, A. Soutar & C. Vathakanon, 1988. Early diagenesis of organic matter in Peru continental margin sediments: phosphorite precipitation. Mar. Geol. 80: 309-343.

Gächter, R., J.S. Meyer & A. Mares, 1988. Contribution of bacteria to release and fixation of phosphorus in lake sediments. Limnol. Oceanogr. 33: 1542-1558.

Gächter, R. & J.S. Meyer, 1992. The role of microorganisms in sediment phosphorus dynamics in relation to mobilization and fixation of phosphorus. Hydrobiologia 253: 103-121.

Garber, J.H., 1984. Laboratory study of nitrogen and phosphorus remineralization during the decomposition of coastal plankton and seston. Est. Coast. Shelf Sci. 18: 685-702.

Graf, G., 1982. Benthic response to sedimentation of a spring phytoplankton bloom process and budget. Mar. Biol 67: 201-208.

Graf, G., 1987. Benthic energy flow during a simulated autumn bloom sedimentation. Mar. Ecol. Prog. Ser. 39: 23-29.

Graf, G., 1989. Benthic-pelagic coupling in a deep-sea benthic community. Nature 341: 437-439.

Hargrave, B.T., 1973. Coupling carbon flow through some pelagic and benthic communities. J. Fish Res. Board Can. 35: 1317-1326.

Helder W. & J.F. Bakker, 1985. Shipboard comparison of micro- and minielectrodes for measuring oxygen distribution in marine sediments. Limnol. Oceanogr. 30: 1106-1109.

Hieltjes A.H.M. & L. Lijklema, 1980. Fractionation of inorganic phosphates in calcareous sediments. J. Envir. Qual. 9: 405-407.

Hopkinson, Jr. C.S., 1987. Nutrient regeneration in shallow-water sediments of the estuarine plume region of the nearshore Georgia Bight, U.S.A. Mar. Biol. 94: 127-142.

Hüttel, M., 1990. Influence of the lugworm *Arenicola marina* on porewater nutrient profiles of sand flat sediments. Mar. Ecol. Prog. Ser. 62: 241-248.

Hylleberg J. & K. Hendriksen, 1982. The central role of bioturbation in sediment mineralization and element recycling. Ophelia 1: 1-16.

Jenness, M.I. & G.C.A. Duineveld, 1985. Effects of tidal currents on chlorophyll-a content of sandy sediments in the southern North Sea. Mar. Ecol. Prog. Ser. 21: 283-287.

Jensen, M.H., E. Lomstein, J. Sørensen, 1990. Benthic NH_4^+ and NO_3^- flux following sedimentation of a spring phytoplankton bloom in Aarhus Bight, Denmark. Mar. Ecol. Prog. Ser. 61: 87-96.

Kelly, J.R. & S.W. Nixon, 1984. Experimental studies of the effect of organic deposition on the metabolism of a coastal marine bottom community. Mar. Ecol. Prog. Ser. 17: 157-169.

Klump, J.V. & C.S. Martens, 1981. Biogeochemical cycling in an organic-rich coastal marine basin. II. Nutrient sediment-water exchange processes. Geochim. Cosmochim. Acta 45: 101-121.

Klump, J.V. & C.S. Martens, 1987. Biogeochemical cycling in an organic-rich coastal marine basin. 5. Sedimentary nitrogen and phosphorus budgets based upon kinetic models, mass balances and the stoichiometry of nutrient regeneration. Geochim. Cosmochim. Acta 51: 1161-1173.

Kristensen, E. & T.H. Blackburn, 1987. The fate of organic carbon and nitrogen in experimental marine sediment systems: influence of bioturbation and anoxia. J. Mar. Res. 45: 231-257.

Krom, M.D. & R.A. Berner, 1980. Adsorption of phosphate in anoxic marine sediments. Limnol. Oceanogr. 25: 797-806.

Krom M.D. & R.A. Berner, 1981. The diagenesis of phosphorus in a nearshore marine sediment. Geochim. Cosmochim. Acta 45: 207-216.

Laane, R.W.P.M, 1980. Conservative behaviour of dissolved organic carbon in the Ems-Dollart Estuary and the Western Wadden Sea. Neth. J. Sea Res. 14: 192-199.

Lancelot, C., G. Billen, A. Sournia, T. Weisse, F. Colijn, M.J.W. Veldhuis, A. Davies & P. Wasman, 1987. *Phaeocystis* blooms and nutrient enrichment in the continental coastal zones of the North Sea. Ambio 16: 38-46.

Levesque, M. & M. Schnitzer, 1966. Effects of NaOH concentration on the extraction of organic matter and of major inorganic constituents from a soil. Can J. Soil Sci. 46: 7-12.

Lijklema, L. 1977. The role of iron in the exchange of phosphate between water and sediments. p313-317. In: H.L. Golterman, ed. Interactions between sediments and freshwater. Junk, The Hague.

Martens, C.S., R.A. Berner & J.K. Rosenfeld, 1978. Interstitial water chemistry of anoxic Long Island Sound sediments. 2. Nutrient regeneration and phosphate removal. Limnol. Oceanogr. 23: 605-617.

Meyer-Reil, L.A., 1983. Benthic response to sedimentation events during autumn to spring at a shallow water station in the western Kiel-Bight. II. Analysis of benthic bacterial populations. Mar. Biol. 77: 247-256.

Mortimer, C.H., 1941. The exchange of dissolved substances between mud and water in lakes. J. Ecol. 280-329.

Nixon, S.W., J.R. Kelly, B.N. Furnas, C.A. Oviatt & S.S. Hale, 1980. Phosphorus regeneration and the metabolism of coastal marine benthic communities. p219-242. In: K.R. Tenore & B.C. Coull, eds. Marine benthic dynamics. Univ. of South Carolina Press, Columbia.

Peeters, J.C.H. & L. Peperzak, 1990. Nutrient limitation in the North Sea: a bioassay approach. Neth. J. Sea Res. 26: 61-73.

Postma, H., 1985. Eutrophication of Dutch Coastal waters. Neth. J. Zool. 35: 348-359.

Redfield, A.C., B. Ketchum & F. Richard, 1963. The influence of organisms on the composition of seawater. p26-77. In: M. Hill, ed. The Sea. Vol. 2. Interscience, New York.

Reeburgh, W.S. 1967. An improved interstitial water sampler. Limnol. Oceanogr. 12: 163-170.

Riegman, R., F. Colijn, J.F.P. Malschaert, H.T. Kloosterhuis & G.C. Cadée, 1990. Assessment of growth rate limiting nutrients in the North Sea by the use of nutrient uptake kinetics. Neth. J. Sea Res. 26: 53-60.

Rutgers van der Loeff, M.M., 1980. Nutrients in the interstitial water of the Southern Bight of the North Sea. Neth. J. Sea Res. 14: 144-171.

Strickland J.D.H. & T.R. Parsons, 1972. A practical handbook of seawater analysis. 2nd edn. Bull. Fish. Res. Bd. Can. 167: 1-311.

Van Duyl, F.C., A.J. Kop, A. Kok & A.J.J. Sandee, 1992. The impact of organic matter and macrozoobenthos on bacterial and oxygen variables in marine sediment boxcosms. Neth. J. Sea Res. 29: 343-355.

Van Raaphorst, W., H.T. Kloosterhuis, A. Cramer & K.J.M. Bakker, 1990. Nutrient early diagenesis in the sandy sediments of the Doggerbank area, North Sea: pore water results. Neth. J. Sea Res. 26: 25-52.

Van Raaphorst, W., H.T. Kloosterhuis, E.M. Berghuis, A.J. Gieles, J.F.P. Malschaert, G.J. Van Noort, 1992. Nitrogen cycling in two sediments of the southern North Sea (Frisian Front, Broad Fourteens): Field data and mesocosm results. Neth. J. Sea. Res. 28: 293-316.

Verardo, D.J., P.N. Froelich & A. McIntyre, 1990. Determination of organic carbon and nitrogen in sediments using the Carlo Erba Na-1500 analyzer. Deep-Sea Res. 37: 157-165.

Westernhagen, H. v., W. Hickel, E. Bauerfernd, U. Niermann & J. Kröncke, 1986. Sources and effects of oxygen deficiencies in the south-eastern North Sea.. Ophelia 26: 457-473.

Yingst, J.Y. & D.C. Rhoads, 1980. The role of bioturbation in the enhancement of bacterial growth rates in marine sediments. p407-421. In: K.R. Tenore & B.C. Coull, eds. Marine benthic dynamics. Univ. South Carolina Press, Columbia.

Chapter 3

Phosphorus binding by poorly crystalline iron oxides in North Sea sediments[*]

ABSTRACT

Differential X-ray powder diffraction (DXRD) and extraction procedures were used to characterize the iron oxides present in four sediments from contrasting environments in the North Sea. Stations were located in depositional areas on the southern shelf (German Bight) and on the north-eastern shelf-slope transition (Skagerrak) and in areas with no net deposition in the southern North Sea. Poorly crystalline ferrihydrite and akageneite (extractable with 0.1 M HCl and 0.2 M NH_4-oxalate) were identified in the fine sediment fraction (<10 μm) of surface samples at all locations. Evidence for the dominant role of these Fe oxides in the binding of phosphorus in North Sea sediments was obtained from the good relationship of both the content of Fe-bound P and the linear adsorption coefficient for phosphate with NH_4-oxalate extractable Fe. A tight coupling of porewater Fe^{2+} and HPO_4^{2-} was observed at 3 stations. Porewater Fe^{2+}/HPO_4^{2-} ratios at maximum porewater concentrations of Fe^{2+} were similar to NH_4-oxalate Fe/Fe-bound P ratios for surface sediment at these locations, and were in the range known for synthetic poorly crystalline Fe oxides. This suggests that porewater HPO_4^{2-} production at the time of core collection was dominated by release from poorly crystalline Fe oxides. In contrast, at the German Bight station, much higher HPO_4^{2-} levels and a decoupling of porewater Fe^{2+} and HPO_4^{2-} was observed, suggesting a larger contribution of mineralization of organic matter to porewater HPO_4^{2-} than at the other sites. Solid phase P analyses indicate possible redistribution of Fe-bound P to another inorganic phase at depth at the Skagerrak station, but not at the other stations. The persistence with depth of poorly crystalline Fe oxides and Fe-bound P suggests that these Fe phases can act as both a temporary and permanent sink for P in continental margin sediments.

INTRODUCTION

Iron oxides, hydroxides and oxyhydroxides (henceforth called Fe oxides) can provide sorption sites for compounds with a high affinity for the Fe oxide surface such as many trace metals, silica and phosphorus (P). The large effect of these sorption processes on the cycling of P in marine sediments is well-documented. Fe oxides present in the oxidized surface layer of the sediment can act as a 'trap' for porewater HPO_4^{2-} diffusing upwards (Krom and Berner, 1980; Sundby et al., 1992; Slomp and Van Raaphorst, 1993). Rapid sorption and release of P from 'reactive' Fe oxides can control porewater HPO_4^{2-} concentrations and thus directly affect sediment-water exchange (Sundby et al., 1992; Van

Raaphorst and Kloosterhuis, 1994). Simultaneous release of P and fluoride from Fe oxides may provide the necessary conditions for early diagenetic carbonate fluorapatite (CFA) precipitation (Ruttenberg and Berner, 1993). The persistence of some Fe oxides with depth, as has been observed in many marine sediments (e.g. Sundby et al., 1992; Jensen and Thamdrup, 1993; Kostka and Luther, 1994), enables Fe-bound P to become an important permanent reservoir for P in marine sediments (Ruttenberg, 1993). As the mineralogy and crystallinity of Fe oxides strongly influence their HPO_4^{2-} sorption characteristics (Borggaard, 1983a; Parfitt, 1989; Ruttenberg, 1992) and their susceptibility to reduction (Schwertmann, 1991), knowledge of the character of these Fe phases in marine sediments is essential for a correct understanding of their role in the P cycle.

The reported occurrences of Fe oxides in the marine environment compiled by Murray (1978) and Burns and Burns (1980) mostly apply to concretions or nodules found in deep sea sediments. Very little is known about the mineral forms of Fe oxides in coastal marine sediments. Direct determination with conventional techniques (e.g. X-ray powder diffraction, X-ray microanalysis) is difficult due to their low concentrations, their (presumably) poor crystallinity, and the fact that they are generally present as coatings on other particles. As an alternative, extraction techniques which have been tested for their selectivity using pure mineral phases are widely employed (e.g. Canfield, 1988, 1989; Kostka and Luther, 1994). When applied to natural materials these techniques are only operationally defined. Firstly, extractants always suffer from a lack of absolute specificity in mineral or phase separation. Secondly, mineral phases in sediments may have very different solubilities compared to the standard materials used for calibration, e.g., due to another mode and environment of formation and variations in the extent of weathering prior to deposition.

Sequential X-ray powder diffraction measurements in combination with extraction schemes (Differential XRD: DXRD) partly circumvent the above mentioned problems by lowering the detection limit for Fe oxides and making direct identification of extracted phases possible (Schulze, 1981; Van der Gaast, 1991; Wang et al., 1993). In this study the DXRD technique is applied to the fine sediment fraction (<10 μm) of surface samples from four contrasting environments in the North Sea with the aim of identifying the Fe oxides present. The DXRD results are combined with bulk sediment solid phase speciation (determined using extraction procedures) and porewater profiles of Fe^{2+} and HPO_4^{2-} to determine whether the identified Fe oxides are responsible for the binding of P in these sediments. The results show that poorly crystalline akageneite and ferrihydrite are the most important Fe oxides in these continental margin sediments and that these Fe phases are responsible for the binding of P.

MATERIALS AND METHODS

Study sites and sample collection. The North Sea is a semi-enclosed part of the north-west European shelf with water depths gradually increasing from less than 30 m in the south to about 200 m in the area between the Shetlands and the Norwegian coast. To the northeast, in the Skagerrak/Norwegian channel, the seafloor slopes down to a depth of 700 m. The water circulation and transport of suspended matter are predominantly counterclockwise (Fig. 1). Net sedimentation of material is negligible outside the deposition areas of the inner German Bight and the Skagerrak/Norwegian Channel (Eisma and Kalf, 1987), where estimated sedimentation rates vary between 0.5-1 cm yr^{-1} (Von Haugwitz et al., 1988; Eisma and Kalf, 1987) and 0.1-0.5 cm yr^{-1} (Van Weering et al., 1987; Anton et al., 1993), respectively. An estimated 50 to 70% of total North Sea suspended matter eventually is deposited in the Skagerrak/Norwegian Channel (Eisma and Kalf, 1987). Local sources of suspended matter, due to past dredging and dumping of harbour sludge, may be of some importance in the German Bight (Irion et al., 1987). In contrast to the Skagerrak area, large seasonal variations in deposition and mineralization rates of organic matter occur in the German Bight area, leading to sediment anoxia in summer (Lohse et al., 1995).

Four locations with a wide range of sediment characteristics (Table 1) were selected for this study. Stations 9 and 13 (medium silt) are located in the main depositional areas (Skagerrak and German Bight), whereas stations 5 and 14 (fine sand) are both located in areas with no net deposition. Station 14 lies right outside the German Bight depositional area.

In February 1992 sediment cores were obtained with a cylindrical box corer (31 cm i.d.) which enclosed 30 to 50 cm of sediment column together with 15 to 25 l of overlying bottom water. Subsamples were taken from the box core with acrylic liners which were closed with rubber stoppers. Only cores without any visible surface disturbance were used. At all stations a brown surface layer was observed, varying in thickness from ~ 5-7 cm (st. 5, 13, 14) to ~10 cm (st. 9). The underlying sediment was either black (st. 13), brown/black (st. 5, 9) or grey/black (st. 14).

Porewater and solid phase analysis. To obtain porewater, sediment from 10-15 subcores (i.d. 3.1 cm) was sliced in a nitrogen flushed box immediately after collection. Slices from 9 depth intervals (0-0.4, 0.4-1, 1-1.5, 1.5-2, 2-3, 3-4, 4-6, 6-8, 8-10 cm) were pooled in polyethylene centrifuge tubes with a built-in filter specially designed for sandy, low porosity sediments (Saager et al., 1990) at stations 5 and 14, and in 50 ml polypropylene centrifuge tubes at stations 9 and 13. These were centrifuged for 10 min. at 1700 g. The filtered (cellulose acetate, 0.45 µm) samples were acidified to pH $\approx$ 1 and stored at 4°C
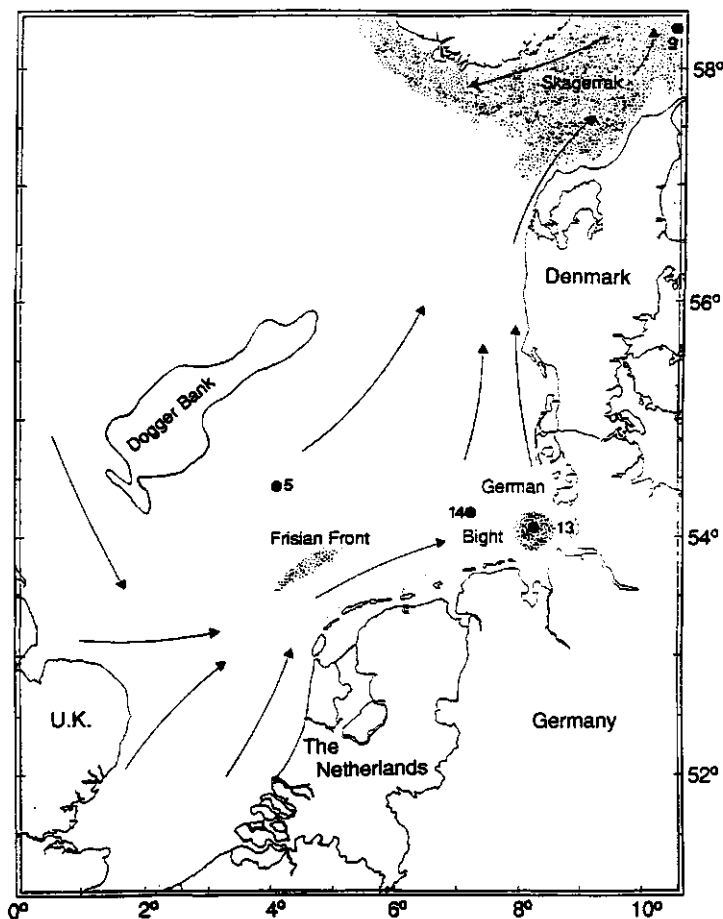
Fig. 1. Map of the North Sea showing the sampling locations and station numbers. Main transport routes of water and suspended matter in the North Sea are indicated (arrows). Stippled areas indicate main depositional regions.

Table 1. Location, depth and some general characteristics of the sediment at the sampling locations (median grain size determined in the upper 0-0.5 cm of the sediment, all other parameters are averages for the 0-1.0 cm layer). Sediment classification is based on the Wentworth size scale (Pettijohn et. al., 1972).

St. no.	Location Lat.	Long.	Water depth	Poro-sity	Org. C	Org. N	Org.P	CaCO₃	<10µm fraction	Median grain size	Sediment classification
	N	E	(m)	(v/v)	(%)	(%)	(%)	(%)	(%)	(µm)	
5	54°25'	4°04'	49	0.49	0.17	0.027	0.0023	1.7	8	103	very fine sand
9	58°20'	10°27'	330	0.89	2.83	0.338	0.0291	9.6	72	6	medium silt
13	54°05'	8°09'	19	0.64	0.82	0.097	0.0108	10.3	42	15	medium silt
14	54°14'	7°20'	39	0.56	0.36	0.047	0.0050	6.5	7	98	very fine sand

until analysis for HPO_4^{2-}, Fe^{2+} and Mn^{2+}. All sample manipulations took place at in situ temperature (4.4 to 6.4°C).

Sliced sediment from 8-10 additional subcores was pooled and stored frozen (-20°C) until solid phase analysis. Sediment from 7 depth intervals (0-0.5, 0.5-1, 1-2, 2-4, 4-6, 6-8, 8-12 cm) was subjected to five (non-sequential) extraction procedures for Fe: (1) 0.1 M HCl for 18 h (Duinker et al., 1974); (2) 1 M HCl for 24 h (Canfield, 1988); (3) 0.2 M NH_4-oxalate/oxalic acid buffer (pH = 3.0) for 2 h under oxic conditions in the dark (Schwertmann and Cornell, 1991); (4) 0.5 M oxalic acid for 2 h (pH = 1.7) (Schwertmann and Cornell, 1991); (5) Citrate-dithionite-bicarbonate solution (CDB, pH = 7.3, 8 h, 20°C) (Ruttenberg, 1992). We tested the effect of the use of a higher temperature (70°C) and a shorter extraction time (15 min.) as suggested in the original procedure for CDB-extractable Fe (Mehra and Jackson, 1960) using surface sediment from stations 5 and 9. We found no significant difference with the 8 hour extraction at room temperature (20°C), even upon repeated (2x) extraction. Oven-dried (60°C), ground (teflon mortar and pestle) material was used for the HCl extractions. Untreated, wet sediment was used for all other procedures. Oven-drying may lead to phase modification and transformation of particularly poorly crystalline Fe oxides, and this may result in changes in their solubility (Schwertmann and Cornell, 1991). We checked whether this occurred at our relatively low oven-temperature by extracting both oven-dried and wet surface sediment from station 5 with 1 M HCl. We found no significant difference between the quantities of Fe extracted. All extraction procedures were performed with sediment under oxic conditions, therefore all Fe profiles include oxidized FeS. We have no data on FeS in these sediments, but based on results of other studies on Fe in North Sea sediments (Jørgensen, 1989; Canfield et al, 1993) we assume that FeS accounted for less than 10% of CDB-Fe.

Table 2 gives an overview of the percentages of Fe that are extracted from common Fe-containing phases as determined using standard minerals and four types of extraction solutions with similar active components (i.e. oxalic acid, 1 M HCl, oxalate and dithionite) to those applied in this study. A part of the observed variation in the efficiency of the extractions can be attributed to differences in the extraction conditions used in each study (extraction time, buffer system, etc.). Oxalate extractable Fe is often used as a rough indication of the amount of poorly crystalline Fe oxides in a sediment. 1 M HCl would be expected to additionally extract Fe from clay minerals. Although no evidence from experiments with standard minerals are available, oxalic acid may also extract clay mineral Fe (due to its low pH) and would be expected to give results comparable to 1 M HCl. Dithionite extractable Fe should give a measure for total Fe oxide Fe. No tests of 0.1 M

Table 2. Percentages of Fe extracted from common Fe-containing phases as determined either directly or estimated using standard minerals and four types of extraction solutions under various extraction conditions.

Mineral	Oxalate % Fe	ref	1 M HCl % Fe	ref	Oxalic ac. % Fe	ref	Dithionite % Fe	ref
amorphous Fe oxide	40-70	b	34-72	b	95	b		
ferrihydrite (Fe$_5$HO$_8$.4H$_2$O)	47-82,70-80,100	d,f,ag	100	a			100	a,l,g
akageneite (β-FeOOH)	<3,+	f,e						
lepidocrocite (γ-FeOOH)	<2, 42, 50	f,d,a	7	a			100	a
goethite (α-FeOOH)	<1,<3, 35	gab,f,b	<0.5, <3	b,a	4-6	b	60-93,100	fikg,a,l
hematite (α-Fe$_2$O$_3$)	<1, <5	gab,f	<0.5,<3	b,a	7-12	b	5-30,63,98,100	f,g,a,kl
magnetite (Fe$_3$O$_4$)	20, 60, 70, 95	b,g,f,a	< 0.5,<3	b,a	28-35,100	b,m	3,90	a,g
amorphous Fe sulfide	100	g	100	c			100	g
mackinawite (FeS)			92	c				
greigite (Fe$_3$S$_4$)			40-67	c				
pyrite (FeS$_2$)			0	c			-	h
chlorite	<3, 3	a,g	32	a			2, 5, 7	i,g,a
smectite	-	j					-	j
vermiculite							+	k
nontronite	<3	a	7	a			27	a
illite	-	j					-	j
glauconite	<3	a	10	a			10	a
biotite	<3	a	22	a				
garnet	<3	a	<3	a			<3	a

Key to the references: (a) Canfield, 1988; (b) Chao and Zhuo, 1983; (c) Cornwell and Morse, 1987; (d) Karim, 1984; (e) Kauffman and Hazel, 1975; (f) Kodama and Ross, 1991 (g) Kostka and Luther, 1994; (h) Lord, 1982; (i) Lucotte and d'Anglejan, 1985; (j) McKeague and Day, 1966; (k) Mehra and Jackson, 1960; (l) Ruttenberg, 1992; (m) Schwertmann and Cornell, 1991. + and - indicate substantial and minor dissolution, respectively, but % Fe extracted unknown. Letters not subdivided by commas refer to the same percentage in the table.

HCl extractions with standard minerals are known, but it is assumed to extract the same phases as 1 M HCl with less attack on clay minerals (Duinker et al., 1974).

CDB-extractable P is used as a measure for total Fe-bound P (Ruttenberg, 1992). Inorganic and total P were determined as 1 M HCl-extractable P (24 h) before and after ignition of the sediment at 550°C (2h). The difference between total and inorganic P is used as a measure for organic-P (Aspila et al, 1976; Ruttenberg, 1992). Dilute (0.1 M) HCl, NH$_4$-oxalate, and oxalic acid extractions can partially solubilize apatite P (Lucotte and d'Anglejan, 1985) and P attached to surfaces of crystalline Fe oxides. Therefore, it is not possible to differentiate directly between P bound to different types of Fe oxides with these extractions.

Porosity was determined by weight loss of the sediment after drying at 60°C for 48 h and assuming a specific sediment weight of 2.65 kg dm^{-3}. Grain size distribution was determined with a Malvern particle analyzer. Total C and N and organic C were measured with a Carlo Erba 1500-2 elemental analyzer (Verardo et al., 1990). All sediment N was assumed to be in an organic form. $CaCO_3$ contents were calculated from inorganic C contents. A good correlation with $CaCO_3$ values calculated from 1 M HCl extractable Ca was found (HCl-$CaCO_3$ = 0.93 x Inorg.C-$CaCO_3$ + 0.11; R^2= 0.93).

Differential X-ray powder diffraction. The < 10 μm fraction of surface sediment from all four stations was used for the XRD analysis for two reasons. Firstly, Fe oxides are expected to be mostly present in the fine sediment fraction, either in the form of coatings on other particles such as clay minerals or as very small crystals (5-150 nm in size; Schwertmann, 1991). Secondly, the particle size of substances analyzed with XRD is preferred to be below 10 μm (Van der Gaast, 1991).

In order to concentrate the Fe oxides the <10 μm fraction of sediment from 0.5-1.0 cm depth (insufficient material was available from the 0-0.5 cm depth layer) was separated by repeated centrifugation and resuspension. Microscopic examination (1000x magnification) showed that indeed very few particles larger than 10 μm were present. Calcium carbonate was removed by a 1 h extraction with 1 M sodium acetate buffer (pH=5) to prevent the formation of a Ca-oxalate complex during extraction with oxalic acid or NH_4-oxalate. The XRD characteristics of smectites depend on the type of cation that they hold in their exchange sites. To ensure that the exchange sites of the sediment smectites were always saturated with Ca, the sediment was exchanged with Ca using a $CaCl_2$ solution after each extraction step. This was followed by a rinse to remove the excess Ca. An ethanol-water mixture (1/1) was used for this rinse, to minimize hydrogen ion substitution for the exchangeable Ca (Moore and Reynolds, 1989). XRD analysis was performed on vacuum dried samples before and after each extraction. The sediment portions from each station were extracted non-sequentially with NH_4-oxalate and oxalic acid. The sample from station 5 was also extracted with 0.1 M HCl. Only following the oxalic acid extraction the sediment residues were subjected to two sequential CDB-extractions.

Randomly oriented specimens were prepared by gently pressing ~10 mg of sample material in a depression of a monocrystalline Si-disc which provides a very low background and no diffraction peaks. The XRD analysis was carried out using CoKα-radiation (40 kV, 40 mA) and a wide angle goniometer (PW 1050/25, Philips). The apparatus was equipped with a long fine focus X-ray tube, a graphite monochromator and a vacuum-helium device. Further details on instrumentation and methodology are given by Van der Gaast (1991).

DXRD patterns were obtained by subtraction of the XRD pattern after treatment from that before treatment. The patterns were normalized by calculating an intensity-ratio from a part of the pattern between 15 and 18° 2θ, from which only incoherent radiation was detected. After subtraction, the patterns were smoothed over nine points of equal weight. The removal of Fe oxides from sediments often results in an improved orientation of clay minerals (Moore and Reynolds, 1989). This causes an increase in their 00*l* (i.e. the diagnostic reflections used for the identification of the clay minerals) and a decrease in their *hk* (non-diagnostic) reflections. As a consequence, subtraction results in negative and positive peaks in the DXRD pattern, at the positions of the diagnostic and non-diagnostic reflections, respectively. These positive peaks are thus not indicative of clay mineral dissolution but solely reflect the change in clay mineral orientation. The same holds for positive peaks in the DXRD pattern for feldspar and quartz.

Due to a strong shift in the reflections of smectite as a result of NH_4 fixation in all samples extracted with NH_4-oxalate, interpretation of the matching XRD and DXRD diagrams was not possible (also see Kodama and Ross, 1991). We tried using Na-oxalate as an alternative, but found that a precipitate was formed when making a 0.2 M buffer solution of pH 3. Consequently, DXRD could only be applied to the 0.1 M HCl, oxalic acid and CDB extracted sediments.

Chemical analysis. Total Fe and Mn in the porewater (mostly present as Fe^{2+} and Mn^{2+}), Fe and Mn in the sediment extracts, and Ca in the 1 M HCl extracts were determined with a Perkin Elmer 5100 PC Atomic Absorption Spectrophotometer. Porewater HPO_4^{2-} and 1 M HCl-extractable P were determined on a Shimadzu Double beam Spectrophotometer with the method of Strickland and Parsons (1972). Total Fe, Al, Si and P in the NH_4-oxalate, the oxalic acid and the CDB solutions and in the DXRD-0.1 M HCl solution for station 5 were determined with an ICP Spectroflame (Spectro Analytical Instruments). Oxalic acid extractable elements were only analyzed for three sediment depths (5-10, 20-40, 60-80 mm). There was a good agreement between the Fe analysis with the AAS and ICP (R^2=0.93). Reproducibility of the analysis of the porewater and of the sediment extractions of bulk samples and of the <10 μm fraction was generally better than 4%, 5% and 15%, respectively. The relatively large variation for the extractions of the fine material can be explained by the larger effect of sample heterogeneity when using small quantities of sample.

RESULTS

Differential X-ray powder diffraction (< 10 μm fraction). XRD and DXRD analysis of the fine sediment fraction from 0.5-1.0 cm depth at all four stations gave essentially the same results. To avoid repetition of very similar patterns only those for station 5 and 14 are presented. When 'reading' the diagrams in Fig. 2-5, it should be kept in mind that (1) peak positions (each mineral is characterized by a 'set' of peaks) indicate which mineral has been detected, (2) peak itensities or height may be used to, very roughly, quantify the amount of this mineral, and (3) peak width indicates how well-crystalline a mineral is. As DXRD patterns are obtained by subtraction of the XRD diagram after treatment from the XRD diagram obtained before treatment, minerals that have been dissolved will appear as positive peaks in the pattern.

Chlorite, mica/illite, kaolinite, feldspar, pyrite and quartz were identified in all 'start' diagrams (Fig. 2 and 3). The broad peak at 15.2 Å, overlain by a small, sharp chlorite peak, is indicative of smectite. The more pronounced broadening of this peak at station 14 (and 13) then at station 5 (and 9) suggests the presence of a poorly crystalline smectite at the first two stations. Based on the peak height a decrease in chlorite, mica/illite and kaolinite contents was observed in the stations sequence: $5 > 9 > 13 \approx 14$. Highest pyrite contents were found at station 13, subsequently decreasing in the stations sequence $14 > 5 \approx 9$.

In the XRD patterns (Fig. 2 and 3), an increase in intensity of the diagnostic clay mineral reflections and a decrease in intensity of the feldspar and quartz and the non-diagnostic (*hk*) clay mineral reflections were observed after oxalic acid and 0.1 M HCl extraction. This resulted in negative peaks at the locations of the diagnostic clay mineral reflections and positive peaks at the locations of the quartz, feldspar and non-diagnostic clay mineral reflections in the corresponding DXRD patterns (Fig. 4A and B and 5A). These peaks are attributed to changes in mineral orientation (see methods section) and thus do not indicate mineral dissolution. Instead of the expected increase in intensity of the diagnostic chlorite peak at 14.1 Å after the oxalic acid treatment, a decrease was observed at stations 9, 13 and 14 (shown for stat. 14 in Fig. 3), resulting in positive peaks in the DXRD patterns (shown for station 14 in Fig. 5A). This suggests dissolution of chlorite or alteration of the chlorite Fe/Mg-hydroxide interlayer upon oxalic acid extraction.

All DXRD patterns obtained after the oxalic acid extraction, as shown for stations 5 and 14 (Fig. 4A and 5A), showed several broad bulges (indicated with curved lines) underlying the sharper reflection peaks. Similar broad bulges were obtained in the DXRD patterns after the 0.1 M HCl extraction at station 5 (Fig. 4B). These broad bulges suggest dissolution of poorly crystalline material with oxalic acid and 0.1 M HCl. The positions of the bulges in the DXRD patterns in Fig. 4A, 4B and 5A, suggest dissolution of opal (4.1Å), ferrihydrite
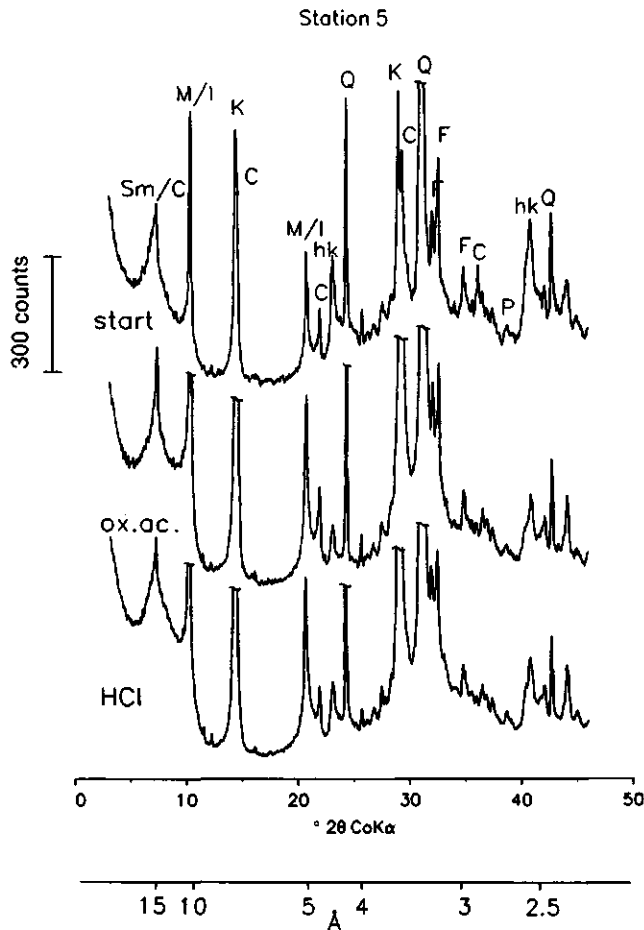
Fig. 2. X-ray powder diffraction (XRD) patterns for the < 10 μm sediment fraction from station 5. Patterns labelled 'start', 'ox.ac.' and 'HCl', were made before extraction, after oxalic acid extraction, and after 0.1 M HCl extraction, respectively. Sm = Smectite, C = Chlorite, M/I = Mica/Illite, K = Kaolinite, Q = Quartz, F = Feldspar, P = Pyrite, hk = non-diagnostic clay mineral reflections.

(2.6Å) and akageneite (2.5 and 3.3Å). Schematic XRD patterns for opal (Van der Gaast, 1991), natural siliceous ferrihydrite (Parfitt et al., 1992) and synthetic akageneite (Schwertmann and Cornell, 1991) are shown in Fig. 4C and 5C for comparison. The 5.3 and 7.4 Å reflections (at 19 and 14°2θ) observed for synthetic akageneite by Schwertmann and Cornell (1991) are weak or absent in our patterns. As the presence, width and intensity of the observed reflections are a direct result of the morphology of the particles, this suggests that the akageneite in our samples may be of different morphology than the synthetic akageneite of Schwertmann and Cornell (1991).
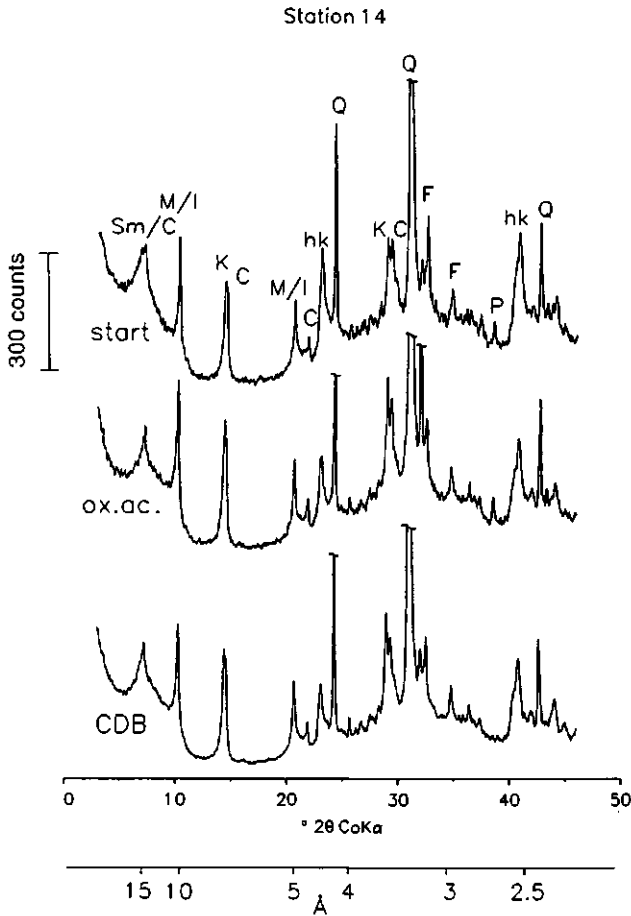
Fig. 3. X-ray powder diffraction (XRD) patterns for the < 10 μm sediment fraction from station 14. Patterns labelled 'start', 'ox.ac' and 'CDB', were made before extraction, after oxalic acid extraction, and after two sequential CDB extractions, respectively. Peak labels as in Fig. 2.

As removal of several wt% of organic matter may also give this type of bulges in DXRD patterns (Van der Gaast, 1991), the effect of oxalic acid and 0.1 M HCl on organic material was addressed. Organic C and N contents on average increased ~ 10% upon extraction with oxalic acid (Table 3). After the 0.1 M HCl extraction for station 5 a similar increase in inorganic N and even a larger increase in organic C (~ 25%) was found. The increase can be explained by weight loss during extraction due to dissolution of Fe oxides (up to ~ 5 wt%) and other compounds. Obviously, extraction of organic material cannot account for the
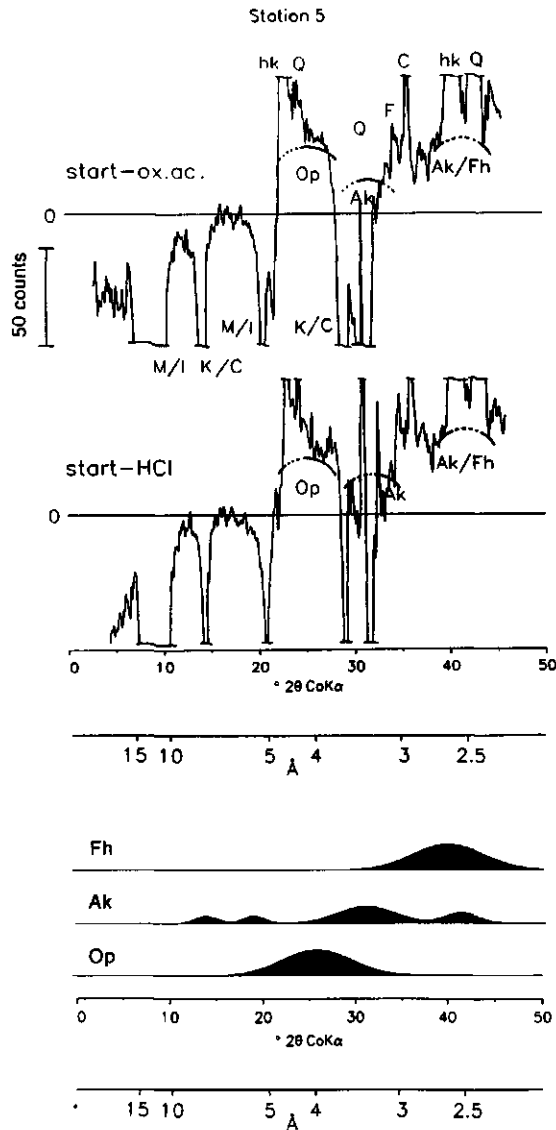
Fig. 4. Differential X-ray powder diffraction (DXRD) patterns for the < 10 μm sediment fraction from station 5. Patterns labelled (A) 'start-ox.ac.' and (B) 'start-HCl', were obtained through subtraction of the 'ox.ac.' diagram from the 'start' diagram and through subtraction of the 'HCl' diagram from the 'start' diagram. Op = Opal, Fh = Ferrihydrite, Ak = Akageneite. Patterns labelled (C) Op, Fh and Ak are schematic XRD patterns for opal (Van der Gaast, 1991), natural siliceous ferrihydrite (Parfitt et al., 1992) and synthetic akageneite (Schwertmann and Cornell, 1991), respectively. All further peak labels as in Fig. 2.
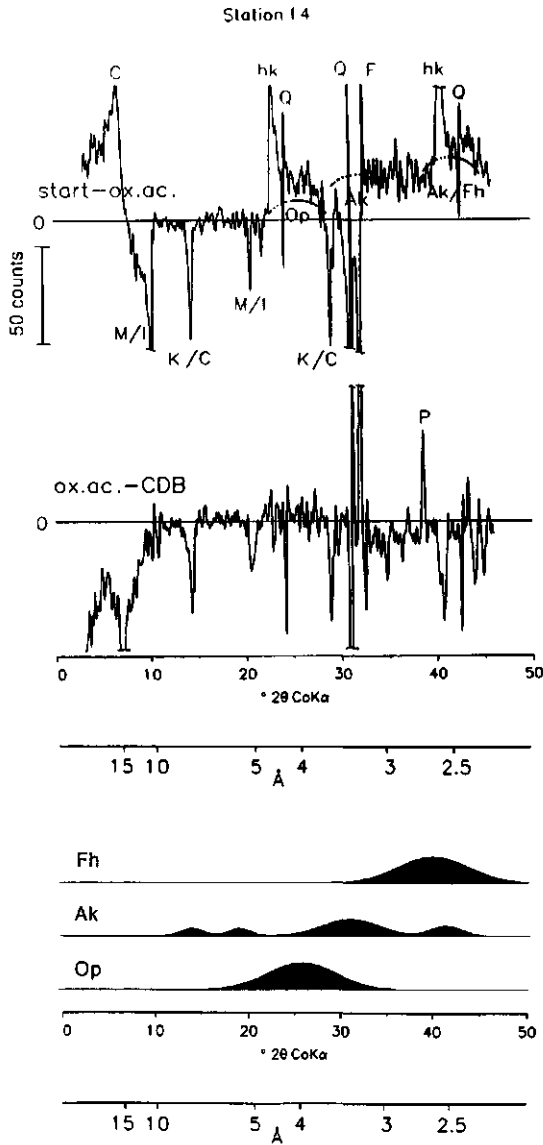
Fig. 5. Differential X-ray powder diffraction (DXRD) patterns for the < 10 μm sediment fraction from station 14. Patterns labelled (A) 'start-ox.ac.' and (B) 'ox.ac-CDB', were obtained through subtraction of the 'ox.ac.' diagram from the 'start' diagram and through subtraction of the 'CDB' diagram from the 'ox.ac.' diagram. Patterns labelled (C) Op, Fh and Ak are schematic XRD patterns for opal (Van der Gaast, 1991), natural siliceous ferrihydrite (Parfitt et al., 1992) and synthetic akageneite (Schwertmann and Cornell, 1991), respectively. All peak labels as in Fig. 2 and 4.

Table 3. Organic C and N contents (in wt %) in the <10 μm fraction before and after oxalic acid and 0.1 M HCl extraction.

	Before extraction		Oxalic acid treated		0.1 M HCl treated	
Station	Org. C (%)	Org. N (%)	Org. C (%)	Org. N (%)	Org. C (%)	Org. N (%)
5	3.17	0.41	3.63	0.59	4.34	0.46
9	4.05	0.47	4.34	0.46	-	-
13	4.74	0.56	5.35	0.63	-	-
14	4.25	0.54	4.70	0.55	-	-

(positive) bulges in Fig. 4A, 4B and 5A. We conclude that, although identification of ferrihydrite and akageneite based on one or two broad peaks remains provisional, it is the most likely explanation for the observed DXRD patterns.

After two extractions with the CDB-solution (only shown for station 14 in Fig. 5B), the intensity of the diagnostic clay mineral reflections (especially chlorite) further increased. All DXRD patterns showed almost complete removal of pyrite, as shown for station 14 in Fig. 5B.

Chemistry of sediment extractions (<10 μm fraction). The sum of the Fe extracted by consecutive oxalic acid and CDB treatments varied between 375 (st. 9) and 482 μmol g^{-1} (st. 5) or 2.1-2.7 wt% Fe (Table 4). Most Fe (60-69% of total extracted Fe) was dissolved in the oxalic acid step. Oxalic acid always extracted more Fe than NH_4-oxalate (a factor 1.8 and 2.0, and 1.3 and 1.4, at stations 5 and 9, and 13 and 14, respectively), whereas NH_4-oxalate extracted only slightly more (1.2 times) Fe than 0.1 M HCl (st.5).

Of the total extractable Al and Si, oxalic acid extracted 52-58% and 9-14%, respectively. The remaining extractable Al and Si was extracted in the two following CDB steps. No large differences between stations could be observed for oxalic acid and CDB-extractable Al. CDB-extractable Si showed a clear gradient, however, decreasing in the station sequence: 13 > 14 > 9 > 5. Generally, the amount of Fe extracted relative to Al and Si decreased with each successive extraction step resulting in a decrease in Fe/Al and Fe/Si ratios.

Oxalic acid dissolved 64-86% of total extractable P. The remaining P was dissolved in the first CDB step. Generally, similar amounts were extracted at all stations, both with oxalic acid and NH_4-oxalate. Only at station 9, less P was extracted than at the other stations (11 versus 19-25 μmol g^{-1}). Fe/P ratios at all stations were very similar (~9-11 for NH_4-oxalate, ~12-14 for oxalic acid with the exception of the value of 20 for st. 9). Fe/P ratios for the first CDB step ranged from 16 to 25. 77-90% of total Mn was extracted in the

Table 4. Fe, Al, Si, and P (in μmol g^{-1}) extracted from the fine sediment fraction (<10 μm) with 0.1 M HCl (st. 5), NH$_4$-oxalate and sequentially with oxalic acid and CDB (all stations).

Solution	Station	Fe μmol/g	Al μmol/g	Si μmol/g	P μmol/g	Mn μmol/g	Fe/Al mol/mol	Fe/Si mol/mol	Si/Al mol/mol	Fe/P mol/mol
0.1M HCl	5	131	167	198	n.d.	1.4	0.8	0.7	1.2	-
NH$_4$-	5	166	27	64	19	1.5	6.1	2.6	2.3	8.9
oxalate	9	114	27	50	12	1.8	4.2	2.3	1.9	9.4
	13	222	50	80	25	5.5	4.5	2.8	1.6	8.7
	14	211	41	55	19	6.0	5.2	3.8	1.4	11.3
Oxalic	5	307	110	52	26	2.5	2.8	5.8	0.5	12
acid	9	224	98	64	11	1.9	2.3	3.5	0.7	20
	13	287	103	75	23	4.6	2.8	3.8	0.7	12
	14	290	97	89	21	5.3	3.0	3.3	0.9	14
CDB-I	5	145	48	235	5.7	0.8	3.0	0.6	4.9	25
	9	125	55	321	6.1	0.5	2.2	0.4	5.8	21
	13	109	58	539	6.3	0.8	1.9	0.2	9.3	17
	14	107	59	426	6.7	0.6	1.8	0.3	7.2	16
CDB-II	5	29	31	81	0	0	0.9	0.4	2.6	-
	9	27	29	85	0	0	0.9	0.3	2.9	-
	13	26	33	201	0	0	0.8	0.1	6.1	-
	14	26	32	164	0	0	0.8	0.2	5.2	-
Sum	5	482	189	369	31	3.3	2.5	1.3	2.0	15
	9	375	183	470	17	2.4	2.1	0.8	2.6	22
	13	422	194	814	29	5.4	2.2	0.5	4.2	14
	14	423	188	680	28	5.9	2.3	0.6	3.6	15

oxalic acid step. Mn contents at stations 5 and 9 are a factor 2 lower than at stations 13 and 14.

Of the non-sequential extraction procedures used, oxalic acid extracted the most Fe at all stations. Much less Fe was extracted in the two following CDB extractions. No clear relationship was observed between extracted Fe and Si, Al and Mn.

Porewater profiles. Porewater profiles of Fe^{2+} and HPO$_4^{2-}$ (Fig. 6), and solid phase Mn and porewater Mn^{2+} profiles (not shown) indicate the presence of an oxidized surface layer at all stations. This is confirmed by simultaneously measured NO$_3^-$ profiles (Lohse et al., 1995), which show that NO$_3^-$ was virtually absent below 2-3 cm depth at all stations. Here, porewater Fe^{2+} (Fig. 6) reaches maximum values of ~ 50 μmol l^{-1} at the sandy stations (5 and 14) and ~ 120 and ~ 100 μmol l^{-1} at the silty stations (9 and 13). At all stations Fe^{2+}
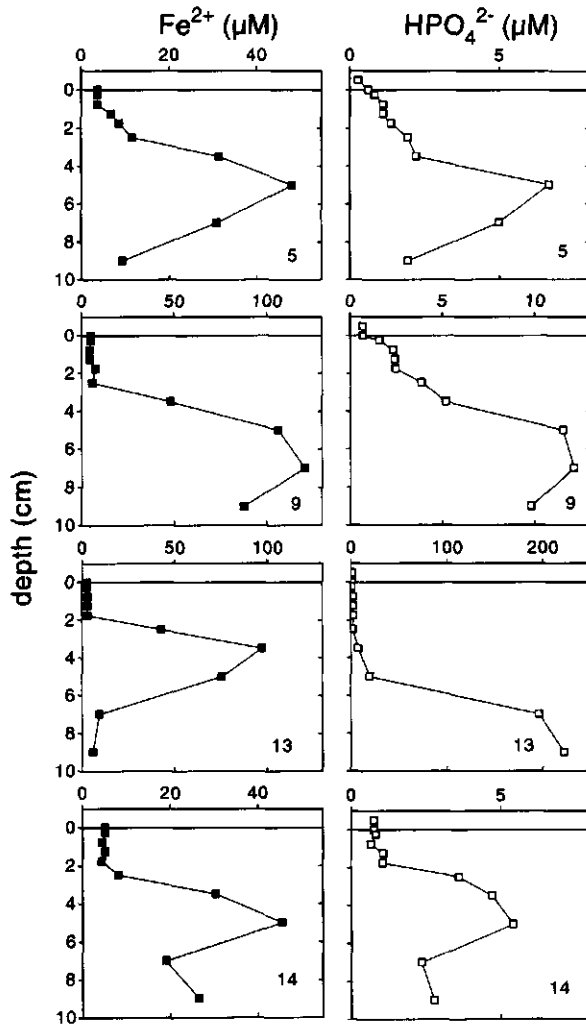
Fig. 6. Porewater profiles of Fe^{2+} and HPO_4^{2-} (μmol l^{-1}) at the four stations.

concentrations drop sharply to relatively constant values between 2.5 and 5 μmol l^{-1} in the oxidized surface layer, implying precipitation of Fe^{2+} in the upper 2-3 cm of the sediment.

Porewater HPO_4^{2-} profiles show a strong resemblance to the Fe^{2+} profiles at stations 5, 9 and 14, with maximum values which are a factor 7-10 lower than those for Fe^{2+}, and relatively constant values in the oxidized surface layer between 0.8 and 2 μmol l^{-1}. At station 13, much higher HPO_4^{2-} concentrations (~200 μmol l^{-1}) and a decoupling of porewater Fe^{2+} and HPO_4^{2-} is observed.

Fe (µmol.g⁻¹)
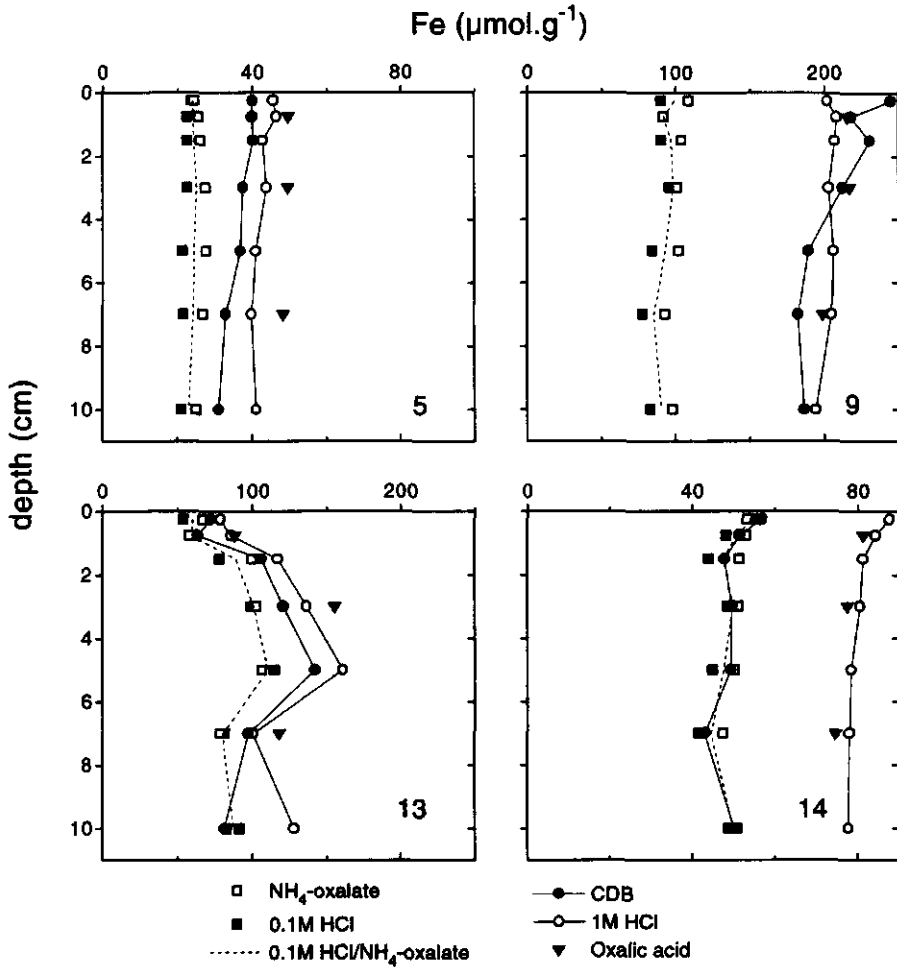
Fig. 7. Solid phase profiles of Fe (µmol g⁻¹) as obtained with five (non-sequential) extraction procedures.

Solid phase profiles. Solid phase profiles of Fe obtained with the various extraction solutions are shown for each location in Fig. 7. NH_4-oxalate extracted ~10% more Fe than 0.1 M HCl, but both extractants give similar profiles. Oxalic acid extracted 1.8-2.4 and 1.5-1.6 times more Fe than NH_4-oxalate at stations 5 and 9, and 13 and 14, respectively. Oxalic acid extracted equal or higher amounts of Fe compared to 1 M HCl but overall, there was a good correlation (Fe-oxalic acid = 1.08 x Fe-1 M HCl -1.12, R^2 = 0.98; n=12). CDB dissolved similar amounts of Fe as NH_4-oxalate and 0.1 M HCl at station 13 (3 depths) and

P (μmol.g^{-1})
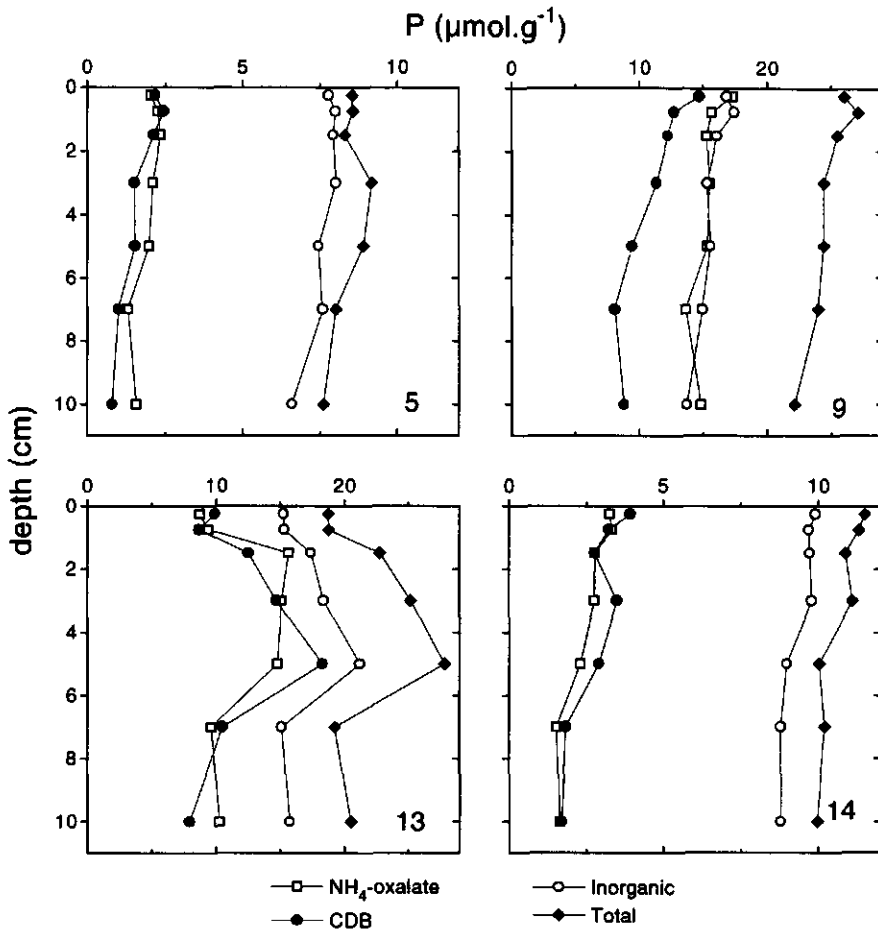
Fig. 8. Solid phase profiles of P (μmol g^{-1}) as obtained with four (non-sequential) extraction procedures.

14, but much higher amounts at stations 5 and 9. The profile shapes obtained with the 5 methods are quite consistent at stations 13 and 14, but are much more variable at stations 5 and 9. Sediment analysis (particle size, porosity, organic C, N, P, microscopic examination (8-50x magnification)) indicated an enrichment in aggregated particles (presumably faecal pellets) comprised of fine material between 1.5 and 7 cm at station 13. This observed enrichment correlates with the high extractable Fe, suggesting a relationship.

Extraction with CDB (which gives a measure of Fe-bound P) and NH$_4$-oxalate resulted in similar profiles for P at stations 5, 13 and 14 (Fig. 8). At station 9, however, much more

P was extracted with NH_4-oxalate than with CDB and the profile of NH_4-oxalate P was almost identical to that of inorganic P. This indicates that NH_4-oxalate dissolved apatite P besides Fe-bound P at this station. Fe-bound P and inorganic P both show a decrease with depth at stations 5, 9 and 14. Only at station 9 the decrease of Fe-bound P is significantly larger than that of inorganic P (and total P), suggesting an increase of another inorganic phase containing P with depth. From the difference between inorganic and CDB P this non-Fe-bound inorganic P phase can be estimated to increase from ~2 μmol g^{-1} in the surface sediment to ~7 μmol g^{-1} in deeper layers. Fe-bound P on average accounts for ~21 and 30%, and ~ 68 and 70% of inorganic P at the sandy (5 and 14) and silty (13 and 9) stations, respectively. Total P profiles relative to those for inorganic P suggest a slight decrease of organic P with depth at stations 9 and 14 and an enrichment of organic P between 1.5 and 7 cm at stations 5 and 13. Organic P on average contributes to 10 and 12%, and 22 and 37% of total P at the sandy (5 and 14) and silty (13 and 9) locations, respectively.

DISCUSSION

Sediment composition (< 10 μm fraction). The similar mineralogical composition of the fine sediment fraction at all four locations suggests a common source for most of the deposited fine material. This is in line with the large contribution (up to 85%) of well-mixed North Atlantic, Channel and seafloor erosion derived material to suspended matter transported through the North Sea (Eisma and Kalf, 1987; Fig. 1). The suggested presence of a poorly crystalline smectite at the German Bight stations (13,14) may be indicative of the contribution of more local sources in this area (Irion et al., 1987).

The much higher pyrite contents (Fig. 2 and 3) in the fine sediment at stations 13 and 14 (German Bight) when compared to stations 5 and 9 (Oystergrounds and Skagerrak, respectively) can be attributed to diagenetic processes, since only the sediments at the former stations become completely anoxic in summer (Lohse et al., 1995). Despite their difference in grain-size, a greater degree of consistency between the Fe extraction results (e.g. NH_4-oxalate and oxalic acid Fe ratios) was observed for stations 13 and 14 than for stations with a more comparable grain size (st. 9 and 5, respectively). This could also be explained by diagenetic processes. A higher clay mineral content of the fine sediment fraction at the latter stations, and perhaps a different clay mineral composition are more likely explanations, however, as will become clear from the calibration of the Fe extractions with DXRD further in the text.
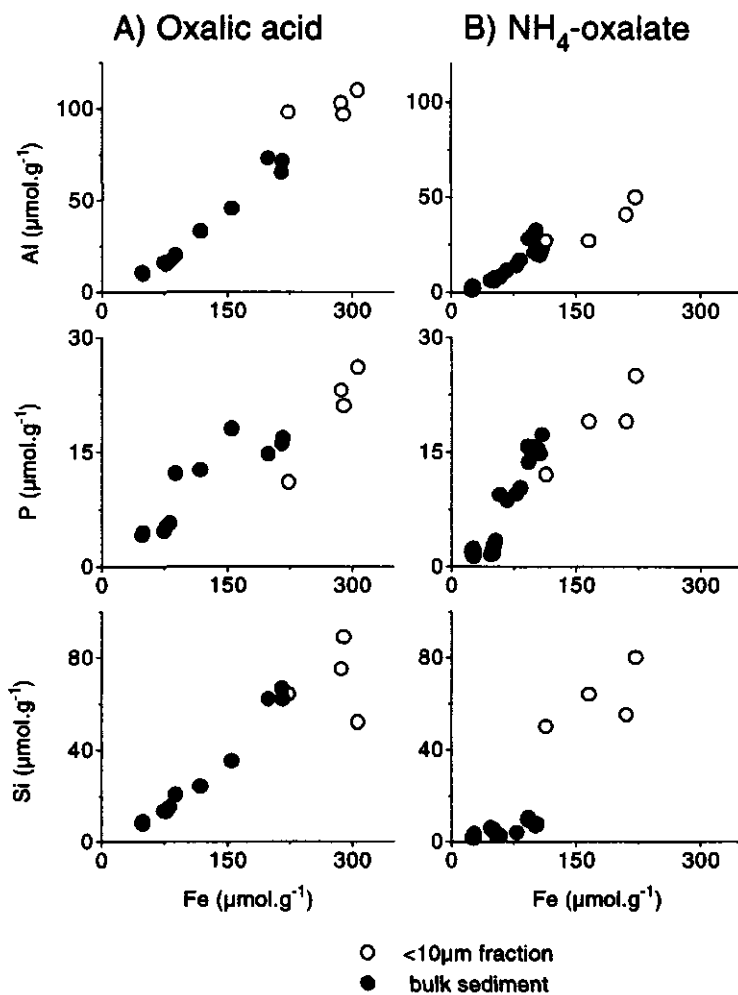
Fig. 9. Relationship between the quantity of Fe, Al, P, and Si extracted from the fine sediment fraction (open circles) and from bulk sediment samples (filled circles) at all four stations using (A) oxalic acid and (B) NH_4-oxalate.

Identification of Fe oxides with DXRD (< 10 μm fraction). The results of the DXRD analysis (Fig. 4 and 5) indicate that both poorly crystalline ferrihydrite and akageneite were dissolved with oxalic acid and 0.1 M HCl during the extraction of the fine sediment fraction. Results from laboratory and field studies suggest that both ferrihydrite and akageneite could form under conditions typical for coastal marine environments. Ferrihydrite is a relatively common Fe oxide in soil and sediment environments where oxidizing and reducing conditions alternate and hence an active Fe turnover exists

(Schwertmann, 1988a; Schwertmann and Cornell, 1991). Inhibitors, such as phosphate, silicate and organics are known to stabilize ferrihydrite and to retard its transformation into more crystalline minerals (Karim, 1984; Cornell, 1985; Cornell et al., 1987; Schwertmann and Cornell, 1991). Akageneite, in contrast, is very rare in soils. The conditions for formation of akageneite in the marine environment are favourable, however, as high Cl^- (or F^-) concentrations are a prerequisite for its formation (Childs et al., 1980; Schwertmann and Cornell, 1991). Murray (1978) found it to be the form of Fe that precipitates from Fe^{3+} in seawater and suggested (1979) that hydrolysis of Fe^{2+} in seawater may also produce akageneite.

No evidence for the presence of goethite, which is the most probable crystalline Fe oxide in temperate regions (Schwertmann, 1988a), was found in the XRD or DXRD patterns. As the detection limit for goethite in our laboratory is ~0.5% wt% ($\approx$ 55 µmol g^{-1}), it can account for some but not all of the Fe dissolved during the two CDB extractions. At stations 13 and 14 pyrite dissolution (~1 wt% FeS_2 = 83 µmol g^{-1}) contributes substantially to extracted Fe, as indicated by the DXRD diagram for station 14 (Fig 5), which showed almost complete removal with CDB. Due to the low pyrite contents at stations 5 and 9, another source should be responsible for most of the extracted Fe there. The dissolution of pyrite by CDB was unexpected (Table 2; Kostka and Luther, 1994), but may be explained by the strong complexing activity of the citrate and, possibly, by instability of the pyrite after exposure to oxidized conditions. Again, this illustrates the pitfalls involved in the use of extraction procedures for natural sediments.

Calibration of the extraction procedures for bulk sediment samples. Oxalic acid dissolved Al, Si, Fe and P in similar proportions both from the fine sediment fraction and from the bulk sediment samples (Fig. 9A). This was also the case for NH_4-oxalate extractable Al, Fe and P (Fig. 9B). Only NH_4-oxalate extractable Si contents relative to Fe (and Al) were grain size dependent. Ratios of NH_4-oxalate and oxalic acid extractable Fe were similar for the fine (1.8 and 2.0, and 1.3 and 1.4, at stations 5 and 9, and 13 and 14, respectively) and bulk sediment (1.8 and 2.4, and 1.5 and 1.6). This implies that the same Fe phases were dissolved from the fine and bulk sediment samples with both extractants. Thus it is possible to use the DXRD and extraction results for the < 10 µm fraction as a calibration of the non-sequential extraction procedures for Fe for bulk sediment samples.

Only a fraction of total sediment Al and Si was extracted with oxalic acid, NH_4-oxalate and CDB. Due to the large differences in affinity of oxalate and citrate for Al, Si and Fe (Furrer and Stumm, 1986; Bennett, 1991; Kodama and Ross, 1991) and the many mineral sources possible (besides Fe oxides also clay minerals, amorphous silica, quartz), the

quantity of Al and Si extracted and the Fe/Al, Fe/Si and Si/Al ratios can not be used for direct identification of Fe sources in the extractions. For example, it is apparent that CDB-I-Fe and CDB-I-Si have a different source (Table 4), given the fact that samples from stations where the highest quantities of Fe were dissolved showed the least release of Si, and vice versa. All calibration is thus solely based on the amount of Fe extracted with each procedure and the DXRD results.

The DXRD diagrams for the < 10 µm fraction from station 5 indicate that ferrihydrite and akageneite were dissolved both with 0.1 M HCl and oxalic acid (Fig. 4 and 5). The amount of Fe extracted with 0.1 M HCl was less than half of that extracted with oxalic acid (Table 4). A good correlation between 0.1 M HCl Fe and NH_4-oxalate Fe was observed (Fig. 7). This suggests that (1) 0.1 M HCl Fe and NH_4-oxalate Fe are both a good measure for the ferrihydrite and akageneite content in these sediments, and that (2) oxalic acid extracts additional Fe from another source. The ratios of NH_4-oxalate/oxalic acid Fe indicate that this source is more important at stations 5 and 9 than at stations 13 and 14.

The CDB extractions can not be calibrated in a similar manner, as the extraction of the < 10 µm fraction was performed as part of a sequential extraction scheme, in contrast to the non-sequential bulk sediment extractions. It is clear, however, that the various sources of Fe in the < 10 µm fraction and in the bulk sediment samples do not contribute to CDB Fe in similar proportions. Pyrite dissolution accounts for an important part of CDB Fe in the < 10 µm fraction at stations 13 and 14. CDB, 0.1 M HCl and NH_4-oxalate Fe were approximately equal in the bulk sediment samples at these stations (Fig. 7). Therefore, pyrite dissolution cannot contribute substantially to the CDB Fe extracted from the bulk sediment samples either at stations 13 and 14 or 5 and 9. This is in line with previous observations that bulk sediment pyrite contents in North Sea sediments are low (Jørgensen, 1989; Canfield et al., 1993). As CDB Fe was substantially higher than 0.1 M HCl and NH_4-oxalate Fe in the bulk sediment extractions for stations 5 and 9 (Fig. 7), this leaves us with an unknown source of CDB Fe at these locations.

As mentioned earlier, goethite may account for some but not all of this CDB Fe. Minor quantities of Fe^{2+} are known to catalyze the reduction and dissolution of crystalline Fe oxides in the presence of oxalate (Sulzberger et al., 1989; Kostka and Luther, 1994). This catalysis reaction does not occur when using 0.1 M HCl as an extractant for poorly crystalline Fe oxides. The good correlation between 0.1 M HCl and NH_4-oxalate Fe at all stations and the much higher quantities of CDB Fe at stations 5 and 9 suggest that this catalysis reaction did not occur during the oxalate extraction. This provides further support for only a minor contribution of crystalline Fe oxides to CDB Fe.

Both oxalic acid and CDB may extract Fe from chlorite interlayers (Harward and Theisen, 1962; Weaver and Pollard, 1972). The higher chlorite content of the sediments at

stations 5 and 9 relative to those of stations 13 and 14 supports the role of chlorite as an important source of the 'extra' Fe. Additional evidence in the case of the oxalic acid extraction is provided by the alteration of the chlorite peaks in the DXRD patterns (Fig. 5A), and the good correlation of oxalic-acid extractable Fe with 1 M HCl extractable-Fe (bulk sediment extractions; Fig. 7), as 1 M HCl should dissolve some fraction of the clay minerals but not the most crystalline Fe oxides (Table 2).

Combining these results with the Fe profiles in Fig. 7, we conclude that at stations 13 and 14, ferrihydrite and akageneite are practically the only Fe oxide phases present. At stations 5 and 9, ferrihydrite and akageneite are also present but account for only $\sim$ 65 and $\sim$ 50% of CDB-Fe in the surface sediment. Remarkably, NH_4-oxalate and 0.1 M HCl extractable Fe show no gradient with depth at stations 5 and 9, whereas CDB-Fe does. Substantial release of Fe from clay minerals upon burial at these locations is unlikely (e.g. Hathaway, 1979). Incomplete extraction of the less crystalline Fe oxides by the NH_4-oxalate and 0.1 M HCl, e.g., due to protection by adsorbed Si, P or organics (Karim, 1984; Borggaard, 1991; Schwertmann, 1991), is a more probable explanation.

Fe oxides and the binding of P in North Sea sediments. A close relationship between P adsorption or the amount of Fe-bound P, and the concentration of total or poorly crystalline Fe oxides has been demonstrated frequently for different types of soils and sediments (e.g. Borggaard, 1983b; Jensen and Thamdrup, 1993). Both experiments with natural and synthetic mineral phases (Borggaard, 1983a and b; Schwertmann, 1988b; Parfitt, 1989; Torrent et al., 1992) have shown that the specific surface area of Fe oxides largely determines their P sorption capacity and intensity and that, due to their larger surface areas, poorly crystalline or 'amorphous' Fe oxides have a larger potential for P sorption than more crystalline Fe phases.

Evidence for the dominant role of poorly crystalline Fe oxides in the binding of P in North Sea sediments was obtained by plotting Fe-bound P and the buffer intensity for HPO_4^{2-} (linear adsorption coefficient K at $[HPO_4^{2-}] = 1$ μmol l^{-1}, including results from four additional stations; Slomp and Van Raaphorst, 1993; Slomp et al., 1997) versus NH_4-oxalate Fe and CDB Fe (Fig. 10A and B, respectively). K and the concentration of Fe-bound P are well correlated with NH_4-oxalate Fe and CDB Fe at all stations where similar amounts of Fe were extracted with both solutions. At station 9 the 'extra' Fe phase (relative to NH_4-oxalate Fe) extracted with CDB apparently had no affinity for P and did not contribute to Fe-bound P. Fe contents at station 5 were too low to enable similar observations. This strongly supports binding of P to poorly crystalline ferrihydrite and akageneite in these sediments, and provides further support for the suggested minor
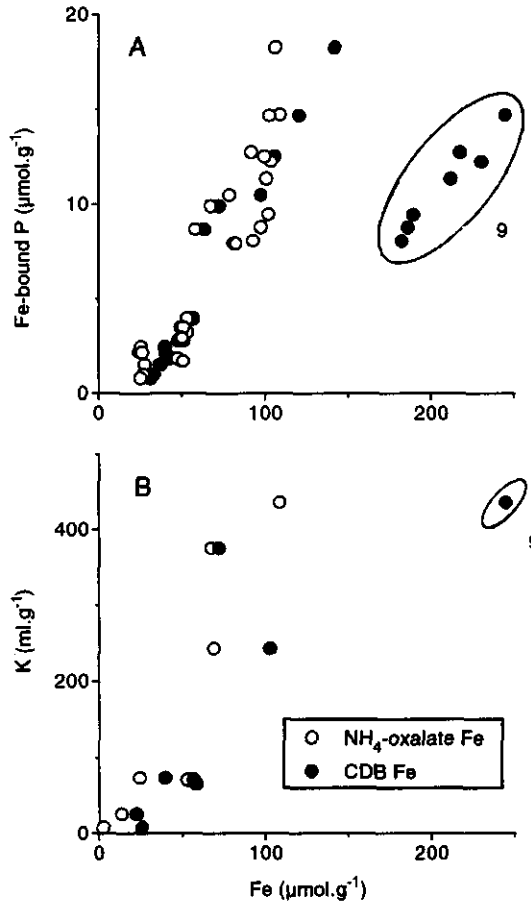
Fig. 10. (A) Relationship between Fe-bound P and NH_4-oxalate (open circles) and CDB (filled circles) extractable Fe at four North Sea stations (Fe-bnd P = 0.15 x NH_4-ox.-Fe - 3.19, R^2 = 0.84, n=28; Fe-bnd P = 0.16 x CDB-Fe - 4.41, R^2 = 0.96, n=21, excluding st. 9); (B) Relationship between the linear adsorption coefficient (K) for HPO_4^{2-} and NH_4-oxalate (open circles) and CDB (filled circles) extractable Fe at 8 North Sea stations (K values from Slomp and Van Raaphorst, 1993; Slomp et al., 1997; K = 4.1 x NH_4-ox.-Fe - 43.6, R^2 = 0.74, K=3.6 x CDB-Fe - 72.5, R^2 = 0.56, excluding st. 9).

contribution of crystalline Fe oxides to the 'extra' CDB Fe at stations 5 and 9, as a contribution to P binding would be expected for crystalline Fe oxides but not necessarily for clay minerals (Krom and Berner, 1980; Parfitt, 1989).

A tight coupling of porewater HPO_4^{2-} and Fe^{2+} was observed at stations 5, 9 and 14. Here, Fe^{2+}/HPO_4^{2-} ratios at maximum porewater concentrations of Fe (~7-14) were in the same range as NH_4-oxalate Fe/Fe-bound P ratios for the fine fraction (~9-11), and for bulk sediment samples (~7-13) from the upper layer, and as Fe/P values known for synthetic poorly crystalline Fe oxides (~10; Borggaard, 1983a; Gerke and Hermann, 1992). This suggests that at these three stations porewater HPO_4^{2-} production at the time of core collection (February 1992) was dominated by release from poorly crystalline Fe oxides. Only at station 13, a decoupling of porewater Fe^{2+} and HPO_4^{2-} was observed. At the maximum in porewater Fe^{2+}, the Fe^{2+}/HPO_4^{2-} ratio (~13) was still in the range suggesting release from Fe oxides, but at depth in the sediment much higher HPO_4^{2-} concentrations (~200 μmol l^{-1}), and much lower Fe^{2+}/HPO_4^{2-} ratios were observed. This suggests a larger production of HPO_4^{2-} due to organic matter mineralization in deeper layers than at the other stations. The NH_4-oxalate Fe/Fe-bound P ratios are comparable to amorphous Fe/Fe-bound P ratios found previously for the Kattegat (~8) and Aarhus Bay (~8-9) (Jensen and Thamdrup, 1993) and to total Fe-oxide Fe/Fe-bound P (~10) in Laurentian Trough sediments (Sundby et al., 1992). Jensen and Thamdrup (1993) found higher amorphous Fe/Fe-bound P ratios (~17) in Skagerrak sediment and concluded that here the Fe oxides might be less capable of adsorbing P or were less saturated with P. They determined amorphous Fe as the difference between total Fe extracted with 0.5 M HCl and Fe(II) extracted with oxalate buffer under anoxic conditions. As 0.5 M HCl probably extracts more Fe from clay minerals than NH_4-oxalate (Table 2), and as we found the same high Fe/P ratio of 17 in Skagerrak surface sediment when using CDB or oxalic acid Fe as a measure for Fe in Fe oxides, it is probable that they attributed Fe from clay minerals to amorphous Fe. We conclude that ratios of poorly crystalline Fe oxides and Fe-bound P are very similar (~10) in many marine sediments.

HPO_4^{2-} released to the porewater can (1) (re)adsorb to Fe oxides in the upper part of the sediment; (2) escape to the overlying water or (3) precipitate as an authigenic phase in the sediment. The decrease with depth of both Fe-bound and inorganic P at the stations where no net sedimentation of material occurs (st. 5 and 14; Fig. 8) suggests that here most of the P released upon reduction of Fe oxides (Fig. 6) is readsorbed in the upper part of the sediment or released to the overlying water. Only in the depositional area of the Skagerrak (st. 9) a substantial increase of another inorganic phase containing P with depth can be inferred from Fig. 8. Although non-steady state changes in composition of the deposited material cannot be ruled out, this may be indicative of an early diagenetic 'sink switching' from Fe oxides to another inorganic phase (e.g. CFA), as has recently been suggested for Laurentian Trough sediments (Lucotte et al., 1994).

Poorly crystalline Fe oxides and Fe-bound P clearly persisted into the reduced zone (down to 10-12 cm), thus making these Fe oxides at least a temporary sink for P in North Sea sediments. Persistence of Fe-bound P with depth (down to 160 cm) at a deeper Skagerrak station (Jensen and Thamdrup, 1993) suggests that poorly crystalline Fe oxides may also form a permanent sink for P, as has been observed for other continental margin sediments (e.g. Ruttenberg and Berner, 1992; Berner et al., 1993). This implies that these Fe oxide forms are protected against reduction, presumably due to coatings with reduced iron compounds (Postma, 1993) and due to the presence of surface bound P, Si and organics (Borggaard, 1991; Biber et al., 1994).

The absence or only minor role of crystalline Fe oxides, such as goethite, in North Sea surface sediments, despite their higher resistance against reduction compared to poorly crystalline phases, can be attributed to three factors. First, there is a relatively low input of terrestrial material adding crystalline Fe oxides in this shelf sea due to trapping of material in estuaries (Eisma et al., 1982; Eisma and Kalf, 1987). Second, long residence times of material on the shelf due to frequent deposition and resuspension prior to burial in the main deposition areas (Eisma and Kalf, 1987), combined with a frequent cycling of Fe between oxidized and reduced Fe forms (Canfield et al., 1993), promote formation of poorly crystalline Fe oxides. Third, inhibition of formation of crystalline Fe oxides in continental margin sediments is expected due to the abundant presence of P, Si and organics (Cornell, 1985; Cornell et al., 1987).

CONCLUSIONS

In this study, a combination of extraction procedures and X-ray powder diffraction has been used to identify the Fe oxides responsible for the binding of P in four sediments from contrasting environments on a continental margin. Poorly crystalline akageneite and ferrihydrite (extractable with 0.2 M NH_4-oxalate or 0.1 M HCl) were found to be the most important Fe oxides at all locations. A good relationship of both the concentration of Fe-bound P and the linear adsorption coefficient for HPO_4^{2-} with NH_4-oxalate Fe provides evidence for the dominant role of this poorly crystalline ferrihydrite and akageneite in the binding of P in these sediments. The ratios of NH_4-oxalate Fe/Fe-bound P were comparable to values found for synthetic poorly crystalline Fe oxides, and for amorphous Fe or total Fe-oxide/Fe-bound P ratios in other marine sediments. This suggests that ratios of poorly crystalline Fe oxides and Fe-bound P may be very similar ($\sim$10) in many marine sediments.

Porewater HPO_4^{2-} can be produced both due to organic matter decomposition and due to release from Fe oxides. The tight coupling of porewater Fe^{2+} and HPO_4^{2-} and the observed Fe^{2+}/HPO_4^{2-} ratios at maximum porewater Fe^{2+} concentrations at three locations suggest that here, porewater HPO_4^{2-} production at the time of core collection was dominated by

release from poorly crystalline Fe oxides. Only at the German Bight station, the much higher HPO_4^{2-} levels and decoupling of porewater Fe^{2+} and HPO_4^{2-} suggest a larger direct contribution from mineralization of organic matter to porewater HPO_4^{2-} than at the other sites.

The solid phase P profiles at the stations with no net sedimentation suggest that here HPO_4^{2-} released to the porewater is either readsorbed to Fe oxides in the upper part of the sediment or released to the overlying water. In the Skagerrak, however, the decrease with depth of Fe-bound P and the suggested increase of another inorganic phase containing P, may indicate an early diagenetic 'sink switching' of P.

The persistence of poorly crystalline Fe oxides and Fe-bound P with depth, as observed in this study, is in line with the large range in susceptibility to reduction known for Fe oxides in sediments. This enables these Fe phases to act as both a temporary and permanent sink for P in continental margin sediments.

REFERENCES

Anton K.K., Liebezeit G., Rudolph C. and Wirth H., 1993. Origin, distribution and accumulation of organic carbon in the Skagerrak. Mar. Geol. 111: 287-297.

Aspila K.I., Agemian H. and Chau A.S.Y., 1976. A semi-automated method for the determination of inorganic, organic and total phosphate in sediments. Analyst 101: 187-197.

Bennett P.C., 1991. Quartz dissolution in organic-rich aqueous systems. Geochim. Cosmochim. Acta 55: 1781-1797.

Berner R.A., Ruttenberg K.C., Ingall E.D., and Rao J.-L., 1993. The nature of phosphorus burial in modern marine sediments. p365-378. In: R. Wollast et al., eds. Interactions of C, N, P, and S. Biogeochemical Cycles and Global Change, NATO ASI Series Vol. 14. Springer.

Biber M.V., Dos Santos Afonso M., and W. Stumm, 1994. The coordination chemistry of weathering: IV. Inhibition of the dissolution of oxide minerals. Geochim. Cosmochim. Acta 58: 1999-2010.

Borggaard O.K., 1983a. Effect of surface area and mineralogy of iron oxides on their surface charge and anion-adsorption properties. Clays Clay Miner. 31: 230-232.

Borggaard O.K., 1983b. The influence of iron oxides on phosphate adsorption by soil. J. Soil Sci. 34: 333-341.

Borggaard O.K., 1991. Effects of phosphate on iron oxide dissolution in ethylenediamine-N,N,N',N'-Tetraacetic acid and oxalate. Clays Clay Miner. 39: 324-328.

Burns R.G. and Burns V.M., 1980. Manganese oxides. p1-46. In: R.G. Burns, ed. Marine Minerals. Reviews in Mineralogy Vol. 6. Mineralogical Society of America.

Canfield D.E.,1988. Sulfate reduction and the diagenesis of iron in anoxic sediments. Ph.D. thesis, Yale Univ.

Canfield D.E., 1989. Reactive iron in marine sediments. Geochim. Cosmochim. Acta. 53: 619-632.

Canfield D.E., Thamdrup B., and Hansen J.W., 1993. The anaerobic degradation of organic matter in Danish coastal sediments: iron reduction, manganese reduction, and sulfate reduction. Geochim. Cosmochim. Acta 57: 3867-3883.

Chao T.T. and Zhuo L., 1983. Extraction techniques for selective dissolution of amorphous iron oxides from soils and sediments. Soil Sci. Soc. Am. J. 47: 225-232.

Childs C.W., Goodman, B.A., Paterson E. and Woodhams F.W.D., 1980. The nature of iron in akageneite (β-FeOOH). Aust. J. Chem. 33: 15-26.

Cornell R.M., 1985. Effect of simple sugars on the alkaline transformation of ferrihydrite into goethite and hematite. Clays Clay Miner. 33: 219-227.

Cornell R.M., Giovanoli R. and Schindler P.W., 1987. Effect of silicate species on the transformation of ferrihydrite into goethite and hematite in alkaline media. Clays Clay Miner. 35: 21-28.

Cornwell J.C. and Morse J.W., 1987. The characterization of iron sulfide minerals in anoxic marine sediments. Mar. Chem. 22: 193-206.

Duinker J.C., Van Eck G.T.M. and Nolting R.F., 1974. On the behaviour of copper, zinc, iron and manganese, and evidence for mobilization processes in the Dutch Wadden Sea. Neth. J. Sea Res. 8: 214-239.

Eisma D., Cadee G.C. and Laane R., 1982. Supply of suspended matter and particulate and dissolved organic carbon from the Rhine to the coastal North Sea. Mitt. Geol.-Paläont. Inst. Univ. Hamburg. 52: 483-505.

Eisma D. and Kalf J., 1987. Dispersal, concentration and deposition of suspended matter in the North Sea. J. Geol. Soc. London. 144: 161-178.

Furrer G. and Stumm W., 1986. The coordination chemistry of weathering: I. Dissolution kinetics of δ-Al$_2$O$_3$ and BeO. Geochim. Cosmochim. Acta 50: 1847-1860.

Gerke J. and Hermann R., 1992. Adsorption of orthophosphate to humic-Fe-complexes and to amorphous Fe-oxide. Z. Pflanzenernähr. Bodenk. 155: 233-236.

Harward M.E. and Theisen A.A., 1962. Problems in clay mineral identification by X-ray diffraction. Soil Sci. Soc. Proc. 26: 335-341.

Hathaway J.C., 1979. Clay minerals. p123-150. In: R.G. Burns, ed. Marine Minerals. Reviews in Mineralogy Vol. 6. Mineralogical Society of America.

Irion G., Wunderlich F. and Schwedhelm E., 1987. Transport of clay minerals and anthropogenic compounds into the German Bight and the provenance of fine-grained sediments SE of Helgoland. J. Geol. Soc. London. 144: 153-160.

Jensen H.S. and Thamdrup B., 1993. Iron-bound phosphorus in marine sediments as measured by bicarbonate-dithionite extraction. Hydrobiologia 253: 47-59.

Jørgensen B.B., 1989. Sulfate reduction in marine sediments from the Baltic Sea-North Sea transition. Ophelia 31: 1-15.

Karim Z., 1984. Characteristics of ferrihydrites formed by oxidation of FeCl$_2$ solutions containing different amounts of silica. Clays Clay Miner. 32: 181-184.

Kauffman K. and Hazel F., 1975. Infrared and Mössbauer spectroscopy, electron microscopy and chemical reactivity of ferric chloride hydrolysis products. J. Inorg. Nucl. Chem. 37: 1139-1148.

Kodama H. and Ross G.J., 1991. Tiron dissolution method used to remove and characterize inorganic components in soils. Soil. Soc. Am. J. 55: 1180-1187.

Kostka J.E. and Luther III G.W., 1994. Partitioning and speciation of solid phase iron in saltmarsh sediments. Geochim. Cosmochim. Acta 58: 1701-1710.

Krom M.D. and Berner R.A., 1980. Adsorption of phosphate in anoxic marine sediments. Limnol. Oceanogr. 25: 797-806.

Lohse L., Malschaert J.F.P., Slomp C.P., Helder W., and Van Raaphorst W., 1995. Sediment-water fluxes of inorganic nitrogen compounds along the transport route of organic matter in the North Sea. Ophelia 41: 173-197.

Lord C.J., 1982. A selective and precise method for pyrite determination in sedimentary materials. J. Sediment. Petrol. 52: 664-666.

Lucotte M. and d'Anglejan B., 1985. A comparison of several methods for the determination of iron hydroxides and associated orthophosphates in estuarine particulate matter. Chem. Geol. 48: 257-264.

Lucotte M., Mucci A., and Hillairemarcel A., 1994. Early diagenetic processes in deep Labrador Sea sediments - reactive and nonreactive iron and phosphorus. Can. J. Earth Sci. 31: 14-27.

McKeague J.A. and Day J.H., 1966. Dithionite- and oxalate-extractable Fe and Al as aids in differentiating various classes of soils. Can. J. Soil Sci. 46: 13-22.

Mehra O.P. and Jackson M.L., 1960. Iron oxide removal from soils and clays by a dithionite-citrate system buffered with sodium bicarbonate. Clays Clay Miner. 7: 317-327.

Moore D.M. and Reynolds R.C., 1989. X-ray diffraction and the identification and analysis of clay minerals. Oxford University Press.

Murray J.W., 1978. β-FeOOH in marine sediments. Eos 59: 411-412. (abstr.).

Murray J.W., 1979. Iron oxides. p47-98. In: R.B. Burns, ed. Marine Minerals. Reviews in Mineralogy Vol. 6. Mineralogical Society of America.

Parfitt R.L., 1989. Phosphate reactions with natural allophane, ferrihydrite and goethite. J. Soil Sci. 40: 359-369.

Parfitt R.L., Van der Gaast S.J., and Childs C.W., 1992. A structural model for natural siliceous ferrihydrite. Clays Clay Miner. 40: 675-681.

Pettijohn, F.J., Potter P.E. and R. Siever, 1972. Sand and sandstone. Springer, New York. 618p.

Postma D., 1993. The reactivity of iron oxides in sediments: a kinetic approach. Geochim. Cosmochim. Acta 57: 5027-5034.

Ruttenberg K.C., 1992. Development of a sequential extraction method for different forms of phosphorus in marine sediments. Limnol. Oceanogr. 37: 1460-1482.

Ruttenberg K.C., 1993. Reassessment of the oceanic residence time of phosphorus. Chem. Geol. 107: 405-409.

Ruttenberg K.C. and Berner R.A., 1993. Authigenic apatite formation and burial in sediments from non-upwelling, continental margin environments. Geochim. Cosmochim. Acta 57: 991-1007.

Saager P.M., Sweerts J.P. and Ellermeijer H.J., 1990. A simple pore-water sampler for coarse sandy sediments of low porosity. Limnol. Oceanogr. 35: 747-751.

Schulze D.G., 1981. Identification of soil iron minerals by differential X-ray diffraction. Soil Sci. Soc. Am. J. 45: 437-440.

Schwertmann U., 1988a. Occurrence and formation of iron oxides in various pedoenvironments. p267-308. In: J.W. Stucki et al., eds. Iron in soils and clay minerals, Reidel.

Schwertmann U., 1988b. Some properties of soil and synthetic oxides. p203-250. In: J.W. Stucki et al., eds. Iron in soils and clay minerals, Reidel.

Schwertmann U., 1991. Solubility and dissolution of iron oxides. Plant Soil 130: 1-25.

Schwertmann U. and Cornell R.M., 1991. Iron oxides in the laboratory. VCH.

Schwertmann U., Schulze D.G. and Murad E., 1982. Identification of ferrihydrite in soils by dissolution kinetics, differential X-ray diffraction and Mössbauer Spectroscopy. Soil Sci. Soc. Am. J. 46: 869-875.

Slomp C.P. and Van Raaphorst W., 1993. Phosphate adsorption in oxidized marine sediments. Chem. Geol. 107: 477-480.

Slomp, C.P., Malschaert, J.F.P. and Van Raaphorst, W., 1997. The role of sorption in sediment-water exchange of phosphate in North Sea continental margin sediments. Limnol. Oceanogr., submitted.

Strickland J.D. and Parsons T.R., 1972. A practical handbook of seawater analysis. 2nd. ed. Bull. Fish. Res. Bd. Can. 167: 1-311.

Sulzberger B., Suter D., Siffert C., Banwart S. and Stumm W., 1989. Dissolution of Fe(III)(hydr)oxides in natural waters; Laboratory assessment on the kinetics controlled by surface coordination. Mar. Chem. 28: 127-144.

Sundby B., Gobeil C., Silverberg N. and Mucci A., 1992. The phosphorus cycle in coastal marine sediments. Limnol. Oceanogr. 37: 1129-1145.

Torrent J., Schwertmann U., and Barrón V., 1992. Fast and slow phosphate sorption by goethite-rich natural materials. Clays Clay Miner. 40: 14-21.

Van der Gaast S.J., 1991. Mineralogical analysis of marine particles by X-ray powder diffraction. Geophys. Monogr. 63: 343-362.

Van Raaphorst W. and Kloosterhuis H.T., 1994. Phosphorus sorption in superficial intertidal sediments. Mar. Chem. 48: 1-16.

Van Weering T.C.E., Berger G.W. and Kalf J., 1987. Recent sediment accumulation in the Skagerrak, northeastern North Sea. Neth. J. Sea Res. 21: 177-189.

Verardo D.J., Froelich P.N. and McIntyre A., 1990. Determination of organic carbon and nitrogen in sediments using the Carlo Erba Na-1500 analyzer. Deep-Sea Res. 37: 157-165.

Von Haugwitz W., Wong H.K. and Salge U., 1988. The mud area southeast of Helgoland: A seismic study. Mitt. Geol.-Paläont. Inst. Univ. Hamburg. 65: 409-422.

Wang H.D., White G.N., Turner F.T. and Dixon J.B., 1993. Ferrihydrite, lepidocrocite, and goethite in coatings from East Texas vertic soils. Soil Sci. Soc. Am. J. 57: 1381-1386.

Weaver C.E. and Pollard L.D., 1972. The chemistry of clay minerals. Elsevier.

Chapter 4

Iron and manganese cycling in different sedimentary environments on the North Sea continental margin[*]

ABSTRACT

Pore water O_2, NO_3^-, Fe^{2+} and Mn^{2+} and solid phase Fe and Mn profiles were measured in sediments located in 4 different types of sedimentary environments in the southern and eastern North Sea in August 1991 and February 1992. A steady-state diagenetic model describing solid phase and pore water metal profiles was developed and applied to Mn and Fe data for 11 and 3 stations, respectively. The quality and quantity of the organic matter deposited in each sedimentary environment are shown to determine whether sediments become sufficiently depleted of O_2 and NO_3^- to allow for (1) Fe and Mn reduction and (2) escape of dissolved Fe^{2+} and Mn^{2+} to the overlying water, thus determining whether these metal cycles extend into the water column. Reversible sorption in combination with sediment mixing is shown to enhance diffusive transport of dissolved metals. Precipitation of Fe^{2+} and Mn^{2+} in the form of reduced authigenic minerals is suggested to be responsible for the reversal in gradient of pore water Fe^{2+} and Mn^{2+} at depth at many stations. Most North Sea sediments are relatively poor in Fe and Mn oxides. High surface concentrations of Fe and Mn oxides (up to 245 and 13 $\mu mol\ g^{-1}$, respectively) were only found in the areas receiving significant amounts of terrigenous material, i.e. the German Bight and Skagerrak. Comparison of model calculated rates of Mn and Fe reduction to O_2 uptake rates indicates that Fe and Mn oxides do not play an important role as redox intermediates in organic C oxidation (accounting for <4%) in most North Sea sediments. Only in the depositional environment of the Skagerrak, model results suggest that metal oxide reduction may contribute substantially to organic C oxidation (~20%).

INTRODUCTION

A substantial proportion (up to 50%) of pelagic primary production may reach the sea floor in continental margin environments (Jørgensen, 1983). Most of this deposited organic matter is mineralized close to the sediment-water interface, with O_2, NO_3^-, Mn and Fe oxides or SO_4^{2-} acting as electron acceptors (Froelich et al., 1979). Oxic respiration and SO_4^{2-} reduction have been assumed each to account for roughly half of the total organic matter decomposition in most continental margin sediments, leaving only a minor role for NO_3^- and metal oxide reduction (Jørgensen, 1982). More recent work has shown, however, that when surface sediments are strongly enriched in Mn or Fe oxides and are characterized by high physical or biological mixing rates, Fe and Mn reduction coupled to organic matter

---

water column
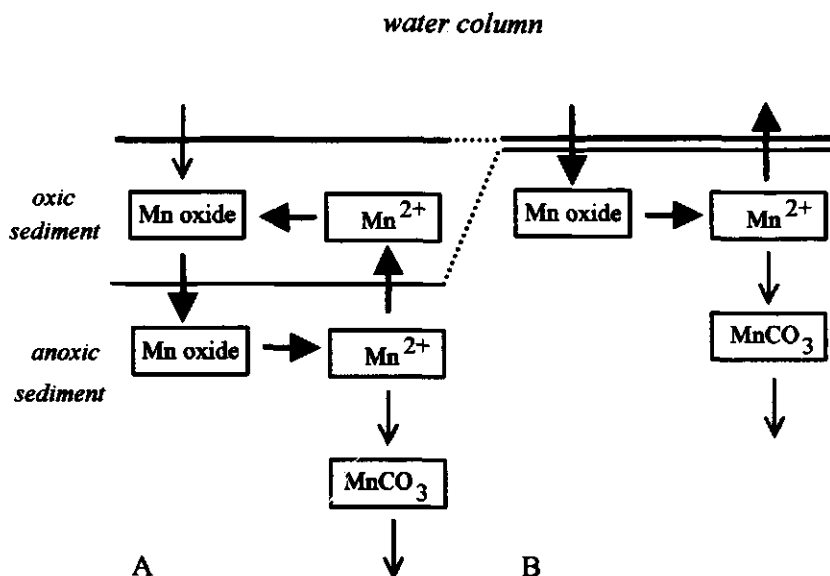
Fig. 1. Schematic representations of the sedimentary Mn cycle in sediments to illustrate the difference between (A) internal and (B) external cycling of metals. When the Mn cycle is largely internal, all of the dissolved Mn^{2+} produced due to Mn oxide reduction is reoxidized in the surface sediment and practically no Mn^{2+} escapes to the overlying water. When the cycle is completely external, Mn^{2+} oxidation takes place outside the sediment and Mn oxide reduction in the sediment is dependent on the flux of Mn oxide from the overlying water. Precipitation of Mn^{2+} as reduced authigenic minerals may take place in both cases (e.g. Aller, 1994). For simplicity we denote these phases as $MnCO_3$ or Mn carbonate, although in reality calcite or a mixed Mn-Ca carbonate phase may also control Mn solubility (Middelburg et al., 1987; Shimmield and Pedersen, 1990). The Fe cycle is very similar except that (1) the redox boundary for Fe lies at a greater depth than that for Mn (2) FeS and FeS_2 are formed instead of a carbonate phase and (3) these Fe sulfides are known to be largely reoxidized to Fe oxides upon upward mixing in most sediments (e.g. Jørgensen, 1982 and 1989).

oxidation can become important (Aller, 1986, 1990 and 1994; Burdige, 1993; Canfield et al., 1993a and b). This coupling is either direct, with the Fe and Mn oxides acting as electron acceptors in the decomposition of organic material (Aller, 1990), or indirect, with Fe and Mn oxides acting as an intermediate between, for example, sulfide produced during SO_4^{2-} reduction and O_2 (Canfield et al., 1993a and b; Aller, 1994). In both cases, a large proportion of the sediment O_2 uptake may be used for the reoxidation of the reduced metals and oxic decomposition of organic matter may be relatively unimportant.

Strong surface enrichments in Fe and Mn oxides occur in areas where the flux of metal oxides from the overlying water is large and/or as a result of long-term internal cycling of

Fe and Mn (Fig. 1). A large flux of metal oxides can be supported by a high input from nearby riverine sources (e.g. on the Amazon shelf; Aller et al., 1986), by redeposition of metal oxide-rich material eroded from other areas (e.g. in coastal environments; Aller, 1994; Thamdrup et al., 1994b), or by deposition of metal oxides formed in the water column. The importance of internal cycling of Fe and Mn depends on the redox conditions in the sediment and the overlying water and, thus, is usually closely linked to the quality and quantity of the organic matter deposited on the sediment and the rate at which it is decomposed (Hunt, 1983; Aller, 1994).

In the present study, we examine the Mn and Fe cycle at 15 stations in 4 different types of sedimentary environments on the North Sea continental margin. These environments differ with respect to the input of both organic and terrigenous material. The aims of our study are (1) to determine and explain differences in the cycling of Fe and Mn and (2) to investigate whether Fe and Mn reduction can play an important role, direct or indirect, in the decomposition of organic matter in these environments. To reach these aims, pore water O_2, NO_3^-, Fe^{2+} and Mn^{2+} and solid phase Fe and Mn profiles were measured in August 1991 and February 1992, and a simple reaction-diffusion model for Fe and Mn diagenesis was developed and applied to the data.

STUDY SITES

The North Sea is a semi-enclosed shelf sea with water depths gradually increasing from less than 30 m in the south to about 200 m in the area between the Shetlands and the Norwegian coast. To the northeast, in the Skagerrak/Norwegian Channel, the seafloor slopes down to a depth of 700 m. The water circulation and transport of suspended matter are predominantly counterclockwise (Fig. 2). Most of the suspended matter is concentrated along the coast. An estimated 30-50% of total North Sea suspended matter is deposited in the inner German Bight (sedimentation rate: 0.5-1 cm yr^{-1}; Eisma and Kalf, 1987; Von Haugwitz et al., 1988), on tidal flats and in rivermouths. The Skagerrak/Norwegian Channel acts as a sink for the remaining 50-70% (sedimentation rate: 0.1-0.5 cm yr^{-1}; Van Weering et al., 1987; Anton et al., 1993).

A total of 15 stations in the southern and eastern North Sea, including the Skagerrak were sampled during 2 cruises on the RV Pelagia in August 1991 and February 1992 (Fig. 2). Geographical positions and water depths of these stations are listed in Table 1. Station 3 was only visited during the August cruise. Seasonal changes in bottom water temperature are related to the depth of the stations (Table 1). The largest seasonal variation occurred at the shallow station in the German Bight (st. 13), whereas temperature changes are negligible at the deepest station in the Skagerrak (st. 9). Bottom water O_2 concentrations were close to saturation values at most stations in both seasons.
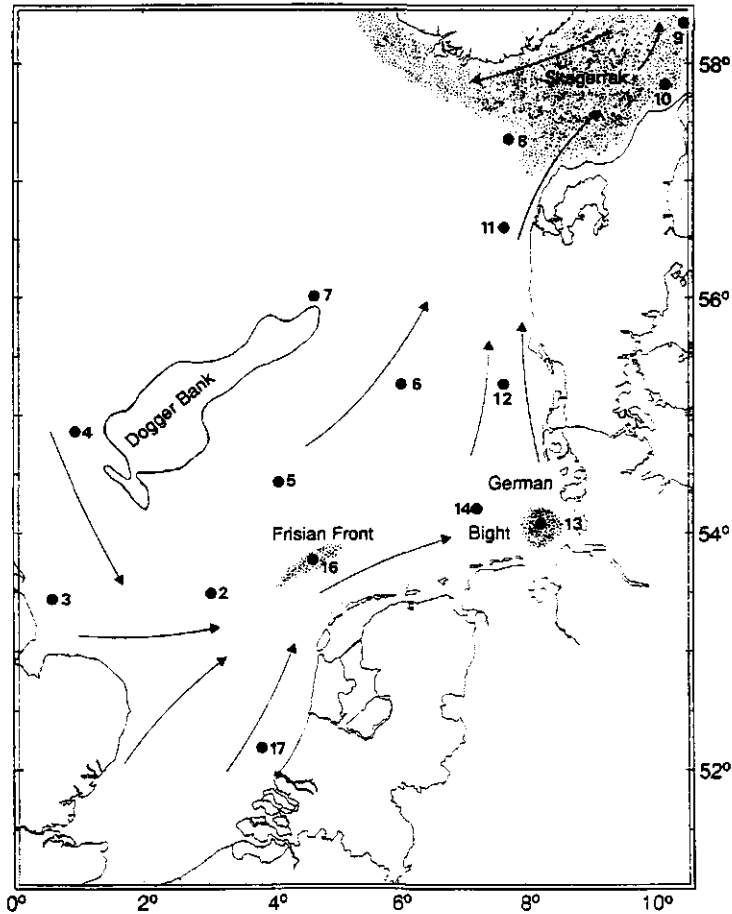
Fig. 2. Map of the North Sea showing the sampling locations and station numbers. Main transport routes of water and suspended matter are indicated by arrows. Stippled areas indicate main depositional regions.

Based on sediment grain size distributions, Lohse et al. (1995) grouped these stations into 3 clusters (Table 2). Cluster I consists of stations with silty sediments which are found in the depositional areas of the inner German Bight and the Skagerrak (st. 9, 10, 13). Cluster II consists of stations with fine sandy sediment characterized by frequent temporary deposition of organic material (st. 2, 5, 6, 7, 8, 12, 14, 16) during periods of minor wind or slack tide (see Jago et al., 1993). Cluster III, finally, includes stations with medium sands where erosion is dominant and where organic matter deposition is limited (st. 3, 4, 11, 17).

Lohse et al. (1995) further differentiated the German Bight station 13 and the Skagerrak stations 9 and 10 as clusters IA and IB, respectively, because the nature of the organic

matter deposited in these areas is quite different. In the shallow area of the German Bight large amounts of locally produced fresh organic matter (Joint and Pomroy, 1993) are deposited in summer. In the Skagerrak, local primary production is of less importance, and organic matter inputs are dominated by the inflow of relatively refractory organic matter from other areas, such as the Scandinavian mainland, the Baltic and, in particular, the North Sea shelf (Van Weering et al., 1987; Anton et al., 1993). Sediment-water exchange rates of NO_3^- and NH_4^+ (Lohse et al., 1995), $Si(OH)_4$ (Gehlen et al., 1995) and HPO_4^{2-} (Slomp et al., 1997), measured at these stations exhibit a distinct spatial pattern: (1) high effluxes of nutrients and an extremely large seasonal variation in these fluxes were observed in the German Bight (cluster IA), (2) low nutrient fluxes and minor seasonal variations were encountered in the Skagerrak (cluster IB) and (3) intermediate exchange rates of nutrients and a distinct seasonal variation in these fluxes were found in the areas dependent on temporary organic matter deposition (clusters II and III), with the lowest fluxes at the cluster III stations. Macrofaunal abundance is highest at the German Bight stations (cluster IA: ~4000 m^{-2}). Lower numbers are found in the Skagerrak (cluster IB: ~ 800 m^{-2}), and at the cluster II (~1500 m^{-2}) and cluster III (~400 m^{-2}) stations (average values for August 1991 and February 1992; H.W. van der Veer, pers. comm.). Both the nutrient fluxes and the macrofaunal abundance results support the suggested classification; we will use this classification as an aid in presenting our results.

EXPERIMENTAL METHODS

Sampling. Sediment cores were obtained with a cylindrical box corer (31 cm i.d.) which enclosed 30 to 50 cm of sediment column together with 15 to 25 l of overlying bottom water. Subsamples were taken from the box core with acrylic liners and were closed with rubber stoppers. Only cores without any visible surface disturbance were used. All subsequent sediment handling took place at in situ temperature.

Pore water profiles of O_2, NO_3^-, Fe^{2+} and Mn^{2+}. Immediately after obtaining the cores, pore water O_2 profiles were determined using Clark-type oxygen-microelectrodes as described previously (Lohse et al., 1993 and 1996). To obtain porewater for NO_3^-, Fe^{2+} and Mn^{2+} measurements, sediment from 10-15 subcores (i.d. 3.1 cm) was sliced under N_2 atmosphere immediately after collection. Slices from 9 depth intervals (0-0.4, 0.4-1.0, 1.0-1.5, 1.5-2.0, 2.0-3.0, 3.0-4.0, 4.0-6.0, 6.0-8.0, 8.0-10.0 cm) were placed in polyethylene centrifuge tubes with a built-in filter specially designed for low porosity sandy sediments (Saager et al., 1990). At the stations with silty sediments (st. 9 and 13), disposable polypropylene centrifuge tubes (50 ml) were used instead. After centrifugation for 10 min. at 1700 *g*, the filtered (cellulose acetate, 0.45 µm) samples were split into two portions. One

Table 1. Number, name, geographical position, water depth, bottom water temperature and oxygen concentration (August 1991 and February 1992) at the 15 visited stations.

No.	Station	Geographical position Lat. N	Long. E	Water depth (m)	Temperature (°C) Aug-91	Feb-92	O_2 concentration (μmol dm^{-3}) Aug-91	Feb-92
2	Boundary	53°30'	03°01'	33	16.8	5.8	210	338
3	Silverpit	53°28'	00°40'	89	14.4	-	272	-
4	Doggerbank	54°50'	01°00'	58	8.2	6.4	267	326
5	Oystergrounds	54°25'	04°04'	49	10.2	6.4	209	321
6	Weiss Bank	55°17'	06°00'	49	12.2	5.8	227	337
7	Tail End	56°00'	04°38'	50	9.5	6.1	230	333
8	Skagerrak W.	57°26'	07°37'	130	7.3	6.4	311	317
9	Skagen	58°20'	10°27'	330	6.9	7.0	276	313
10	Hirtshals	57°50'	10°01'	64	12.2	6.8	243	319
11	Jutland	56°40'	06°43'	41	10.0	5.2	175	330
12	Esbjerg	55°12'	07°38'	25	17.7	4.8	241	345
13	Helgoland Bight	54°05'	08°09'	19	18.7	4.4	196	353
14	Elbe Rinne	54°14'	07°20'	39	16.5	5.4	186	329
16	Frisian Front	53°42'	04°32'	39	17.4	6.3	232	327
17	Hook of Holland	52°07'	03°45'	26	18.5	5.8	259	329

Table 2. General sediment characteristics and CDB-Fe at the 15 stations. Clusters indicate (IA and B) depositional, (II) transitional, and (III) erosional areas (Lohse et al., 1995). Porosities are averages over the upper 3 cm of the sediment in August 1991 and February 1992. All other sediment parameters were determined in the 0-0.5 cm sediment layer collected in February 1992. Sediment classification is based on the Wentworth size scale (Pettijohn et al., 1972).

Cluster	St. no.	Org. C (wt %)	CaCO$_3$ (wt %)	porosity (dm^3 dm^{-3})	CDB-Fe (μmol g^{-1})	Median grain size (μm)	Sediment classification
IA	13	0.74	10.26	0.66	72	15	medium silt
IB	9	2.76	9.64	0.88	245	6	medium silt
	10	0.82	8.43	0.69	103	36	coarse silt
II	2	0.19	4.14	0.47	43	128	fine sand
	5	0.17	1.73	0.46	40	103	very fine sand
	6	0.17	1.80	0.46	40	96	very fine sand
	7	0.15	0.00	0.41	12	125	fine sand
	8	0.14	0.64	0.42	22	175	fine sand
	12	0.07	0.03	0.39	17	187	fine sand
	14	0.39	6.52	0.51	57	98	very fine sand
	16	0.28	8.95	0.53	59	75	very fine sand
III	3	-	-	0.37	-	>350	medium sand
	4	0.03	2.23	0.40	60	>295	medium sand
	11	0.03	0.58	0.43	59	>300	medium sand
	17	0.04	1.21	0.37	26	>340	medium sand

portion was analyzed on board for NO_3^- on a TRAACS-800 autoanalyzer according to the method of Strickland and Parsons (1972). The other portion was acidified to pH $\approx$ 1 and stored at 4°C. Total dissolved Fe and Mn was determined in these samples with a Perkin Elmer 5100 PC Atomic Absorption Spectrophotometer within several weeks. No loss of dissolved Fe and Mn occurred during the storage period. All dissolved Fe and Mn is assumed to be present as Fe^{2+} and Mn^{2+}. The analytical precision for pore water NO_3^- and for Fe and Mn was generally better than 1% and 5%, respectively. Detection limits for Fe and Mn were 0.5 μmol dm^{-3} and 0.2 μmol dm^{-3}, respectively.

Solid phase profiles of Fe and Mn. Sediment from 7 depth intervals (0-0.5, 0.5-1.0, 1.0-2.0, 2.0-4.0, 4.0-6.0, 6.0-8.0, 8.0-12.0 cm) from 8-10 additional subcores was stored frozen (-20°C) until solid phase analysis. Four non-sequential extraction procedures for sediment Fe and Mn oxides were applied: (1) 0.1 M HCl for 18 h; (2) 1 M HCl for 24 h; (3) 0.2 M NH_4-oxalate/oxalic acid buffer (pH = 3.0) for 2 h under oxic conditions in the dark; (4) Citrate-dithionite-bicarbonate solution for 8 h (CDB, pH = 7.3, 20°C). Further details on sample preparation and extraction procedures are given by Slomp et al. (1996). The 0.1 M HCl extraction was applied to all sediment samples from the August 1991 cruise. Profiles of 0.1 M HCl, 1 M HCl, NH_4-oxalate and CDB extractable metals were obtained for 5 stations (Cluster IA: 13; IB: 9; II: 5 and 14; III: 4) sampled in February. These extractions were also applied to the surface sediment (0-0.5 cm) collected at the 10 remaining stations in February. Dissolved Fe and Mn in the extracts was measured in a similar manner as described for pore water Fe and Mn.

Both 0.1 and 1 M HCl should dissolve Mn carbonate phases and 'reactive' Mn oxides (most probably in the form of amorphous or poorly crystalline δ-MnO_2 or vernadite; Burns and Burns, 1980). NH_4-oxalate and CDB are expected to be more selective for Mn oxides (e.g. Canfield et al., 1993a) and to leave Mn carbonate phases largely intact. The Fe phases extracted from North Sea sediments (Cluster IA: 13; IB: 9 II: 5 and 14) with the four applied methods have been discussed previously (Slomp et al., 1996). Here, we will use the CDB-Fe profiles to obtain an estimate of the change with depth of 'reactive' Fe-oxides.

General sediment characteristics. Sediment porosity was determined from the weight loss of the sediment after drying at 60°C for 48h and assuming a specific weight of 2.65 kg dm^{-3}. Total and organic C were measured with a Carlo Erba 1500-2 elemental analyzer. Organic C was determined as the concentration of C in the sample after treatment with sulfurous acid (Verardo et al., 1990). $CaCO_3$ contents were calculated from inorganic C contents as determined from the difference between total and organic C. A good correlation with $CaCO_3$ values calculated from 1 M HCl extractable Ca was found. Grain size

distribution in sediment from the 0-0.5 cm depth interval at each station was determined with a laser diffraction particle sizer (Malvern 2600 E; McCave et al., 1986) after removal of carbonates and organic matter with HCl and H_2O_2.

DESCRIPTION OF THE MODEL

Several multicomponent early diagenetic models have recently been developed that explicitly describe the coupling of the cycles of Mn and Fe to those of O_2, C, S, and N (Rabouille and Gaillard, 1991; Boudreau, 1996; Dhakar and Burdige, 1996; Soetaert et al., 1996; Van Cappellen and Wang, 1996). We use a more simple approach (1) to limit the number of free or not well-defined parameters, (2) to ensure that the uncertainties in the model description or in the results for other elements do not affect our results for Mn and Fe and (3) to allow the presentation and quantitative interpretation of the Mn and Fe data for as many of the North Sea stations as possible.

Most continental margin environments are dynamic environments. It is assumed here that this can be approximated by a series of steady states. Although pore water metal concentrations can be strongly suppressed by anoxic precipitation (Aller, 1990; Canfield et al., 1993a and b) and sorption processes (Canfield et al., 1993a and b), none of the steady state models currently available for the description of the sedimentary cycles of Mn (Robbins and Callender, 1975; Aller, 1980, 1990, Burdige and Gieskes, 1983; Gratton et al., 1990) and Fe (Aller, 1980) include both these processes. We, therefore, develop a steady state reaction-diffusion model that includes anoxic precipitation and sorption.

The model is applied to pore water Mn^{2+} and Fe^{2+} and solid phase Mn and Fe profiles measured in North Sea sediments. In order to reduce the length of this paper, only the equations for Mn are presented. Where Mn^{2+}, Mn oxide, Mn carbonate are mentioned in the following description of the model, Fe^{2+}, Fe oxide, Fe sulfide may be substituted to obtain the corresponding equations for Fe. Mn^{2+} and Fe^{2+} are assumed to be oxidized by O_2 and NO_3^-, respectively. The boundaries below which Mn and Fe switch from an oxidized to a reduced state are given, therefore, by the maximum depth of O_2 penetration (i.e. the oxic/anoxic interface) and the maximum depth of NO_3^- penetration.

A one-dimensional model is assumed; thus, spatial variability and lateral transport are ignored. Dissolved Mn^{2+} (C) and Mn oxide (S) profiles are considered to be at steady state. The sediment column is divided into two zones, an oxic surface zone (I: $0 \leq x \leq L_1$) and an anoxic zone (II: $x > L_1$). Transport of solid phase Mn in both zones is assumed to be the result of sediment accumulation and bioturbational/physical mixing (described as a biodiffusion process). Transport of dissolved Mn^{2+} in both zones takes place through molecular diffusion. Oxidation of dissolved Mn^{2+} occurs only in the oxic surface zone (I) and is described as a first-order process in the dissolved Mn concentration with k_{ox} as the

oxidation rate constant. In the anoxic zone (II), both production and removal of dissolved Mn^{2+} occur. Dissolved Mn^{2+} production due to Mn oxide reduction is described as a first-order process in the reactive Mn oxide concentration with k_r as the dissolution rate constant and S_r as the concentration of unreactive Mn oxide. Mn^{2+} removal due to authigenic Mn carbonate formation is described as a first order process, assuming the dissolved Mn^{2+} concentration to approach an equilibrium value (C_a) with depth and k_a as the precipitation rate constant. Instantaneous reversible sorption of dissolved Mn^{2+} is assumed (Berner, 1976; Schink and Guinasso, 1978) with K_s as the linear sorption coefficient (the amount of Mn sorbed to the sediment = $K_s \times C$). The molecular diffusion (D_s in m^2 d^{-1}) and biodiffusion (D_b in m^2 d^{-1}) coefficents, all rate constants (k_{ox}, k_r, k_a in d^{-1}), the sorption coefficient (K_s in dm^3 dm^{-3}), and sediment porosity (ϕ in dm^3 dm^{-3}) are assumed to be depth-independent in each relevant layer. The sedimentation rate (ω in m d^{-1}) is assumed to be constant. Pore water Mn^{2+} and solid phase Mn have units of mol per m^3 pore water and μmol per gram of dry sediment, respectively. A factor ϑ (gram of dry sediment per cm^3 of pore water) allows conversion between these components of the model:

$$\vartheta = \rho_s[(1-\phi)/\phi] \tag{1}$$

where ρ_s is the average density of the sediment (2.65 g cm^{-3}).

The differential equations for the one-dimensional distribution of dissolved Mn^{2+} and solid phase Mn oxide are given in part A of the Appendix. These equations were solved analytically after assuming continuity in concentrations and fluxes of both dissolved Mn^{2+} and solid phase Mn at the boundary of the two sediment zones (L_1) and appropriate conditions at the external boundaries of the system (see Appendix, part B). C_0 stands for the dissolved Mn^{2+} concentration in the overlying water, and $J_{S_{x=0}}$ is the flux of Mn oxide at the sediment-water interface. The solutions are given in part C of the Appendix.

Four parameters (k_r, k_a, S_r and $J_{S_{x=0}}$) were varied to fit the model to experimental data. Variance-weighted sums of squares for both the pore water Mn^{2+} and Mn oxide were minimized simultaneously using iteratively reweighted regression (Draper and Smith, 1967). All other parameters (k_{ox}, L_1, D_s, D_b, ω, K_s, C_0, C_a) were fixed, based on experimental results obtained in this study and on literature data.

EXPERIMENTAL RESULTS

General sediment characteristics. Organic C concentrations and sediment porosity were highest in the silty sediments (cluster IA and B) and lowest in the medium sands (cluster III, Table 2). Highest $CaCO_3$ concentrations (~8.4-10.3 wt %) were observed at stations 9,

10, 13 (cluster IA and B) and 16 (cluster II). At the remaining stations, $CaCO_3$ concentrations ranged between 0 (st. 7) and 6.5 wt % (st. 14).

Sediment porosity, organic C and $CaCO_3$ concentrations were similar in August and February. Sediment porosity generally decreased with depth. Over the depth interval sampled here (0-12 cm), this decrease was on average 9%. At station 13 (cluster IA), a broad subsurface maximum in porosity was observed between 1.5 and 7 cm depth. Organic C and $CaCO_3$ concentrations generally showed very little change with depth. At station 13, however, a subsurface maximum in organic C was found at the same depth as the porosity maximum. Microscopic examination (8-50× magnification) and grain size analysis of untreated sediment indicated an enrichment in aggregated particles in this same zone.

Pore water profiles of O_2, NO_3^-, Mn^{2+} and Fe^{2+}. As pore water profiles of O_2 are discussed elsewhere (Lohse et al., 1993 and 1996), only the depths of O_2 penetration in both seasons (Fig. 3) are presented here. Penetration depths varied between less than 250 μm (the resolution of the profiles) and ~2.5 cm at cluster IA, IB and II stations. O_2 penetrated much deeper into the sediment of the cluster III stations, with a maximum of ~15 cm at station 11 in February. At almost all cluster IA, IB and II stations, penetration depths in February were higher than in August. All stations with penetration depths less than 250 μm in August (st. 12, 13, 14) are located in the German Bight region. No significant seasonal change in O_2 penetration was found at the deep station in the Skagerrak (st. 9).

NO_3^- pore water profiles exhibited a similar seasonal pattern as that observed for O_2 at the cluster IA, IB and II stations (Fig. 4A and B). At most stations, NO_3^- concentrations were high in a broad surface sediment zone (down to ~2 to 5 cm depth) in February, whereas in August the sediment was almost completely depleted of NO_3^- below ~1-2 cm depth. Except for station 4, little seasonal change in the NO_3^- concentrations was found at the cluster III stations (Fig. 4C). For further details on the NO_3^- profiles, see Lohse et al. (1995).

At depths where the sediment became depleted of O_2 (Fig 2), Mn^{2+} appeared in the pore water at most stations (Fig. 5). Mn^{2+} concentrations were highest at the cluster IA and B stations, ranging up to ~220 μmol dm^{-3}. Cluster II stations mostly had concentrations below 20 μmol dm^{-3}, whereas those of cluster III (with the exception of st. 4) did not rise above 2 μmol dm^{-3}. Dissolved Mn^{2+} concentrations in the upper sediment layer of stations 13 and 10 (cluster IA and B) were higher in August than in February. A reverse seasonal pattern was observed below ~0.5 cm depth at all cluster IA and B stations. At the cluster II stations, pore water Mn^{2+} concentrations were generally higher in August than in February. No seasonal pattern was observed at the cluster III stations, except at station 4, where results were similar to those for cluster II. The high dissolved Mn^{2+} concentrations in the upper 0.4
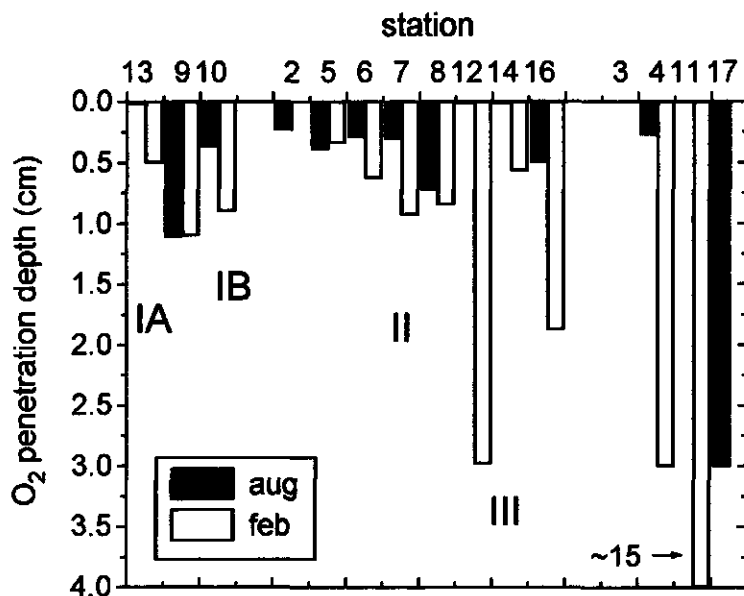
Fig. 3. Maximum O_2 penetration depths (cm) at all stations in August (black bars) and February (white bars).

cm of the sediment at most cluster IA, IB and II stations in August indicate that Mn^{2+} can escape to the overlying water at this time of the year. There is a distinct reversal in gradient of pore water Mn^{2+} at depth in the sediment at many cluster IA, IB and II stations indicating removal of pore water Mn^{2+}.

Increased levels of pore water Fe^{2+} (Fig. 6) appeared upon depletion of sediment NO_3^- (Fig. 4). Maxima in pore water Fe^{2+} occurred at greater depths than those for Mn^{2+}. As with Mn^{2+}, the highest Fe^{2+} concentrations (up to ~180 μmol dm^{-3}) were observed at the cluster I stations. At the cluster II and III stations, Fe^{2+} concentrations mostly remained below ~70 and ~5 μmol dm^{-3}, respectively. The seasonal variation in pore water Fe^{2+} was similar to that observed for Mn^{2+}, with high Fe^{2+} concentrations in the surface sediment of station 10 and 13 (Cluster I) and at most cluster II stations in August compared to February, and the reverse seasonal pattern in the deeper sediment layers at the cluster IA and B stations. Except for station 4, little seasonal change was observed at the cluster III stations. The pore water profiles at many cluster IA, IB and II stations point at removal of Fe^{2+} at depth in the sediment.

A. Cluster IA and B

NO$_3^-$ (μmol dm^{-3})

B. Cluster II

NO$_3^-$ (μmol dm^{-3})

C. Cluster III

NO$_3^-$ (μmol dm^{-3})

Fig. 4. Pore water NO$_3^-$ profiles (μmol dm^{-3}; A: Cluster IA and B, B: Cluster II, C: Cluster III) in August (filled circles) and February (open circles).

Fig. 5. Pore water profiles of Mn^{2+} ($\mu mol\ dm^{-3}$; A: Cluster IA and B, B: Cluster II, C: Cluster III) in August (filled circles) and February (open circles).
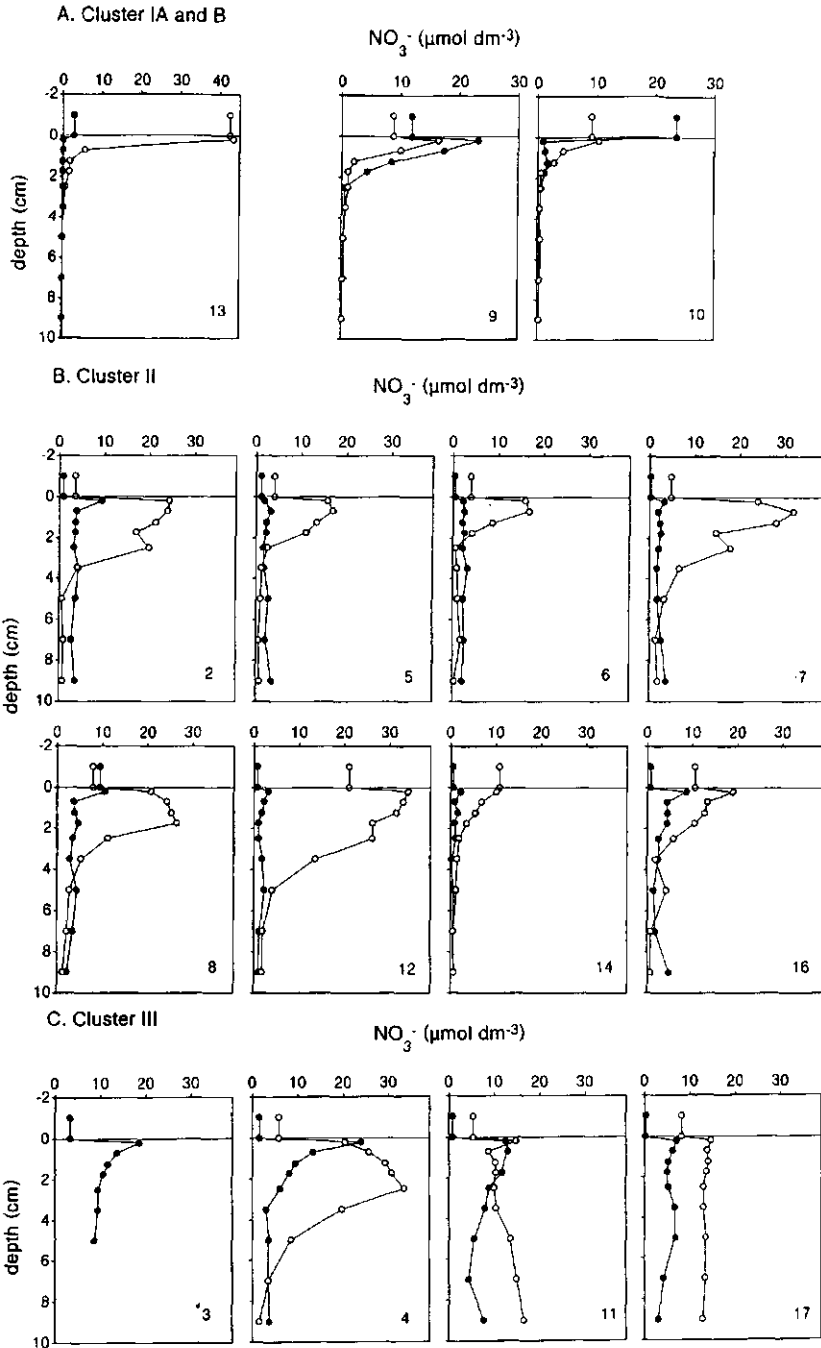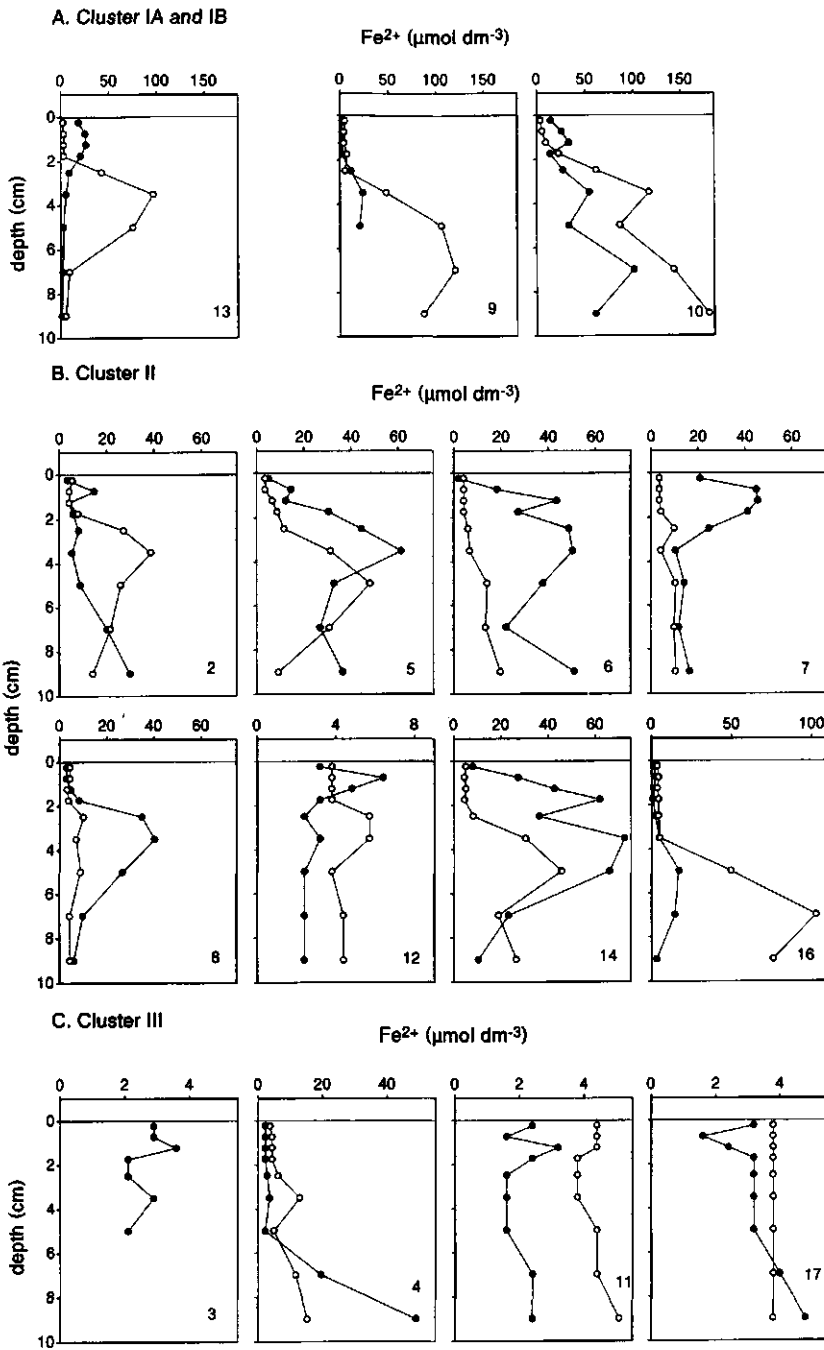
Fig. 6. Pore water profiles of Fe^{2+} (μmol dm^{-3}; A: Cluster IA and B, B: Cluster II, C: Cluster III) in August (filled circles) and February (open circles).
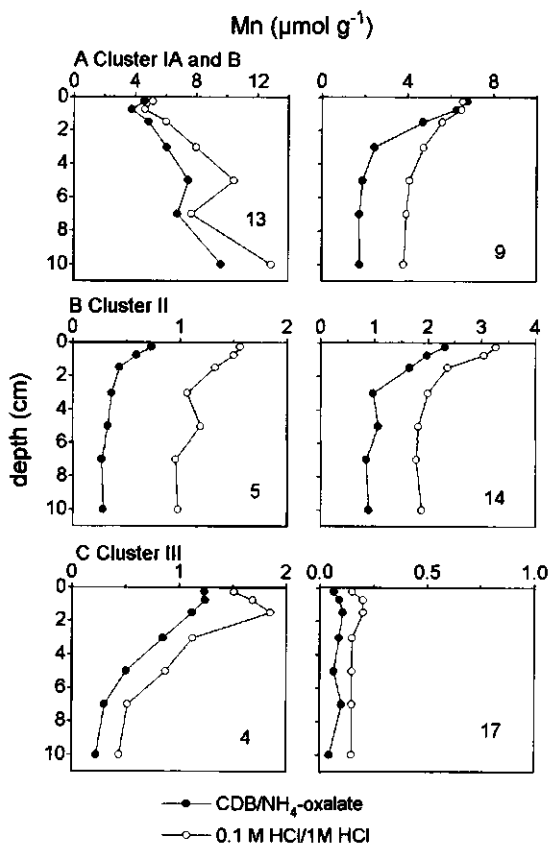
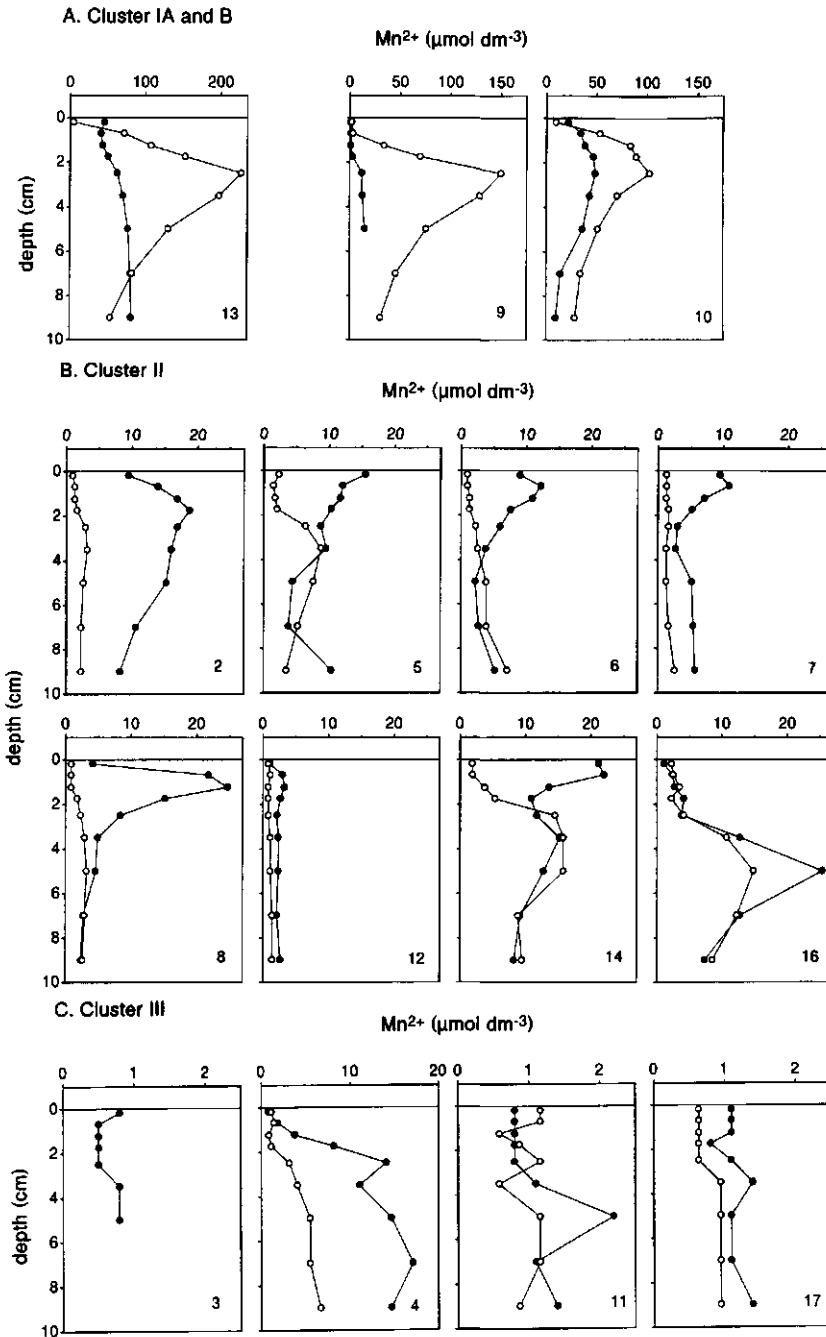Fig. 7. Depth distributions of 0.1 M HCl/1 M HCl Mn (μmol g^{-1}; open circles) and NH$_4$-oxalate/CDB Mn (μmol g^{-1}; filled circles) at stations from each cluster (A: Cluster IA and B, B: Cluster II, C: Cluster III) in February 1992.

Solid phase profiles of Mn and Fe. NH$_4$-oxalate buffer and CDB extracted similar amounts of sediment Mn (slope = 1.0; R^2 = 0.93; n= 52). The same holds for the 0.1 and 1 M HCl solutions (slope = 1.0; R^2 = 0.96, n = 52). Average depth distributions for both sets of extractions at 6 stations are presented in Fig. 7. HCl always extracted more Mn than NH$_4$-oxalate/CDB, which is in line with the dissolution of Mn carbonate phases, in addition to Mn oxides, by HCl. The results suggest that Mn carbonate concentrations increase with depth at stations 13 and 9 (cluster IA and B), whereas they remain relatively constant with depth at the other stations. Only the 0.1 M HCl extration was applied to the sediments from all stations. Therefore, we will use the results of this extraction, which provides a measure of the Mn present as Mn carbonate and Mn oxide, for comparison of the solid phase Mn contents at the different stations.
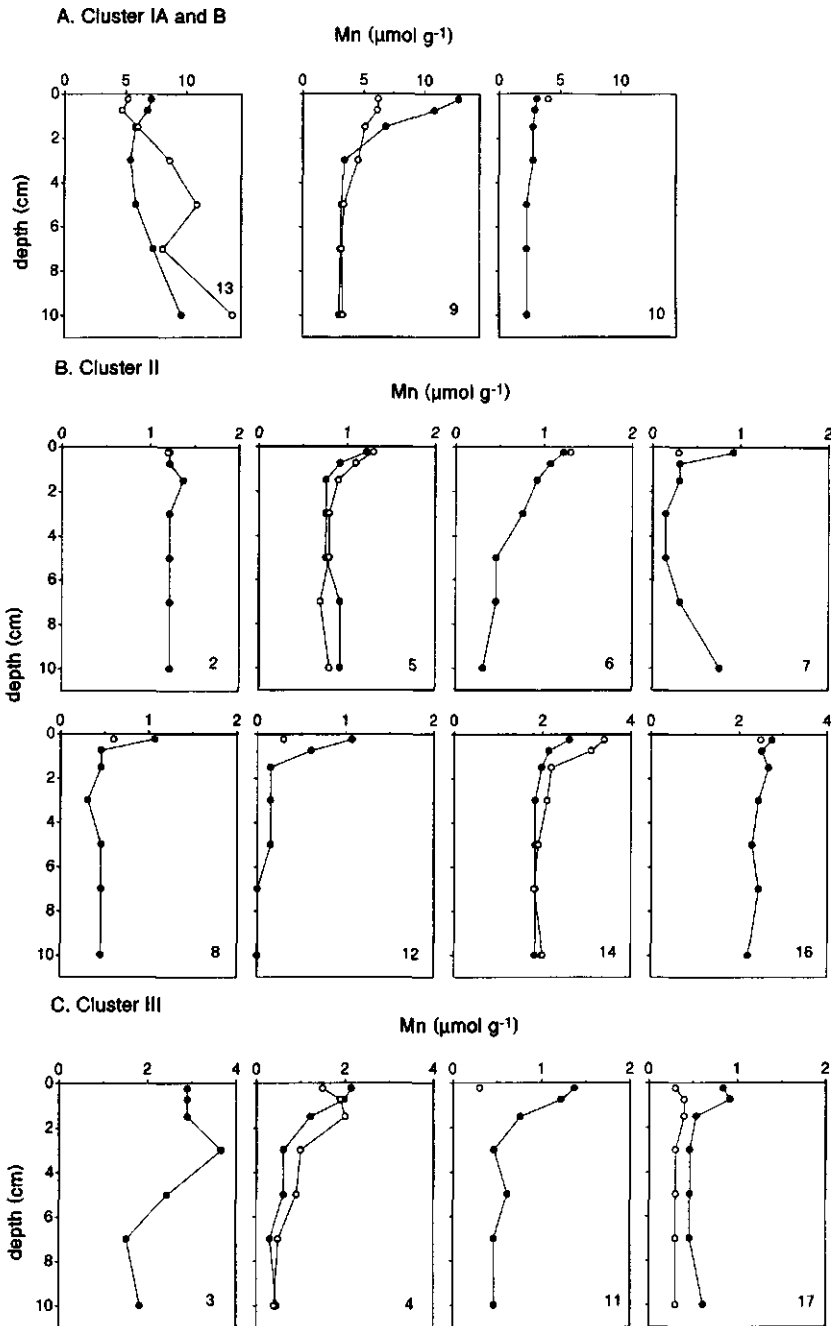
Fig. 8. Solid phase profiles of 0.1 M HCl Mn (μmol g^{-1}; A: Cluster IA and B, B: Cluster II, C: Cluster III) in August (filled circles) and February (open circles).
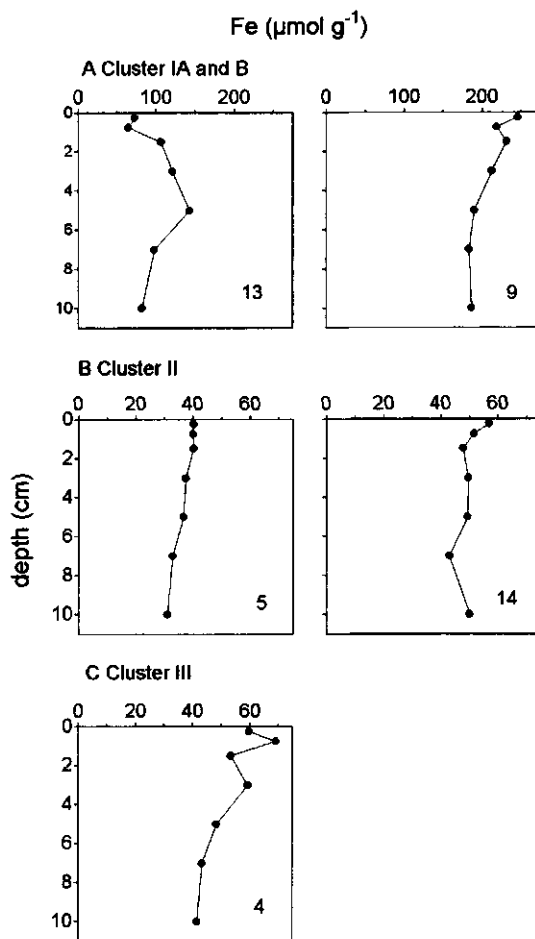
Fig. 9. Solid phase profiles of CDB-Fe (μmol g^{-1}; A: Cluster IA and B, B: Cluster II, C: Cluster III) in February.

Highest solid phase Mn concentrations (up to ~13 μmol g^{-1}) were observed at the stations in the Skagerrak (cluster IB: st. 9 and 10) and the German Bight (cluster IA: st. 13) (Fig. 8). At all other stations, surface Mn concentrations were mostly between 1 and 3 μmol g^{-1}. At most stations, surface enrichments typical for Mn oxides were found. Only at station 13, high concentrations of Mn were found at depth. Apart from station 9, where much higher Mn contents were observed in summer than in winter, no significant seasonal changes in Mn contents were observed at the stations where whole profiles were available.

At several of the cluster II and III stations (st. 7, 8, 11, 12, 17), surface Mn contents were lower in winter than in summer.

Highest concentrations of CDB-Fe (up to ~110 and 245 μmol g^{-1}) were found at the cluster I stations (Table 2). CDB-Fe profiles at four of the five selected stations (Fig. 9) decrease with depth. At station 13 a broad subsurface maxium in CDB-Fe was found between 1.5 and 7 cm depth.

APPLICATION OF THE MODEL

The model was applied to stations where profiles of both solid phase (0.1 M HCl Mn and CDB Fe) and pore water metals were available. The Mn profiles of stations 13 (cluster IA) and 3, 11 and 17 (cluster III) and the Fe profiles of stations 13 (cluster IA) and 4 (cluster III) were not modelled, however. At these stations, the pore water and solid phase profiles suggest an important role for processes not included in the model. At station 13, high concentrations of CDB- and HCl-Mn and of CDB-Fe at depth (Fig. 7, 8 and 9) coincided with a maximum in porosity, organic C and aggregated particles. This may be due to a local enrichment with faecal pellets containing fine material in this zone. At the cluster III stations 3, 11, 17 a Mn oxide-rich surface zone was observed (Fig. 8). Active redox cycling cannot be responsible for this enrichment as O_2 is abundant in these sediments (Fig. 3) and pore water Mn^{2+} concentrations are very low and do not change appreciably with depth (Fig. 5). The same holds for station 4 in February, where CDB-Fe decreases with depth (Fig. 9) although NO_3^- is present throughout the whole interval sampled.

In the model calculations, two rate constants (k_r and k_a), the flux of Mn or Fe oxide from the overlying water ($J_{S_{x=0}}$), and the metal oxide concentration at which no further release of dissolved metal occurs (S_r) were used as fitting parameters. Values for the fixed parameters (L_1, D_s, D_b, ω, k_{ox}, K_s, C_0, C_a) are listed in Table 3 with references to their origin. Additional model runs, in which (1) S_r was set to the lowest metal oxide concentration measured in each sediment core or (2) C_a was used as a fitting parameter, were carried out for all stations. Generally, only minor differences were observed between the model results with and without C_a or S_r as fitting parameters. The model was very insensitive to the values assumed for k_{ox}. Consequently, the value of this parameter had to be fixed. The biodiffusion coefficient, D_b, which is a critical parameter in the model, is derived from the equation:

$$D_b = 15.7\omega^{0.6} \tag{2}$$

with ω in units of cm y^{-1} and D_b in units of cm^2 y^{-1} (Boudreau, 1994) at the cluster I stations (Table 3). This equation cannot be used at the cluster II stations as ω is unknown.

Table 3. The fixed parameters used for the model calculations.

		(1)	(2)	(3)	(4)	(5)	(6)	(7)	(8)
	Parameter	L_1	D_s	D_b	ω	k_{ox}	K_s	C_o	C_a
	Unit	(m)	(10^{-5} m^2 d^{-1})	(10^{-6} m^2 d^{-1})	(10^{-6} m d^{-1})	(d^{-1})	(-)	(mol m^{-3})	(mol m^{-3})
Mn model									
	Station								
IB	9 aug	0.025	3.04	2.74	13.7	1	4	0.0001	0.013
	10 aug	0.0037	2.02	2.74	13.7	1	4	0.0001	0.005
II	2 aug	0.0023	2.27	1.37	0.027	1	1	0.0001	0.005
	5 aug	0.0039	1.83	1.37	0.027	1	1	0.0001	0.004
	6 aug	0.0029	1.95	1.37	0.027	1	1	0.0001	0.002
	7 aug	0.0031	1.60	1.37	0.027	1	1	0.0001	0.004
	8 aug	0.0073	1.52	1.37	0.027	1	1	0.0001	0.004
	12 aug	0.00025	1.93	1.37	0.027	1	1	0.0001	0.0024
	14 aug	0.00025	2.44	1.37	0.027	1	1	0.0001	0.009
	16 aug	0.025	2.60	1.37	0.027	1	1	0.0001	0.005
III	4 aug	0.0028	1.49	0.027	0.027	1	1	0.0001	0.005
IB	9 feb	0.011	2.77	2.74	13.7	1	4	0.0001	0.010
II	5 feb	0.020	1.61	1.37	0.027	1	1	0.0001	0.005
	14 feb	0.017	1.72	1.37	0.027	1	1	0.0001	0.009
III	4 feb	0.03	1.43	0.027	0.027	1	1	0.0001	0.005
Fe model									
	station								
IB	9 feb	0.02	2.89	2.74	13.7	10	4	0.0001	0.050
II	5 feb	0.03	1.68	1.37	0.027	10	1	0.0001	0.008
	14 feb	0.025	1.79	1.37	0.027	10	1	0.0001	0.025

Sources: (1) L_1: depth of O_2 penetration (Mn model) or NO_3^- penetration (Fe model) unless indicated otherwise in the text; (2) D_s: derived from the data of Li and Gregory (1974) correcting for temperature and ϕ (Ullman and Aller, 1982); (3) ω: see study sites for cl. IB, at the cl. II and III stations, a value of 0.001 cm y^{-1} is assumed to enable a model solution; (4) D_b: see text; (5) k_{ox}: for Mn^{2+} the value was based on a first-order rate constant calculated from the work of Thamdrup et al. (1994a); the oxidation kinetics for Fe^{2+} are assumed to be more rapid (e.g. Aller, 1980); (6) K_s: for cluster IB the value observed in Mn-poor Skagerrak sediments (S6; Canfield et al., 1993a) and assumed for Long Island Sound sediments by Aller (1994) is used; for cluster II and III a lower value is assumed; (7) C_o is set at a value that is typical for oxygenated North Sea water (e.g. Tappin et al., 1995); (8) C_a is set equal to or slightly lower than the lowest observed metal concentration at depth.

Here, a D_b value of 5 cm^2 y^{-1} was assumed. This value is close to the maximum D_b value observed in low sedimentation environments (ω < 0.01 cm y^{-1}) as compiled by Boudreau (1994). For station 4 of cluster III, the D_b was set to 0.10 cm^2 y^{-1}, as no model solutions could be obtained for higher D_b values. It should be noted, however, that this low value is not necessarily correct since one of our model assumptions could be wrong. The range in

Fig. 10. Model fits (solid lines) to profiles of pore water Mn^{2+} (μmol dm^{-3}; filled circles) and 0.1 M HCl Mn (μmol g^{-1}; open circles) at 11 stations (A: Cluster IB, B: Cluster II, C: Cluster III) in August. Dashed lines indicate the depth of O_2 penetration.

C. Cluster III
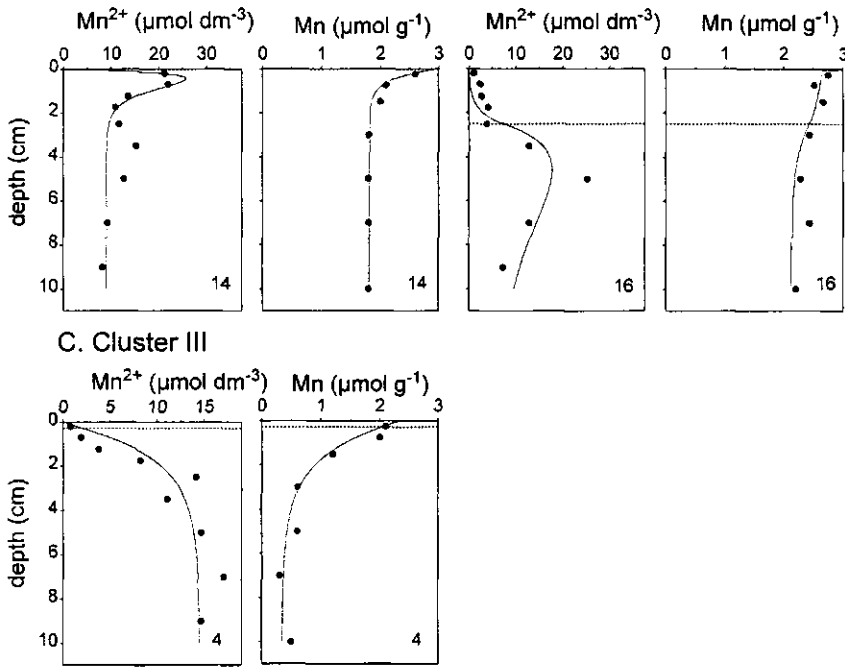
Fig. 10. (continued)

D_b values used here is similar to the range of 0.5-12 cm^2 y^{-1} estimated for North Sea sediments from ^{210}Pb profiles (Albrecht, 1991, cited in Pohlmann and Puls, 1994). We have not accounted for possible seasonal changes in sediment mixing. At 4 stations (9 and 16 in August and 5 and 14 in February), pore water Mn^{2+} profiles suggest that NO_3^-, not O_2, acts as the oxidant for dissolved Mn^{2+} (Fig. 3, 4 and 5). Although never demonstrated directly, this is theoretically possible and has been suggested previously in order to explain concave-upward Mn^{2+} distributions in anoxic sediment (Aller, 1990). For these stations, the depth of NO_3^- penetration is used as the depth (L_1) at which Mn shifts from an oxidized to reduced state.

Model fits for Mn and Fe. Model fits to the Mn oxide and pore water Mn^{2+} profiles for 11 stations in August and 4 stations in February are shown in Fig. 10 and 11, respectively. As no model fit could be obtained when using 0.1 M HCl Mn as a measure for solid phase Mn at station 9 in February, the result of the CDB/NH_4 oxalate extraction was used for this station (Fig. 7 and 11). Model fits to the solid phase Fe and pore water Fe^{2+} profiles for 3 stations in February are shown in Fig. 12. The model gives a reasonably good description of the measured metal profiles at most stations, particularly when the zone where metal
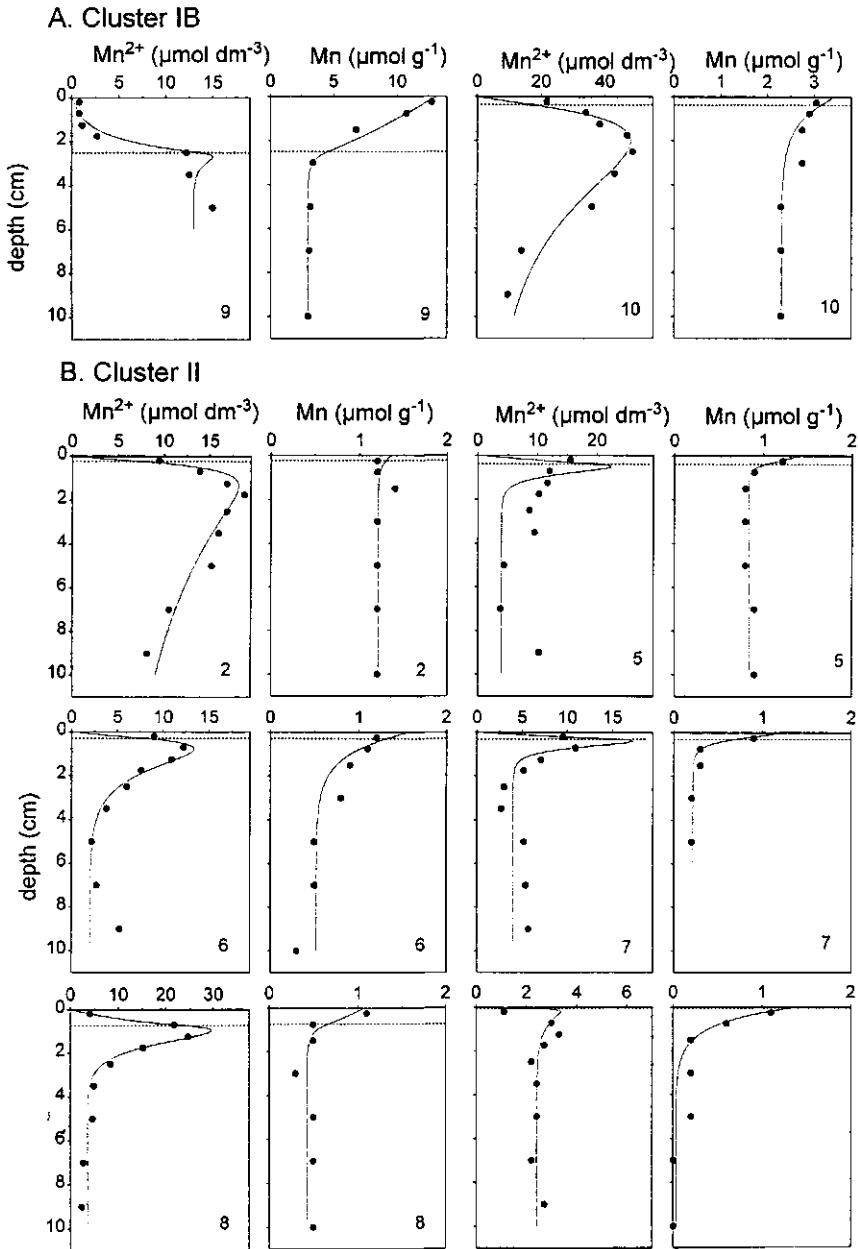
Fig. 11. Model fits (solid lines) to profiles of pore water Mn^{2+} (µmol dm^{-3}; filled circles) and 0.1 M HCl Mn (µmol g^{-1}; open circles) at 3 stations (A: Cluster IB, B: Cluster II, C: Cluster III) in February. Dashed lines indicate the depths of O_2 penetration.
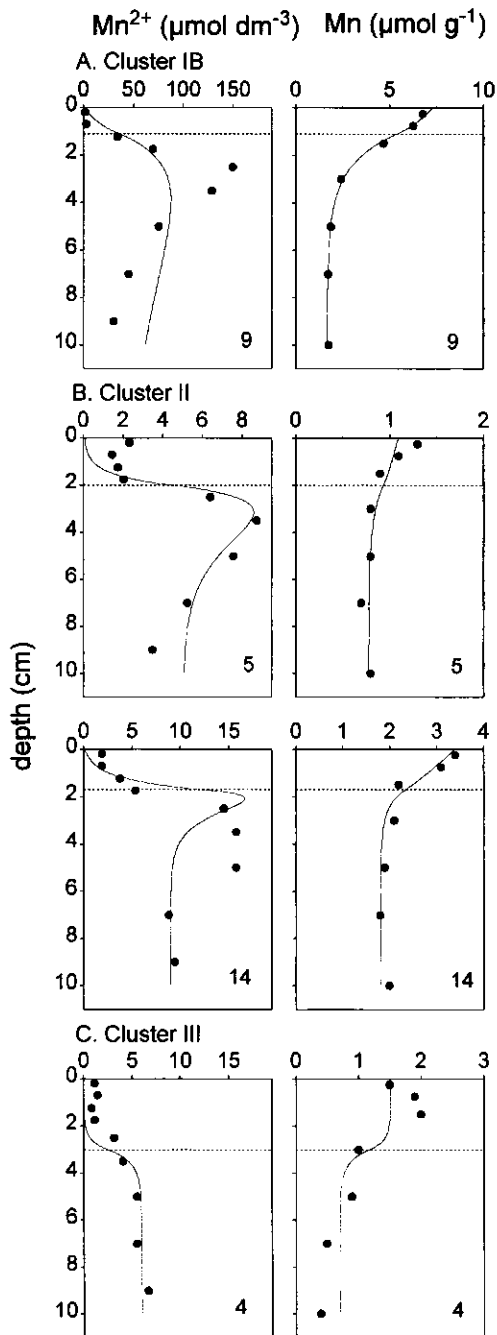
Table 4. First-order rate constants for Mn and Fe reduction (k_r) and precipitation of reduced authigenic Mn and Fe (k_a), and the concentrations of unreactive Mn and Fe oxide (S_r) obtained by fitting the model to pore water and solid phase profiles of these metals.

	Parameter		k_r	k_a	S_r
	Unit		(d^{-1})	(d^{-1})	$(\mu mol\ g^{-1})$
Mn model	Station				
IB	9	aug	0.2	25	3.00
	10	aug	0.024	0.025	2.30
II	2	aug	0.092	0.0053	1.21
	5	aug	0.41	2.9	0.84
	6	aug	0.015	1.4	0.41
	7	aug	0.20	14	0.21
	8	aug	0.11	0.78	0.43
	12	aug	0.024	100	0.03
	14	aug	0.069	2.7	1.82
	16	aug	0.0057	0.025	2.13
III	4	aug	0.00012	1.0×10^{-11}	0.35
IB	9	feb	0.017	0.0036	1.69
II	5	feb	0.0072	0.27	0.78
	14	feb	0.030	2.0	1.82
III	4	feb	0.010	1.0×10^{-11}	0.70
Fe model	Station				
IB	9	feb	0.016	0.70	186.5
II	5	feb	0.0032	0.29	33.0
	14	feb	0.0025	0.52	47.0

oxidation takes place is thin (Fig. 10). The model underestimates dissolved metal concentrations in the oxidation zone at most stations when this zone extends to greater depths (Fig. 10, 11 and 12).

Values for k_r and k_a estimated from the model fits are listed in Table 4. Rate constants for Mn reduction (k_r) range from 0.00012 to 0.41 d^{-1}. Rate constants for anoxic precipitation of Mn^{2+} (k_a) range from 0.0053 to 100 d^{-1} (no anoxic precipitation is taking place at st. 4). For Fe, ranges of 0.0025 to 0.016 d^{-1} and 0.29 to 0.70 d^{-1} were found for k_r and k_a, respectively. The fitted values for the Mn and Fe oxide flux from the overlying water ($J_{Sx=0}$) and calculated rates of Mn and Fe oxide reduction, Mn and Fe oxide precipitation, anoxic precipitation of Mn^{2+} and Fe^{2+} and sediment-water exchange of Mn^{2+} and Fe^{2+} are listed in Table 5. Rates of Mn and Fe reduction range from 0.0039 to 0.46 mmol m^{-2} d^{-1}, and 0.18 to 2.1 mmol m^{-2} d^{-1}, respectively. A large proportion of the Mn^{2+} and Fe^{2+} liberated at most stations (generally ranging from ~50 to ~90% for Mn^{2+} and ~60 to ~70% for Fe^{2+}) is precipitated as a reduced authigenic mineral in zone II

Table 5. The metal oxide flux obtained by fitting the model to experimental data and model calculated rates of metal oxide reduction, formation of metal oxides, authigenic mineral formation and the flux of dissolved metals across the sediment-water interface. Rates of metal oxide reduction are compared to calculated rates of O_2 uptake.

	Parameter	(1) oxide flux at x=0 (JSx=0)	(2) oxide red. rate zone II	(3) oxide prec. rate zone I	(4) auth. min. prec. rate zone II	(5) diss. metal flux at x = 0	(6) O_2-uptake calc.	(7) contr.Fe or Mn red. to C-ox.
	Unit Station			(mmol m^{-2} d^{-1})				(%)
Mn model								
IB	9 aug	0.30	0.37	0.08	0.29	0.00	5.2	4%
	10 aug	0.18	0.17	0.02	0.04	0.10	9.4	1%
II	2 aug	0.041	0.045	0.004	0.002	0.039	8.8	0%
	5 aug	0.19	0.20	0.02	0.14	0.05	4.4	2%
	6 aug	0.16	0.16	0.00	0.13	0.03	6.9	1%
	7 aug	0.38	0.39	0.01	0.34	0.04	8.9	2%
	8 aug	0.11	0.14	0.03	0.09	0.02	1.9	4%
	12 aug	0.38	0.38	0.00	0.34	0.04	28.4	1%
	14 aug	0.46	0.46	0.00	0.24	0.21	24.8	1%
	16 aug	0.012	0.033	0.021	0.009	0.000	6.7	2%
III	4 aug	0.0037	0.0048	0.0011	0.0000	0.0037	-	-
IB	9 feb	0.12	0.25	0.13	0.02	0.08	5.3	2%
II	5 feb	0.013	0.022	0.009	0.013	0.000	9.4	0%
	14 feb	0.10	0.13	0.03	0.10	0.00	5.0	1%
III	4 feb	0.0000	0.0039	0.0039	0.0000	0.0000	0.8	0%
Fe model								
IB	9 feb	2.1	2.1	0.8	1.3	0.00	5.2	19%
II	5 feb	0.22	0.30	0.09	0.21	0.00	4.9	2%
	14 feb	0.12	0.18	0.07	0.11	0.00	4.8	2%

DISCUSSION

Internal and external metal cycling and rates of Fe and Mn reduction. Fe and Mn reduction rates in sediments depend on (1) the supply of metal oxides from an internal or external source (Fig. 1) and on (2) the reducing capacity of the sediment. The depths of NO_3^- and O_2 penetration in a sediment and the rates of sediment mixing determine the importance of internal metal cycling. In many continental margin sediments, in-situ formation of metal oxides is the dominant source for metal oxides (Fig. 1A). As a result, high surface concentrations of metal oxides develop, and Fe and Mn reduction rates often become orders of magnitude higher than suggested by the supply rates from the overlying water (Table 6).

In North Sea sediments outside the major depositional areas, comparatively minor surface enrichments of Fe and Mn oxides are present (Fig. 8), suggesting less efficient retention of metal oxides. Even when sediment mixing is substantial, as assumed for most of our stations, Fe and Mn reduction rates remain comparatively low (Table 6). Detailed studies on the sedimentary Mn cycle in coastal environments (Aller, 1994; Thamdrup et al., 1994b) have shown seasonal shifts from a largely internal cycle to an external cycle, following the almost complete disappearance of O_2 from the surface sediment in summer. As the flux of dissolved Mn^{2+} out of the sediment was larger than the external supply of Mn oxides, these sediments were depleted of Mn at this time of year. When oxic conditions were reestablished in winter, the external input from the overlying water was sufficient to allow for a rapid build-up of surface Mn oxide concentrations. Similar seasonal variations in the redox conditions in surface sediments are observed in most non-depositional North Sea environments. We cannot accurately evaluate the magnitude of the seasonal change in the balance between external and internal supply of Mn oxide in these sediments without knowledge of the D_b values. Nevertheless, the results in Table 5 indicate that internal cycling of Mn is more important in winter than in summer. The external Mn oxide supply in winter is apparently insufficient to cause a large build-up of Mn oxide concentrations at this time of year (st. 5, 14 and 4; Fig. 8). We conclude that in most non-depositional North Sea sediments (cluster II and III) high surface concentrations of Fe and Mn oxides do not develop. At typical D_b values for continental margin sediments this leads to relatively low rates of Fe and Mn reduction in these sediments.

In a previous study on Fe and Mn reduction in the depositional area of the Skagerrak (Table 6; Canfield et al., 1993a and b), a high Mn reduction rate was observed in a sediment from the deepest part of the Skagerrak (S9, 695m) where the surface sediment was strongly enriched in Mn oxides. At two other stations outside this deep area (S4, 190m; S6, 380 m), surface sediments were rich in Fe oxides instead of Mn oxides. At these latter stations, Mn reduction rates were low but Fe reduction rates were high. The surface enrichments were attributed to long-term internal metal cycling at all locations. We also find low rates of Mn reduction at our stations located at 330 and 64 m depth (st. 9 and 10, respectively). The rate of Fe reduction calculated for station 9 is substantially higher than that observed in any of the other North Sea environments, but it is still a factor 10 lower than that reported by Canfield et al. (1993a and b) for station S6 at a comparable depth. There are three possible explanations. First, Canfield et al. (1993a and b) calculated metal reduction rates from sediment incubation results (Table 6) and may have overestimated actual rates in the sediment and, as a result, the D_b values necessary to sustain these rates. Second, we may have underestimated the D_b value at station 9. In view of the low number of macrofauna
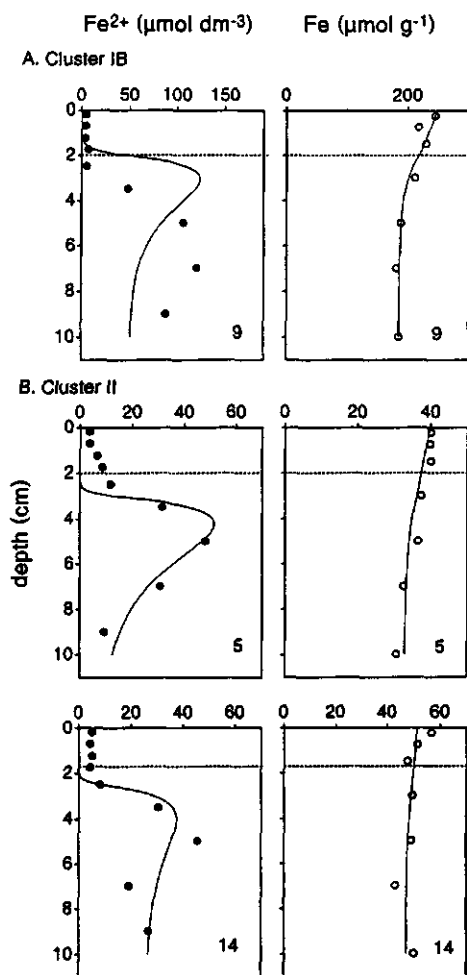
Fig. 12. Model fits (solid lines) to profiles of pore water Fe^{2+} (μmol dm^{-3}; filled circles) and CDB-Fe (μmol g^{-1}; open circles) at 3 stations (A: Cluster IB, B: Cluster II) in February. Dashed lines indicate the depths of NO_3^- penetration.

encountered at station 9 (see study sites), it is unlikely, however, that we greatly underestimated the actual D_b value. Third, there may be very large spatial variations in sediment mixing rates and, as a consequence, rates of metal oxide reduction in the Skagerrak.

First-order rate constants for Mn reduction derived from model calculations in the literature vary over a wide range. Values of 3.1 x 10^{-5} and 4.7 x 10^{-5} d^{-1} have been found for east equatorial Atlantic (Burdige and Gieskes, 1983) and Chesapeake Bay (Holdren et

al., 1975) sediments, respectively. Aller (1980) calculated a range of 0.022 - 0.068 d^{-1} for Long Island Sound sediments, whereas Gratton et al. (1990) found a value of 0.68 d^{-1} for Laurentian Trough sediments. This wide range is not surprising as this parameter lumps a great number of processes and, thus, depends on several factors, including the reactivity of the Mn oxides and the type of reductant involved. The values calculated here (Table 5) cover a similar wide range. Except for the fact that the lowest value is found for the cluster III station 4, there is no evidence for a link between the sedimentary environment and the value for k_r. No estimates of rate constants for in-situ Fe oxide reduction are available in the literature for comparison. Rate constants for Fe reduction at stations 9, 5 and 14 are respectively equal to, a factor of 2 lower and a factor of 10 lower than those for Mn at these same stations. The latter observations are in line with the fact that Mn oxides are generally more easily reduced than Fe oxides (Froelich et al., 1979).

Fe and Mn reduction and organic C oxidation. The potential direct or indirect role of Fe and Mn in the decomposition of organic matter in each of these North Sea environments is evaluated by comparing the rates of Fe and Mn reduction to total rates of sediment O_2 uptake, calculated from O_2 profiles (Table 5; for details, see Lohse et al., 1996). Sediment O_2 uptake can be viewed as a rough measure for total organic C oxidation, if NH_4-oxidation and denitrification are relatively unimportant and all O_2 is utilized for oxic decomposition of organic material or for oxidation of reduced products of anoxic decomposition processes (Fe^{2+}, Mn^{2+} and H_2S). In addition, there must be no net storage of reduced by-products (e.g. FeS, FeS_2, etc.). If Fe and Mn reduction are coupled to organic C oxidation, 4 and 2 moles of Fe and Mn oxides must be reduced, respectively, for each mole of organic C that is oxidized and, thus, for each mole of O_2 taken up by the sediment (Canfield et al., 1993b).

The results in Table 5 show that, at most stations, the calculated contribution of Fe or Mn reduction to organic C oxidation ranges between 0 and 4%. The only exception is the Skagerrak station 9 where ~19% of organic C oxidation can be linked to Fe reduction in February. We conclude that Fe and Mn oxides do not play an important role in organic C oxidation in most North Sea sediments. The contribution from metal oxide reduction may be substantial only in the Skagerrak.

The fate of the dissolved Fe^{2+} and Mn^{2+}. Dissolved metal produced by metal oxide reduction can precipitate as a reduced authigenic mineral, or after upward transport, reprecipitate as an oxide in the surface sediment or escape to the overlying water. The diffusive transport of the dissolved metals may be enhanced due to reversible sorption on to sediment particles in combination with sediment mixing (Schink and Guinasso, 1978).

Table 6. Comparison of D_b values, fluxes of Mn and Fe oxides from the overlying water and Fe and Mn reduction rates from this study to those determined in other studies on metal cycling in continental margin sediments*.

Source	Location	D_b (cm² y⁻¹)	Mn oxide flux at x = 0 (mmol m⁻² d⁻¹)	Fe oxide flux at x = 0 (mmol m⁻² d⁻¹)	Mn reduction rate (mmol m⁻² d⁻¹)	Fe reduction rate (mmol m⁻² d⁻¹)
This study	Skagerrak, st. 9, cl. 1B	10	0.12-0.30	2.1	0.25-0.37	2.1
	Skagerrak, st. 10, cl. 1B	10	0.18	-	0.17	-
	North Sea, cl. II	5	0.012-0.46	0.12-0.22	0.022-0.46	0.18-0.30
	North Sea, cl. III	0.1	0.0000-0.00037	-	0.0039-0.0048	-
Sundby & Silverberg, 1985	Laurentian Trough, st. 20	0.05	0.23	-	0.31	-
	Laurentian Trough, st. 23	3.1	0.38	-	1.16	-
	Laurentian Trough, st. 24	12	0.86	-	4.62	-
Aller, 1980	Long Island Sound	14	-	-	0.57-4.6	7-34
Aller, 1994	Long Island Sound	3-180	-0.14-0.07	-	0.29-133	-
Thamdrup et al., 1994b	Aarhus Bay	17	0.04	-	2.3	4.6
Canfield et al., 1993a & b	Skagerrak, S4, 190m	80	-	0.19-0.38	0	20
	Skagerrak, S6, 380m	87	-	0.17-0.34	0	21
	Skagerrak, S9, 695m	19	0.14-0.28	-	20	0

(*) In these studies, Fe and Mn reduction rates were calculated from D_b values determined from radionuclide profiles and from gradients of metal oxides in the surface sediment. Only in the study of Canfield et al. (1993a and b) Fe and Mn reduction rates were determined from sediment incubation results and D_b values were calculated *from* these Fe and Mn reduction rates and measured concentration gradients of Fe and Mn oxides. Metal oxide fluxes were calculated in several different ways and should be viewed as rough estimates.

To illustrate the potential effect of reversible sorption on the pore water metal profiles in North Sea sediments, the model results for pore water Mn^{2+} for station 10 (cluster IB), 8 (cluster II) and 4 (cluster III) in August (Fig. 10) are compared to model scenarios with both larger and smaller sorption coefficients (Fig. 13 A, B and C). The greatest sorption coefficient used here is the maximum value observed for an extremely Mn oxide-rich (475 μmol g^{-1}), silty sediment in the Skagerrak (assuming a porosity of 0.9 dm^3 dm^{-3} and a sediment density of 2.65 g cm^{-3}; Canfield et al., 1993a). The model results show that at the small D_b values, such as those assumed at the cluster III station 4 (0.1 cm y^{-1}), sorption has very little effect on the pore water profiles of Mn^{2+} (Fig. 13 C). At larger D_b values, such as assumed at the cluster IB and II stations (10 and 5 cm y^{-1}, respectively), reversible sorption can have a substantial effect on pore water distributions of Mn^{2+} (Fig. 13A and B).

Anoxic authigenic mineral formation can be responsible for the reversal in gradient of the pore water metal profiles at depth. This is illustrated for Mn in Fig. 13D and E where the model results for pore water Mn^{2+} at stations 10 and 8 are compared to a model scenario where anoxic precipitation of Mn^{2+} is absent. The results show that this process also may lead to lower maximum pore water metal concentrations. The model results for station 4 (Fig. 13F) remain unchanged as no anoxic removal occurs at this station. It should be noted, however, that biological irrigation at depth in the sediment can also result in a reversal in gradient of pore water profiles (Aller, 1980 and 1990; Emerson et al., 1984). Since this process is not included in our model, the calculated rates of anoxic precipitation of dissolved Fe^{2+} and Mn^{2+} may overestimate actual rates.

Rates of SO_4^{2-} reduction in southern North Sea sediments mostly are <1 mmol SO_4^{2-} m^{-2} d^{-1} in winter. Over 80% of the SO_4^{2-} in these sediments is reduced to acid volatile sulfides (AVS = H_2S and FeS; Upton et al., 1993). Slightly higher SO_4^{2-} reduction rates, ranging up to 4 mmol m^{-2} d^{-1} have been observed in Skagerrak sediments. A large proportion of the reduced sulfur in these sediments is converted to FeS (Jørgensen, 1989; Canfield et al., 1993b). This indicates that the rates of reduced authigenic mineral formation calculated for Fe at our North Sea stations (Table 5) are not unreasonable. Furthermore, it suggests that most of the dissolved Fe^{2+} precipitates as FeS. Relatively little of this FeS is permanently stored in these marine sediments, either as FeS or FeS_2, as evidenced by solid phase analysis. The reason is that most of the Fe^{2+} in these Fe sulfides is (1) redissolved to Fe^{2+} and reoxidized or (2) directly converted to Fe oxide upon upward mixing into the oxidized sediment or upon changes in sediment redox conditions (Jørgensen, 1982; Canfield et al., 1993a and b; Thamdrup et al., 1994b). In the second case, this results in an additional internal cycle of Fe in which the reduced Fe does not pass through the dissolved Fe^{2+} phase, and thus cannot escape the sediment through diffusion. Consequently, Fe sulfide formation may limit the extent to which the Fe cycle extends into the water column,
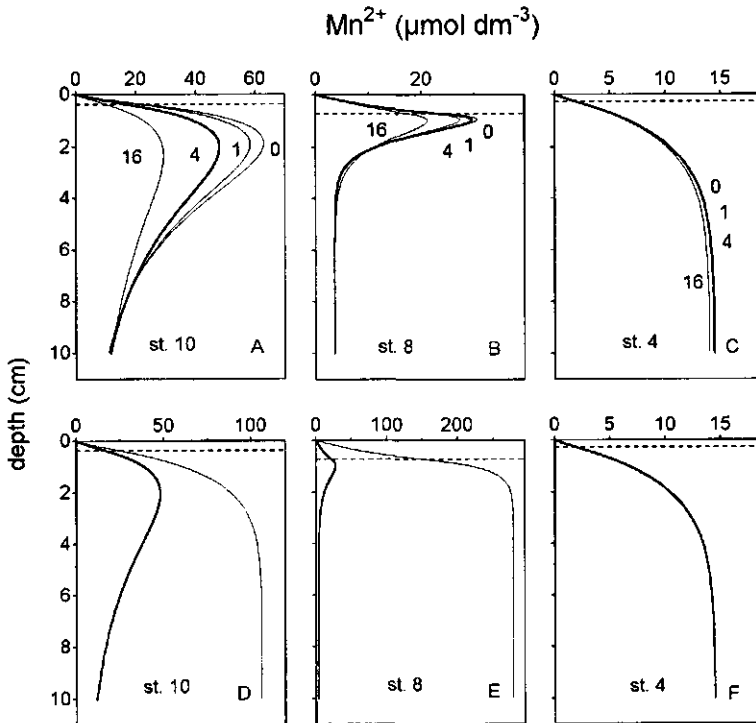
Fig. 13. Comparison of model results for pore water Mn^{2+} from Fig. 9 (thick solid line) to alternative model scenarios (thin solid line). Panels (A, B and C) show the effect of variations in the value of the sorption coefficient (K_s: 0, 1, 4 and 16) for stations 10, 8 and 4. Panels (D, E and F) show what happens at these stations when anoxic precipitation is absent (k_a: 1.0×10^{-11} d^{-1}). All other parameters are as in Tables 3 and 4. Note the difference in scale of D, E and F when compared to A, B and C.

even under steady state conditions. A similar argument may hold for Mn carbonate formation and the Mn cycle.

We could not include a description of this second internal metal cycle in the model as this would require (1) detailed information about the reduced mineral forms of Fe and Mn in these sediments (2) more insight in to the reoxidation processes involved and (3) greater sampling resolution for both pore water and solid phase metals. When upward transport and reoxidation of authigenic reduced Fe and Mn minerals is an important source for Fe and Mn oxides, this omission could result in an overestimation of the metal oxide fluxes from the overlying water calculated for our North Sea sediments ($J_{Sx=0}$; Table 5).

The Fe^{2+} and Mn^{2+} produced due to metal oxide reduction that is not precipitated as a reduced authigenic mineral will diffuse upwards and will be oxidized in the surface layer of

the sediment or will escape to the overlying water. The efficiency of the oxidation process depends on the rate of oxidation and the thickness of the oxidized sediment zone. Fe^{2+} is oxidized more rapidly than Mn^{2+} (Table 3; Stumm and Morgen, 1981) and, as a result, the former metal will more easily be retained in the sediment. The seasonal variation in the thickness of the oxidized sediment zone has important consequences for the retention of both metals. This is demonstrated by the model calculations for Mn at stations 5, 14 and 4 in August and February (Table 5). Whereas dissolved Mn^{2+} may escape the sediment in August, this loss is limited in February.

It should be noted, however, that the simplified model description of the oxidation process causes this seasonal difference to be exaggerated. This particularly becomes apparent from the discrepancy between the measured and modelled pore water metal profiles in the surface zone in February (Fig. 11 and 12). There are two reasons for this poor model fit. Firstly, a single, first-order oxidation rate constant (k_{ox}) cannot adequately describe oxidative removal of dissolved metals (see Thamdrup et al., 1994a; Yeats and Strain, 1990). Secondly, 'background' concentrations of several $\mu mol\ dm^{-3}$ of both Mn^{2+} and Fe^{2+} in the surface oxidized zone at all stations (Fig. 5 and 6) are not accounted for by the model. This background Fe^{2+} and Mn^{2+} may be associated with dissolved organic compounds or may be the product of Fe and Mn oxide reduction in reduced micro-sites in the surface sediment (Burdige, 1993).

To obtain a more accurate estimate of the fluxes across the sediment-water interface, we calculated diffusive fluxes directly from the measured pore water profiles with Fick's first law. An advantage of this approach was that this enabled us to obtain an estimate of rates of sediment-water exchange at all stations and not only those to which the model was applied. The average concentration in the 0-0.4 cm depth interval was assumed to be representative for the dissolved metal concentration at 0.2 cm, and the concentration in the overlying water was set at zero. Parameters ϕ and D_S are as given in Tables 2 and 3, respectively. Figure 14 shows that very little Fe^{2+} and Mn^{2+} is released from the sediments of cluster III. In the cluster II environments, enhanced release of dissolved Mn^{2+} may occur in August; conversely, this only holds for two stations in the case of Fe^{2+}. At the depositional site in the German Bight (st. 13; cluster IA) and at the shallowest station in the Skagerrak region (st. 10; cluster IB) sediment-water exchange of both Fe^{2+} and Mn^{2+} display a seasonal pattern with highest release rates in August. The reverse pattern is observed at the other Skagerrak site (st. 9; cluster IB). These results are explained below.

Fe and Mn cycling in the different sedimentary environments. The porewater and solid phase metal profiles (Fig. 5, 6, 7, 8 and 9), diffusive fluxes of Mn^{2+} and Fe^{2+} across the sediment-water interface (Fig. 14) and model results (Table 5) indicate distinct differences
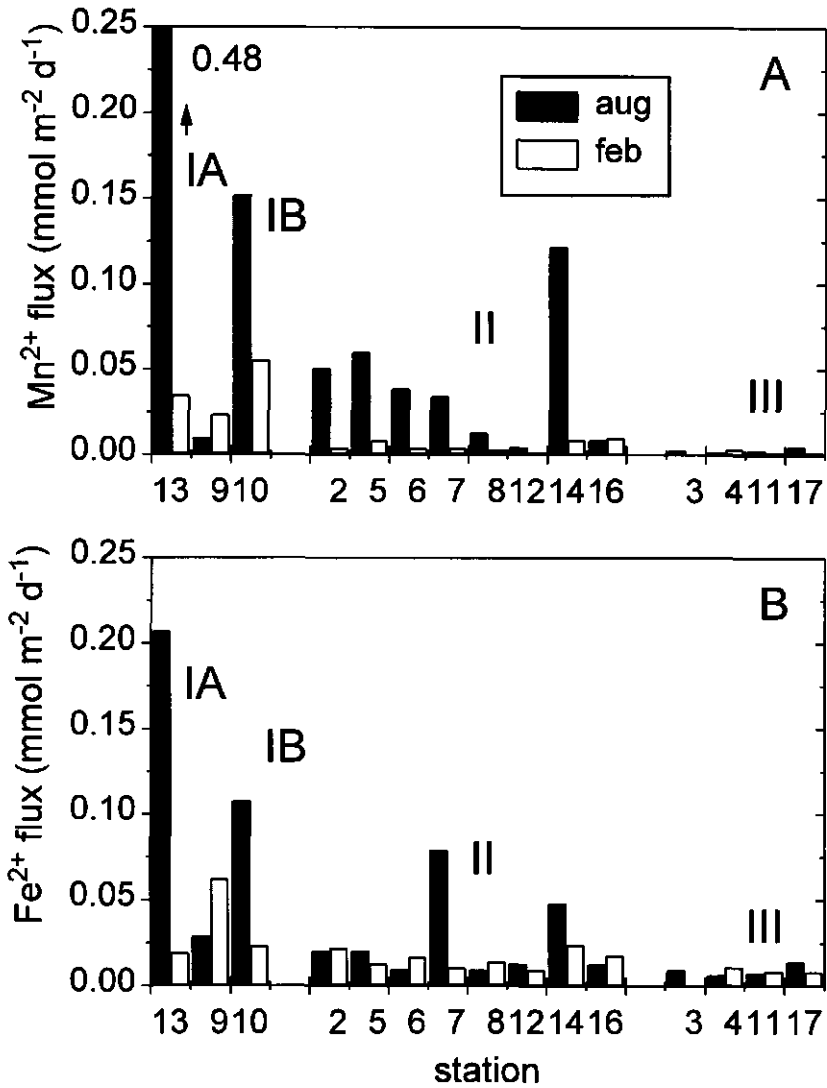
Fig. 14. Calculated diffusive fluxes of (A) Mn^{2+} and (B) Fe^{2+} (in mmol m^{-2} d^{-1}) across the sediment-water interface at 15 North Sea stations in August 1991 (black bars) and February 1992 (white bars).

in the cycling of Fe and Mn in the four types of sedimentary environments encountered in the North Sea during this study. These differences can be explained largely by seasonal and spatial variations in the amount and quality of the deposited organic material and the supply of metal oxides.

In the areas where erosion is dominant (cluster III), organic matter deposition is limited to short periods during the slack tide (Jenness and Duineveld, 1985). Sediment accumulation rates in these areas are low and sediment mixing is probably limited to a relatively thin surface layer. As a result, most of the organic matter is decomposed close to the sediment-water interface. Mineralization rates are so low, both in August and February, that with the exception of station 4, the sediments are not sufficiently depleted of O_2 and NO_3^- to allow for Fe and Mn oxide reduction (Fig. 3, 4, 5 and 6) within the upper 10 cm of the sediment. The enrichment of the surface sediment with Mn oxide in August (Fig. 8) at stations 3, 11 and 17 is either a 'relict' dating from more reduced conditions in other parts of the year, e.g. immediately following the spring bloom, or the result of a biological or physical redistribution process. Resuspension of surface sediment during storms is common in the southern North Sea (Eisma and Kalf, 1987; Jago et al., 1993) and has been suggested to account for elevated concentrations of Fe and Mn in North Sea suspended matter in winter (Tappin et al., 1995). Upon resedimentation during calmer periods, this may result in a concentration of Mn-rich fine-grained particles in the surface layer of cluster III sediments. The large seasonal change in the Mn oxide concentration in the surface sediment at stations 11 and 17 (Fig. 8) supports this view.

In the areas where temporary deposition of organic matter is more frequent (cluster II), organic matter decomposition rates are so rapid in August that the O_2-containing sediment layer becomes very thin or even is absent (Fig. 3). In February, the input of organic matter is low, and the O_2-containing sediment zone extends to greater depths. As a result, the Mn cycle shifts seasonally between an external cycle in summer, when Mn^{2+} can escape to the overlying water, and an internal cycle in winter, when in-situ Mn oxide formation results in retention of most dissolved Mn^{2+} in the sediment (Fig. 5 and 14; Table 5). This is in line with the seasonal pattern in dissolved Mn^{2+} concentrations, with largest values in summer, reported for southern and central North Sea surface waters by Tappin et al. (1995). A tight coupling between sediment redox conditions and the release of dissolved Mn^{2+} to the water column has also been suggested previously for several sandy southern North Sea sediments (Dehairs et al., 1989). NO_3^- penetrates deeper into the sediment than O_2 and creates a barrier that allows the Fe cycle to remain largely internal in both summer and winter (Fig. 14; Table 5). Mn oxides can also act as an oxidant for Fe^{2+} (Postma, 1985; Myers and Nealson, 1988) and, thus, may contribute to this barrier. The presence of 'background' concentrations of dissolved Fe^{2+} in the oxidized surface sediment suggests that,

nevertheless, some dissolved Fe^{2+} may escape to the overlying water. Despite the partial internal cycling, sediment mixing rates and surface enrichments with Fe and Mn oxides are not sufficient to allow Mn and Fe reduction to play a quantitatively important role in organic C oxidation in these sediments.

The two depositional areas, the German Bight (cluster IA) and the Skagerrak (cluster IB), are the only sedimentary environments studied here that receive substantial amounts of terrigenous material. In both areas, dissolved Fe^{2+} and Mn^{2+} concentrations at depth in the sediment are higher in winter than in summer (Fig. 5A and 6A), indicating a seasonal shift in the balance between production and removal of both dissolved metals. SO_4^{2-} reduction and, thus, Fe sulfide precipitation rates are expected to vary seasonally in the German Bight, but this is less likely in the deeper parts of the Skagerrak. An alternative explanation is the occurrence of an enhanced input of Fe and Mn oxide-rich mineral material which has been eroded from cluster III and, perhaps also cluster II (see st. 7, 8 and 12, Fig. 8 and Tappin et al., 1995) type environments by winter storms.

The large difference in the types of organic matter deposited in the German Bight and the Skagerrak has large consequences for the cycling of Fe and Mn. Large quantities of mostly locally produced fresh organic matter reach the sediment in the shallow, inner German Bight in spring and summer. As a result, the sediments become almost completely depleted of O_2 and NO_3^- in August (Fig. 3 and 4). At this time of the year, SO_4^{2-} reduction rates are very high (e.g. 17 mmol m^{-2} d^{-1}; Jørgensen, 1989), and precipitation of Fe sulfide in the sediment strongly suppresses pore water concentrations of Fe^{2+} (Fig. 6). Pore water profiles of Mn^{2+} suggest both production and removal of dissolved Mn^{2+} in the upper anoxic 2 cm of the sediment. Some of the dissolved Mn^{2+} and Fe^{2+} will escape to the overlying water (Fig. 14). We cannot quantify Fe and Mn reduction at station 13, but such rates are probably substantial in summer, as concentrations of both Fe and Mn oxides are high (Fig. 8 and 9) and a large number of macrofauna are present (see study sites), ensuring high sediment mixing rates. In winter, input rates of organic matter and mineralization rates are lower than in summer, and the O_2 and NO_3^- containing surface layer is reestablished (Fig. 3 and 4). Dissolved Mn^{2+} and Fe^{2+} concentrations in the surface sediment are now lower than in summer, and less of these metals will escape to overlying water (Fig. 5, 6 and 14).

The Skagerrak (cluster IB), finally, is characterized by a regular input of large amounts of refractory organic matter. Primary production rates are substantially lower than in the German Bight region, and due to the greater water depths (ranging from <50 m to ~700 m), only a relatively small proportion of this 'fresh' authochtonous material will reach the sediment. Despite the high flux of organic material to the sediment, mineralization rates are, therefore, relatively low in this region (Table 5; also see Jørgensen, 1989; Canfield et al.,

1993b). In the shallower parts of the Skagerrak, such as at station 10, which is located at a depth of 64 m, the increased input of authochtonous material and increase in bottom water temperature in summer (Table 1) are nevertheless sufficient to cause a seasonal change in mineralization rates and thus in the redox conditions in the sediment (Fig. 3, 4, 5 and 6). Here, both the Fe and Mn cycle may extend in to the water column in summer (Fig. 14). Surface enrichments with Mn oxides remain low, and Mn reduction coupled to organic C oxidation is unimportant (Table 5). We have no insight in the role of Fe reduction in this area.

In the deeper parts of the Skagerrak, such as at station 9, which is located at 330 m depth, bottom water temperature is constant throughout the year (Table 1). Here, the input of authochtonous material is so low that the organic matter flux to the sediment and mineralization rates are independent of season (Table 5). The results suggest that, at this station, the reduced sediments are permanently 'capped' with an O_2 and NO_3^- containing sediment layer (Fig. 3 and 4). This allows the build-up of higher concentrations of Mn oxide than at station 10, but does not completely preclude loss of dissolved Mn^{2+} and Fe^{2+} to the overlying water (Fig. 14). Mn reduction linked to organic C oxidation is still not very important at this station (Table 5), but the contribution of Fe reduction may be substantial (Table 5 and 6). In deeper parts of the Skagerrak than sampled in our study (down to ~700 m), the thickness of the oxidizing 'cap' increases further (Canfield et al., 1993a and b) thus acting as a more efficient trap for both Mn^{2+} and Fe^{2+} and accounting for very large surface enrichments of these oxides (Nolting and Eisma, 1988; Canfield et al., 1993a and b; Jensen and Thamdrup, 1993). As shown for Mn by Canfield et al. (1993a and b), metal oxide reduction coupled to organic C oxidation may be very important here.

CONCLUSIONS

Most North Sea sediments are relatively poor in Fe and Mn oxides. High surface concentrations are found only in the depositional areas receiving significant amounts of terrigenous material, i.e. the German Bight and Skagerrak. Results of a reaction-diffusion model developed to describe the sedimentary Fe and Mn cycles indicate that Fe and Mn oxides play only a minor role in organic C oxidation in most North Sea sediments. In the depositional environment of the Skagerrak, and perhaps also in the German Bight, metal oxide reduction may contribute substantially to organic C oxidation.

With our model, we demonstrate that reversible sorption, in combination with sediment mixing enhances the diffusive transport of dissolved metals. Formation of reduced authigenic minerals can be responsible for the reversal in gradient of pore water Fe^{2+} and Mn^{2+} at depth at many stations. If this is so, little permanent storage of these reduced

phases occurs. The efficiency of the oxidation of dissolved Fe^{2+} and Mn^{2+} in the surface sediment is shown to depend on the thickness of the NO_3^- and O_2 containing zones.

Pore water and solid phase metal profiles, diffusive fluxes of Fe^{2+} and Mn^{2+} across the sediment-water interface and model results indicate distinct differences in the cycling of Fe and Mn in the 4 different types of sedimentary environments encountered in the southern and eastern North Sea. These differences are shown to be determined by (1) the quality and quantity of the deposited organic matter and (2) the supply of metal oxides in each environment.

REFERENCES

Aller, R.C., 1980. Diagenetic processes near the sediment-water interface of Long Island Sound II. Fe and Mn. Adv. Geophys. 22: 351-415.

Aller, R.C., 1990. Bioturbation and manganese cycling in hemipelagic sediments. Phil. Trans. R. Soc. London A 331: 51-68.

Aller, R.C., 1994. The sedimentary Mn cycle in Long Island Sound: its role as intermediate oxidant and the influence of bioturbation, O_2, and C_{org} flux on diagenetic reaction balances. J. Mar. Res. 52: 259-295.

Aller, R.C., J.E. Mackin and R.T. Knox Jr., 1986. Diagenesis of Fe and S in Amaxon inner shelf muds: apparent dominance of Fe reduction and implications for the genesis of ironstones. Cont. Shelf Res.. 6: 263-289.

Anton, K.K., G. Liebezeit, C. Rudolph and H. Wirth, 1993. Origin, distribution and accumulation of organic carbon in the Skagerrak. Mar. Geol. 111: 287-297.

Berner, R.A., 1976. Inclusion of adsorption in the modelling of early diagenesis. Earth Planet. Sci. Lett. 29: 333-340.

Boudreau, B.P., 1994. Is burial velocity a master parameter for bioturbation? Geochim. Cosmochim. Acta 58: 1243-1249.

Boudreau, B.P., 1996. A method-of-lines code for carbon and nutrient diagenesis in aquatic sediments. Computers and Geosciences. 2: 479-496.

Burdige, D.J., 1993. The biogeochemistry of manganese and iron reduction in marine sediments. Earth-Sci. Rev. 35: 249-284.

Burdige, D.J. and J.M. Gieskes, 1983. A pore water/solid phase diagenetic model for manganese in marine sediments. Am. J. Sci. 283: 29-47.

Burns R.G. and V.M. Burns, 1980. Manganese oxides. p1-46. In: R.G. Burns, ed. Marine Minerals, Reviews in Mineralogy Vol. 6. Mineralogical Society of America.

Canfield D.E., B. Thamdrup and J.W. Hansen, 1993a. The anaerobic degradation of organic matter in Danish coastal sediments: iron reduction, manganese reduction, and sulfate reduction. Geochim. Cosmochim. Acta 57: 3867-3883.

Canfield, D.E., B.B. Jorgensen, H. Fossing, R. Glud, J. Gundersen, N.B. Ramsing, B. Thamdrup, J.W. Hansen, L.P. Nielsen and P.O.J. Hall, 1993b. Pathways of organic carbon oxidation in three continental margin sediments. Mar. Geol. 113: 27-40.

Dehairs, F., W. Baeyens and D. Van Gansbeke, 1989. Tight coupling between enrichment of iron and manganese in North Sea suspended matter and sedimentary redox processes: Evidence for Seasonal variability. Est. Coast. Shelf Sci. 29: 457-471.

Dhakar, S.P. and D.J. Burdige, 1996. A coupled, non-linear, steady state model for early diagenetic processes in pelagic sediments Am. J. Sci. 296: 296-330.

Draper, N.R. and H. Smith, 1967. Applied regression analysis. John Wiley, 407p.

Eisma D. and J. Kalf, 1987. Dispersal, concentration and deposition of suspended matter in the North Sea. J. Geol. Soc. London. 144: 161-178.

Emerson, S., R. Jahnke and D. Heggie, 1984. Sediment-water exchange in shallow water estuarine sediments. J. Mar. Res. 42: 709-730.

Froelich, P.N., G. Klinkhamer, M.L. Bender, N.A. Luedtke, G.R. Heath, D. Cullen, P. Dauphin, D. Hammond, B. Hartman, V. Maynard, 1979. Early oxidation of organic matter in pelagic sediments of the eastern equatorial Atlantic: suboxic diagenesis. Geochim. Cosmochim. Acta 43: 1075-1090.

Gehlen, M., J.F.P. Malschaert and W. Van Raaphorst, 1995. Spatial and temporal variability of benthic silica fluxes in the southeastern North Sea. Cont. Shelf Res. 15: 1675-1696.

Gratton, Y., H.M. Edenhorn, N. Silverberg and B. Sundby, 1990. A mathematical model for manganese diagenesis in bioturbated sediments. Am. J. Sci. 290: 246-262.

Holdren, G.R., Jr., O.P. Bricker III and G. Matisoff, 1975. A model for the control of dissolved manganese in the interstitial water of Chesapeake Bay. p364-381. In: T.M. Church, ed. Marine chemistry in the coastal environment. ACS Symposium Series 18.

Hunt, C.D., 1983. Variability in the benthic Mn flux in coastal marine ecosystems resulting from temperature and primary production. Limnol. Oceanogr. 28: 913-923.

Jago, C.F., A.J. Bale, M.O. Green, M.J. Howarth, S.E. Jones, I.N. McCave, G.E. Millward, A.W. Morris, A.A. Rowden and J.J. Williams, 1993. Resuspension processes and seston dynamics, southern North Sea. Phil. Trans. R. Soc. London A 343: 379-596.

Jenness, M.I. and G.C. Duineveld, 1985. Effects of tidal currents on chlorofyll-a content of sandy sediments in the southern North Sea. Mar. Ecol. Prog. Ser. 21: 283-287.

Jensen, H.S. and B. Thamdrup, 1993. Iron-bound phosphorus in marine sediments as measured by bicarbonate-dithionite extraction. Hydrobiologia 253: 47-59

Joint, I. and A. Pomroy, 1993. Phytoplankton biomass and production in the southern North Sea. Mar. Ecol. Prog. Ser. 99: 169-182.

Jørgensen, B.B., 1982. Mineralization of organic matter in the sea bed - the role of sulphate reduction. Nature 296: 643-645.

Jørgensen, B.B., 1983. Processes at the sediment-water interface. p477-515. In: B. Bolin and R.B. Cook, eds. The major biogeochemical cycles and their interactions. John Wiley, Chichester.

Jørgensen B.B., 1989. Sulfate reduction in marine sediments from the Baltic Sea-North Sea transition. Ophelia 31: 1-15.

Li, Y.H. and S. Gregory, 1974. Diffusion of ions in sea water and deep sea sediments. Geochim. Cosmochim. Acta 38: 703-714.

Lohse L., J.F.P. Malschaert, C.P. Slomp, W. Helder and W. Van Raaphorst, 1993. Nitrogen cycling in North Sea sediments: interaction of denitrification and nitrification in offshore and coastal areas. Mar. Ecol. Prog. Ser. 101: 283-296.

Lohse L., J.F.P. Malschaert, C.P. Slomp, W. Helder and W. Van Raaphorst, 1995. Sediment-water fluxes of inorganic nitrogen compounds along the transport route of organic matter in the North Sea. Ophelia 41: 173-197.

Lohse L., E.H.G. Epping, W. Helder and W. van Raaphorst, 1996. Oxygen pore water profiles in continental shelf sediments of the North Sea: turbulent versus molecular diffusion. Mar. Ecol. Prog. Ser. 145: 63-75.

McCave, I.N., R.J. Bryant, H.F. Cook and C.A. Coughanowr, 1986. Evaluation of a laser diffraction size analyzer for use with natural sediments. J. Sed. Petrol. 56: 561-564.

Middelburg, J.J., G.J. de Lange and C.H. van der Weijden, 1987. Manganese solubility control in marine pore waters. Geochim. Cosmochim. Acta 51: 759-763.

Myers, C.R. and K.H. Nealson, 1988. Microbial reduction of manganese oxides: Interactions with iron and sulfur. Geochim. Cosmochim. Acta 52: 2727-2732.

Nolting, R.F. and D. Eisma, 1988. Elementary composition of suspended particulate matter in the North Sea. Neth. J. Sea Res. 22: 219-236.

Pettijohn, F.J., P.E. Potter and R. Siever, 1972. Sand and sandstone. Springer, New York. 618p.

Pohlmann, T. and W. Puls, 1994. Currents and transport in water. p345-402. In: J. Sündermann, ed. Circulation and contaminant fluxes in the North Sea. Springer.

Postma, D., 1985. Concentration of Mn and separation from Fe in sediments- I. Kinetics and stoichiometry of the reaction between birnessite and dissolved Fe(II) at 10°C. Geochim. Cosmochim. Acta 49: 1023-1033.

Rabouille, C. and J.F. Gaillard, 1991. Towards the EDGE: Early diagenetic global explanation. A model depicting the early diagenesis of organic matter, O_2, NO_3, Mn and PO_4. Geochim. Cosmochim. Acta 55: 2511-2525.

Robbins, J.A. and E. Callender, 1975. Diagenesis of manganese in Lake Michigan sediments. Am. J. Sci. 275: 512-533.

Saager P.M., J.P. Sweerts and H.J. Ellermeijer, 1990. A simple pore-water sampler for coarse sandy sediments of low porosity. Limnol. Oceanogr. 35: 747-751.

Schink, D.R. and N.L. Guinasso, 1978. Redistribution of dissolved and adsorbed materials in abyssal marine sediments undergoing biological stirring. Am. J. Sci. 278: 687-702.

Shimmield, G.B. and T.F. Pedersen, 1990. The geochemistry of reactive trace metals and halogens in hemipelagic continental margin sediments. Rev. Aq. Sci. 3: 255-279.

Slomp, C.P., S.J. Van der Gaast and W. Van Raaphorst, 1996. Phosphorus binding by poorly crystalline iron oxides in North Sea sediments. Mar. Chem.52: 55-73.

Slomp, C.P., J.F.P. Malschaert and W. Van Raaphorst, 1997. The role of sorption in sediment-water exchange of phosphate in North Sea continental margin sediments. Limnol. Oceanogr., submitted.

Soetaert, K., P.M.J. Herman and J.J. Middelburg, 1996. A model of early diagenetic processes from the shelf to abyssal depths. Geochim. Cosmochim. Acta 60: 1019-1040.

Strickland, T.R. and J.D. Parsons, 1972. A practical handbook of seawater analysis. 2nd. edition, Bulletin 167, Fisheries Research Board of Canada, 311p.

Stumm, W. and J.J. Morgan, 1981. Aquatic Chemistry. 2nd edition. Wiley, New York, 780p.

Sundby, B. and N. Silverberg, 1985. Manganese fluxes in the benthic boundary layer. Limnol. Oceanogr. 30: 374-382.

Tappin, A.D., G.E. Millward, P.J. Statham, J.D. Burton and A.W. Morris, 1995. Trace metals in the central and southern North Sea. Est. Coast. Shelf Sci. 41: 275-323.

Thamdrup, B., R.N. Glud and J.W. Hansen, 1994a. Manganese oxidation and in situ manganese fluxes from a coastal sediment. Geochim. Cosmochim. Acta 58: 2563-2570.

Thamdrup, B., H. Fossing and B.B. Jorgensen, 1994b. Manganese, iron, and sulfur cycling in a coastal marine sediment, Aarhus Bay, Denmark. Geochim. Cosmochim Acta 58: 5115-5129.

Ullman, W.J. and R.C. Aller, 1982. Diffusion coefficients in nearshore marine sediments. Limnol. Oceanogr. 27: 552-556.

Upton, A.C., D.B. Nedwell, R.J. Parkes and S.M. Harvey, 1993. Seasonal benthic microbial activity in the southern North Sea; oxygen uptake and sulphate reduction. Mar. Ecol. Prog. Ser. 101: 273-281.

Van Cappellen, P. and Y. Wang, 1996. Cycling of iron and manganese in surface sediments: a general theory for the coupled transport and reaction of carbon, oxygen, nitrogen, sulfur, iron and manganese. Am. J. Sci. 296: 197-243.

Van Weering T.C.E., G.W. Berger and J. Kalf, 1987. Recent sediment accumulation in the Skagerrak, northeastern North Sea. Neth. J. Sea Res. 21: 177-189.

Verardo D.J., P.N. Froelich and A. McIntyre, 1990. Determination of organic carbon and nitrogen in sediments using the Carlo Erba Na-1500 analyzer. Deep-Sea Res. 37: 157-165.

Von Haugwitz W., H.K. Wong and U. Salge, 1988. The mud area southeast of Helgoland: A seismic study. Mitt. Geol.-Paläont. Inst. Univ. Hamburg. 65: 409-422.

Yeats, P.A. and P.M. Strain, 1990. The oxidation of manganese in seawater: Rate constants based on field data. Est. Coast. Shelf Sci. 31: 11-24.

APPENDIX

A. The differential equations for dissolved Mn^{2+} and Mn oxide in the oxic (I: $0 \leq x \leq L_1$) and anoxic (II: $x > L_1$) sediment zone are:

Dissolved Mn^{2+} (C)

$$[(1 + K_s)D_b + D_s]\frac{d^2 C_I}{dx^2} - \omega(1 + K_s)\frac{dC_I}{dx} - k_{ox}C_I = 0 \qquad (A1)$$

$$[(1 + K_s)D_b + D_s]\frac{d^2 C_{II}}{dx^2} - \omega(1 + K_s)\frac{dC_{II}}{dx} - k_a(C_{II} - C_a) + 9k_r(S_{II} - S_r) = 0 \qquad (A2)$$

Mn oxide (S)

$$D_b \frac{d^2 S_I}{dx^2} - \omega \frac{dS_I}{dx} + \frac{k_{ox}}{9} C_I = 0 \tag{A3}$$

$$D_b \frac{d^2 S_{II}}{dx^2} - \omega \frac{dS_{II}}{dx} - k_r (S_{II} - S_r) = 0 \tag{A4}$$

B. With $D_s^* = (1 + K_s)D_b + D_s$ and $\omega^* = (1 + K_s)\omega$, the boundary conditions used to solve equations (A1)-(A4) are:

at $x = 0$

$$C_I = C_o \tag{B1}$$

$$J_{S\,x=0} = -[D_b \frac{dS_I}{dx} - \omega S_I]\phi 9 \tag{B2}$$

at $x = L_1$

$$C_I = C_{II} \tag{B3}$$

$$S_I = S_{II} \tag{B4}$$

$$D_s^* \frac{dC_I}{dx} - \omega^* C_I = D_s^* \frac{dC_{II}}{dx} - \omega^* C_{II} \tag{B5}$$

$$D_b \frac{dS_I}{dx} - \omega S_I = D_b \frac{dS_{II}}{dx} - \omega S_{II} \tag{B6}$$

at $x \to \infty$

$$C_{II} = C_a \tag{B7}$$

$$S_{II} = S_r \tag{B8}$$

C. With the boundary conditions (B1) to (B8) the solutions of equations (A1) to (A4) for the oxic (I: $0 \le x \le L_1$)) and anoxic (II: $x > L_1$) zone are:

$$C_I = A_1 \exp[(O + P)x] + A_2 \exp[(O - P)x] \tag{C1}$$

$$C_{II} = B_2 \exp[(O - Q)x] + G_1 \exp[(M - N)(x - L_1)] + C_a \tag{C2}$$

$$S_I = C_1 + C_2 \exp[(\frac{\omega}{D_b})x] + D_1 \exp[(O + P)x] + D_2 \exp[(O - P)x] \tag{C3}$$

$$S_{II} = E_2 \exp[(M - N)(x - L_1)] + S_r \tag{C4}$$

where

$$M = \frac{\omega}{2D_b}; \quad N = \frac{\sqrt{\omega^2 + 4k_r D_b}}{2D_b}; \quad O = \frac{\omega^*}{2D_s^*}; \quad P = \frac{\sqrt{\omega^{*2} + 4k_{ox} D_s^*}}{2D_s^*}; \quad Q = \frac{\sqrt{\omega^{*2} + 4k_a D_s^*}}{2D_s^*};$$

$$\beta = \exp[(O + P)L_1] \; ; \; \gamma = \exp[(O - P)L_1] \; ; \; \delta = \exp[(O - Q)L_1] \; ; \; \eta = \exp[(\frac{\omega}{D_b})L_1] \; ;$$

$$A_1 = C_o - A_2 \; ; \; A_2 = \frac{C_o \beta(P + Q) + C_a(O - Q) + G_1(O - Q - M + N)}{\gamma(P - Q) + \beta(P + Q)} = a_1 + a_2 G_1 \; ;$$

$$B_2 = \frac{A_1 \beta + A_2 \gamma - C_a - G_1}{\delta} \; ;$$

$$C_1 = \frac{D_1 D_b(O + P) + D_2 D_b(O - P) - \dfrac{J_{Sx=0}}{\phi \vartheta}}{\omega} - (D_1 + D_2) \; ; \quad C_2 = \frac{E_2 + S_r - C_1 - D_1 \beta - D_2 \gamma}{\eta} \; ;$$

$$D_1 = -\frac{k_{ox} A_1}{\vartheta[D_b(O + P)^2 - \omega(O + P)]} = d_1 A_1$$

$$D_2 = -\frac{k_{ox} A_2}{\vartheta[D_b(O - P)^2 - \omega(O - P)]} = d_2 A_2 \; ; \; G_1 = -\frac{\vartheta k_r E_2}{D_s^*(M - N)^2 - \omega^*(M - N) - k_a} = g_1 E_2 \; ;$$

$$E_2 = \frac{t_2(\dfrac{\omega}{D_b}) - t_4}{t_1(\dfrac{\omega}{D_b}) - t_3} \; ; \; t_1 = 1 + (d_1 g_1 a_2)(\frac{D_b(O + P)}{\omega} + \beta - 1) - (d_2 g_1 a_2)(\frac{D_b(O - P)}{\omega} + \gamma - 1) \; ;$$

$$t_2 = -\frac{J_{Sx=0}}{\omega \phi \vartheta} - S_r + (d_1 C_o - d_1 a_1)(\frac{D_b(O + P)}{\omega} + \beta - 1) + (a_1 d_2)(\frac{D_b(O - P)}{\omega} + \gamma - 1) \; ;$$

$$t_3 = (M - N) + d_1 g_1 a_2 \beta(O + P) - d_2 g_1 a_2 \gamma(O - P) \; ; \; t_4 = \beta(O + P)(d_1 C_o - d_1 a_1) + \gamma(O - P)d_2 a_1 .$$

D. Depth integrated processes:

Oxic prec. rate $\quad = \phi k_{ox} \int_0^{L_1} C_I = \phi k_{ox} \dfrac{A_1}{(O + P)}(1 - \beta) + \phi k_{ox} \dfrac{A_2}{(O - P)}(1 - \gamma)$

Anoxic prec. rate $\quad = \phi k_a \int_{L_1}^{L_2} (C_{II} - C_a) = \phi k_a \dfrac{B_2}{(O - Q)}(\delta - \tau) + \phi k_a \dfrac{G_1}{(M - N)}(1 - \lambda)$

with $\tau = \exp[(O - Q)L_2]$; $\lambda = \exp[(M - N)(L_2 - L_1)]$

and with L_2 being the lower boundary of the sediment-column under study

Mn oxide red. rate $\quad = \phi \vartheta k_r \int_{L_1}^{L_2} (S - S_r) = \phi \vartheta k_r \dfrac{E_2}{(M - N)}(\lambda - 1)$

Sediment-water exchange rate of dissolved Mn^{2+}:

$$= D_s^* \phi(\frac{dC_I}{dx})_{x=0} = D_s^* \phi[A_1(O + P) + A_2(O - P)]$$

Chapter 5

The role of sorption in sediment-water exchange of phosphate in North Sea continental margin sediments[*]

ABSTRACT

The effect of sorption on the sediment-water exchange of HPO_4^{2-} was investigated for sediments located in 4 different types of sedimentary environments in the southern and eastern North Sea in August 1991 and February 1992. Non-linear sorption isotherms for oxidized sediment from 8 stations indicate that North Sea sediments differ widely in their capacity to sorb HPO_4^{2-}. A good correlation between the value of the sorption coefficient at a HPO_4^{2-} concentration of 1 μmol dm^{-3} and NH_4-oxalate Fe was observed. Results of kinetics experiments for 2 stations show that the sorption process can be adequately modelled assuming concurrent equilibrium and first-order kinetic sorption. A combination of the sorption data with pore water HPO_4^{2-} profiles, solid phase results, and measured and calculated rates of sediment-water exchange of HPO_4^{2-} for 15 stations in both August and February indicates that sorption plays an important role in controlling sediment-water exchange of HPO_4^{2-} during at least a part of the year in 3 of the 4 North Sea environments. At most stations, HPO_4^{2-} adsorption constrains the flux of HPO_4^{2-} to the overlying water. At one station in the depositional environment of the Skagerrak, however, desorption is responsible for the maintenance of a flux of HPO_4^{2-} to the overlying water. A one-dimensional reaction-diffusion model describing pore water HPO_4^{2-} and solid phase P profiles was developed and applied to results for 2 stations. The model results show that both enhanced retention and enhanced release of HPO_4^{2-} due to sorption can be adequately described when simultaneous equilibrium and first-order kinetic reversible sorptive reactions are assumed.

INTRODUCTION

A substantial proportion (10-50%) of the pelagic primary production may reach the sea floor in continental margin environments (Jørgensen, 1983). When this organic material is mineralized in the sediment, this results in a release of dissolved HPO_4^{2-} to the pore water. This HPO_4^{2-} can be retained in the sediment but may also escape to the overlying water, where it once again can become available for uptake by phytoplankton (e.g. Howarth et al., 1995).

Phosphorus (P) retention and release in marine sediments at short time scales are usually considered to be redox-dependent. When an oxidized surface layer is present, substantial amounts of HPO_4^{2-} can be retained in the sediment through sorption to Fe oxides (e.g.

Krom and Berner, 1980b and 1981; Sundby et al., 1992; Jensen et al., 1995). This sorption process generally results in a buffering of pore water HPO_4^{2-} concentrations to low values in the oxidized sediment zone (Froelich, 1988; Sundby et al., 1992), thus allowing only limited diffusive transport of HPO_4^{2-} to the overlying water. When, in contrast, the oxidized surface layer is thin or absent, the HPO_4^{2-} released from organic matter and from Fe oxides upon their reduction can escape to the overlying water. This was first decribed for lake sediments by Einsele (1936) and Mortimer (1941, 1942). Redox-dependent sediment HPO_4^{2-} release has also been simulated in long-term bell-jar incubations of coastal sediments (Balzer, 1984; Sundby et al., 1986) and has been observed in several continental margin environments (Ingall and Jahnke, 1994).

The presence of an oxidized surface layer containing Fe oxides does not preclude release of dissolved HPO_4^{2-} from sediments, however. There are three reasons for this. First, organic matter deposited on the sediment can be mineralized rapidly at or close to the sediment-water interface, allowing a large proportion of the released HPO_4^{2-} to escape directly to the overlying water (Martens et al., 1978). Second, sediment irrigation may result in direct, non-local transport of pore water from below the oxidized zone to the overlying water (e.g. Aller, 1980, Emerson et al., 1984; Boudreau, 1984; Aller and Yingst, 1985). Third, the sorption to Fe oxides is rapid and at least partly reversible (Carritt and Goodgal, 1954; Froelich, 1988; Sundby et al., 1992). Thus, sorption may allow the sustainment of a sharp gradient in dissolved HPO_4^{2-} near the sediment-water interface. This may result in a substantial flux of dissolved HPO_4^{2-} to the overlying water, even when HPO_4^{2-} concentrations in the oxidized surface sediment are low. This has been demonstrated for intertidal sediments with a kinetic model for HPO_4^{2-} sorption in surface sediments (Van Raaphorst et al., 1988; Van Raaphorst and Kloosterhuis, 1994).

Such a desorption enhanced flux can only be maintained over longer periods of time when there is a sufficient supply of HPO_4^{2-} to the sediment near the sediment-water interface. Since the buffering of pore water HPO_4^{2-} concentrations precludes supply through aqueous diffusive transport of HPO_4^{2-}, this P must be supplied as desorbable Fe-bound P. This Fe-bound P may be deposited from the overlying water or may be formed near the redox boundary and subsequently transported upward through bioturbation. The importance of this latter mechanism depends on the rate of sediment mixing and the in-situ sorption coefficient, as was demonstrated with an equilibrium model for sorption by Schink and Guinasso (1978).

In the current models used to describe the effect of sorption on sediment-water exchange of dissolved constituents, sorption is assumed to be either instantaneous (Schink and Guinasso, 1978) or is assumed to follow first-order kinetics (Van Raaphorst et al., 1988). Many laboratory studies with synthetic and natural Fe oxides have shown, however, that P

sorption comprises both fast and slow reactions. Rapid P sorption presumably results from the reaction of P with surface sites on Fe oxides (Parfitt, 1978). Slow P sorption has been attributed to slow diffusion into Fe-oxide crystals (Barrow, 1983; Parfitt, 1989) or aggregates of crystals (Madrid and Arambarri, 1985; Willett et al., 1988; Torrent et al., 1992), and slow formation of P-containing precipitates (Van Riemsdijk et al., 1984). Slow sorption is usually found to be more pronounced for poorly ordered Fe oxides, such as e.g. ferrihydrite, than for more crystalline minerals such as hematite and goethite (Parfitt, 1989; Torrent et al., 1992). The Fe oxides that are formed in-situ in marine sediments and that are responsible for the binding of P are probably mainly poorly crystalline (Slomp et al., 1996a). Consequently, the present practice of assuming only one type of sorption reaction when modelling the effect of sorption on sediment-water exchange of HPO_4^{2-} in marine environments may strongly bias the results.

The aim of this study was to determine the role of HPO_4^{2-} sorption to Fe oxides in controlling sediment-water exchange of dissolved HPO_4^{2-} in different types of continental margin environments. To reach this aim, we measured pore water profiles of HPO_4^{2-} and Fe^{2+}, rates of sediment-water exchange of HPO_4^{2-} and solid phase P and Fe concentrations in the surface sediment at 15 locations in the southern and eastern North Sea, in August 1991 and February 1992. The results for 2 stations are combined with data on HPO_4^{2-} sorption and profiles of solid phase P (Fe-bound, organic and Ca-bound P) using a one-dimensional reaction-diffusion model. This model describes the sedimentary cycle of P and takes both fast and slow HPO_4^{2-} sorption kinetics into account.

STUDY SITES

A total of 15 stations located in the southern and eastern North Sea, including the Skagerrak, were visited during 2 cruises with RV Pelagia in August 1991 and February 1992 (Fig. 1). The positions, water depths and bottom water temperatures of these stations are listed in Table 1. An extensive description of the general characteristics of the stations visited (Lohse et al., 1995; Slomp et al., 1997) as well as data on O_2 dynamics, NH_4 sorption and Fe, Mn, N and Si cycling are given elsewhere (Gehlen et al., 1995; Lohse et al., 1993, 1995, 1996; Slomp et al., 1996a, 1997; Van Raaphorst and Malschaert, 1996). The stations are located along the main transport route of suspended matter in the North Sea (Fig. 1). Based on sediment grain size and the quality of the organic matter deposited at these stations, 4 clusters of stations are distinguished (Table 2 and Lohse et al., 1995). Cluster IA and IB consist of stations with silty sediments located in the depositional environments of the German Bight and the Skagerrak with sedimentation rates of 0.5-1 cm y^{-1} (Eisma and Kalf, 1987; Von Haugwitz et al., 1988) and 0.1-0.5 cm y^{-1} (Van Weering et
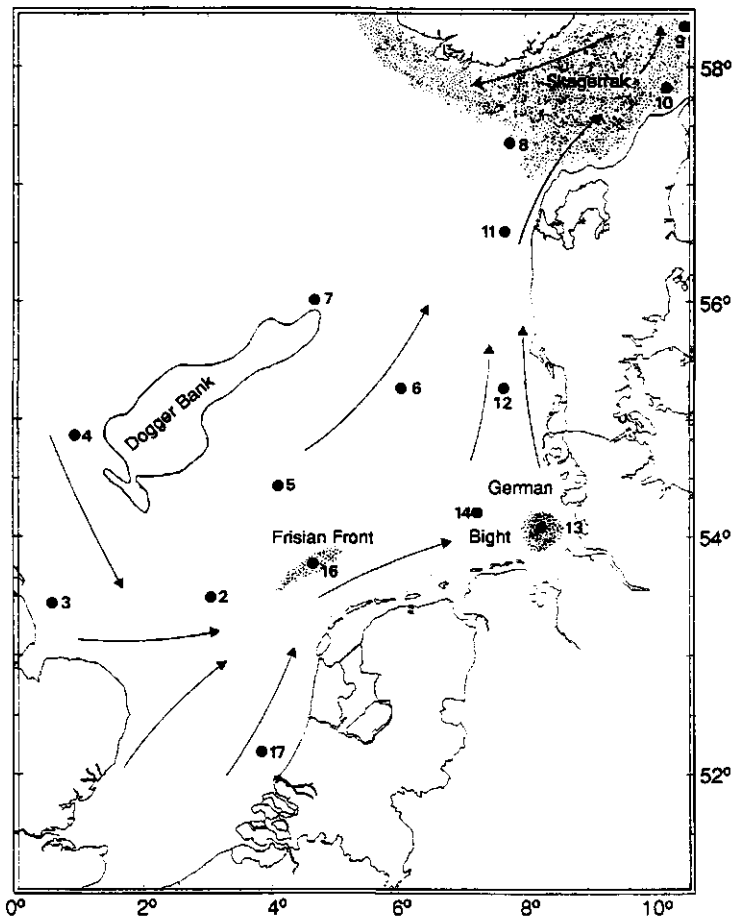
Fig. 1. Map of the North Sea showing the sampling locations and station numbers. Arrows indicate the main transport routes of water and suspended matter in the North Sea. Stippled areas indicate main depositional regions.

al., 1987; Anton et al., 1993), respectively. Large amounts of fresh organic material are deposited in the shallow area of the German Bight in summer. Organic matter inputs in the Skagerrak are dominated by a more or less constant inflow of relatively refractory compounds from other areas. Cluster II consists of stations with fine sandy sediment in areas with frequent temporary deposition of organic matter. Cluster III, finally, consists of stations with medium sandy sediments, where erosion is dominant and where organic matter deposition is restricted to periods of calm weather.

Table 1. Number, name, geographical position, water depth and bottom water temperature (February, August) at the 15 visited stations.

No.	Station	Geographical position		Water depth	Temperature (°C)	
		N	E	(m)	Aug-91	Feb-92
2	Boundary	53°30'	03°01'	33	16.8	5.8
3	Silverpit	53°28'	00°40'	89	14.4	-
4	Doggerbank	54°50'	01°00'	58	8.2	6.4
5	Oystergrounds	54°25'	04°04'	49	10.2	6.4
6	Weiss Bank	55°17'	06°00'	49	12.2	5.8
7	Tail End	56°00'	04°38'	50	9.5	6.1
8	Skagerrak W.	57°26'	07°37'	130	7.3	6.4
9	Skagen	58°20'	10°27'	330	6.9	7.0
10	Hirtshals	57°50'	10°01'	64	12.2	6.8
11	Jutland	56°40'	06°43'	41	10.0	5.2
12	Esbjerg	55°12'	07°38'	25	17.7	4.8
13	Helgoland Bight	54 05'	08°09'	19	18.7	4.4
14	Elbe Rinne	54°14'	07°20'	39	16.5	5.4
16	Frisian Front	53°42'	04°32'	39	17.4	6.3
17	Hook of Holland	52°07'	03°45'	26	18.5	5.8

EXPERIMENTAL METHODS

Sample collection. Sediment cores were collected with a cylindrical box corer (31 cm i.d.) which enclosed 30 to 50 cm of sediment column together with 20 to 40 cm of overlying water. Subcores were taken with plastic liners. All subsequent sediment handling took place on board ship at in situ temperature.

Pore water and solid phase analysis. To obtain pore water, sediment was sliced in 9 depth intervals (0-0.4, 0.4-1.0, 1.0-1.5, 1.5-2.0, 2.0-3.0, 3.0-4.0, 4.0-6.0, 6.0-8.0, 8.0-10.0 cm) under N_2 immediately after core collection. Slices from each interval were pooled and centrifuged at 1700 g for 10 minutes. Bottom water samples were obtained from the overlying water from one of the box cores. The filtered (cellulose acetate, 0.45 μm) samples were acidified to pH $\approx$ 1 and stored at 4°C until analysis for HPO_4^{2-} and Fe^{2+}. Unacidified samples gave erroneously low HPO_4^{2-} concentrations for slices from below the oxidized zone, presumably due to Fe oxide precipitation in the sample vials (see Bray et al., 1973).

Sediment sliced from 7 depth intervals (0-0.5, 0.5-1.0, 1.0-2.0, 2.0-4.0, 4.0-6.0, 6.0-8.0, 8.0-12.0 cm) was stored frozen (-20°C) until solid phase analysis. Porosity was determined by weight loss of the sediment after drying at 60°C for 48 h and assuming a specific sediment weight of 2.65 kg dm^{-3}. Organic C and total N were measured with a Carlo Erba 1500-2 elemental analyzer. Organic C was determined as the C concentration in the samples after treatment with sulfurous acid (Verardo et al., 1990). All sediment N was assumed to be present in an organic form. Grain size distribution was determined with a

Malvern particle analyzer (McCave et al., 1986) after removal of carbonate and organic matter with HCl and H_2O_2.

Three non-sequential extraction procedures were used for the determination of the sediment P speciation: (1) Citrate-dithionite-bicarbonate extractable P (CDB P; pH=7.3, 8 h, 20°C) was assumed to represent total Fe-bound P (Ruttenberg, 1992); (2) 1 M HCl extractable P (24h, 20°C) was used as a measure for inorganic P; (3) 1 M HCl extractable P after ignition of the sediment (24 h, 550°C) was assumed to represent total P. Organic P was determined as the difference between total and inorganic P (Aspila et al., 1976; Ruttenberg, 1992). The difference between inorganic and Fe-bound P was used as a measure for Ca-bound P (presumably detrital and authigenic apatite and perhaps also some $CaCO_3$-bound P). Untreated, wet sediment was used for the CDB procedure. Oven-dried (60°C), ground (teflon mortar and pestle) material was used for the HCl extractions. The extractions were applied to surface samples (0-0.5 cm) from all stations collected in February (CDB, HCl) and August (HCl). Complete profiles were only obtained for stations 9 (February) and 14 (February and August). The precision of the individual P extractions was generally ~5%. At stations where organic P concentrations were low (< 2 μmol g^{-1}), the organic P concentration was equal to the very small difference between relatively large numbers. This resulted in large uncertainties in the organic P concentrations (on average ~50 %) and these results should therefore be interpreted with caution.

0.2 M NH_4-oxalate/oxalic acid buffer (2 h, oxic conditions in the dark; Schwertmann and Cornell, 1991) was used to dissolve Fe present in poorly crystalline Fe oxides (Slomp et al., 1996a) in surface sediment (0-0.5 cm) collected at all stations in February 1992.

Sediment-water exchange rates of HPO_4^{2-}. Fluxes of HPO_4^{2-} across the sediment-water interface were measured using 5 intact sediment cores (i.d. 10 cm) of which the overlying water was carefully replaced by 0.75 dm^3 of filtered (cellulose acetate, 0.45 μm) bottom water to exclude effects of algae or suspended particles on the measured fluxes. All cores were incubated for 6 h at in-situ temperature under constant bubbling of air which kept the overlying water well-mixed and saturated with O_2 (Van Raaphorst and Kloosterhuis, 1994). Samples (a total of 7) were taken each 30-120 minutes, filtered (cellulose acetate, 0.45 μm) and analyzed for HPO_4^{2-} on board. Fluxes were calculated from the change in the amount of dissolved HPO_4^{2-} in the overlying water corrected for the volume change due to sampling.

Diffusive fluxes were calculated from the pore water profiles using Fick's first law. The concentration gradient at the sediment-water interface was estimated from the dissolved HPO_4^{2-} concentration in the overlying water and the average concentration in the 0-0.4 cm

Table 2: General sediment characteristics at the 15 stations. Clusters indicate depositional (IA and B), transitional (II) and erosional (III) areas. All sediment parameters were determined for the 0-0.5 cm sediment layer in February 1992 (with the exception of station 3). Sediment classification is based on the Wentworth size scale (Pettijohn et al, 1972).

Cluster	Station no.	Organic C (wt %)	Organic N (wt %)	Porosity (vol vol^{-1})	Median grain size (μm)	Sediment classification (Wentworth)
IA	13	0.74	0.092	0.63	15	medium silt
IB	9	2.76	0.334	0.89	6	medium silt
	10	0.82	0.099	0.73	36	coarse silt
II	2	0.19	0.034	0.50	128	fine sand
	5	0.17	0.026	0.49	103	very fine sand
	6	0.17	0.023	0.58	85	very fine sand
	7	0.15	0.025	0.42	125	fine sand
	8	0.14	0.018	0.41	175	fine sand
	12	0.07	0.014	0.40	187	fine sand
	14	0.39	0.049	0.57	98	very fine sand
	16	0.28	0.033	0.54	75	very fine sand
III	3	-	-	-	>350	medium sand
	4	0.03	0.004	0.44	>295	medium sand
	11	0.03	0.008	0.36	>300	medium sand
	17	0.04	0.002	0.37	>340	medium sand

depth interval in the sediment. The diffusion coefficient (D_s) was calculated from the data of Krom and Berner (1980a) correcting for temperature and porosity.

Sorption experiments. Sorption isotherms were determined for 8 stations (st. 5, 8, 9, 10, 13, 14, 16 and 17) directly after sediment retrieval in February. Centrifuge tubes (50 cm^3) were filled with 5 or 15 cm^3 of fresh wet surface sediment (0-0.5 cm depth) and 30 or 15 cm^3 of filtered (0.2 μm), low nutrient ([HPO_4^{2-}] = 0.05 μmol dm^{-3}), ocean water spiked with various amounts of dissolved HPO_4^{2-}. The added amounts of HPO_4^{2-} were such that final HPO_4^{2-} concentrations at the end of each experiment mostly ranged between 0.5 and 10 μmol dm^{-3}. The total volume of the sediment slurries was either 30 or 35 cm^3. All tubes were shaken vigorously immediately, then every 15 minutes during the first hour and subsequently, every few hours until final sampling after 48 hours. After centrifugation (1700 g, 15 min.) the supernatant was removed, filtered (0.45 μm) and analyzed for HPO_4^{2-} and $Si(OH)_4$. The $Si(OH)_4$ analysis was included to determine whether silicate sorbed to Fe oxides was displaced by HPO_4^{2-}. The sediment residue was dried (60°C) and weighed. The amount of P sorbed to the sediment was calculated from the change in the HPO_4^{2-} concentration during the experiment.

To obtain insight in the kinetics of sorption, 4-6 centrifuge tubes were filled with 15 cm³ of fresh wet sediment and incubated with 15 cm³ of oceanwater. Initial concentrations of HPO_4^{2-} ranged between 6 and 10 µmol dm⁻³. The tubes were removed at different time intervals during the 48 hour incubation (the first at t = 15 min.). Additional incubations were carried out with sediment from 2 North Sea locations representative for stations 5 and 17 during a separate cruise in February 1993. In this case, 18 to 20 tubes were filled with 5 cm³ wet sediment and 30 cm³ ocean water and initial HPO_4^{2-} concentrations were higher: 55.4 (st. 5) and 41.2 µmol dm⁻³ (st. 17).

Sorption isotherms were obtained by plotting the amount of HPO_4^{2-} adsorbed on or desorbed from the sediment, calculated from the change in dissolved HPO_4^{2-} during the experiment, on the y-axis, and the final HPO_4^{2-} concentration in solution on the x-axis. The results were described with a Freundlich isotherm:

$$NAP + P_{sor} = K_F C^{1/n} \qquad (1)$$

where NAP (Native Adsorbed P) is the amount of P sorbed to the sediment at the start of the experiment (µmol g⁻¹), P_{sor} is the amount of P sorbed to the sediment during the experiment (µmol g⁻¹), K_F (dm³ g⁻¹) and n (dimensionless) are empirical constants and C is the final HPO_4^{2-} concentration (µmol dm⁻³). Values for NAP, K_F and n were obtained by fitting equation (1) directly to the experimental data by minimizing the sum of squared differences between the measured and calculated amounts of sorbed P. The HPO_4^{2-} concentration at which no sorption or desorption of HPO_4^{2-} occurs (Equilibrium Phosphate Concentration or EPC_o; e.g. Froelich, 1988), was calculated from:

$$EPC_o = 10^{n\log(\frac{NAP}{K_F})} \qquad (2)$$

Sorption coefficients (K_F') were calculated from the slope of the isotherms:

$$K_F' = \frac{K_F}{n} C^{(1/n-1)} \qquad (3)$$

The value of K_F' thus depends on the HPO_4^{2-} concentration. At C = 1 µmol dm⁻³, K_F' is equal to K_F/n. Dimensionless sorption coefficients (K_{dim}) were obtained by multiplying K_F' by a conversion factor ϑ, the in-situ solid-solution ratio in gram of dry sediment per dm³ of pore water (Krom and Berner, 1980b):

$$\vartheta = \rho_s[(1-\phi)/\phi] \tag{4}$$

where ρ_s is the average density of the sediment particles (2650 g dm^{-3}) and ϕ is the sediment porosity (dm^3 dm^{-3}).

A simple model was developed to describe the change in the HPO$_4^{2-}$ concentration with time during the kinetics experiments. The model is compatible with the assumption that two types of sorption sites are present which differ in their accessibility for HPO$_4^{2-}$ (Fuller et al., 1993; Lookman et al., 1995). These are presumably surface sites on Fe oxides and sites in Fe oxide crystals or aggregates of crystals (see introduction). HPO$_4^{2-}$ sorption is assumed to consist of 2 simultaneous, reversible reactions: an instantaneous, equilibrium reaction and a first-order process:

$$(1+K_{lin})\frac{dC}{dt} = -\Gamma k_k S(C-C_e) \tag{5}$$

where K_{lin} is a linear sorption coefficient for equilibrium sorption (dimensionless), C is the HPO$_4^{2-}$ concentration (μmol dm^{-3}), t is time (d^{-1}), Γ is the solid-solution ratio during the incubation (g dm^{-3}), k_k is the sorption mass transfer coefficient for the first-order reaction (dm d^{-1}), S is the specific surface area of the sorbing solids (dm^2 g^{-1}), and C_e is the equilibrium HPO$_4^{2-}$ concentration (μmol dm^{-3}) for the first-order reaction. It is important to note that the first-order approach gives a rather simple, non-mechanistic description of the slow sorption processes. The equilibrium that is assumed to be reached is an apparent, not actual equilibrium and the constant value of C_e has no direct physical or chemical relevance. Equation (5) was solved for the boundary conditions: $C = C_0$ at $t = 0$, where C_0 is the equilibrium concentration for the instantaneous sorption reaction and $C \rightarrow C_e$ when $t \rightarrow \infty$. This gives:

$$C = (C_0 - C_e)e^{-(\frac{\Gamma k_k S}{(1+K_{lin})})t} + C_e = (C_0 - C_e)e^{-\beta t} + C_e \tag{6}$$

Values of β, C_0 and C_e were estimated by fitting equation (6). An additional fit procedure was carried out in which C_e was set equal to the EPC$_0$ value calculated from the sorption isotherm (Table 4). K_{lin} was calculated as:

$$K_{lin} = \frac{P_{sor}}{(C_o - EPC_o)} = \frac{(C_i - C_o)}{(C_o - EPC_o)} \tag{7}$$

with C_i being equal to the initial HPO$_4^{2-}$ concentration of the incubation solution (μmol dm^{-3}) and P_{sor} to the amount of P sorbed to the sediment (μmol dm^{-3}) through equilibrium

sorption. The value of $k_k \times S$ was then calculated from β (equation 6). At in-situ sediment-solution ratios the first-order rate constant for the slow reaction is equal to $k_k \times S \times \vartheta$ (d^{-1}).

Chemical analysis of P, Fe and Si. HPO_4^{2-} was measured as soluble reactive P according to the method of Strickland and Parsons (1972) using either a Shimadzu Spectrophotometer (HCl extracts, pore water) or a TRAACS-800 autoanalyzer (sorption and flux experiments). Total P in the CDB solutions was measured using an Inductively Coupled Plasma-Atomic Emisson Spectrophotometer (ICP-AES; Spectro Analytical Instruments). Total Fe in the pore water samples (mostly present as Fe^{2+}) and in the NH_4-oxalate buffer solutions was measured using a Perkin Elmer 5100 Atomic Absorption Spectrophotometer. $Si(OH)_4$ in the sorption samples was measured on a TRAACS-800 autoanalyzer following the procedure of Strickland and Parsons (1972).

DESCRIPTION OF THE REACTION-DIFFUSION MODEL

To obtain more insight in the effect of sorption in surface sediments on the sediment-water exchange of HPO_4^{2-}, a one-dimensional reaction-diffusion model describing the sedimentary P cycle was developed. The steady state model describes the concentration change with depth of pore water HPO_4^{2-} (C), and 4 forms of particulate P, i.e. organic P (G), Fe-bound P (M), sorbed P (S), and Ca-bound P (A) which includes both detrital Ca-P, $CaCO_3$-P and authigenically formed carbonate fluorapatite (CFA; Van Cappellen and Berner, 1988; Ruttenberg and Berner, 1993; Slomp et al., 1996b). Transport of solid phase P is assumed to occur through bioturbational/physical mixing, described as a biodiffusion process, and through sediment accumulation. Transport of dissolved HPO_4^{2-} additionally is assumed to take place through molecular diffusion and burrow irrigation. The latter process is modelled by including a non-local source/sink term that permits the exchange of pore water from any depth in the sediment (within the depth interval under study; this should not exceed the depth where burrowers can be active) and the overlying water (Emerson, et al., 1984; Boudreau, 1984).

The sediment column is divided into 2 zones (Fig. 2): an oxidized surface zone (I: $0 \leq x \leq L_1$) and a reduced sediment zone (II: $x > L_1$). The processes included are (1) release of HPO_4^{2-} from organic P due to organic matter mineralization (zone I and II), (2) reversible kinetic sorption of HPO_4^{2-} to Fe oxides resulting in Fe-bound P formation (zone I), (3) reversible equilibrium sorption of HPO_4^{2-} assuming a linear isotherm resulting in the presence of sorbed P (zone I and II), (4) release of HPO_4^{2-} from Fe-bound P due to reductive dissolution of Fe oxides (zone II) and (5) precipitation of an authigenic Ca-P mineral (zone II). All release and removal processes, with the exception of (3) are described as first-order reactions, with the rate being equal to a rate constant times the difference
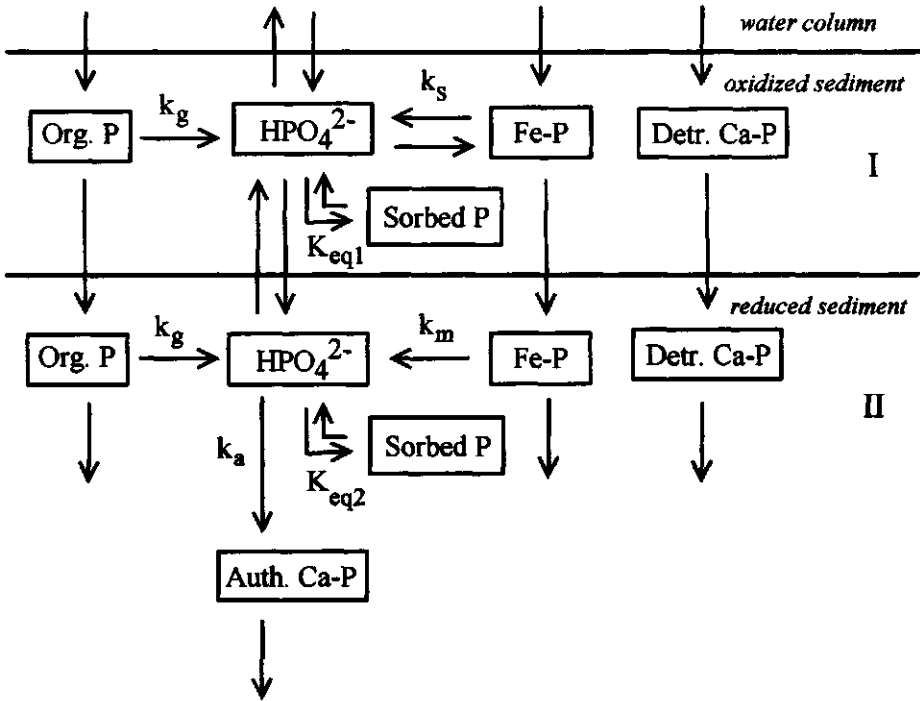
Fig. 2. Schematic representation of the sedimentary P cycle as assumed in the model. For an explanation of the symbols, see the text.

between the actual concentration and an equilibrium (pore water) or asymptotic (solid phase) value. The rate constants for the processes (1), (2), (4) and (5) listed above are k_g, k_s, k_m, and k_a, respectively. The pore water equilibrium concentrations for kinetic sorption and for authigenic P precipitation are C_s and C_a, respectively. The particulate P concentrations of Fe-bound and organic P at which no further release occurs are equal to M_∞ and G_∞. The dimensionless sorption coefficients for equilibrium sorption in zone I and II are K_{eq1} and K_{eq2}, respectively.

Pore water HPO_4^{2-} and the particulate P forms have units of mol per m^3 pore water and µmol per gram of dry sediment, respectively. A conversion factor 9 (equation 4, in units of g cm^{-3}) is used to enable combination of dissolved HPO_4^{2-} and solid phase P in one model. The molecular (D_s) and biodiffusion (D_b) coefficients (both in units of m^2 d^{-1}), the sedimentation rate (ω, in units of m d^{-1}), the non-local transport coefficient (α, in units of d^{-1}), the reaction rate constants (k_g, k_s, k_m and k_a in units of d^{-1}), the sorption coefficients

for equilibrium sorption in each zone (K_{eq1} and K_{eq2}) and sediment porosity (ϕ, in units of $m^3 \, m^{-3}$) are assumed to be constant with depth in each relevant layer.

The set of differential equations for the one-dimensional distribution of pore water HPO_4^{2-} (C) and three particulate P forms (G, M, A) are given in the Appendix (A1-A8). Instantaneous, reversible linear equilibrium sorption makes the amount of sorbed P (S) a known function of pore water HPO_4^{2-} (Appendix: A9-A10). The equations A1-A8 were solved analytically assuming continuity in concentrations and fluxes of both dissolved HPO_4^{2-} and solid phase P at the boundary between the two sediment zones ($x = L_1$) and considering appropriate conditions at $x = 0$ and $x \to \infty$. Constant fluxes of organic P, Fe-bound P and Ca-bound P from the overlying water to the sediment were assumed at $x = 0$ ($J_{Gx=0}$, $J_{Mx=0}$, $J_{Ax=0}$, respectively). The pore water HPO_4^{2-} concentration at $x = 0$ was assumed to be equal to the bottom water concentration (C_0). When $x \to \infty$, asymptotic values for organic P and Fe-bound P (G_∞ and M_∞) are assumed to be reached. Additionally, the pore water HPO_4^{2-} concentration is assumed to reach a constant value (E), and the gradient in authigenic P (A) is assumed to be zero. This latter assumption only holds when $C_a = C_0$, so when including authigenic P formation in the model calculations, C_a must always be set equal to C_0. The mathematical expressions for these boundary conditions are given in the Appendix (A11-A26).

Three model settings (termed model i, ii and iii) were used when applying the model to measured pore water HPO_4^{2-} and solid phase P profiles. Further details are given in the model application section. In each model setting, up to 8 of the following 9 parameters ($J_{Gx=0}$, $J_{Ax=0}$, $J_{Mx=0}$, G_∞, M_∞, k_s, k_g, k_a, α) were varied to fit the model to experimental data using iteratively reweighted regression (Draper and Smith, 1967). Variance-weighted sums of squares of the difference between the modelled and experimental values were minimized for all 4 components, i.e. HPO_4^{2-}, organic P, Fe-bound P and Ca-bound P, simultaneously. This means that up to 8 fit parameters were used for 4 profiles with a total of 30 data points. The relatively large number of parameters did not lead to a large degree of freedom when fitting the parameters, due to the strongly coupled nature of the equations (see Van Cappellen and Wang, 1996). The other parameters (L_1, ϕ, D_s, D_b, ω, C_0, C_a, C_s, K_{eq1}, K_{eq2}, k_m) were fixed based on experimental results obtained in this study and data from the literature.

EXPERIMENTAL RESULTS

Sediment characteristics. Sediment porosity, organic C, N and P and inorganic P concentrations were considerably higher in the silty sediments (cluster IA and B) than in the sandy sediments (cluster II and III; Tables 2 and 3). There was no significant seasonal difference in organic C, N and P, and inorganic P concentrations in the surface sediment

Table 3. Sediment P speciation and 0.2 M NH$_4$-oxalate/oxalic acid extractable Fe for the 0-0.5 cm sediment layer at 15 North Sea locations in August 1991 (in italics) and February 1992. No representative sample for station 3 could be obtained due to the very coarse and heterogeneous nature of the sediment.

Cluster	Station no.	Org. P (µmol g^{-1})		Inorg. P (µmol g^{-1})		Fe-bnd. P (µmol g^{-1})	NH$_4$-ox. Fe (µmol g^{-1})
IA	13	*4.75*	3.50	*15.39*	15.22	9.90	67.2
IB	9	*11.35*	9.16	*18.79*	16.87	14.70	108.8
	10	*3.59*	3.33	*13.38*	13.66	7.97	68.8
II	2	*1.31*	1.13	*8.02*	7.64	2.97	33.6
	5	*0.97*	0.76	*3.70*	7.77	2.17	24.4
	6	*0.28*	0.96	*5.36*	6.03	2.31	27.6
	7	*0.59*	0.40	*5.81*	4.80	2.18	9.8
	8	*1.38*	0.31	*4.52*	4.17	2.30	13.5
	12	*0.86*	0.27	*3.58*	2.74	1.58	2.7
	14	*1.52*	1.58	*9.92*	9.91	3.90	53.3
	16	*2.54*	1.20	*9.48*	8.79	2.52	57.8
III	3	-	-	-	-	-	-
	4	*0.48*	0.75	*7.75*	5.84	4.10	32.0
	11	*1.68*	1.66	*7.49*	2.62	4.06	5.8
	17	*1.11*	1.65	*2.84*	1.91	1.52	4.4

(paired t-test, p = 0.05). Fe-bound P is correlated with NH$_4$-oxalate Fe in February (Fe-bnd. P = 0.11 × NH$_4$-ox. Fe + 0.60, r^2 = 0.75, n = 14). Fe-bound P accounts for between 25 and 60% of total P in these sediments.

Pore water profiles of Fe^{2+} and HPO$_4$$^{2-}$. The redox conditions in February 1991 and August 1992 at these 15 stations have been discussed in detail in a separate paper on Fe and Mn cycling (Slomp et al., 1997). In short, maximum depths of O$_2$ and NO$_3$$^-$ penetration ranged between < 250 µm to ~2.5 cm and ~1 to ~5 cm, respectively, at most cluster IA, IB and II stations. O$_2$ and NO$_3$$^-$ penetrated much deeper into the sediment at the cluster III stations (for O$_2$ mostly between ~3 to ~15 cm depth). With the exception of these latter stations and the deep station in the Skagerrak (cl. IB; st. 9), penetration depths of both O$_2$ and NO$_3$$^-$ were significantly larger in February than in August. All stations with O$_2$ penetration depths less than 250 µm in August are located in the German Bight region (st. 12, 13 and 14). Increased levels of pore water Mn^{2+} and Fe^{2+} were generally observed at depths where the sediment became depleted of O$_2$ and NO$_3$$^-$, respectively. Only the Fe^{2+} profiles are repeated here.
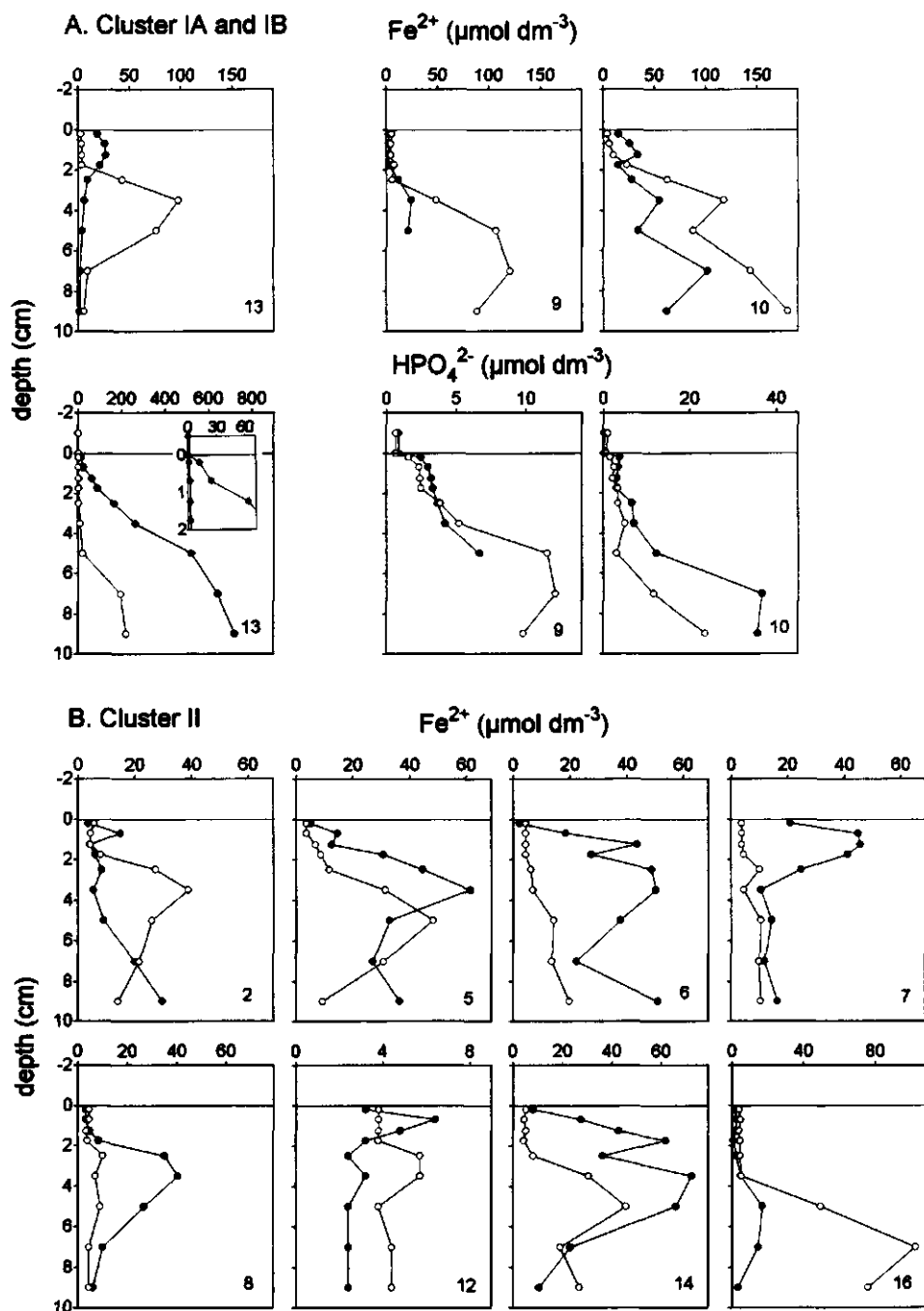
Fig. 3. Pore water profiles of HPO_4^{2-} and Fe^{2+} (μmol dm^{-3}) at all stations (A: Cluster IA and B, B: Cluster II, C: Cluster III) in August 1991 (filled circles) and February 1992 (open circles).
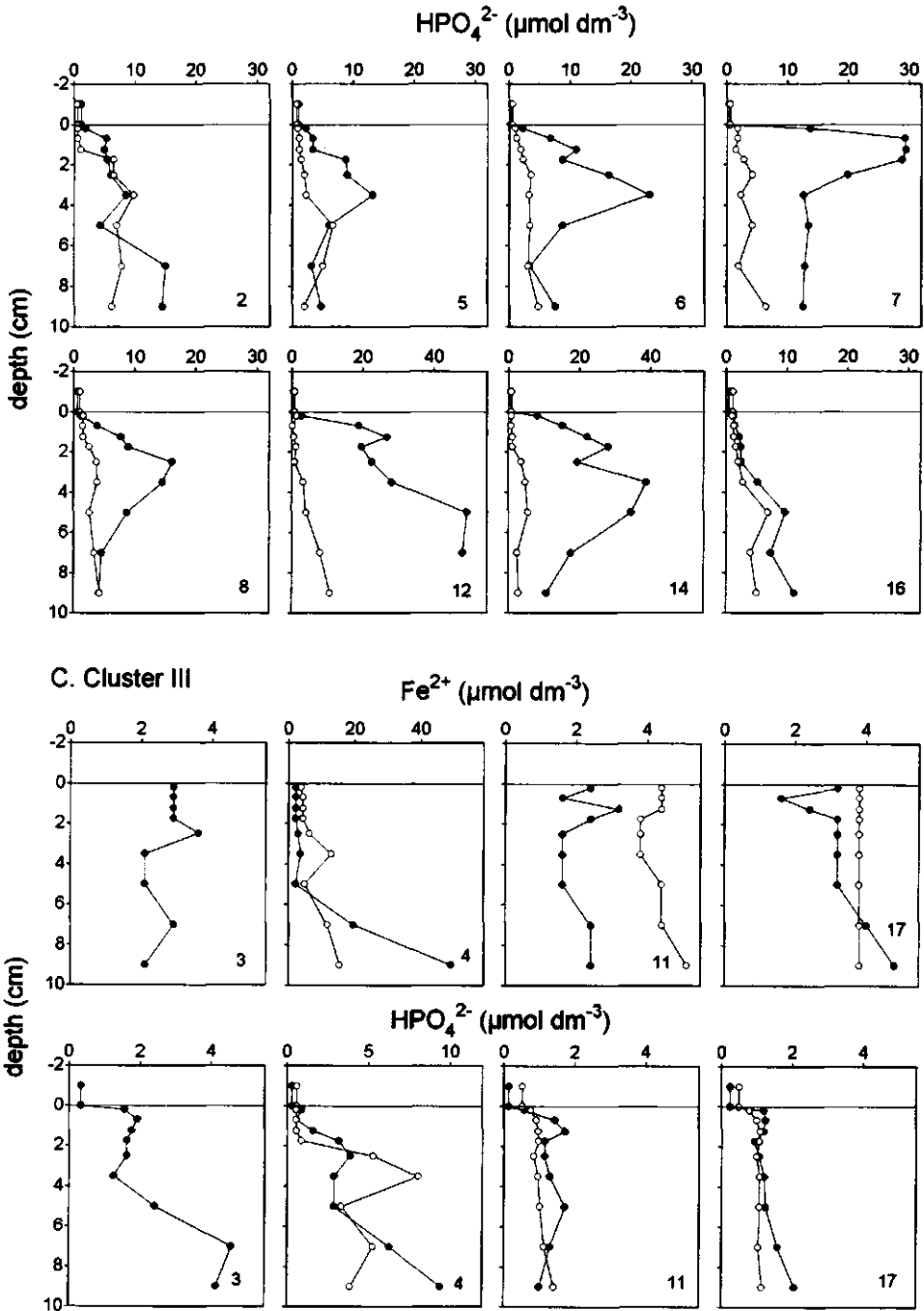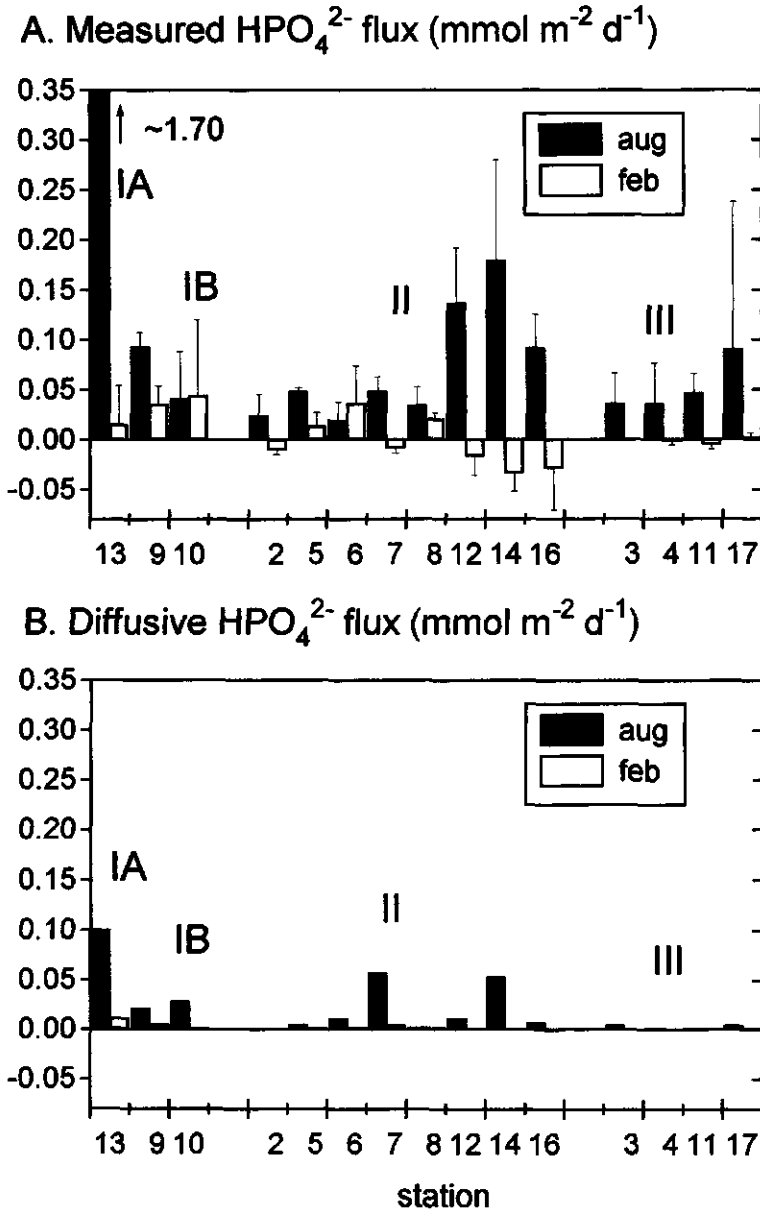
Fig. 3. (continued)

A. Measured HPO$_4$$^{2-}$ flux (mmol m^{-2} d^{-1})

B. Diffusive HPO$_4$$^{2-}$ flux (mmol m^{-2} d^{-1})

Fig. 4. Rates of sediment-water exchange of HPO$_4$$^{2-}$ at all stations in August 1991 (black bars) and February 1992 (white bars) as (A) measured in flux core incubations and (B) calculated assuming molecular diffusion. Positive fluxes are directed to the water column. Error bars in (A) indicate the standard deviation (n=5). Note the difference in scale in panels (A) and (B).

Comparison of the pore water Fe^{2+} and HPO_4^{2-} profiles (Fig. 3) shows that HPO_4^{2-} concentrations were generally much lower in oxidized sediment than in reduced sediment. This is presumably due to removal of HPO_4^{2-} in oxidized sediment through sorption to Fe oxides. S-shaped HPO_4^{2-} profiles were found at stations in the depositional environments of cluster IA and IB. This type of profile is characterized by a sharp increase in pore water HPO_4^{2-} concentrations when going from the bottom water to the oxidized surface sediment, nearly constant pore water concentrations in the oxidized zone, and a rapid increase below this region. Remarkably, the HPO_4^{2-} pore water profiles of station 13 suggest that sorptive removal of HPO_4^{2-} extended into the reduced zone both in August and February. The effect of seasonal changes in sediment redox conditions on pore water HPO_4^{2-} concentrations was most pronounced for station 13 (cl. IA) and many cluster II stations. Here, sharp HPO_4^{2-} gradients were found near the sediment-water interface in August which were absent in February. At many cluster II stations, a decrease of the HPO_4^{2-} concentration with depth was observed in a part of the reduced zone. Concentrations of both Fe^{2+} and HPO_4^{2-} were very low at the cluster III stations.

Sediment-water exchange of HPO_4^{2-}. The flux of dissolved HPO_4^{2-} was directed from the sediment to the bottom water at all stations in August (Fig. 4A). The highest effluxes (up to 1.7 mmol m^{-2} d^{-1}) were measured at stations 12, 13 and 14 in the German Bight where the sediment was almost completely anoxic at this time of year. In February, both small influxes and effluxes of HPO_4^{2-} were measured at the cluster II and III stations. The effluxes were generally lower than in August. The largest seasonal change occurred at station 13 (cluster IA) where the efflux of HPO_4^{2-} in February was a factor 110 lower than that in August.

Diffusive fluxes calculated from the pore water profiles (Fig. 4B) were much lower (up to a factor 30) than measured fluxes at most stations. Station 16 was the only station for which a minor influx of HPO_4^{2-} was calculated in February.

Sorption experiments. At all 8 stations, the Freundlich equation gave a good description of the isotherms (Fig. 5). Values for EPC_o were approximately equal to or lower than measured pore water concentrations in the upper 0.4 cm of the sediment (Table 4). Sorption coefficients at a HPO_4^{2-} concentration of 1 μmol dm^{-3} ($K_F'=K_F/n$) were well correlated with sediment porosity, NH_4-oxalate Fe, Fe-bound P and % organic C (r^2: 0.71-0.84). Dimensionless sorption coefficients (K_{dim}) ranged from 32 at station 17 (cluster III) to 584 at station 13 (cluster IA). There was a linear relationship between the amount of P sorbed to the sediment and silicate release from the sediment above a large background release of
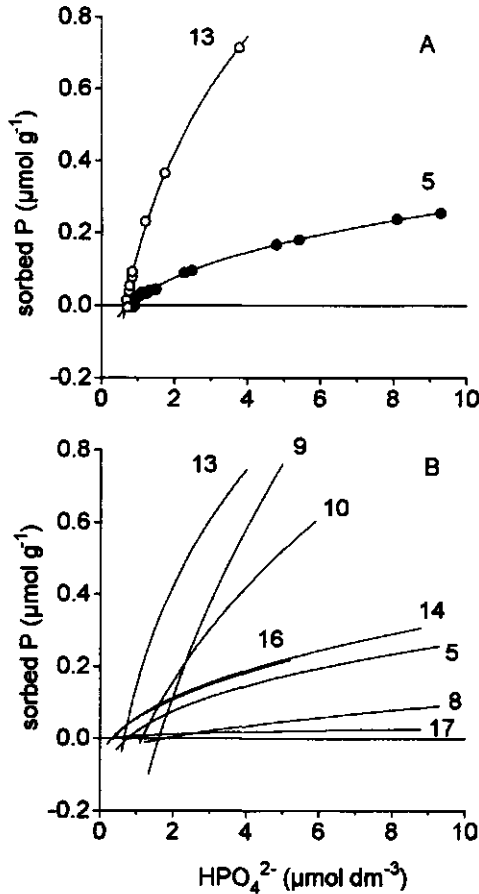
Fig. 5. Sorption isotherms for (A) stations 5 and 13 (including data points) and (B) stations 5, 8, 9, 10, 13, 14, 16 and 17 (data points omitted for clarity). Final HPO_4^{2-} concentrations at t = 2 days are given on the x-axis. The amount of P adsorbed to or desorbed from the sediment during the sorption experiments (P_{sor}; equation 1) is given on the y-axis. Lines are Freundlich isotherms fitted to the data (mean $r^2 = 0.95$ for the linear form).

silicate at all stations. This indicates a displacement of sorbed silicate by HPO_4^{2-}. The ratio between the amount of HPO_4^{2-} sorbed and the extra $Si(OH)_4$ released ranged from 8.3 to 50 mol mol^{-1} (Table 4).

Practically all of the HPO_4^{2-} sorbed to the sediment during the kinetics experiments at low intial HPO_4^{2-} concentrations, was removed from solution within the first 15 minutes, as shown for stations 9 and 13 in Fig. 6A and B. In the experiments where higher initial HPO_4^{2-} concentrations were used, HPO_4^{2-} was also removed rapidly from solution (Fig. 6C
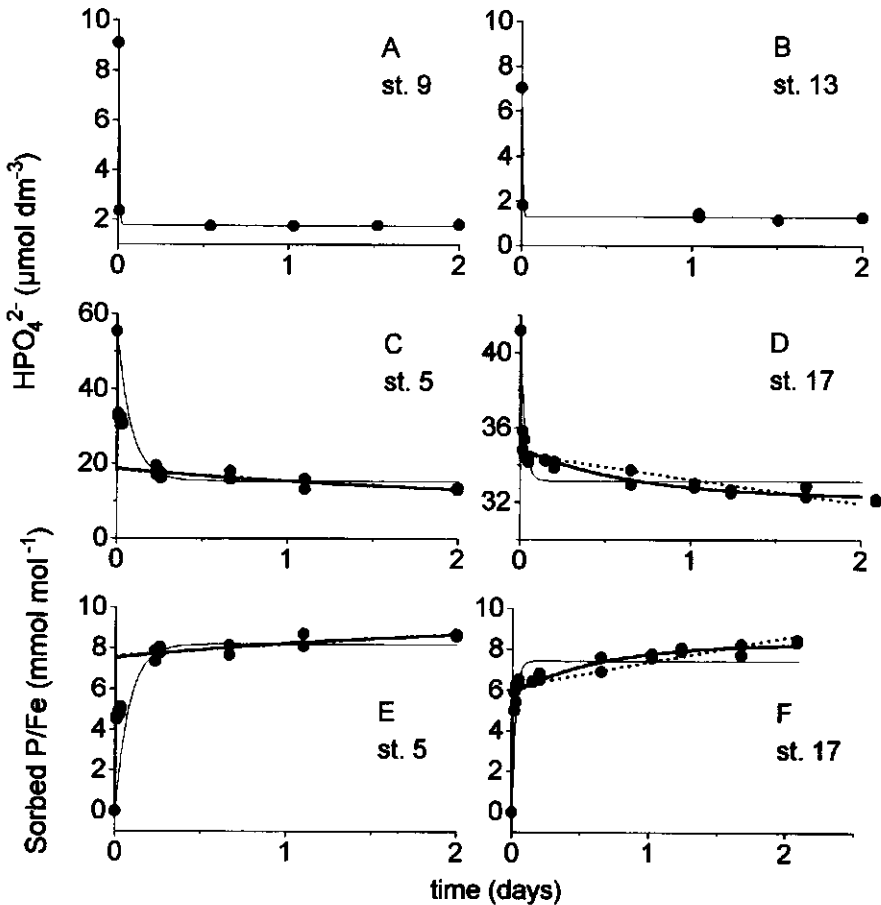
Fig. 6. Changes in the HPO_4^{2-} concentration ($\mu mol\ dm^{-3}$) with time during kinetics experiments with low (A, B) and high (C, D) initial HPO_4^{2-} concentrations for stations 9, 13, 5 and 17, respectively. The molar ratio of P sorbed during the experiment with high initial HPO_4^{2-} concentrations and NH_4-ox.-Fe for stations (E) 5 and (F) 17. Thin solid lines indicate fits to a first-order model. Fits to the model assuming simultaneous equilibrium and first-order sorption (equation 6) are indicated with thick solid (C_e free) and thick dotted (C_e fixed) lines.

and D). In this case, however, HPO_4^{2-} concentrations continued to decrease slowly throughout the experiment. The corresponding plots of sorbed P normalized to concentrations of solid NH_4-oxalate Fe are given in Fig. 6E and F. Model fits to the data using both a first-order model and the model assuming simultaneous equilibrium and first-order kinetic sorption (equation 6) are shown in Fig. 6C-F. At both stations, the latter model gives the best description of the results, regardless of whether C_e is a free or fixed parameter. Fitted values of C_e were 10.0 and 32.2 $\mu mol\ dm^{-3}$ and corresponding values of
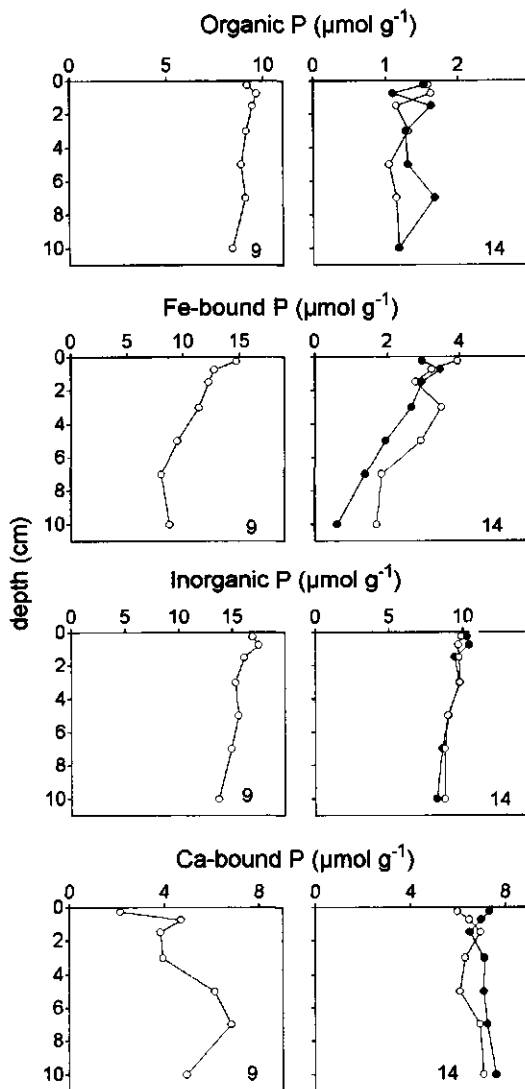
Fig. 7. Organic P, Fe-bound P and residual P at station 9 (cluster IB) and station 14 (cluster II) in February (open circles) and August (filled circles).

$k_k \times S$ amounted to 7.5 and 7.4 cm^3 g^{-1} d^{-1} for stations 5 and 17, respectively. When C_e was fixed at the value for EPC$_0$ (st. 5: 0.77; st. 17: 0.36; Table 4) fitted values for $k_k \times S$ were 2.7 and 0.2 cm^3 g^{-1} d^{-1}, for these stations. The corresponding in-situ sorption coefficients ($k_k \times S \times 9$) are 20 d^{-1} and 33 d^{-1} (C_e fixed) and 7.2 and 0.9 d^{-1} (C_e free).

Table 4. The empirical constants for the Freundlich isotherms (K_F, n), the calculated amount of Native Adsorbed Phosphorus (NAP) and the calculated equilbrium phosphate concentration (EPC_0), pore water HPO_4^{2-} concentrations measured in the upper 0.4 cm of the sediment (pw. HPO_4^{2-}), sorption coefficients calculated from the gradient of the isotherms at $C = 1$ μmol dm^{-3} (K_F/n) and corresponding dimensionless sorption coefficients (K_{dim}), and the ratio between the amount of HPO_4^{2-} sorbed to and $Si(OH)_4$ released from the sediment during the sorption experiments (-dP/dSi).

St. no.	K_F (dm^3 g^{-1})	n (-)	NAP (μmol g^{-1})	EPC_0 (μmol dm^{-3})	pw. HPO_4^{2-} (μmol dm^{-3})	K_F/n (cm^3 g^{-1})	K_{dim} (-)	-dP/dSi (mol mol^{-1})
5	0.22	3.08	0.21	0.77	0.82	73	201	18
8	0.05	1.84	0.06	1.78	1.52	25	94	8.3
9	1.06	2.43	1.29	1.62	1.58	436	143	8.7
10	0.58	2.39	0.62	1.16	1.67	243	238	15
13	1.81	4.82	1.66	0.67	1.39	375	584	6.5
14	0.16	2.32	0.11	0.37	0.82	70	139	18
16	0.14	2.08	0.08	0.34	0.93	65	147	10
17	0.030	4.26	0.023	0.36	0.79	7	32	50

Sediment P profiles. Organic P concentrations decrease slightly with depth at station 9 (Fig. 7). At station 14, organic P concentrations are very low and show substantial scatter.At both stations, concentrations of Fe-bound and total inorganic P decrease with depth. Ca-bound P concentrations increase with depth at station 9, but remain relatively constant with depth at station 14. Apart from Fe-bound P, no clear seasonal change in sediment P speciation was observed at station 14.

APPLICATION OF THE REACTION-DIFFUSION MODEL

To obtain more insight in the role of sorption in controlling sediment-water exchange of HPO_4^{2-} in both high and low sedimentation environments, the model was applied to the pore water HPO_4^{2-} and solid phase P profiles of station 9 (cluster IB) for February and station 14 (cluster II) for February and August.

Three model settings (termed model i, ii and iii) were used. In model (i) P sorption is solely decribed as a reversible equilibrium process. All Fe- and Ca-bound P is supplied from the overlying water. In model (ii), both equilibrium and kinetic sorption are assumed to be operative. Slow, kinetic sorption is responsible for in-situ formation of Fe-bound P. All Ca-bound P but only a part of the Fe-bound P is supplied from the overlying water. In model (iii), conditions are as in model (ii) except now all Ca-bound P is assumed to have been formed in the sediment. Model calculated rates of non-local transport are directly linked to rates of HPO_4^{2-} production and to rates of HPO_4^{2-} removal through authigenic Ca-bound P formation. By comparing the results of model (iii) and (ii) it is possible to evaluate whether, at a given rate of HPO_4^{2-} production, it is likely that non-local transport

Table 5. The fixed parameters used for the model calculations (models i, ii, iii) with their source. + indicates that the parameter value is given in Table 6.

Parameter	Description	Units	Station 9-Feb	Station 14-Feb	Station 14-Aug	Source
All calculations (i, ii, iii)						
L_1	boundary oxidized/reduced zone	m	0.02	0.025	0.002	(1)
ϕ	sediment porosity	$m^3\ m^{-3}$	0.88	0.51	0.51	(2)
D_s	whole sediment diffusion coefficient	$m^2\ d^{-1}$	3.4×10^{-5}	1.9×10^{-5}	2.6×10^{-5}	(3)
ω	sedimentation rate	$m\ d^{-1}$	2.7×10^{-6}	2.7×10^{-8}	2.7×10^{-8}	see text
D_b	sed. mixing or biodiffusion coefficient	$m^2\ d^{-1}$	1.1×10^{-6}	5.5×10^{-7}	5.5×10^{-7}	see text
C_o	overlying water HPO_4^{2-} concentration	$mol\ m^{-3}$	0.69×10^{-3}	0.76×10^{-3}	0.62×10^{-3}	(4)
C_a	equilibrium conc. for CFA precipitation	$mol\ m^{-3}$	0.69×10^{-3}	0.76×10^{-3}	0.62×10^{-3}	(5)
K_{eq1}	equil. sorption coefficient zone I	-	108	243	243	(6)
K_{eq2}	equil. sorption coefficient zone II	-	2	2	2	(7)
k_m	rate constant for Fe-bound P release upon Fe oxide reduction in zone II	d^{-1}	5.3×10^{-4}	5.3×10^{-4}	5.3×10^{-4}	(8)
k_g	rate constant for organic P decomposition	d^{-1}	+	+	6.3×10^{-4}	(9)
Kinetic sorption (ii, iii)						
k_s	rate constant for kinetic sorption	d^{-1}	+	+	0.49	(10)
C_s	equilibrium concentration for P sorption	$mol\ m^{-3}$	1.62×10^{-3}	0.37×10^{-3}	0.37×10^{-3}	(11)
Authigenic P precipitation (iii)						
$JA_{x=0}$	flux of Ca-P to the sediment	$\mu mol\ m^{-2}\ d^{-1}$	0	0	0	(12)

Source: (1) Slomp et al. (1997); (2) mean porosity top 3 cm; (3) Krom and Berner (1980a); (4) measured bottom water HPO_4^{2-} concentration; (5) as defined in model description; (6) K_{dim} at EPC_O (eq. 3 and 4); (7) Krom and Berner (1980b); (8) Slomp et al. (1996b); (9) and (10) k_g and k_s values obtained by fitting model (ii) to the data for station 14 in February as given in Table 6; (11) EPC_O, Table 4; (12) see description model (iii).
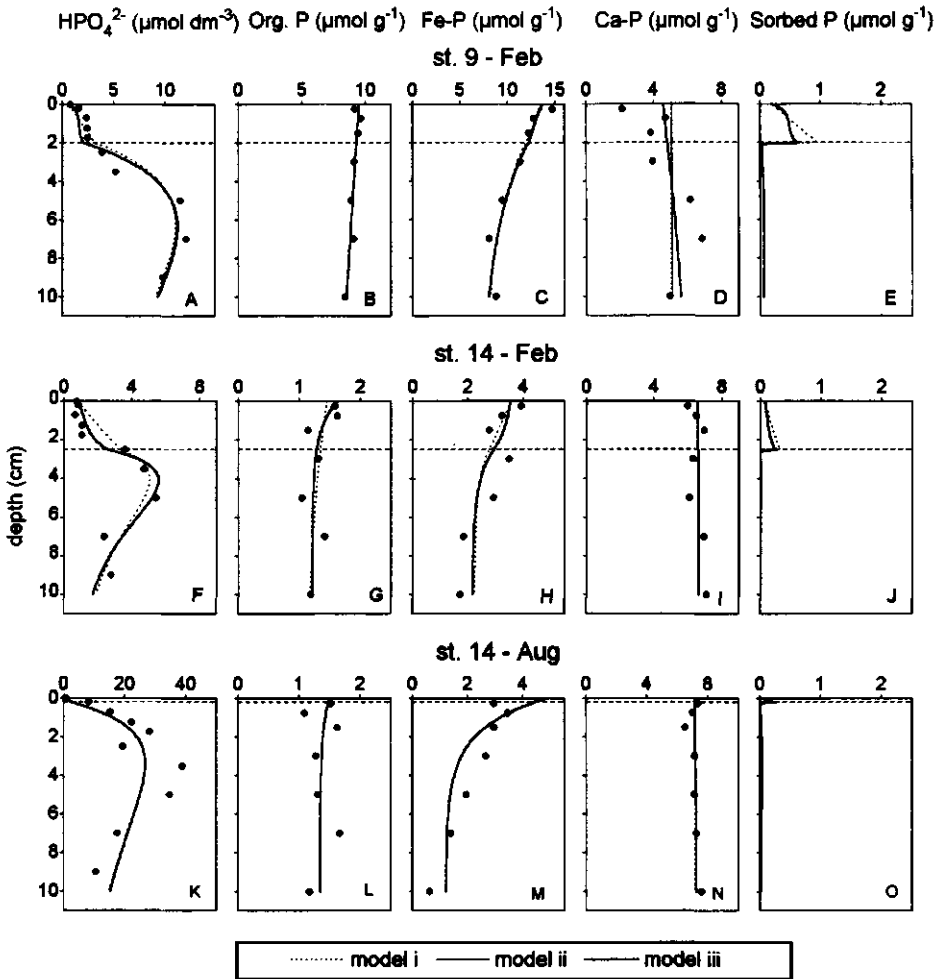
Fig. 8. Model fits to profiles of pore water HPO_4^{2-}, organic P, Fe-bound P, Ca-bound P and sorbed P for the 4 model settings for stations 9 (February) and 14 (February and August).(i): dotted lines, (ii): thin solid lines, (iii) thick solid lines. The dashed lines indicate the depth of the redox boundary at each station.

contributes substantially to HPO_4^{2-} removal in the sediment and to sediment-water exchange of HPO_4^{2-}.

Fixed parameters. The fixed parameters used in the model calculations are listed in Table 5. The sedimentation rate of 0.1 cm y^{-1} assumed for station 9 is at the low end of the range known for the Skagerrak (Van Weering et al., 1987). A value of 4 cm^2 y^{-1} for the sediment mixing rate (D_b) at station 9 is derived from the equation:

Table 6. Values of the parameters for station 9 and 14 obtained by fitting the model to the data. i, ii and iii are the three model settings studied. - indicates that the relevant process was excluded. + indicates that the parameter is given in Table 5.

Para-meter	Description	Units	st. 9 - February			st. 14 - February			st. 14 - August		
			(i)	(ii)	(iii)	(i)	(ii)	(iii)	(i)	(ii)	(iii)
$JG_{x=0}$	flux of org. P to the sed.	$\mu mol\ m^{-2}\ d^{-1}$	12.0	11.9	11.8	0.9	4.9	5.1	1.9	1.9	1.9
$JM_{x=0}$	flux of Fe-P to the sed.	$\mu mol\ m^{-2}\ d^{-1}$	44.1	68.2	68.5	5.9	1.9	1.8	35.9	35.3	34.8
$JA_{x=0}$	flux of Ca-P to the sed.	$\mu mol\ m^{-2}\ d^{-1}$	4.4	4.4	+	0.2	0.2	+	0.3	0.3	+
G_∞	asymptotic conc. of org. P	$\mu mol\ g^{-1}$	4.1	3.3	3.6	1.1	1.2	1.2	1.3	1.3	1.3
M_∞	asymptotic conc. of Fe- P	$\mu mol\ g^{-1}$	7.3	7.1	7.0	2.2	2.2	2.1	1.2	1.2	1.2
α	non-local transport coeff.	d^{-1}	$2.1x10^{-2}$	$2.2x10^{-2}$	$1.8x10^{-2}$	$2.7x10^{-2}$	$3.7x10^{-2}$	$3.5x10^{-2}$	$4.0x10^{-3}$	$4.0x10^{-3}$	$3.7x10^{-3}$
k_g	rate const. for org. P decomp.	d^{-1}	$9.9x10^{-6}$	$7.8x10^{-6}$	$8.1x10^{-6}$	$2.2x10^{-5}$	$6.3x10^{-4}$	$6.5x10^{-4}$	+	+	+
k_s	rate const. for kinetic sorption	d^{-1}	-	$1.5x10^{+1}$	$1.5x10^{+1}$	-	$4.9x10^{-1}$	$5.0x10^{-1}$	+	+	+
k_a	rate const. for auth. P form.	d^{-1}	-	-	$4.1x10^{-3}$	-	-	$1.9x10^{-3}$	-	-	$1.6x10^{-4}$

$$D_b = 15.7\omega^{0.6} \tag{8}$$

with ω in units of cm y^{-1} and D_b in units of cm^2 y^{-1} (Boudreau, 1994). Net sedimentation outside the main depositional environments in the North Sea is negligible (Eisma and Kalf, 1987). For station 14, a sedimentation rate of 0.001 cm y^{-1} is assumed to enable a model solution. The D_b at this station is set at 0.5 cm^2 y^{-1}. These D_b values fall within the range of 0.5-12 cm^2 y^{-1} estimated for North Sea sediments from ^{210}Pb profiles (Albrecht, 1991, cited in Pohlmann and Puls, 1994) and are a factor 2.5 and 10 lower than the values assumed for stations 9 and 14, respectively, in our study on Fe and Mn cycling in North Sea sediments (Slomp et al., 1997). In the latter study we used very large values to ensure that we did not underestimate the role of Fe and Mn reduction. The lower values assumed here are probably closer to the actual values.

Model fits. Model fits for all 3 model settings agree reasonably well with the measured profiles of pore water HPO$_4$$^{2-}$ and solid phase P at station 9 in February and station 14 in August and February (Fig. 8). In February, the best description of the pore water HPO$_4$$^{2-}$ profile in the oxidized surface sediment at both stations is obtained when describing sorption as a combination of an equilibrium and kinetic process (ii and iii) (Fig. 8A and F). In August, including kinetic sorption has no effect on the model fit to the pore water HPO$_4$$^{2-}$ profiles (Fig. 8K). Modelled profiles of organic, Fe-bound and Ca-bound P are very similar in all cases (Fig. 8B-D, G-I, L-N). This particularly holds for models (ii) and (iii). Model calculated concentrations of sorbed P decrease when going upwards from the redox boundary to the sediment-water interface (Fig. 8E, J, O). Sorbed P concentrations are low compared to values for Fe-bound P (sorbed P/Fe-bound P < 5%).

The fitted parameters for all 3 model settings and both stations are listed in Table 6. The values of the rate constants are in line with ranges estimated from laboratory experiments and other diagenetic models (for α see Emerson et al., 1984; for the other rate constants see discussion in Slomp et al., 1996b). Calculated rates of HPO$_4$$^{2-}$ production and removal in the sediment are given in Table 7. Release from Fe-bound P is the major source for dissolved HPO$_4$$^{2-}$ at both stations in all model calculations. In the case of model (i), most of the produced HPO$_4$$^{2-}$ is released to the overlying water. Non-local transport accounts for an important part of the sediment-water exchange flux at both stations in February, but is relatively unimportant at station 14 in August.

Table 7. Rates of HPO_4^{2-} production and removal for stations 9 (February) and 14 (February and August) as calculated with the three model settings (i, ii, iii).

Rates in $\mu mol\ m^{-2}\ d^{-1}$	St. 9 - February			St. 14 - February			St. 14 - August		
	(i)	(ii)	(iii)	(i)	(ii)	(iii)	(i)	(ii)	(iii)
HPO_4^{2-} production									
Release from solid phase P									
- org. P zone I	0.3	0.3	0.3	0.2	4.0	4.2	0.2	0.2	0.2
- org. P zone II	1.2	1.1	1.1	0.4	0.9	0.9	1.6	1.6	1.6
- Fe-bnd. P zone I	-	37.2	37.5	-	0.0	0.0	-	0.0	0.0
- Fe-bnd. P zone II	30.6	33.5	33.7	5.7	8.4	8.4	35.8	35.8	35.3
Sedimentation flux at x = 0	0.2	0.2	0.2	0.0	0.0	0.0	0.0	0.0	0.0
Total	*32.3*	*72.3*	*72.8*	*6.4*	*13.3*	*13.5*	*37.6*	*37.6*	*37.2*
HPO_4^{2-} removal									
Formation of solid phase P									
- Fe-bnd. P zone I	-	16.5	16.7	-	6.6	6.8	-	0.6	0.6
- auth. P zone II	-	-	2.6	-	-	0.2	-	-	0.2
Sediment-water exchange									
- diffusive flux	16.4	39.3	39.7	2.7	1.9	1.9	31.2	30.6	30.3
- non-local	13.3	13.8	11.1	3.4	4.5	4.3	4.1	4.1	3.8
Flux at lower system boundary									
- diffusive flux	2.5	2.6	2.6	0.3	0.3	0.3	2.3	2.3	2.3
- sedimentation flux	0.1	0.1	0.1	0.0	0.0	0.0	0.0	0.0	0.0
Total	*32.3*	*72.3*	*72.8*	*6.4*	*13.3*	*13.5*	*37.6*	*37.6*	*37.2*

The total production of HPO_4^{2-} calculated with model (ii) at stations 9 and 14 in February is more than twice as high as that calculated with model (i). At station 9, the sediment-water exchange of HPO_4^{2-} is also substantially higher. This is the result of a higher diffusive flux due to a sharper HPO_4^{2-} gradient at the sediment-water interface compared to model (i). The model results for this station indicate that substantial desorption of HPO_4^{2-} occurs in the top cm of zone I. This desorption exceeds the adsorption in the 1-2 cm interval below. This implies that there is no net sorptive removal of HPO_4^{2-} at this station. At station 14 in February, in contrast, the importance of the diffusive flux for sediment-water exchange of HPO_4^{2-} has decreased. Here, only adsorption occurs in zone I and Fe-bound P is a net sink for HPO_4^{2-}. There is little difference between the results of model (i) and (ii) for station 14 in August.

The results of model (iii) show that the assumption that all Ca-bound P has been formed in-situ has very little effect on the magnitude of the non-local exchange flux.

DISCUSSION

Sorption of HPO_4^{2-} to North Sea sediments. The results of the sorption isotherms indicate that North Sea surface sediments differ widely with respect to their capacity to sorb HPO_4^{2-}. The good correlation between the value of the sorption coefficient, calculated from the gradient of the sorption isotherm at $[HPO_4^{2-}] = 1$ µmol dm^{-3} (K_F/n), and NH_4-oxalate Fe suggests that the HPO_4^{2-} is sorbed mostly to poorly crystalline Fe oxides (also see Slomp et al., 1996a). The enhanced release of $Si(OH)_4$ upon HPO_4^{2-} sorption, with dP/dSi ratios largely in the range known for silicate displacement from Fe oxide surfaces (~1-17 for ferrihydrite and goethite; Parfitt, 1989; Torrent et al., 1992), supports this view. Fits of HPO_4^{2-} sorption isotherms to the Freundlich equation are compatible with a heterogeneous type of adsorbing surface (Weber et al., 1992) and are common for natural and synthetic Fe oxides (Torrent et al., 1992; Colombo et al., 1994).

Controls on sediment-water exchange of HPO_4^{2-} in the North Sea. Combination of the sorption, solid phase and pore water data with measured and calculated rates of sediment-water exchange of HPO_4^{2-} enables us to distinguish the most likely controls on sediment-water exchange of HPO_4^{2-} in the 4 types of North Sea environments studied here, and thus, to determine where sorption may be important.

Organic matter mineralization rates in the cluster III sediments are so low that these are not sufficiently depleted of O_2 and NO_3^- to allow for substantial Fe oxide reduction either in August or February (Fig. 3C). The low pore water HPO_4^{2-} concentrations at these stations reflect low rates of HPO_4^{2-} release to the pore water and are not the result of strong sorption (Fig. 5B, Tables 3 and 4). Despite the lack of a seasonal variation in the HPO_4^{2-} pore water profiles (Fig. 3C) and calculated diffusive fluxes (Fig. 4B), measured rates of sediment-water exchange of HPO_4^{2-} (Fig. 4A) were distinctly higher in August than in February. Results from previous studies suggest that in these sediments temporarily deposited organic matter is decomposed close to the sediment-water interface (Lohse et al., 1995; Slomp et al., 1997). This decomposition is not resolved with our relatively coarse pore water sampling procedure. We conclude that in the cluster III sediments release of HPO_4^{2-} from organic matter at or close to the sediment-water interface controls the sediment-water exchange of HPO_4^{2-} and sorption is relatively unimportant.

At the cluster II stations, in comparison, deposition of organic matter is much more frequent. Most deposition takes place in summer leading to a distinct seasonal variation in the depths of O_2 and NO_3^- penetration (Lohse et al., 1995; Slomp et al., 1997). This has important consequences for the control of sediment-water exchange at these stations. The shapes of the pore water Fe^{2+} and HPO_4^{2-} profiles for February indicate removal of upward diffusing Fe^{2+} and HPO_4^{2-} in the oxidized surface sediment (Fig. 3B). The results of the

sorption experiments (Fig. 5; Table 4) and the solid phase analyses (Table 3) indicate that most of these surface sediments have the capacity to sorb HPO_4^{2-}. Calculated diffusive fluxes suggest that little HPO_4^{2-} escapes out of the sediment at this time of the year (Fig. 4B). Measured fluxes of HPO_4^{2-}(Fig. 4A) even suggest influxes of HPO_4^{2-} at 5 stations in February. We conclude that, in February, sorption can play an important role in limiting the flux of HPO_4^{2-} to the overlying water at many cluster II stations.

In August, the oxidized surface layer is very thin at most cluster II stations. The shape of the pore water HPO_4^{2-} and Fe^{2+} profiles suggests that the role of sorption is limited to this very thin surface layer. Measured fluxes of HPO_4^{2-} are substantially (up to a factor 19) higher than calculated fluxes at most stations suggesting that if sorption is operative, it does not lead to a retention of HPO_4^{2-} in the sediment. Release of HPO_4^{2-} from organic material at the sediment-water interface, and enhancement of the HPO_4^{2-} flux due to turbulent diffusion in the upper millimetres of the sediment (Lohse et al., 1996) and due to non-local, bioirrigative transport may be important at this time of year.

The sorption experiments demonstrate that the surface sediments in the depositional environments of cluster IA and IB all have a strong affinity for HPO_4^{2-}, and that HPO_4^{2-} sorption may be important at in-situ conditions, particularly at station 13 (Table 4). Pore water HPO_4^{2-} profiles for both clusters show a distinct S-shape, which is generally attributed to sorptive removal of HPO_4^{2-} (e.g. Sundby et al., 1992). Despite these similarities, there are distinct differences in the cycling of P in the German Bight (cluster IA) and the Skagerrak (cluster IB) which are related to the quality and quantity of the organic matter deposited in each area.

In the German Bight (cluster IA; station 13), large amounts of mostly fresh produced organic matter are known to reach the sediment in spring and summer. Pore water concentrations of HPO_4^{2-} in the reduced zone are exceptionally high, ranging up to ~200 $\mu mol \, dm^{-3}$ in February and ~700 $\mu mol \, dm^{-3}$ in August. In February, O_2 and NO_3^- penetrate down to depths of ~0.5 and ~ 2 cm, respectively (Lohse et al., 1995; Slomp et al., 1997). Both the measured and calculated fluxes indicate that very little dissolved HPO_4^{2-} escapes out of the sediment, suggesting effective retention of HPO_4^{2-} in the sediment. In August, the sediment is almost completely depleted of O_2 and NO_3^- and high concentrations of HPO_4^{2-} occur in the upper 0-0.4 cm of the sediment. Fluxes to the overlying water are substantial although measured rates are a factor ~17 higher than calculated diffusive fluxes. This difference is presumably due to a combination of sediment irrigation, release of HPO_4^{2-} from organic matter at the sediment-water interface and an underestimation of the actual gradient at the sediment-water interface. The concave-upward shapes of the pore water HPO_4^{2-} profiles, starting at ~5 and 6 cm depth, in both August and February suggest sorptive removal of HPO_4^{2-} is not limited to the zone of NO_3^- penetration. Non-local

mixing of 'fresh' sediment Fe oxides with unoccupied sorption sites into the reduced zone could explain these results. The sub-surface maximum of NH_4-oxalate Fe observed between 2 and 6 cm depth at this station in February (Slomp et al., 1996a) supports this conjecture.

In the Skagerrak (cluster IB), mostly refractory organic matter is deposited and organic matter mineralization rates are relatively low and show little seasonal change. This particularly holds for the deeper stations, such as station 9. Here, the depths of O_2 and NO_3^- penetration and the pore water HPO_4^{2-} profiles show very little change between August and February (Lohse et al., 1995; Slomp et al., 1997). The pore water HPO_4^{2-} profiles indicate strong sorptive removal of the HPO_4^{2-} diffusing upwards from the reduced zone into the oxidized zone. Nevertheless, a relatively sharp gradient in pore water HPO_4^{2-} at the sediment-water interface (Fig. 3A) and a flux of HPO_4^{2-} to the overlying water are maintained in both seasons (Fig. 4A and B). Rapid release of HPO_4^{2-} from organic material close to the sediment-water interface is unlikely due to the refractory nature of the organic matter. Therefore, desorption of HPO_4^{2-} from Fe oxides probably supplies the necessary HPO_4^{2-}. The discrepancy between the measured and calculated rates of sediment-water exchange is presumably largely due to the fact that the gradient determined from the pore water profile underestimates the actual gradient at the sediment-water interface.

Summarizing, the results show that sorption plays an important role in controlling sediment-water exchange of HPO_4^{2-} during at least a part of the year in 3 of the 4 North Sea environments studied here. The role of sorption is most important when the oxidized sediment zone is relatively thick, which is the case at all cluster IA, IB and II stations in February and at station 9 in February and August. Then, HPO_4^{2-} sorption limits the flux to the overlying water at most stations. At station 9, however, sorption is suggested to be responsible for the maintenance of a flux of HPO_4^{2-} to the overlying water throughout the year.

The effect of sorption on sediment-water exchange of HPO_4^{2-}. The results of the sorption kinetics experiments (Fig. 6) indicate concurrent fast and slow sorption of HPO_4^{2-}. The rate constants for the slow sorption process found for stations 5 and 17 in these experiments (0.9 to 33 d^{-1}) are reasonably close to the values obtained with the reaction-diffusion model for stations 9 and 14 (0.5 to 15 d^{-1}). The results of the reaction-diffusion model (Fig. 8) show that the best description of pore water HPO_4^{2-} concentrations in the oxidized surface layer is obtained when including both fast and slow processes by assuming concurrent equilibrium and first-order kinetic sorption (models ii and iii) instead of only equilibrium sorption (model i).

In model (i), where only instantaneous, reversible equilibrium sorption is assumed, sorption in combination with bioturbation enhances vertical transport through aqueous

diffusion of dissolved HPO_4^{2-} in the oxidized surface zone (Schink and Guinasso, 1978). The enhancement depends on the values of D_b and K_{eq1} (see equation A1 of the Appendix) and amounts to a factor of 4.5 and 2.8 at stations 9 and 14, repectively. This allows a substantial diffusive flux of HPO_4^{2-} to the overlying water to be maintained at these stations, even when modelled pore water HPO_4^{2-} gradients are relatively low. With this model, substantial retention of HPO_4^{2-} in the sediment, one of the most important effects of HPO_4^{2-} sorption to Fe oxides in sediments, can not be adequately described.

When including instantaneous, equilibrium sorption and relatively slow kinetic sorption (model ii and iii), sorption can cause (1) a decrease of the flux from the sediment to the overlying water and (2) an enhancement of this flux. The first effect is the classical view of sorption in which the oxidized zone acts as a trap for upward diffusing HPO_4^{2-} from the reduced zone (Einsele, 1936; Mortimer, 1941, 1942). This is observed when the apparent equilibrium HPO_4^{2-} concentration (C_s) is equal to or lower than the overlying water concentration (C_o). Kinetic sorption results in adsorption of HPO_4^{2-} and net Fe-bound P formation in the oxidized zone. Equilibrium sorption in combination with bioturbation enhances the aqueous diffusion through the oxidized zone. When the pore water HPO_4^{2-} gradient in the oxidized zone, and the D_b and K_{eq1} values are small, this enhancement is relatively unimportant. This is the situation as calculated for station 14 in February (model ii and iii; Fig. 8, Tables 5 and 7). Release of HPO_4^{2-} from organic P in zone I and upward diffusion of HPO_4^{2-} from zone II supply the P for Fe-bound P formation. Release of HPO_4^{2-} from organic P accounts for the relatively sharp gradient in the model calculated HPO_4^{2-} profile close to the sediment-water interface and thus supplies the HPO_4^{2-} that still manages to escape out of the sediment through diffusion.

The second effect, an enhancement of the flux to the overlying water, occurs when the equilibrium HPO_4^{2-} concentration (C_s) is higher than the overlying water concentration (C_o). Desorption of HPO_4^{2-} from Fe-bound P now allows a sharp gradient at the sediment-water interface and thus a flux of HPO_4^{2-} to the overlying water to be maintained. Equilibrium sorption in combination with bioturbation enhances this flux. This situation was observed at station 9 (models ii and iii; Fig. 8, Tables 5 and 7). Under steady-state conditions, a continous re-supply of Fe-bound P to the surface layer is necessary, either through deposition from the overlying water or through formation in deeper parts of the oxidized zone and upward bioturbational transport of Fe-bound P. For station 9, the model calculations (model ii; Tables 6 and 7) suggest that the Fe-bound P necessary to maintain the diffusive flux of HPO_4^{2-} at the sediment-water interface is supplied from the overlying water.

This Fe-bound P must have been formed in an environment with a higher HPO_4^{2-} concentration than that in the overlying water to explain the slow release. With a diagenetic

model for Fe (Slomp et al., 1997), a maximum sedimentation flux of Fe oxides of ~350 μmol m^{-2} d^{-1} can be calculated from the Fe oxide and pore water Fe^{2+} profiles for station 9 using the D_b and ω values of this study. Since the calculated flux of Fe-bound P is ~70 μmol m^{-2} d^{-1} (Table 6), this suggests an Fe/P ratio of the sedimenting Fe oxides of 5. Although similar Fe/P values have been reported previously for Fe oxides in coastal marine sediments (Jensen et al., 1995), this value is rather low (Slomp et al., 1996a). A possible explanation is that we overestimated the flux of Fe-bound P from the overlying water. If sediment mixing at station 9 is not adequately described as a biodiffusive process, and, for example, transport in the surface sediment is actually of a non-local, conveyor-belt nature (Boudreau, 1986), Fe-bound P could also be transported upward across the oxidized zone.

When the oxidized surface zone at station 14 becomes very thin in August and the rate constant for sorption is assumed to be similar to that for February (Table 5), very little Fe-bound P is formed in the sediment (Table 7). Most dissolved HPO$_4$$^{2-}$ produced in the sediment now escapes to the overlying water through diffusion.

The role of sorption in controlling sediment-water exchange of HPO$_4$$^{2-}$ not only depends on the thickness of the oxidized layer but also on the extent to which this layer covers the reduced sediment. Well-irrigated animal burrows provide a means for direct transport of dissolved constituents from the reduced zone to the overlying water (Aller, 1980). When a large number of such burrows are present, the role of sorption in controlling the HPO$_4$$^{2-}$ flux to the overlying water is diminished. We used the approach of non-local exchange to describe the effect of sediment-irrigation. We did not account for possible effects of sorption to Fe oxides formed along burrow linings. Non-local exchange can result in a reversal of pore water gradients at depth in the sediment (Fig. 8) and can account for a substantial proportion of the HPO$_4$$^{2-}$ flux to the overlying water (Table 7). The results of model (iii) show that authigenic Ca-bound P formation can account for only a small part of the HPO$_4$$^{2-}$ removal in the reduced zone at both stations at the D_b values assumed here, suggesting an important role for non-local transport. It should be noted, however, that a D_b value which is too high will lead to an overestimation of the contribution of non-local exchange. A comparison of the model calculated rate of sediment-water exchange of HPO$_4$$^{2-}$ (~51-53 μmol m^{-2} d^{-1}; models ii and iii; Table 7) to the measured flux (~ 35 μmol m^{-2} d^{-1}; Fig. 4A) for station 9 in February suggests that at this station we may have slightly overestimated the actual D_b value and thus the role of non-local exchange. The uncertainty in the measured flux for station 14 in February is too large to enable a similar comparison. At station 14 in August, the measured flux to the overlying water (~180 μmol m^{-2} d^{-1}; Fig. 4A) is much higher than the model calculated flux (~35 μmol m^{-2} d^{-1}; Table 7). At this station, the actual D_b value may be higher at this time of year and non-local exchange may account for a major proportion of the HPO$_4$$^{2-}$ flux. Furthermore, release of HPO$_4$$^{2-}$ from

organic matter at the sediment-water interface or turbulent diffusion in the upper millimetres of the sediment may also be important (Lohse et al., 1996).

CONCLUSIONS

A good correlation between the value of the sorption coefficient at $[HPO_4^{2-}] = 1$ μmol dm^{-3} (K_F/n) and NH$_4$-oxalate Fe and an enhanced release of Si(OH)$_4$ upon HPO$_4^{2-}$ sorption was observed for sediment from 8 North Sea stations. This suggests that the HPO$_4^{2-}$ removed from solution during sorption experiments with oxidized surface sediment was sorbed mostly to Fe oxides. Results of kinetics experiments for 2 stations suggest that the sorption process can be adequately described with a model assuming simultaneous instantaneous equilibrium and first-order kinetic sorption.

Combination of pore water and solid phase data with measured and calculated rates of sediment-water exchange of HPO$_4^{2-}$ indicates that sorption plays an important role in controlling sediment-water exchange of HPO$_4^{2-}$ during at least a part of the year in 3 of the 4 North Sea environments studied here. Sorption is most important when the oxidized sediment zone is relatively thick. At most stations, HPO$_4^{2-}$ sorption is suggested to constrain the flux of HPO$_4^{2-}$ to the overlying water. At one station in the depositional environment of the Skagerrak, however, desorption is suggested to be responsible for the maintenance of a flux of HPO$_4^{2-}$ to the overlying water. Application of a reaction-diffusion model to pore water HPO$_4^{2-}$ and solid phase P profiles for 2 stations demonstrates that both of these effects of sorption on sediment-water exchange of HPO$_4^{2-}$ can be adequately described when instantaneous equilibrium and first-order kinetic sorption is assumed in the model.

REFERENCES

Aller, R.C., 1980. Diagenetic processes near the sediment-water interface of Long Island Sound I. Decomposition and nutrient element geochemistry (S, N, P) Adv. Geophys. 22: 237-350.

Aller, R.C. and J.Y. Yingst, 1985. Effects of marine deposit feeders *Heteromastus filiformis* (Polychaeta), *Macoma balthica* (Bivalvia), and *Tellina texana* (Bivalvia) on averaged sedimentary solute transport, reaction rates, and microbial distributions. J. Mar. Res. 43: 615-645.

Anton K.K., Liebezeit G., Rudolph C. and Wirth H., 1993. Origin, distribution and accumulation of organic carbon in the Skagerrak. Mar. Geol. 111: 287-297.

Aspila, K.I., H. Agemian and A.S.Y. Chau, 1976. A semi-automated method for the determination of inorganic, organic and total phosphate in sediments. Analyst. 101: 187-197.

Balzer, W., 1984. Organic matter degradation and biogenic element cycling in a nearshore sediment (Kiel Bight). Limnol. Oceanogr. 29: 1231-1246.

Barrow, N.J., 1983. A mechanistic model for describing the sorption of phosphate by soil. J. Soil Sci. 34: 733-750.

Berner, R.A., 1976. Inclusion of adsorption in the modelling of early diagenesis. Earth Planet. Sci. Lett. 29: 333-340.

Berner, R.A., 1980. Early diagenesis: a theoretical approach. Princeton University Press, Princeton. 241p.

Berner, R.A., K.C. Ruttenberg, E.D. Ingall, and J.-L. Rao, 1993. The nature of phosphorus burial in modern marine sediments, In: Interactions of C, N, P, and S Biogeochemical Cycles and Global Change, R. Wollast, F.T. Mackenzie and L. Chou, eds., Springer-Verlag, NATO ASI Series Vol. 14, 521p.

Boudreau, B.P., 1984. On the equivalence of nonlocal and radial-diffusion models for pore water irrigation. J. Mar. Res. 42: 731-735.

Boudreau, B.P., 1986. Mathematics of tracer mixing in sediments: II. Nonlocal mixing and biological conveyor-belt phenomena. Am. J. Sci. 286: 199-238.

Boudreau, B.P., 1994. Is burial velocity a master parameter for bioturbation? Geochim. Cosmochim. Acta 58: 1243-1249.

Bray, J.T., O.P. Bricker and B.N. Troup, 1973. Phosphate in interstitial waters of anoxic sediments: oxidation effects during sampling procedures. Science 180: 1362-1364.

Broecker, W.S., 1982. Ocean chemistry during glacial time. Geochim. Cosmochim. Acta 46: 1689-1705.

Carritt, D.E. and S. Goodgal, 1954. Sorption reactions and some ecological implications. Deep-Sea Res. 1: 224-243.

Colombo, C., V. Barrón and J. Torrent, 1994. Phosphate adsorption and desorption in relation to morphology and crystal properties of synthetic hematites. Geochim. Cosmochim. Acta 58: 1261-1269.

Draper, N.R. and H. Smith, 1967. Applied regression analysis. John Wiley, 407p.

Einsele, W., 1936. Über die Beziehungen des Eisenkreislaufs zum Phosphatkreislauf im eutrophen See. Arch. Hydrobiol. 29: 664-686.

Eisma D. and J. Kalf, 1987. Dispersal, concentration and deposition of suspended matter in the North Sea. J. Geol. Soc. London. 144: 161-178.

Emerson, S., R. Jahnke and D. Heggie, 1984. Sediment-water exchange in shallow water estuarine sediments. J. Mar. Res. 42: 709-730.

Froelich, P.N., 1988. Kinetic control of dissolved phosphate in natural rivers and estuaries: a primer on the phosphate buffer mechanism. Limnol. Oceanogr. 33: 649-668.

Fuller, C.C., J.A. Davis and G.A. Waychunas, 1993. Surface chemistry of ferrihydrite: Part 2. Kinetics of arsenate adsorption and coprecipitation. Geochim. Cosmochim. Acta 57: 2271-2282.

Gehlen, M., J.F.P. Malschaert and W. Van Raaphorst, 1995. Spatial and temporal variability of benthic silica fluxes in the southeastern North Sea. Cont. Shelf Res. 15: 1675-1696.

Howarth, R.W., H. Jensen, R. Marino and H. Postma, 1995. Transport to and processing of phosphorus in near-shore and oceanic waters. p323-346. In: Phosphorus in the global environment, H. Tiessen, ed., John Wiley, SCOPE 54, 462p.

Ingall, E.D. and R.A. Jahnke, 1994. Evidence for enhanced phosphorus regeneration from marine sediments overlain by oxygen-depleted waters. Geochim. Cosmochim. Acta 58: 2571-2575.

Jensen, H.S. and B. Thamdrup, 1993. Iron-bound phosphorus in marine sediments as measured by the bicarbonate-dithionite extraction. Hydrobiologia 253: 47-59.

Jensen, H.S., P.B. Mortensen, F.Ø. Andersen, E. Rasmussen and A. Jensen, 1995. Phosphorus cycling in a coastal marine sediment, Aarhus Bay, Denmark. Limnol. Oceanogr. 40: 908-917.

Jørgensen, B.B., 1983. Processes at the sediment-water interface. In: The major biogeochemical cycles and their interactions. B. Bolin and R.B. Cook, editors. John Wiley, Chichester. p477-515.

Krom, M.D. and R.A. Berner, 1980a. The diffusion coefficients of sulfate, ammonium and phosphate ions in anoxic marine sediments. Limnol. Oceanogr. 25: 327-337.

Krom, M.D. and R.A. Berner, 1980b. Adsorption of phosphate in anoxic marine sediments. Limnol. Oceanogr. 25: 797-806.

Krom, M.D. and R.A. Berner, 1981. The diagenesis of phosphorus in a nearshore marine sediment. Geochim. Cosmochim. Acta 45: 207-216.

Lohse L., J.F.P. Malschaert, C.P. Slomp, W. Helder and W. Van Raaphorst, 1993. Nitrogen cycling in North Sea sediments: interaction of denitrification and nitrification in offshore and coastal areas. Mar. Ecol. Prog. Ser. 101: 283-296.

Lohse L., J.F.P. Malschaert, C.P. Slomp, W. Helder and W. Van Raaphorst, 1995. Sediment-water fluxes of inorganic nitrogen compounds along the transport route of organic matter in the North Sea. Ophelia 41: 173-197.

Lohse L., E.H.G. Epping, W. Helder and W. van Raaphorst, 1996. Oxygen pore water profiles in continental shelf sediments of the North Sea: turbulent versus molecular diffusion. Mar. Ecol. Prog. Ser. 145: 63-75.

Lookman, R., D. Freese, R. Merckx, K. Vlassak and W.H. Van Riemsdijk, 1995. Long-term kinetics of phosphate release from soil. Environ. Sci. Technol. 29: 1569-1575.

Lovely, D.R., 1991. Dissimilatory Fe(III) and Mn(IV) reduction. Microbiol. Rev. 55: 259-287.

Madrid, L. and P. Arambarri, 1985. Adsorption of phosphate by two iron oxides in relation to their porosity. J. Soil Sci. 36: 523-530.

Martens, C.S., R.A. Berner and J.K. Rosenfeld, 1978. Interstitial water chemistry of anoxic Long Island Sound sediments. 2. Nutrient regeneration and phosphate removal. Limnol. Oceanogr. 23: 605-617.

McCave, I.N., R.J. Bryant, H.F. Cook and C.A. Coughanowr, 1986. Evaluation of a laser diffraction size analyzer for use with natural sediments. J. Sed. Petrol. 56: 561-564.

Mortimer, C.H., 1941. The exchange of dissolved substances between mud and water in lakes. I. J. Ecol. 30: 280-329.

Mortimer, C.H., 1942. The exchange of dissolved substances between mud and water in lakes. II and IV. J. Ecol. 31: 147-201.

Parfitt, R.L., 1978. Anion sorption by soils and soil materials. Adv. Agron. 30: 1-50.

Parfitt, R.L., 1989. Phosphate reactions with natural allophane, ferrihydrite and goethite. J. Soil Sci. 40: 359-369.

Pettijohn, F.J., P.E. Potter and R. Siever, 1972. Sand and sandstone. Springer, New York. 618p.

Pohlmann, T. and W. Puls, 1994. Currents and transport in water. In: Circulation and contaminant fluxes in the North Sea. J. Sündermann, ed. Springer. p345-402.

Ruttenberg, K.C., 1992. Development of a sequential extraction method for different forms of phosphorus in marine sediments. Limnol. Oceanogr. 37: 1460-1482.

Ruttenberg, K.C. and R.A. Berner, 1993. Authigenic apatite formation and burial in sediments from non-upwelling, continental margin environments. Geochim. Cosmochim. Acta 57: 991-1007.

Schink, D.R. and N.L. Guinasso, 1978. Redistribution of dissolved and adsorbed materials in abyssal marine sediments undergoing biological stirring. Am. J. Sci. 278: 687-702.

Schwertmann U. and Cornell R.M., 1991. Iron oxides in the laboratory. VCH, Weinheim.

Slomp, C.P., S.J. Van der Gaast and W. Van Raaphorst, 1996a. Phosphorus binding by poorly crystalline iron oxides in North Sea sediments. Mar. Chem. 52: 55-73.

Slomp, C.P., E.H.G. Epping, W. Helder and W. Van Raaphorst, 1996b. A key role for iron-bound phosphorus in authigenic apatite formation in North Atlantic continental platform sediments. J. Mar. Res. 54: 1179-1205.

Slomp, C.P., J.F.P. Malschaert, L. Lohse and W. Van Raaphorst, 1997. Iron and manganese cycling in different sedimentary environments on the North Sea continental margin. Cont. Shelf Res., in press.

Strickland, T.R. and J.D. Parsons, 1972. A practical handbook of seawater analysis. 2nd. ed. Bull. Fish. Res. Bd. Can. 167: 1-311.

Sundby, B., L.G. Anderson, P.O.J. Hall, A. Iverfeldt, M.M. Rutgers van der Loeff, S.F.G. Westerlund, 1986. The effect of oxygen on release and uptake of cobalt, manganese, iron and phosphate at the sediment-water interface. Geochim. Cosmochim. Acta 50: 1281-1288.

Sundby, B., C. Gobeil, N. Silverberg and A. Mucci, 1992. The phosphorus cycle in coastal marine sediments. Limnol. Oceanogr. 37: 1129-1145.

Torrent, J. , V. Barrón, U. Schwertmann, 1992. Fast and slow phosphate sorption by goethite-rich natural materials. Clays Clay Miner. 40: 14-21.

Van Cappellen, P. and R.A. Berner, 1988. A mathematical model for the early diagenesis of phosphorus and fluorine in marine sediments. Apatite precipitation. Am. J. Sci. 288: 289-333.

Van Cappellen P. and Y. Wang, 1996. Cycling of iron and manganese in surface sediments: a general theory for the coupled transport and reaction of carbon, oxygen, nitrogen, sulfur, iron, and manganese. Am. J. Sci. 296: 197-243.

Van Raaphorst W., P. Ruardij and A.G. Brinkman, 1988. The assessment of benthic phosphorus regeneration in an estuarine ecosystem model. Neth. J. Sea Res. 22: 23-36.

Van Raaphorst, W., H.T. Kloosterhuis, A. Cramer and K.J.M. Bakker, 1990. Nutrient early diagenesis in the sandy sediments of the Doggerbank area, North Sea: pore water results. Neth. J. Sea Res. 26: 25-52.

Van Raaphorst, W. and H.T. Kloosterhuis, 1994. Phosphate sorption in superficial intertidal sediments. Mar. Chem. 48: 1-16.

Van Raaphorst, W. and J.F.P. Malschaert, 1996. Ammonium adsorption in superficial North Sea sediments. Cont. Shelf Res. 16: 1415-1435.

Van Riemsdijk, W.H., L.J.M. Boumans and F.A.M. de Haan, 1984. Phosphate sorption by soils. I. A model for the reaction of phosphate with metal oxides in soil. Soil Sci. Soc. Am. J. 48: 537-541.

Van Weering, T.C.E., G.W. Berger, J. Kalf, 1987. Recent sediment accumulation in the Skagerrak, northeastern North Sea. Neth. J. Sea Res. 21: 177-189.

Verardo, D.J., P.N. Froelich and A. McIntyre, 1990. Determination of organic carbon and nitrogen in sediments using the Carlo Erba Na-1500 analyzer. Deep-Sea Res., 37, 157-165.

Von Haugwitz W., H.K. Wong and U. Salge, 1988. The mud area southeast of Helgoland: A seismic study. Mitt. Geol.-Paläont. Inst. Univ. Hamburg. 65: 409-422.

Weber, W.J., Jr., P.M. McGingley and L.E. Katz, 1992. A distributed reactivity model for sorption by soils and sediments. 1. Conceptual basis and equilibrium assessments. Environ. Sci. Technol. 26: 1955-1962.

Willett, I.R., C.J. Chartres and T.T. Nguyen, 1988. Migration of phosphate into aggregated particles of ferrihydrite. J. Soil Sci. 39: 275-282.

APPENDIX

The differential equations for each P reservoir in the (I) oxidized surface zone ($0 \le x \le L_1$) and (II) reduced sediment zone ($x > L_1$) are as follows:

Pore water HPO_4^{2-} (C)

$$(1 + K_{eq_1})\frac{\partial C_I}{\partial t} = [D_b(1 + K_{eq_1}) + D_s]\frac{\partial^2 C_I}{\partial x^2} - \omega(1 + K_{eq_1})\frac{\partial C_I}{\partial x} + k_g \vartheta(G_I - G_\infty) + \tag{A1}$$
$$-\alpha(C_I - C_o) - k_s(C_I - C_s) = 0$$

$$(1 + K_{eq_2})\frac{\partial C_{II}}{\partial t} = [D_b(1 + K_{eq_2}) + D_s]\frac{\partial^2 C_{II}}{\partial x^2} - \omega(1 + K_{eq_2})\frac{\partial C_{II}}{\partial x} + k_g \vartheta(G_{II} - G_\infty) + \tag{A2}$$
$$-\alpha(C_{II} - C_o) - k_a(C_{II} - C_a) + k_m \vartheta(M_{II} - M_\infty) = 0$$

Organic P (G)

$$\frac{\partial G_I}{\partial t} = D_b \frac{\partial^2 G_I}{\partial x^2} - \omega \frac{\partial G_I}{\partial x} - k_g(G_I - G_\infty) = 0 \tag{A3}$$

$$\frac{\partial G_{II}}{\partial t} = D_b \frac{\partial^2 G_{II}}{\partial x^2} - \omega \frac{\partial G_{II}}{\partial x} - k_g(G_{II} - G_\infty) = 0 \tag{A4}$$

Fe-bound P (M)

$$\frac{\partial M_I}{\partial t} = D_b \frac{\partial^2 M_I}{\partial x^2} - \omega \frac{\partial M_I}{\partial x} + \frac{k_s}{\vartheta}(C_I - C_s) = 0 \tag{A5}$$

$$\frac{\partial M_{II}}{\partial t} = D_b \frac{\partial^2 M_{II}}{\partial x^2} - \omega \frac{\partial M_{II}}{\partial x} - k_m(M_{II} - M_\infty) = 0 \tag{A6}$$

Authigenic P (A)

$$\frac{\partial A_I}{\partial t} = D_b \frac{\partial^2 A_I}{\partial x^2} - \omega \frac{\partial A_I}{\partial x} = 0 \tag{A7}$$

$$\frac{\partial A_{II}}{\partial t} = D_b \frac{\partial^2 A_{II}}{\partial x^2} - \omega \frac{\partial A_{II}}{\partial x} + \frac{k_a}{\vartheta}(C_{II} - C_a) = 0 \tag{A8}$$

Instantaneous, reversible linear equilibrium sorption gives:

Sorbed P (S)

$$S_I = \frac{K_{eq1}}{9} C_I \qquad (A9)$$

$$S_{II} = \frac{K_{eq2}}{9} C_{II} \qquad (A10)$$

The boundary conditions used to solve the equations (A1) to (A8) are :

at $x = 0$

$$C_I = C_o \qquad (A11)$$

$$J_{G_{x=0}} = -\phi 9 [D_b \frac{\partial G_I}{\partial x} - \omega G_I]_{x=0} \qquad (A12)$$

$$J_{M_{x=0}} = -\phi 9 [D_b \frac{\partial M_I}{\partial x} - \omega M_I]_{x=0} \qquad (A13)$$

$$J_{A_{x=0}} = -\phi 9 [D_b \frac{\partial A_I}{\partial x} - \omega A_I]_{x=0} \qquad (A14)$$

at $x = L_1$

$$C_I = C_{II} \qquad (A15)$$

$$G_I = G_{II} \qquad (A16)$$

$$M_I = M_{II} \qquad (A17)$$

$$A_I = A_{II} \qquad (A18)$$

$$[D_b(1+K_{eq1})+D_s]\frac{\partial C_I}{\partial x} - \omega(1+K_{eq1})C_I = \qquad (A19)$$

$$= [D_b(1+K_{eq2})+D_s]\frac{\partial C_{II}}{\partial x} - \omega(1+K_{eq2})C_{II}$$

$$D_b \frac{\partial G_I}{\partial x} - \omega G_I = D_b \frac{\partial G_{II}}{\partial x} - \omega G_{II} \qquad (A20)$$

$$D_b \frac{\partial M_I}{\partial x} - \omega M_I = D_b \frac{\partial M_{II}}{\partial x} - \omega M_{II} \qquad (A21)$$

$$D_b \frac{\partial A_I}{\partial x} - \omega A_I = D_b \frac{\partial A_{II}}{\partial x} - \omega A_{II} \qquad (A22)$$

when $x \rightarrow \infty$

$$C_{II} = E \qquad (A23)$$

$$G_{II} \rightarrow G_\infty \qquad (A24)$$

$$M_{II} \rightarrow M_\infty \qquad (A25)$$

$$\frac{\partial A_{II}}{\partial x} \rightarrow 0 \qquad (A26)$$

$$E = \frac{(k_a C_a + \alpha C_o)}{(k_a + \alpha)} \qquad (A27)$$

Chapter 6

A key role for iron-bound phosphorus in authigenic apatite formation in North Atlantic continental platform sediments[*]

ABSTRACT

A combination of pore water and solid phase analysis was used to determine whether authigenic carbonate fluorapatite (CFA) is currently forming in the sediment at two locations (OMEX I and II) on the North Atlantic continental platform Goban Spur (southwest of Ireland). Results of selective P extractions suggest that an early diagenetic redistribution of Fe-bound P to an authigenic P phase may be occurring at both stations. A steady-state diagenetic model describing the depth profiles of pore water HPO_4^{2-} and three solid phase forms of P (organic P, Fe-bound P and authigenic P) was developed and applied to the data of station OMEX-I. The model results indicate that CFA formation can account for the observed increase of authigenic P with depth at this station. Furthermore, the results show that an intense cycling of P between Fe-bound P and pore water HPO_4^{2-} at the redox interface can create conditions beneficial for CFA formation. This internal P cycle is driven by downward, bioturbational transport of mainly *in-situ* formed Fe-bound P into the reduced sediment zone. Losses from the internal P cycle due to CFA formation and HPO_4^{2-} diffusion are compensated for by sorption of HPO_4^{2-} released from organic matter to Fe oxides in the oxidized surface sediment. Fe-bound P thus acts as an intermediate between organic P and CFA. CFA can account for between 25 and 70% of the total burial flux of reactive P at station OMEX-I and thus may act as an important sink for P in this low sedimentation, continental margin environment.

INTRODUCTION

Phosphorus (P) is an essential nutrient for marine phytoplankton and has been suggested as the limiting factor for oceanic primary production on geological timescales (Howarth et al., 1995). As sediments form the only important sink for P in the marine environment, changes in the burial rate of P in sediments can modify the oceanic inventory of P and thus profoundly influence marine carbon cycling (Broecker and Peng, 1982). Most removal of P from the water column takes place through sedimentation of organic matter (Berner et al., 1993). Consequently, it is of prime importance to know the fate of the P in organic matter upon reaching the sediment.

As shown in the schematic overview of the sedimentary P cycle in Figure 1, part of the P in organic matter is buried directly as organic P. The nonrefractory portion of the organic matter decomposes, however, resulting in a release of HPO_4^{2-} to the pore water. In the oxidized part of the sediment, this HPO_4^{2-} escapes to the overlying water through upward

diffusion or is sorbed, either reversibly or irreversibly, to sediment Fe oxides (e.g. Sundby et al., 1992; Slomp et al., 1996). In the reduced sediment zone HPO_4^{2-} is not only released from organic matter but also from Fe oxides upon their reduction. In this part of the sediment, dissolved HPO_4^{2-} concentrations can become high enough for authigenic mineral formation to occur (e.g. Van Cappellen and Berner, 1988). Whether this actually takes place is important, as P bound in authigenic minerals may not be solubilized again, whereas Fe-bound and organic P can still be released upon deep burial.

Evidence for authigenic mineral formation in marine sediments outside classical phosphorite accumulation environments in upwelling areas (e.g the Peru continental margin; Froelich et al., 1988) is difficult to obtain. Due to the low concentrations of authigenic P, direct identification with e.g. X-ray diffraction, is often impossible. This makes it necessary to rely on indirect methods. These include calculation of the saturation state of the pore water with respect to authigenic P minerals (Martens et al., 1978; Jahnke et al., 1983), the use of stoichiometric models describing NH_4^+ and HPO_4^{2-} regeneration to detect a possible deficit of HPO_4^{2-} with respect to NH_4^+ (Martens et al., 1978), and application of selective extraction procedures (Ruttenberg, 1992).

Using all of these methods, Ruttenberg and Berner (1993) showed that authigenic carbonate fluorapatite (CFA) formation is occurring in rapidly accumulating continental margin sediments dominated by terrigenous material. Based on mirror-image profiles of organic and authigenic P, they concluded that at their two study sites HPO_4^{2-} released from organic material is almost completely retained in the sediment due to an early diagenetic 'sink-switching' to CFA. Using the same selective extraction procedure for authigenic P, Lucotte et al. (1994) showed that P retention due to CFA formation may also occur in continental rise sediments. In this case, however, Fe-bound P acted as the major source of P and the overall CFA precipitation rate was much lower.

We expect Fe-bound P to play a key role in CFA formation in many marine sediments for two reasons. Firstly, Fe-bound P can act as an intermediate between organic P and CFA. Dissolved HPO_4^{2-} released from labile organic matter, that otherwise would rapidly escape to the overlying water, is retained in the sediment. This HPO_4^{2-} can then cycle between the dissolved and Fe-bound P pool many times, before being permanently bound in CFA. Secondly, HPO_4^{2-} release from Fe oxides has been observed to be accompanied by a simultaneous release of fluoride. The resulting spike of both solutes may provide the condition of supersaturation required for the precipitation of CFA (Heggie et al., 1990; Ruttenberg and Berner, 1993).

In this study, we apply the extraction procedure for authigenic P developed by Ruttenberg (1992) to sediments from two low sedimentation environments on a North Atlantic continental platform. These results are combined with pore water and solid phase
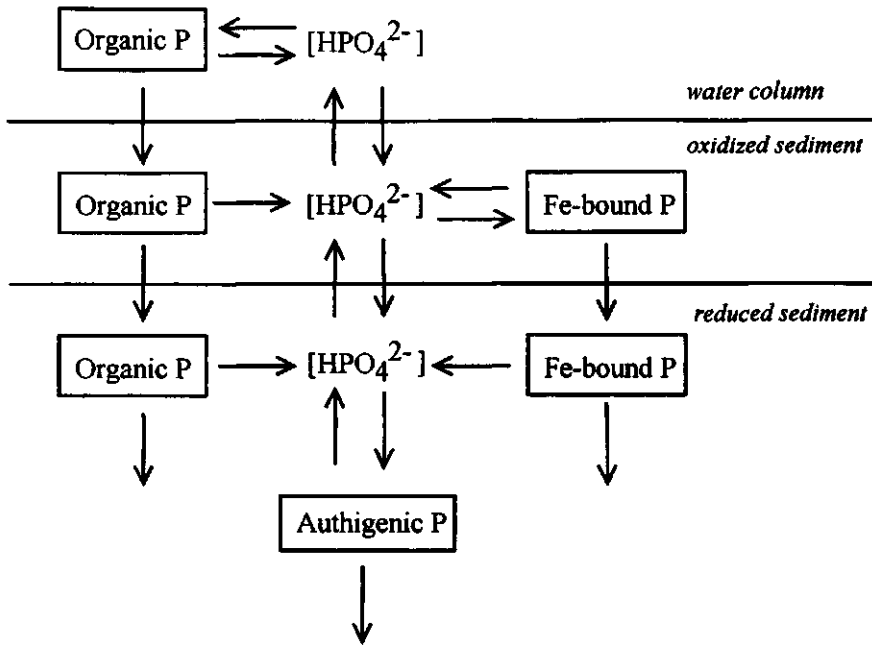
Organic P ⇄ $[HPO_4^{2-}]$

water column

oxidized sediment

Organic P → $[HPO_4^{2-}]$ ⇄ Fe-bound P

reduced sediment

Organic P → $[HPO_4^{2-}]$ ← Fe-bound P

Authigenic P

Fig. 1. A schematic overview of the sedimentary P cycle. Note that in this view, biogenic Ca-P, $CaCO_3$- and clay-bound P and detrital Ca-P are assumed to be unimportant as a source or sink for dissolved reactive phosphorus.

data to determine whether CFA formation is an early diagenetic event in these sediments, and if so, whether there is evidence for a key role of Fe-bound P in CFA formation. A diagenetic model for the sedimentary P cycle is developed and applied to the data to facilitate interpretation of the observed depth profiles.

STUDY SITES

Two locations on the continental platform Goban Spur, which is situated in the North Atlantic Ocean, south-west of Ireland (Fig. 2), were selected for this study. This broad platform (200-2000 m water depth) is connected to the Celtic Sea continental shelf in the east, is incised by deep canyons on its southern side, whereas to the north and west, the platform slopes down into the Porcupine Basin and the Porcupine Abyssal Plain, respectively. Sediment trap and current meter deployments show that the platform is a biologically and physically dynamic environment, dominated by lateral particle transport and high current velocities (Antia and Von Bodungen, in prep.). Samples were collected during an OMEX (Ocean Margin Exchange) cruise with RV Pelagia in October 1993. Station OMEX-I (49°24.72' N, 11°31.86' W) is located on the eastern, relatively shallow

part of the platform (at a water depth of 670 m), whereas station OMEX-II (49°11.20' N, 12 °49.18' W) is located on the deeper, western part of the platform (at a water depth of 1425 m).

Bottom water temperature was higher at station I (10°C) than at the deeper station II (5.9°C). Holocene sediment accumulation rates of 0.0025 and 0.0011 cm y^{-1} were estimated for stations I and II, respectively, using planktonic foraminiferal biostratigraphy and radiocarbon dating (Van Weering and De Stigter, pers. comm.). More than 90% of the macrofauna at these stations were present in the upper 5 cm of the sediment (Flach and Heip, 1996). This indicates that sediment mixing due to bioturbation was mainly limited to this surface layer. Sediment mixing or biodiffusion coefficients (D_b) calculated from excess ^{210}Pb profiles (Van Weering and De Stigter, pers. comm.), assuming a uniformly mixed surface zone of 5 cm overlying undisturbed sediment, amount to 0.18 and 0.05 cm^2 y^{-1} at stations I and II, respectively.

EXPERIMENTAL METHODS

Sampling. Sediment cores with overlying bottom water were obtained with a cylindrical box corer (either 30 or 50 cm i.d.). Subsamples were taken from the box cores with Plexi-glas or acrylic liners (3.1, 5.4 or 10 cm i.d.) which were closed with rubber stoppers. Only cores without any visible disturbance were used.

Pore water analysis. Subcores (3.1 cm i.d.) were sliced into 16 depth intervals down to a depth of 15 cm under nitrogen and at *in-situ* temperature immediately after collection. Pore water was collected from these slices using teflon Reeburgh-type squeezers under N$_2$-pressure (Reeburgh, 1967) and 0.2 µm cellulose acetate filters. Bottom water samples were obtained from the overlying water in one of the subcores. The samples were immediately analyzed for NH$_4^+$ (phenol-hypochlorite method; Helder and De Vries, 1979), NO$_3^-$ and HPO$_4^{2-}$ (Strickland and Parsons, 1972). Aliquots of pore water were acidified to pH $\approx$ 1 and analyzed for Fe^{2+} (ferrozine method; Stookey, 1970) and Mn^{2+} (formaldoxime method; Brewer and Spencer, 1971). All analyses were carried out on a Technicon TRAACS-800 autoanalyzer. The analytical precision of the determinations was 2% for NH$_4^+$ and HPO$_4^{2-}$ and 1% for all other compounds. The acidified pore water samples were additionally analyzed for HPO$_4^{2-}$ to determine whether loss of pore water HPO$_4^{2-}$ due to Fe^{2+} oxidation and subsequent sorption of HPO$_4^{2-}$ (Bray et al., 1973) had occurred in the sample cups. No significant difference in the pore water HPO$_4^{2-}$ concentration in acidified and nonacidified pore water samples was found.
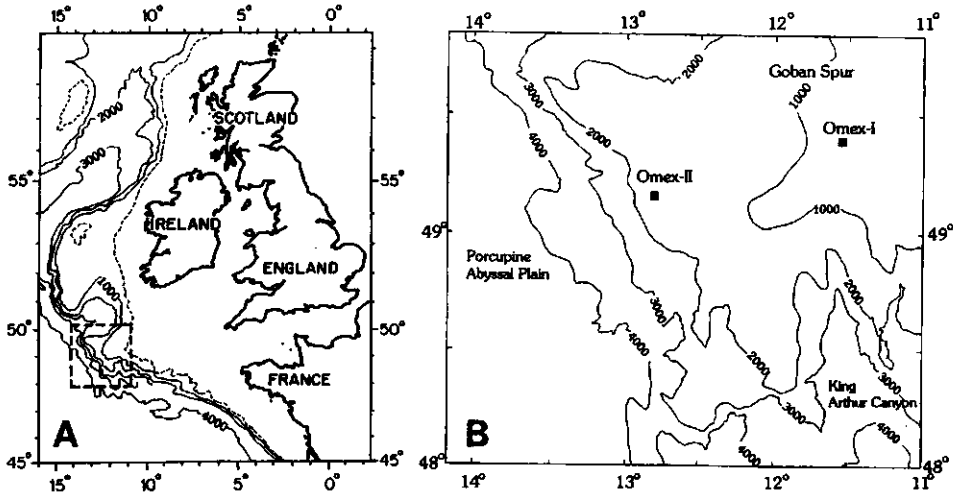
Fig. 2. (A) Location of the deep-water continental platform Goban Spur; (B) positions of the stations OMEX-I and OMEX-II.

Pore water O_2 profiles were determined in subcores (5.4 cm i.d.) on-deck with Clark type micro-electrodes (Diamond Corporation, type 737, 60 μm tip diameter; further details will be given in Epping et al., in prep.).

Solid phase analysis. The sediment remaining after the collection of the pore water was dried (60°C) and ground (teflon mortar and pestle) to < 125 μm. These samples were used for all subsequent solid phase analyses. Inorganic sediment P was fractionated in to Fe-bound P, authigenic P (this includes CFA, biogenic Ca-P, $CaCO_3$-bound P and possibly smectite-bound P) and detrital Ca-P using a sequential extraction procedure modified from the sedex method of Ruttenberg (1992). Fe-bound P was determined as citrate-dithionite bicarbonate (CDB, pH = 7.3, 8 h, 20°C) extractable P. The sediment residue was subsequently extracted with 1 M Na-acetate buffer (pH = 4, 6h, 20°C) and treated with a 1 M $MgCl_2$ (pH = 8, 0.5 h, 20°C) wash solution. Authigenic P was calculated as the sum of the P extracted in these last two steps. The sediment residue was then treated with 1 M HCl (24 h, 20°C) and the amount of extracted P was used as a measure of detrital Ca-P. There are three differences with the original 13-step procedure of Ruttenberg (1992). First, the 1 M $MgCl_2$ step to extract exchangeable or loosely sorbed P was omitted. Our Fe-bound P fraction thus includes easily exchangeable P. Second, we omitted all but one of the $MgCl_2$ washes and all H_2O rinses. These were included in the original procedure to reverse secondary sorption of P on to residual solid surfaces during the extractions. The results of

Ruttenberg (1992) show, however, that this process is not important during the CDB and HCl extractions and can be largely reversed with only one $MgCl_2$ extraction following the acetate buffer treatment. Third, we determined organic P in a separate procedure, since organic P concentrations may be underestimated when using the sequential sedex procedure (Ruttenberg, 1992; Berner et al., 1993).

Organic P was determined nonsequentially as the difference between 1 M HCl extractable P (24 h) before and after ignition of the sediment (550°C, 2h; Aspila et al., 1976). Total P is calculated as the sum of this organic P and the inorganic P determined with the sequential procedure. Inorganic P concentrations determined as the sum of Fe-bound P, authigenic P and detrital Ca-P were approximately equal to P concentrations obtained with the 1 M HCl extraction in the one-step procedure. Only at some depth intervals in the upper 2 cm at stations I and II significantly more P (up to ~ 1 μmol g^{-1}) was extracted with the sequential procedure. We attribute this discrepancy to incomplete extraction of inorganic P (most probably of Fe-bound P) with 1 M HCl.

All extractions were performed in duplicate. The P concentration in the CDB extracts (Fe-bound P) was determined using an Inductively Coupled Plasma-Atomic Emisson Spectrophotometer (ICP-AES; Spectro Analytical Instruments). All other P analyses were carried out using a Shimadzu Spectrophotometer with the method of Strickland and Parsons (1972). Precision of the individual extractions was generally ~5%. As the organic P concentration was determined as the relatively small difference between two large numbers, the uncertainty in the organic P concentrations is large (up to 30%).

The Fe and Mn concentrations in the CDB solutions of the P-extractions were measured using an ICP-AES and a Perkin Elmer 5100 PC Atomic Absorption Spectrophotometer, respectively. CDB-extractable Fe is assumed to be a measure of total Fe bound in Fe oxides (CDB may also extract some Fe from clay minerals and from Fe sulfides; Slomp et al., 1996). CDB extractable Mn is used as a measure of the total Mn oxides in the sediment (Canfield et al., 1993).

Total C and N and organic C were measured on a Carlo Erba 1500-2 elemental analyzer. Organic C was determined as the concentration of C in the sample after treatment with sulfurous acid (Verardo et al., 1990). $CaCO_3$ content was calculated from inorganic C concentrations determined as the difference between total and organic C. All sediment N was assumed to be present in an organic form. Grain size distribution was measured with a laser diffraction particle sizer (Malvern 2600 E). Sediment porosity was measured in samples from three additional subcores (3.1 cm i.d.). These were sliced into 10 depth intervals (slices of 0.5 cm thickness down to a depth of 5 cm) and the samples were dried at 105°C (24 h).

DESCRIPTION OF THE MODEL

To obtain more quantitative insight in the redistribution of sediment P with depth, a mathematical model describing the sedimentary P cycle, as outlined in Fig. 1, was developed and applied to the data. The steady-state model describes the concentration change with depth of pore water HPO_4^{2-}, and three forms of particulate P, i.e., organic P, Fe-bound P and authigenic P. The latter phase is assumed to include all P phases extractable with acetate buffer (see methods section). Transport of solid phase P occurs through bioturbational/physical mixing (described as a biodiffusion process) and sediment accumulation. Transport of dissolved HPO_4^{2-} additionally takes place through molecular diffusion.

The sediment column is divided into 3 zones: an oxidized surface zone (I: $0 \leq x \leq L_1$), a reduced sediment zone with bioturbation (II: $L_1 < x \leq L_2$) and a reduced sediment zone without bioturbation (III: $x > L_2$). The processes included are (1) release of HPO_4^{2-} from organic P due to organic matter mineralization (zone I, II, III), (2) reversible sorption of HPO_4^{2-} to Fe oxides (zone I), (3) release of HPO_4^{2-} from Fe-bound P due to reductive dissolution of the Fe oxides (zone II, III) and (4) CFA precipitation (zone II, III). All release and removal processes are described as first-order reactions, with the rate being equal to a rate constant times the difference between the actual concentration and an equilibrium (pore water) or asymptotic (solid phase) value. The rate constants for the processes (1) to (4) listed above are k_g, k_s, k_m, and k_a, respectively. The pore water equilibrium concentrations for sorption and CFA precipitation are C_s and C_a. The asymptotic Fe-bound P and organic P concentrations are equal to M_∞ and G_∞.

There are two major differences with the only other diagenetic P model known to us that includes both HPO_4^{2-} release from organic matter and release from Fe oxides (Van Capellen and Berner, 1988). Firstly, we include transport through bioturbational/physical mixing in the upper part of the sediment. This increases the downward transport of organic and Fe-bound P and thus enhances the cycling of P in the sediment (as shown for the Mn cycle by Aller (1990)). Furthermore, this results in upward transport of CFA and thus in a 'background' concentration of CFA at the sediment-water interface. Secondly, sorption of HPO_4^{2-} is modeled as a first-order process and not as simple linear equilibrium sorption. Sorption isotherms for oxic sediments may deviate from linearity, and P sorption has been shown to be rapid but not instantaneous (e.g. Slomp and Van Raaphorst, 1993). Description of P sorption as a first-order process has proved to be successful in the past (Van Raaphorst et al., 1988, 1990; Van Raaphorst and Kloosterhuis, 1994).

Pore water HPO_4^{2-} and the particulate P forms have units of μmol per cm^3 pore water and μmol per gram of dry sediment, respectively. A conversion factor ϑ (gram of dry

sediment per cm^3 of pore water) is introduced to enable a combination of dissolved HPO_4^{2-} and solid phase P in one model:

$$\vartheta = \rho_s[(1-\phi)/\phi] \qquad (1)$$

where ρ_s is the average density of the sediment particles (2.65 g cm^{-3}) and ϕ is the porosity of the sediment (in units of cm^3 cm^{-3}). The molecular (D_s) and biodiffusion (D_b) coefficients (both in units of cm^2 d^{-1}), the sedimentation rate (ω, in units of cm d^{-1}), the reaction rate constants (k_g, k_s, k_m and k_a, in units of d^{-1}) and the sediment porosity (ϕ) are assumed to be constant with depth in each relevant layer. This is a common assumption in many diagenetic models (e.g. Berner, 1980).

The set of differential equations for the one-dimensional distribution of pore water HPO_4^{2-} and the three particulate P forms is given in the Appendix (A1-A12). These equations were solved analytically assuming continuity in concentrations and fluxes of both dissolved HPO_4^{2-} and solid phase P at the boundaries between the three depth zones, i.e. at $x = L_1$ and $x = L_2$, and considering appropriate boundary conditions for the system at $x = 0$ and $x \to \infty$. Constant fluxes of organic P, Fe-bound P and authigenic P from the overlying water to the sediment were assumed at $x = 0$ ($J_{Gx=0}$, $J_{Mx=0}$ and $J_{Ax=0}$, respectively). The pore water HPO_4^{2-} concentration at $x = 0$ was assumed to be equal to the bottom water concentration (C_0). When $x \to \infty$, equilibrium values for pore water HPO_4^{2-} (C_a), and asymptotic values for organic and Fe-bound P (G_∞, M_∞) are assumed to be reached. The mathematical expressions for these boundary conditions are given in the Appendix (A13-A35).

It is important to note that three processes can contribute to a 'background' concentration of authigenic P at the sediment-water interface: (1) formation of CFA in the surface layer of the sediment, (2) upward bioturbational/physical transport of CFA formed *in-situ* in deeper layers and (3) deposition of authigenic P which has been formed elsewhere ($J_{Ax=0}$). In the model, it is assumed that the first process is not important when an oxidized surface layer is present. This is a reasonable assumption when sorption of HPO_4^{2-} to Fe-oxides in the oxidized layer is rapid. This results in a buffering of pore water HPO_4^{2-} concentrations to low values in the surface sediment thus presumably precluding supersaturation of the pore water with respect to CFA. The contribution of the other two processes to the background concentration of authigenic P can be calculated with the model when L_1, L_2, D_s, D_b and ω are fixed.

Values of k_g, k_s, k_m, k_a, $J_{Gx=0}$, $J_{Ax=0}$, G_∞, and M_∞ were varied to fit the model to experimental data. Variance-weighted sums of squares of all 4 components were minimized simultaneously using an iteratively reweighted regression (Draper and Smith, 1967). This

Table 1. Sediment characteristics of the surface layer (0-0.25 cm) at stations OMEX-I and -II. The sediment classification is based on the Wentworth size scale (Pettijohn et al., 1972).

	Unit	OMEX-I	OMEX-II
porosity	(v/v)	0.50	0.48
org. C	(wt%)	0.37	0.64
org. N	(wt%)	0.05	0.09
$CaCO_3$	(wt %)	51	61
median grain size	(μm)	92	55
sed. fraction < 2 μm	(%)	0	5
sed. classification		very fine sand	coarse silt

means that 8 fit parameters were used for 4 profiles with a total of 64 data points. The other parameters (L_1, L_2, D_s, D_b, ω, C_0, C_s, C_a, $J_{Mx=0}$) were fixed based on existing data.

EXPERIMENTAL RESULTS

General sediment characteristics. Some general sediment characteristics of the two stations are listed in Table 1. Both sediments have a low porosity, are organic-poor and contain substantial amounts of $CaCO_3$, mainly in the form of foraminiferal remains. The sediment from station II is finer grained and contains higher concentrations of organic C and N and $CaCO_3$ than that from station I.

At both stations, $CaCO_3$ concentrations decrease with depth (Fig. 3A and B). This decrease is confined to the surface 6 cm of the sediment at station I, whereas it occurs between 6 and 14 cm depth at station II. The organic C profile at station I displays a large degree of scatter (Fig. 3C). At station II, organic C concentrations decrease sharply close to the sediment-water interface followed by a more gradual decrease with depth (Fig. 3D). Organic N concentrations rapidly decrease in the upper 2 cm of the sediment at station I, succeeded by relatively constant values with depth (Fig. 3E). At station II, the organic N profile closely follows the trend of the organic C profile (Fig. 3F). Sediment porosity decreases slightly with depth at both stations. The sediment grain size distribution does not change significantly with depth at station I, but the amount of fine sediment material increases between 10 and 15 cm depth at station II (the median grain size decreases from 50 μm to 23 μm in this depth interval).

Pore water profiles. Bottom water O_2 concentration levels were 231 and 241 μmol dm^{-3} at stations I and II, respectively, and were close to saturation values. Maximum O_2 penetration depths were shallower at station I (0.91 cm) than at station II (5.0 cm; complete profiles
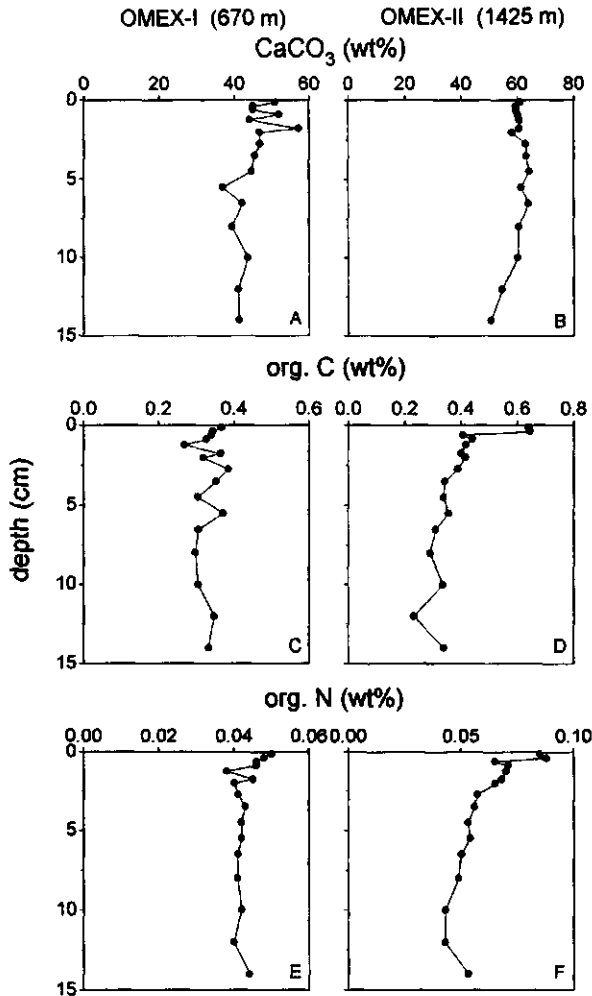
Fig. 3. Profiles of (A,B) CaCO$_3$, (C, D) organic C and (E, F) organic N (wt%) at stations OMEX-I and -II.

will be given in Epping et al., in prep.). Pore water NO$_3^-$ concentrations (Fig. 4A and B) reached a maximum close to the sediment surface at both stations. At station I, NO$_3^-$ concentrations rapidly decreased to low values within the upper 2 cm of the sediment, whereas at station II, NO$_3^-$ penetrated down to 14 cm depth. In the following text, we will use (1) the maximum depth of O$_2$ penetration as the boundary between the *oxic* and *anoxic* sediment zones and (2) the depth where NO$_3^-$ concentrations reach a background value as the boundary between the *oxidized* and *reduced* sediment zones, as relevant for Fe.
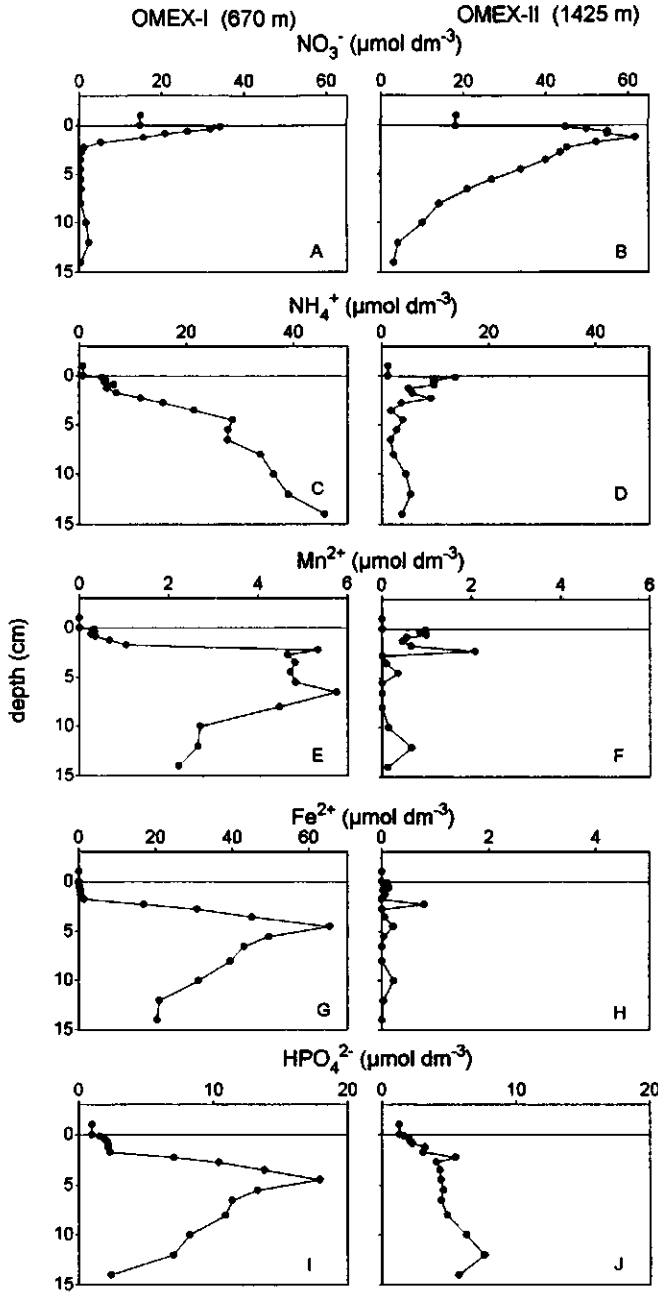
Fig. 4. Pore water profiles of (A, B) NO_3^-, (C, D) NH_4^+, (E,F) Mn^{2+}, (G, H) Fe^{2+} and (I, J) HPO_4^{2-} (μmol dm^{-3}) at stations OMEX-I and -II.
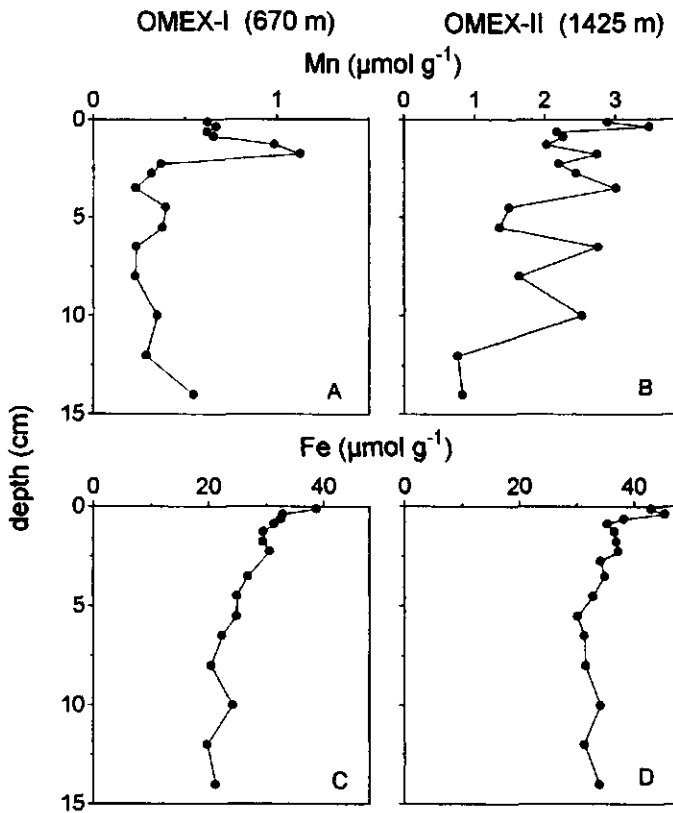
Fig. 5. Solid phase profiles of CDB-extractable (A, B) Mn and (C, D) Fe (μmol g^{-1}) at stations OMEX-I and -II.

Pore water NH_4^+ concentrations rapidly increased with depth (to ~ 45 μmol dm^{-3} at 15 cm) in the reduced zone at station I (Fig. 4C). At station II, the NH_4^+ profile reached a maximum (~14 μmol dm^{-3}) close to the sediment-water interface, followed by a decrease to concentrations below ~5 μmol dm^{-3} at depth (Fig. 4D). Mn^{2+} and Fe^{2+} pore water profiles indicate dissolution of sediment Mn and Fe oxides upon NO_3^- depletion at station I (Fig. 4E and G). At station II, pore water Mn^{2+} and Fe^{2+} concentrations were very low (< 2 μmol dm^{-3}) throughout the sediment (Fig. 4F and H).

The pore water HPO_4^{2-} profile at station I shows a remarkable resemblance to the Fe^{2+} profile, suggesting a coupling between the release of HPO_4^{2-} and Fe^{2+} in the sediment (Fig. 4G and I). HPO_4^{2-} concentrations are buffered to low values (~1-2 μmol dm^{-3}) in the oxidized surface zone of the sediment. The sharp increase in the HPO_4^{2-} concentration with depth below this zone (to ~ 18 μmol dm^{-3}) is followed by a steep decrease below ~5 cm, indicating removal of dissolved HPO_4^{2-} in the reduced part of the sediment. At station II,

the HPO_4^{2-} profile has a distinctly different shape (Fig. 4J). The HPO_4^{2-} concentration increases immediately below the sediment-water interface but the gradient levels off below 2.5 cm. The maximum HPO_4^{2-} concentration reached (~8 μmol dm^{-3}) is much lower than at station I. The small but simultaneous maxima of Mn^{2+}, NH_4^+, Fe^{2+} and HPO_4^{2-} in the 2-2.5 cm depth interval, suggest very local, reduced conditions due to organic matter decomposition in the oxidized sediment at station II (Fig. 4D, F, H and J).

Solid phase profiles of Mn, Fe and P. The sharp subsurface peak in sediment Mn oxide (Fig 5A) at station I is typical for mobilization and reprecipitation of Mn at the redox interface for Mn in a low sedimentation and low bioturbation sediment environment (Burdige and Gieskes, 1983). The redox interface for Mn is generally assumed to occur at the oxic/anoxic interface (Aller, 1990). The depth of the solid phase Mn and pore water Mn^{2+} peaks at station I indicate that either the on-deck O_2 profiles underestimate actual *in-situ* O_2 penetration or that NO_3^- is acting as the main oxidant for Mn^{2+}. At station II, Mn oxide concentrations decrease with depth but show a large variability (Fig. 5B). Several of the local minima in the Mn oxide profile occur in the same depth intervals as maxima in the pore water Mn^{2+} profile (2-2.5, 4-5 and 11-13 cm; Fig. 4F). This suggests that the observed variability in the Mn oxide profile is due to local Mn oxidation and reduction in the 'oxidized' sediment of station II.

A decrease in total Fe oxides with depth is observed at both stations (Fig. 5C and D) with the largest decrease occurring in the upper 2 cm of the sediment. This is followed by a more gradual decrease down to ~8 and ~6 cm at stations I and II, respectively. Reduction of Fe oxides apparently occurs in the 'oxidized' sediment zone at station II.

The sediment P profiles, as determined with the selective extractions, are shown in Fig. 6A-H. Organic P (Fig. 6A and B) remains relatively constant or even slightly increases with depth at station I, whereas a decrease is observed at station II. At both stations, a decrease of Fe-bound P and a concomitant increase of authigenic P (Fig. 6C and D) with depth was found. Detrital Ca-P concentrations (Fig. 6E and F) are relatively constant at station I, but slightly increase with depth at station II. At station I, inorganic and total P concentrations (Fig. 6G and H) increase slightly with depth. At station II, inorganic P concentrations remain relatively constant with depth, whereas total P concentrations decrease.

The acetate extraction is not strictly selective for CFA (see methods section and Ruttenberg, 1992). If foraminiferal shells contain little P, as suggested by the results of Sherwood et al. (1987), an increase of the contribution of $CaCO_3$ to the total sediment flux with time may result in a dilution of acetate extractable P phases which have not been
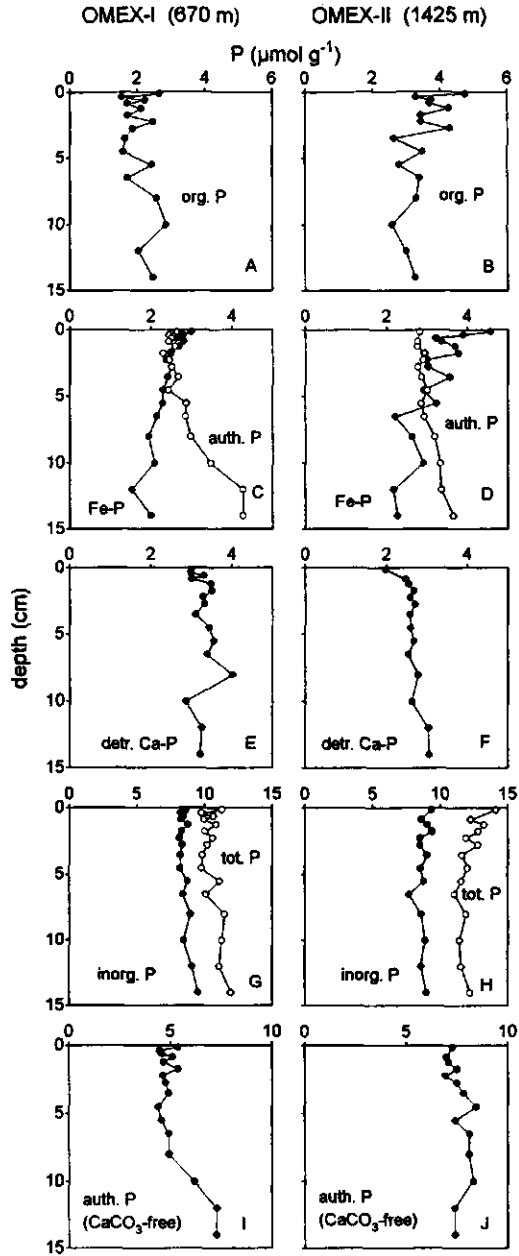
Fig. 6. Solid phase profiles of P (μmol g^{-1}) at stations OMEX-I and -II as determined with the extraction procedures: (A, B) organic P, (C, D) Fe-bound P (filled circles) and authigenic P (open circles), (E, F) detrital Ca-P, (G, H) inorganic P (filled circles) and total P (open circles) and (I, J) authigenic P on a CaCO$_3$ free-basis.

formed *in-situ*. Consequently, lower concentrations of authigenic P will be found at the sediment-water interface than at depth without *in-situ* CFA formation. In this study, $CaCO_3$ concentrations decreased with depth at both stations (Fig. 3A and B). This can be the result of an increase in the contribution of $CaCO_3$ to the sediment flux with time. To assess whether this could account for the observed authigenic P increase, authigenic P concentrations are presented on a $CaCO_3$-free basis in Fig. 6I and J. The results suggest that admixing with $CaCO_3$ cannot account for the increase of authigenic P observed at station I, but may be responsible for a large part of the observed increase with depth at station II.

APPLICATION OF THE MODEL

Both the pore water and solid phase profiles indicate that reduction of Fe and Mn oxides occurs in the oxidized sediment of station II, thus implying a strong heterogeneity of the sediment at this station. As the model is based on a strictly vertical redox zonation, it cannot be applied to the results of station II and we will therefore concentrate on station I.

Fixed parameters. The fixed parameters used for the model fits and their source are listed in Table 2. The burial flux of Fe is calculated from the sediment accumulation rate (Table 2) and the Fe concentration of the material being buried (Fig. 5). Assumption of steady-state requires that all Fe thus removed through burial is replenished through sedimentation of Fe oxides. As these Fe oxides necessarily contain some P, this results in a flux of Fe-bound P to the sediment ($J_{Mx=0}$). The Fe/P ratio of the sedimenting material is of course crucial for the value of this P flux. We assume the Fe/P ratio of these incoming Fe oxides to be equal to 10, which is a value typical for both synthetic (Gerke and Hermann, 1992) and natural (Jensen and Thamdrup, 1993; Sundby et al., 1992; Slomp et al., 1996) poorly crystalline Fe oxides.

Model fits and calculated rate constants. Model fits for pore water HPO_4^{2-} and the three diagenetically active solid phase P forms agree reasonably well with the measured profiles (Fig. 7A-D). The major discrepancy between the model and field results occurs for the pore water HPO_4^{2-} profile (Fig. 7A). The sharp transition from low concentrations in the oxidized sediment zone to 'peak values' below the redox boundary is not accurately described. Due to the large scatter in the organic P data (Fig. 7B), it is difficult to check the validity of the model fit for this component. The organic C profile is of little assistance, as a large variability was also observed in this profile (Fig. 3C). The sharp decrease in organic N (Fig. 3E) in the upper 2 cm of the sediment, however, supports the modeled decrease of organic P with depth. The results of the model calculations indicate that CFA formation can

Table 2. Values of the fixed parameters as used in the diagenetic P model.

Para-meter	Description	Units	Value	Source
L_1	boundary oxidized/reduced zone	cm	2.0	depth where NO_3^- reaches background values (Fig. 4)
L_2	boundary bioturbated/non-biot. zone	cm	5.0	macrofaunal densities (see study sites)
ϕ	sediment porosity	$cm^3\ cm^{-3}$	0.43	mean porosity top 5 cm
D_s	whole sediment diffusion coeff.	$cm^2\ d^{-1}$	2.1×10^{-1}	Krom and Berner (1980)
D_b	sed. mixing or biodiffusion coeff.	$cm^2\ d^{-1}$	4.9×10^{-4}	Van Weering & De Stigter (pers. comm.)
ω	sedimentation rate	$cm\ d^{-1}$	6.9×10^{-6}	Van Weering & De Stigter (pers. comm.)
C_0	overlying water HPO_4^{2-} conc.	$\mu mol\ cm^{-3}$	9.1×10^{-4}	measured bottom water concentration
C_s	equilibrium conc. for P sorption	$\mu mol\ cm^{-3}$	1.0×10^{-3}	Froelich (1988), Slomp & Van Raaphorst (1993)
C_a	equilibrium conc. for CFA prec.	$\mu mol\ cm^{-3}$	3.7×10^{-3}	Atlas & Pytkowicz (1977), assuming pH=7.5
$J_{Mx=0}$	flux of Fe-bound P to the sediment	$\mu mol\ cm^{-2}\ d^{-1}$	0.2×10^{-4}	see text

account for the increase of authigenic P with depth at station I. Fitted values for $J_{Gx=0}$, $J_{Ax=0}$, G_∞ and M_∞ and for the rate constants k_s, k_g, k_m and k_a are listed in Table 3.

DISCUSSION

Diagenetic redistribution of P. Pore water profiles of NO_3^-, Mn^{2+} and Fe^{2+} indicate the presence of an oxidized surface zone of ~2 cm overlying reduced sediment at station I. Both the solid phase P (Fig. 6) and pore water HPO_4^{2-} and Fe^{2+} (Fig. 4) profiles at this station suggest a redistribution of Fe-bound P to an authigenic P phase in the reduced part of the sediment. The model results (Fig. 7) support this view and show that CFA formation can account for the increase of authigenic P at station I. The discrepancy between the pore water model and field results close to the redox-boundary may be explained by the fact that pore water profiles are much more sensitive indicators of short-term, non-steady state events than solid phase profiles. This is illustrated in Fig. 8, which shows the results of a scenario in which the model was fit to the pore water HPO_4^{2-} profile and the corresponding Fe-bound P and authigenic P profiles were subsequently calculated. The organic P profile was assumed to be similar to that of Fig. 7 and deposition of authigenic P from the overlying
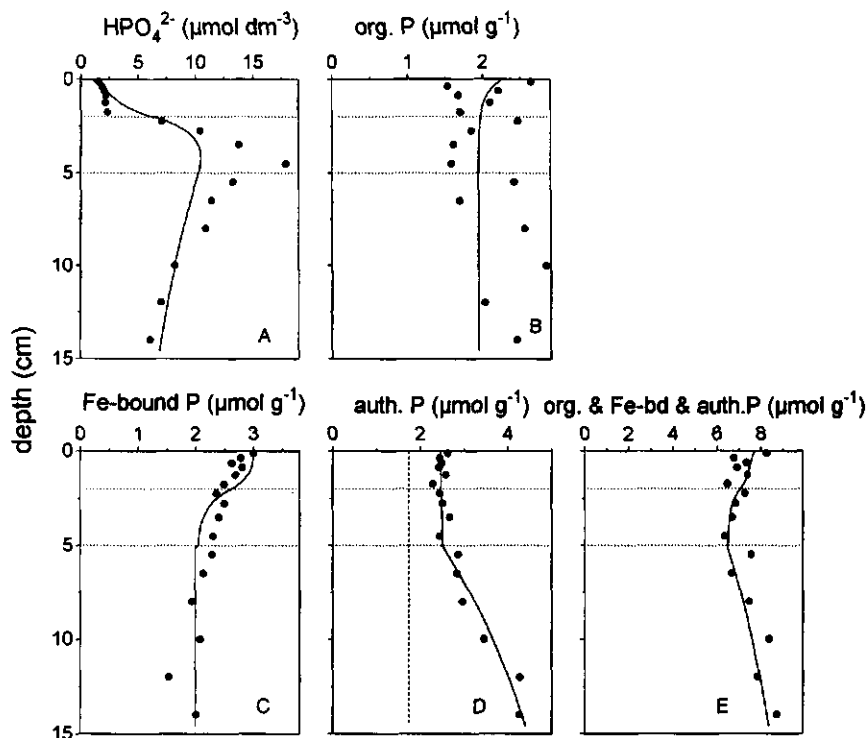
Fig. 7. Model fits (solid lines) to profiles of (A) pore water HPO_4^{2-} ($\mu mol\ dm^{-3}$), (B) organic P, (C) Fe-bound P and (D) authigenic P (all three in $\mu mol\ g^{-1}$) for station OMEX-I. The dotted lines in each panel indicate the boundaries between the oxidized and reduced sediment zones ($L_1 = 2$ cm) and between the bioturbated and nonbioturbated zones ($L_2 = 5$ cm). The dashed line in panel (D) is the profile of the authigenic P which has not been formed *in-situ*. The profile in panel (E) is the sum of the solid phase P forms (B, C, D) and the solid line is the sum of their model fits.

water was assumed to be absent ($J_{Ax=0} = 0$). The sharp peak in the pore water HPO_4^{2-} profile clearly does not match with the measured Fe-bound P and authigenic P profiles. These results can be explained by a very temporary increase of the sediment mixing rate, resulting in a temporary increase of the release of HPO_4^{2-} from Fe oxides in the reduced sediment zone. It is also important to note that uniform rate constants, transport coefficients and equilibrium concentrations throughout each sediment zone are assumed in the model, whereas in reality these will vary with depth, particularly close to the redox boundary. Thus the model gives an overly simplistic description of the complex HPO_4^{2-} sorption, precipitation and release processes.
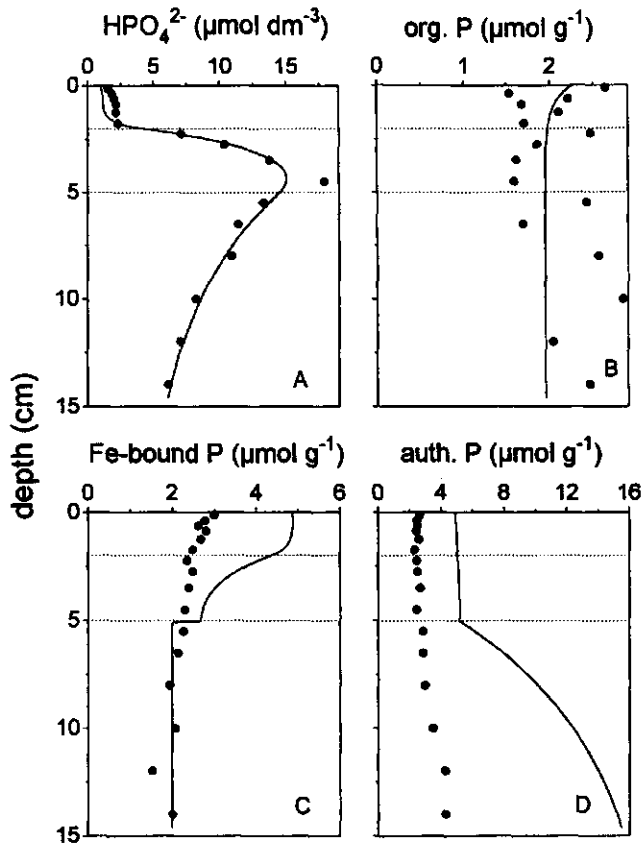
Fig. 8. The model fit (solid line) to the profile of (A) pore water HPO_4^{2-} (μmol dm^{-3}) and model calculated (solid lines) profiles of (B) organic P, (C) Fe-bound P and (D) authigenic P (all three in μmol g^{-1}) for station OMEX-I. The dotted lines in each panel indicate the boundaries between the oxidized and reduced sediment zones (L_1 = 2 cm) and between the bioturbated and non-bioturbated zones (L_2 = 5 cm). k_s = 2.3 d^{-1}, k_a = 4.7 × 10^{-3} d^{-1}, k_m = 2.0 × 10^{-4} d^{-1} and $J_{Ax=0}$ = 0 μmol cm^{-2} d^{-1}. All other parameters are as in Tables 2 and 3.

To illustrate the extent to which the pore water HPO_4^{2-} profile is modified by authigenic P formation, the model results of Fig. 7 are compared to a model scenario in which CFA precipitation is absent and the profiles of Fe-bound P and organic P remain unchanged (Fig. 9). The results show that CFA precipitation suppresses pore water HPO_4^{2-} concentrations and is responsible for the downward gradient of the profile below ~ 4 cm depth. That Fe-bound P and not organic P is acting as the main source of pore water HPO_4^{2-} at station I, is illustrated in Fig. 10. Here, the model fits of Fig. 7 are compared to a model scenario in which Fe-bound P plays no role. The results show that a much larger decrease of organic P
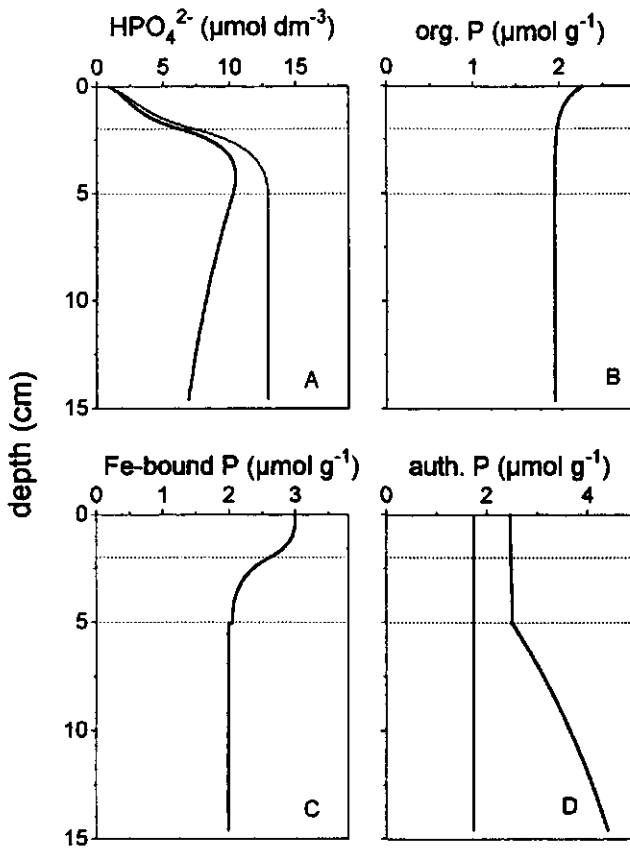
Fig. 9. Model results from Fig. 7 (thick solid lines) for profiles of (A) pore water HPO_4^{2-} (μmol dm^{-3}), (B) organic P, (C) Fe-bound P and (D) authigenic P (all three in μmol g^{-1}) and results of an alternative model scenario (thin solid lines). The dotted lines in each panel indicate the boundaries between the oxidized and reduced sediment zones ($L_1 = 2$ cm) and between the bioturbated and nonbioturbated zones ($L_2 = 5$ cm). For the alternative scenario: $k_a = 1.0 \times 10^{-16}$ d^{-1}, $k_s = 0.2$ d^{-1}. All other parameters are as in Tables 2 and 3.

with depth than could ever be supported by the measured profile must be invoked to explain the profiles of HPO_4^{2-} and authigenic P.

Comparison of the rate constants obtained for the model fits of Fig. 7 (Table 3) to rate constants observed in other sediments should provide insight into the validity of the model calculations. Very little is known, however, about the actual *in-situ* rate constants for the reactions controlling pore water HPO_4^{2-} concentrations in marine sediments. Estimates from diagenetic models for P are only available for the rate constants for sorption (k_s) and authigenic apatite formation (k_a). The present value of the sorption rate constant k_s falls
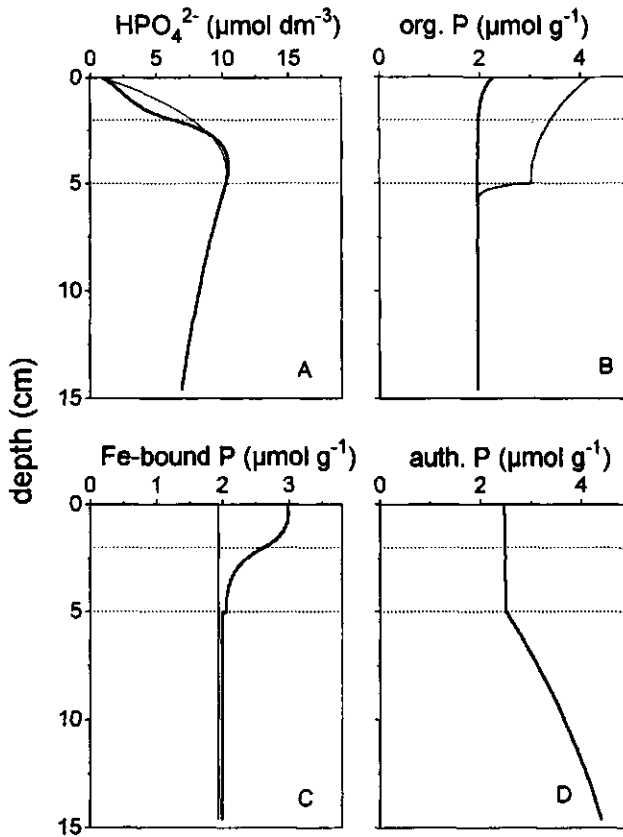
Fig. 10. As in Fig. 9. For the alternative scenario: $k_s = 1.0 \times 10^{-16}$ d^{-1}, $k_m = 1.0 \times 10^{-16}$ d^{-1}, $k_g = 3.8 \times 10^{-5}$ d^{-1} and $J_{Gx=0} = 4.5 \times 10^{-4}$ µmol cm^{-2} d^{-1}.

within the lower part of the range of 0.1-23.8 d^{-1} estimated for sandy North Sea sediments (Van Raaphorst et al., 1990). Van Cappellen and Berner (1988) estimated a first-order rate constant of 0.17 d^{-1} for nonsteady state CFA precipitation in a well-defined layer of a Mexican continental margin sediment. The rate constant determined for dispersed, steady state CFA precipitation (k_a) in our study is substantially lower. Tromp et al. (1995) proposed the following relationship between the oxic degradation rate constant for organic C (k_c in units of y^{-1}) and sedimentation rate (ω in units of cm y^{-1}):

$$k_c = 2.97\omega^{0.62} \tag{2}$$

With a sedimentation rate of 2.5×10^{-3} cm y^{-1} (Table 2) this gives a k_c of ~2.0×10^{-4} d^{-1} for station I. This value is very close to the rate constant for organic P decomposition (k_g)

Table 3. Values of the fitted parameters for station OMEX-I.

Parameter	Description	Units	Value
$J_{Gx=0}$	flux of organic P to the sediment at x = 0	$\mu mol\ cm^{-2}\ d^{-1}$	3.11×10^{-4}
$J_{Ax=0}$	flux of authigenic P to the sediment at x = 0	$\mu mol\ cm^{-2}\ d^{-1}$	0.18×10^{-4}
G_∞	asymptotic conc. for organic P	$\mu mol\ g^{-1}$	1.94
M_∞	asymptotic conc. for Fe-bound P	$\mu mol\ g^{-1}$	1.99
k_s	rate constant for P sorption	d^{-1}	2.6×10^{-1}
k_g	rate constant for organic P decomposition	d^{-1}	7.4×10^{-4}
k_m	rate constant for Fe-bound P release	d^{-1}	5.3×10^{-4}
k_a	rate constant for CFA precipitation	d^{-1}	1.0×10^{-3}
k_g'	$k_g \times \vartheta$	d^{-1}	2.5×10^{-3}
k_m'	$k_m \times \vartheta$	d^{-1}	1.8×10^{-3}

estimated for station I, particularly when taking into account that preferential regeneration of P relative to C oxidation is believed to occur upon oxic decomposition of organic material (Ingall and Van Cappellen, 1990). The rate constant for P release due to reduction of Fe oxides (k_m) observed for station I is lower than most first-order rate constants for reductive dissolution of Fe oxides due to chemical reductants or by microorganisms under laboratory conditions (Lovley, 1991; Schwertmann, 1991; Stumm and Sulzberger, 1992). Canfield et al. (1992), for example, calculated values ranging from 6.0 d^{-1} for amorphous Fe oxide to 0.03 d^{-1} for synthetic hematite upon reduction of these Fe oxides with sulfide (1 mM). We conclude that, with the exception of k_g, the values of the rate constants calculated here are lower than most values obtained in other modeling or laboratory studies, thus suggesting less optimal conditions for the relevant processes in the sediment at station I.

At station II, pore water Fe^{2+}, Mn^{2+}, HPO_4^{2-}, NH_4^+ (Fig. 4) and solid phase Mn (Fig. 5) profiles suggest the occurrence of locally reduced spots associated with organic matter decomposition at several depths in an otherwise oxidized sediment. This concept of micro-environments has been suggested previously to explain both Mn reduction (Kalhorn and Emerson, 1984; Heggie et al., 1986) and SO_4^{2-} reduction (Jørgensen, 1977) in the 'oxic' zone of several sediments. Apparently, organic matter degradation is so rapid locally that the consumption of O_2 is faster than the resupply by molecular diffusion. As O_2 is supplied from the overlying water, most of the Fe^{2+} and Mn^{2+} diffusing out of such micro-sites will be oxidized at the 'top' of each site. When these micro-sites are quantitatively important in a sediment and the rate of sediment accumulation is low, this can eventually result in the net
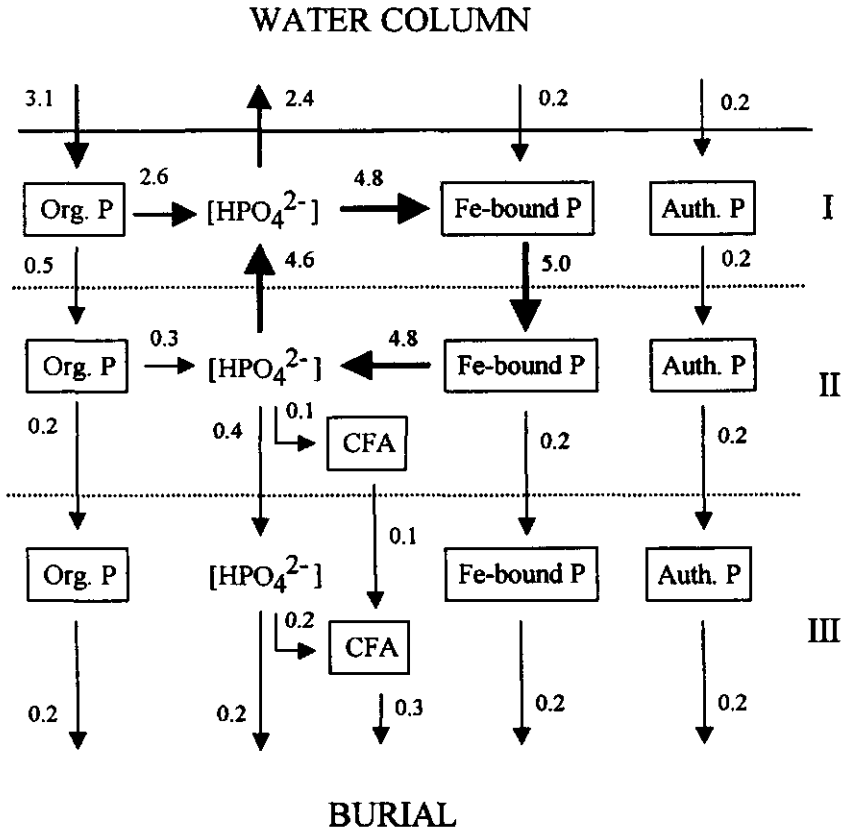
WATER COLUMN

Fig. 11. Fluxes of P (in 10^{-4} μmol cm^{-2} d^{-1}) between the pore water and the sediment P reservoirs as calculated with the model for each sediment zone at station OMEX-I. Zone I ($0 \leq x \leq 2$ cm) is the oxidized surface zone. Zone II (2 cm < x $\leq$ 5 cm) is the reduced sediment zone with bioturbation. Zone III (x > 5 cm) is the reduced sediment zone without bioturbation.

decrease in the amount of Mn and Fe oxides with depth observed here. The results of the sediment P extractions (Fig. 6) suggest that a redistribution of Fe-bound P to CFA may be occurring in these micro-sites below ~6 cm depth at station II. We cannot exclude, however, the possibility that the increase of authigenic P with depth at this station is not due to *in-situ* formation of authigenic P but is the result of a gradual change in the flux of CaCO$_3$ to the sediment with time.

　　In conclusion, the results indicate that CFA may be forming at the expense of Fe-bound P in both Goban Spur sediments. We will concentrate on the results of station I in the further discussion, as the results for this station are less equivocal than those for station II.

A key role for Fe-bound P in CFA formation. Further insight into the mechanism responsible for the early diagenetic redistribution of Fe-bound P to CFA at station I is provided by the fluxes of P between the sediment P reservoirs and pore water HPO_4^{2-} in each sediment zone. These fluxes were calculated with the model and are presented in Fig. 11. Combining Fig. 7 and 11, the following description of the sedimentary P cycle results.

Most P deposited at the sediment-water interface is associated with organic matter. A large proportion (~85%) of this organic P is decomposed in the oxidized surface layer. Most of the thus produced pore water HPO_4^{2-} is released very close to the sediment-water interface and immediately escapes to the overlying water. Some of this HPO_4^{2-} is sorbed to Fe oxides, however, and enters the intense cycle of P at the redox boundary. This cycle of P, which is mainly driven by bioturbation through downward transport of Fe-bound P, is responsible for the continuously high concentrations of pore water HPO_4^{2-} immediately below the redox boundary. These high HPO_4^{2-} concentrations favour CFA precipitation. Losses from the internal P cycle occurring due to CFA formation and due to diffusive escape of HPO_4^{2-} are compensated for by input of HPO_4^{2-} released from organic matter in the oxidized surface zone. Bioturbation causes the CFA, formed in the reduced, bioturbated zone (between L_1 and L_2), to be mixed upwards into the oxidized zone, accounting for a 'background' concentration of CFA at the sediment-water-interface. The total background concentration of authigenic P is higher, however, due to a flux ($J_{Ax=0}$) of authigenic P formed elsewhere. This authigenic P is only truly authigenic, in the sense that its formation has resulted in the removal of reactive P (i.e. potentially biologically available P) from seawater (see Ruttenberg and Berner, 1993), when it has been formed in a marine environment. In the non-bioturbated zone, release of HPO_4^{2-} from organic P and Fe-bound P is small and downward diffusion of HPO_4^{2-} supplies most P for CFA formation. In this zone of the sediment, the CFA profile is no longer disturbed by mixing and the CFA concentration (Fig. 7D) and the sum of organic, Fe-bound and authigenic P (Fig. 7E) gradually increase with depth. This increase will cease when the porewater reaches equilibrium with respect to CFA.

Assuming that all sediment P phases in Fig. 11 consist of reactive P, the total downward flux of reactive P at the lower boundary of the sediment interval under study here (at 15 cm depth) becomes 1.1 μmol m^{-2} d^{-1}. CFA formed *in-situ* accounts for ~25% (0.3 μmol m^{-2} d^{-1}) of this downward flux of reactive P. If the pore water HPO_4^{2-} diffusing downward (0.2 μmol m^{-2} d^{-1}) is also incorporated in CFA, this authigenic mineral phase accounts for ~45% of the downward reactive P flux. If Fe-bound P and authigenic P supplied from the overlying water consist of non-reactive P phases, total reactive P burial decreases to 0.7

μmol m^{-2} d^{-1}. Now the contribution of CFA formed *in-situ* to reactive P burial will be ~40% when downward diffusing HPO$_4^{2-}$ is not incorporated in CFA and ~70% when it is.

In the model calculations we assumed a small flux of Fe oxides from the overlying water with an Fe/P ratio of 10. The Fe/P ratio of the Fe oxides being buried was also ~10 at station I (depth interval 13-15 cm, Fig. 5C and Fig. 6D). Since, under steady-state conditions, the flux of Fe-oxides from the overlying water is equal to the burial flux of Fe, the same also holds for the deposition and burial fluxes of Fe-bound P (Fig. 11). The flux of Fe-bound P from the overlying water is only of minor importance for the internal P cycle at the redox interface as this cycle largely depends on *in-situ* formation of Fe-bound P.

Intercomparison of the rate constants obtained in this study provides more insight in the kinetics of the relevant processes. To enable the values of k_m and k_g (first-order in the solid phase concentrations of Fe-bound P and organic P) to be compared to those of k_a and k_s (first-order in the pore water HPO$_4^{2-}$ concentration), the former constants were multiplied by ϑ, giving k_m' and k_g' (Table 3). The high k_s value relative to k_m' and k_g' indicates that, as expected, sorption of HPO$_4^{2-}$ to Fe oxides in the oxidized sediment zone is a more rapid process than HPO$_4^{2-}$ release from either organic matter or from Fe oxides. The rate constant for CFA precipitation (k_a) is of the same order of magnitude as k_m' and k_g'. This suggests that both Fe-bound P and organic P are kinetically suited as sources of HPO$_4^{2-}$ for CFA. We conclude that CFA formation is sufficiently rapid to keep up with release of HPO$_4^{2-}$ from both sources. Which of the two actually acts as the source of P for CFA depends on the location in the sediment where the HPO$_4^{2-}$ release occurs and on the availability of sufficient pore water fluoride.

Summarizing, these results illustrate how an intense cycling of P between Fe-bound P and pore water HPO$_4^{2-}$ can account for elevated concentrations of HPO$_4^{2-}$ below the redox boundary, thus promoting early diagenetic CFA formation. This internal P cycle is driven by downward transport of *in-situ* formed Fe-bound P and refueled by P release from organic matter. This mechanism, in which Fe-bound P plays a key role in early diagenetic CFA formation, acting as an intermediate between organic P and CFA, may be of particular importance in marine sediments with low sedimentation rates where organic matter decomposition takes place close to the sediment-water interface. Remineralized HPO$_4^{2-}$ which would otherwise escape to the overlying water is thus largely retained in the sediment. This could also explain why Fe-bound P acts as the P source for CFA in a low sedimentation environment in the Labrador Sea (Lucotte et al., 1994). In terrigenous, high sedimentation continental margin environments where relatively labile organic matter is buried rapidly, there is less need for an intermediate role of Fe-bound P. Here, organic P may act as a direct source of HPO$_4^{2-}$ for CFA as suggested by Ruttenberg and Berner (1993) for Long Island Sound and Mississippi Delta sediments.

CFA as a sink for P. The major importance of CFA formation in marine sediments lies in the fact that CFA acts as a permanent sink for reactive P. The contribution of CFA to the total burial flux of reactive P at station I was estimated to range between ~25 and 70%, depending on whether downward diffusing HPO_4^{2-} is assumed to be incorporated in CFA and whether Fe-bound and authigenic P supplied from the overlying water are assumed to consist of reactive P. This indicates that CFA is a very important sink for reactive P in this sediment. Ruttenberg (1993) estimated a contribution of authigenic P to global reactive P burial of ~28 to 50 % based on P speciation results for only three locations: the two high sedimentation, continental margin sites from the study of Ruttenberg and Berner (1993) and one pelagic sediment in the equatorial Atlantic. Our results for a low sedimentation, continental margin environment support this important role of CFA for global reactive P burial.

CONCLUSIONS

The results of solid phase P speciation for sediments from two stations on the North Atlantic continental platform Goban Spur indicate that authigenic carbonate fluorapatite (CFA) may be forming in the sediment at the expense of Fe-bound P.

Application of a diagenetic phosphorus model to solid phase P (organic P, Fe-bound P and authigenic P) and pore water HPO_4^{2-} profiles, indicates that CFA formation can account for the increase of authigenic P with depth at one station. The model results demonstrate that an intense cycling of P between Fe-bound P and pore water HPO_4^{2-} can be responsible for elevated pore water HPO_4^{2-} concentrations below the redox-interface, thus creating conditions beneficial for CFA formation. This cycle is driven by bioturbation through downward transport of *in-situ* formed Fe-bound P and refueled by sorption of HPO_4^{2-} released from organic matter to Fe oxides. This mechanism, in which Fe-bound P plays a key role, acting as an intermediate between organic P and CFA, may be of particular importance in marine sediments with low sedimentation rates where organic matter decomposition takes place close to the sediment-water interface. In these environments, CFA may then become an important sink for P.

REFERENCES

Aller, R.C., 1990. Bioturbation and manganese cycling in hemipelagic sediments. Phil. Trans. R. Soc. London. A. 331: 51-68.

Aspila, K.I., H. Agemian and A.S.Y. Chau, 1976. A semi-automated method for the determination of inorganic, organic and total phosphate in sediments. Analyst 101: 187-197.

Atlas, E. and R.M. Pytkowicz, 1977. Solubility behavior of apatites in seawater. Limnol. Oceanogr. 2: 290-300.

Berner, R.A., 1980. Early diagenesis: A theoretical approach. Princeton University Press, Princeton. 241p.

Berner, R.A., K.C. Ruttenberg, E.D. Ingall, and J.-L. Rao, 1993. The nature of phosphorus burial in modern marine sediments. In: Interactions of C, N, P, and S Biogeochemical Cycles and Global Change, R. Wollast, F.T. Mackenzie and L. Chou, eds. Springer-Verlag, NATO ASI Series Vol. 14. 521p.

Bray, J.T., O.P. Bricker and B.N. Troup, 1973. Phosphate in interstitial waters of anoxic sediments: oxidation effects during sampling procedures. Science 180: 1362-1364.

Brewer, P.G. and D.W. Spencer, 1971. Colorimetric determination of manganese in anoxic waters. Limnol. Oceanogr. 16: 107-110.

Broecker, W.S. and T.-H. Peng, 1982. Tracers in the sea. Eldigio Press, Palisades, 690p.

Burdige, D.J. and J.M. Gieskes, 1983. A pore water/solid phase diagenetic model for manganese in marine sediments. Am. J. Sci. 283: 29-47.

Canfield, D.E., R. Raiswell and S. Bottrell, 1992. The reactivity of sedimentary iron minerals toward sulfide. Am. J. Sci. 292: 659-683.

Canfield, D.E., B. Thamdrup and J.W. Hansen, 1993. The anaerobic degradation of organic matter in Danish coastal sediments: iron reduction, manganese reduction, and sulfate reduction. Geochim. Cosmochim. Acta 57: 3867-3883.

Draper, N.R. and H. Smith, 1967. Applied regression analysis. John Wiley, 407p.

Flach, E. and C. Heip, 1996. Vertical distribution of macrozoobenthos within the sediment along the continental slope in the Goban Spur area (NE Atlantic). Mar. Ecol. Prog. Ser. 141: 55-66.

Froelich, P.N., 1988. Kinetic control of dissolved phosphate in natural rivers and estuaries: a primer on the phosphate buffer mechanism. Limnol. Oceanogr. 33: 649-668.

Froelich, P.N., M.A. Arthur, W.C. Burnett, M. Deakin, V. Hensley, R. Jahnke, L. Kaul, K.-H. Kim, K. Roe, A. Soutar and C. Vathakanon, 1988. Early diagenesis of organic matter in Peru continental margin sediments: phosphorite precipitation. Mar. Geol. 80: 309-343.

Gerke, J. and R. Hermann, 1992. Adsorption of orthophosphate to humic-Fe-complexes and to amorphous Fe-oxide. Z. Planzenernähr. Bodenk.155: 233-236.

Heggie, D.T., D. Kahn and K. Fischer, 1986. Trace metals in metalliferous sediments. MANOP Site M: interfacial pore water profiles. Earth Planet. Sci. Lett. 80: 106-116.

Heggie, D.T., G.W. Skyring, G.W. O'Brein, C. Reimers, A. Herczeg, D.J.W. Moriarty, W.C. Burnett, A.R. Milnes, 1990. Organic carbon cycling and modern phosphorite formation on the East Australian continental margin: An overview. In: Phosphorite research and development, G.J. Notholt and I. Jarvis, eds. Geol. Soc. Spec. Publ. 52: 87-117.

Helder, W. and R.P.T. De Vries, 1979. An automatic phenol-hypochlorite method for the determination of ammonia in sea- and brackish waters. Neth. J. Sea. Res. 13: 154-160.

Howarth, R.W., H. Jensen, R. Marino and H. Postma, 1995. Transport to and processing of phosphorus in near-shore and oceanic waters. In: Phosphorus in the global environment, H. Tiessen, ed., John Wiley, SCOPE 54, 462p.

Ingall, E.D. and P. Van Cappellen, 1990. Relation between sedimentation rate and burial of organic phosphorus and organic carbon in marine sediments. Geochim. Cosmochim. Acta 54: 373-386.

Jahnke, R.A., S.R. Emerson, K.K. Roe and W.C. Burnett, 1983. The present day formation of apatite in Mexican continental margin sediments. Geochim. Cosmochim. Acta 47: 259-266.

Jensen, H.S. and B. Thamdrup, 1993. Iron-bound phosphorus in marine sediments as measured by the bicarbonate-dithionite extraction. Hydrobiologia 253: 47-59.

Jørgensen, B.B., 1977. Bacterial sulfate reduction within reduced microniches of oxidized marine sediments. Mar. Biol. 41: 7-17.

Kalhorn, S. and S. Emerson, 1984. The oxidation state of manganese in surface sediments of the deep sea. Geochim. Cosmochim. Acta 48: 897-902.

Krom, M.D. and R.A. Berner, 1980. The diffusion coefficient of sulfate, ammonium and phosphate ions in anoxic marine sediments. Limnol. Oceanogr. 25: 327-337.

Lovley, D.R., 1991. Dissimilatory Fe(III) and Mn(IV) reduction. Microbiol. Rev. 55: 259-287.

Lucotte, M., A. Mucci and A. Hillairemarcel, 1994. Early diagenetic processes in deep Labrador Sea sediments: reactive and nonreactive iron and phosphorus. Can. J. Earth Sci. 31: 14-27.

Martens, C.S., R.A. Berner and J.K. Rosenfeld, 1978. Interstitial water chemistry of anoxic Long Island Sound sediments. 2. Nutrient regeneration and phosphate removal. Limnol. Oceanogr. 23: 605-617.

Pettijohn, F.J., P.E. Potter and R. Siever, 1972. Sand and sandstone. Springer, New York. 690p.

Reeburgh, W.S., 1967. An improved interstitial water sampler. Limnol. Oceanogr. 12: 163-170.

Ruttenberg, K.C., 1992. Development of a sequential extraction method for different forms of phosphorus in marine sediments. Limnol. Oceanogr. 37: 1460-1482.

Ruttenberg, K.C., 1993. Reassessment of the oceanic residence time of phosphorus. Chem. Geol. 107: 405-409.

Ruttenberg, K.C. and R.A. Berner, 1993. Authigenic apatite formation and burial in sediments from non-upwelling, continental margin environments. Geochim. Cosmochim. Acta 57: 991-1007.

Sherwood, B.A., S.L. Sager and H.D. Holland, 1987. Phosphorus in foraminiferal sediments from North Atlantic Ridge cores and in pure limestones. Geochim.Cosmochim. Acta 51: 1861-1866.

Schwertmann, U., 1991. Solubility and dissolution of iron oxides. Plant Soil 130: 1-25.

Slomp, C.P. and W. Van Raaphorst, 1993. Phosphate adsorption in oxidized marine sediments. Chem. Geol. 107: 477-480.

Slomp, C.P., S.J. Van der Gaast and W. Van Raaphorst, 1996. Phosphorus binding by poorly crystalline iron oxides in North Sea sediments. Mar. Chem. 52: 55-73.

Stookey, L.L., 1970. Ferrozine - A new spectrophotometric reagent for iron. Analyt. Chem., 42, 779-781.

Strickland, T.R. and J.D. Parsons, 1972. A practical handbook of seawater analysis. 2nd. ed. Bull. Fish. Res. Bd. Can. 167: 1-311.

Stumm, W. and B. Sulzberger, 1992. The cycling of iron in natural environments: Considerations based on laboratory studies of heterogeneous redox processes. Geochim. Cosmochim. Acta 56: 3233-3257.

Sundby, B., C. Gobeil, N. Silverberg and A. Mucci, 1992. The phosphorus cycle in coastal marine sediments. Limnol. Oceanogr. 37: 1129-1145.

Tromp, T.K., P. Van Cappellen and R.M. Key, 1995. A global model for the early diagenesis of organic carbon and organic phosphorus in marine sediments. Geochim. Cosmochim. Acta 59: 1259-1284.

Van Cappellen, P. and R.A. Berner, 1988. A mathematical model for the early diagenesis of phosphorus and fluorine in marine sediments: apatite precipitation. Am. J. Sci. 288: 289-333.

Van Raaphorst, W., P. Ruardij and A.G. Brinkman, 1988. The assessment of benthic phosphorus regeneration in an estuarine ecosystem model. Neth. J. Sea Res. 22: 23-36.

Van Raaphorst, W., H.T. Kloosterhuis, A. Cramer and K.J.M. Bakker, 1990. Nutrient early diagenesis in the sandy sediments of the Dogger Bank area: pore water results. Neth. J. Sea Res. 26: 25-52.

Van Raaphorst, W. and H.T. Kloosterhuis, 1994. Phosphate sorption in superficial intertidal sediments. Mar. Chem. 48: 1-16.

Verardo, D.J., P.N. Froelich and A. McIntyre, 1990. Determination of organic carbon and nitrogen in sediments using the Carlo Erba Na-1500 analyzer. Deep-Sea Res. 37: 157-165.

APPENDIX

The differential equations for each P reservoir in the (I) oxidized surface zone ($0 \leq x \leq L_1$), (II) reduced sediment zone with bioturbation ($L_1 < x \leq L_2$) and (III) reduced sediment zone without bioturbation ($x > L_2$), with ϑ as given in equation (1) and all other symbols as listed in Tables 2 and 3, are as follows:

Pore water HPO_4^{2-} (C)

$$\frac{\partial C_I}{\partial t} = [D_b + D_s]\frac{\partial^2 C_I}{\partial x^2} - \omega \frac{\partial C_I}{\partial x} + k_g\vartheta(G_I - G_\infty) - k_s(C_I - C_s) = 0 \tag{A1}$$

$$\frac{\partial C_{II}}{\partial t} = [D_b + D_s]\frac{\partial^2 C_{II}}{\partial x^2} - \omega \frac{\partial C_{II}}{\partial x} + k_g\vartheta(G_{II} - G_\infty) - k_a(C_{II} - C_a) + k_m\vartheta(M_{II} - M_\infty) = 0 \tag{A2}$$

$$\frac{\partial C_{III}}{\partial t} = D_s \frac{\partial^2 C_{III}}{\partial x^2} - \omega \frac{\partial C_{III}}{\partial x} + k_g\vartheta(G_{III} - G_\infty) - k_a(C_{III} - C_a) + k_m\vartheta(M_{III} - M_\infty) = 0 \tag{A3}$$

Organic P (G)

$$\frac{\partial G_I}{\partial t} = D_b \frac{\partial^2 G_I}{\partial x^2} - \omega \frac{\partial G_I}{\partial x} - k_g(G_I - G_\infty) = 0 \tag{A4}$$

$$\frac{\partial G_{II}}{\partial t} = D_b \frac{\partial^2 G_{II}}{\partial x^2} - \omega \frac{\partial G_{II}}{\partial x} - k_g(G_{II} - G_\infty) = 0 \tag{A5}$$

$$\frac{\partial G_{III}}{\partial t} = -\omega \frac{\partial G_{III}}{\partial x} - k_g(G_{III} - G_\infty) = 0 \tag{A6}$$

Fe-bound P (M)

$$\frac{\partial M_I}{\partial t} = D_b \frac{\partial^2 M_I}{\partial x^2} - \omega \frac{\partial M_I}{\partial x} + \frac{k_s}{\vartheta}(C_I - C_s) = 0 \tag{A7}$$

$$\frac{\partial M_{II}}{\partial t} = D_b \frac{\partial^2 M_{II}}{\partial x^2} - \omega \frac{\partial M_{II}}{\partial x} - k_m (M_{II} - M_\infty) = 0 \tag{A8}$$

$$\frac{\partial M_{III}}{\partial t} = -\omega \frac{\partial M_{III}}{\partial x} - k_m (M_{III} - M_\infty) = 0 \tag{A9}$$

Authigenic P (A)

$$\frac{\partial A_I}{\partial t} = D_b \frac{\partial^2 A_I}{\partial x^2} - \omega \frac{\partial A_I}{\partial x} = 0 \tag{A10}$$

$$\frac{\partial A_{II}}{\partial t} = D_b \frac{\partial^2 A_{II}}{\partial x^2} - \omega \frac{\partial A_{II}}{\partial x} + \frac{k_a}{\vartheta} (C_{II} - C_a) = 0 \tag{A11}$$

$$\frac{\partial A_{III}}{\partial t} = -\omega \frac{\partial A_{III}}{\partial x} + \frac{k_a}{\vartheta} (C_{III} - C_a) = 0 \tag{A12}$$

The boundary conditions used to solve the equations (A1) to (A12) are:

at $x = 0$
$$C_I = C_o \tag{A13}$$

$$J_{G_{x=0}} = -\phi\vartheta [D_b \frac{\partial G}{\partial x} - \omega G]_{x=0} \tag{A14}$$

$$J_{M_{x=0}} = -\phi\vartheta [D_b \frac{\partial M}{\partial x} - \omega M]_{x=0} \tag{A15}$$

$$J_{A_{x=0}} = -\phi\vartheta [D_b \frac{\partial A}{\partial x} - \omega A]_{x=0} \tag{A16}$$

at $x = L_1$
$$C_I = C_{II} \tag{A17}$$

$$G_I = G_{II} \tag{A18}$$

$$M_I = M_{II} \tag{A19}$$

$$A_I = A_{II} \tag{A20}$$

$$[D_b + D_s]\frac{\partial C_I}{\partial x} - \omega C_I = [D_b + D_s]\frac{\partial C_{II}}{\partial x} - \omega C_{II} \tag{A21}$$

$$D_b \frac{\partial G_I}{\partial x} - \omega G_I = D_b \frac{\partial G_{II}}{\partial x} - \omega G_{II} \tag{A22}$$

$$D_b \frac{\partial M_I}{\partial x} - \omega M_I = D_b \frac{\partial M_{II}}{\partial x} - \omega M_{II} \tag{A23}$$

$$D_b \frac{\partial A_I}{\partial x} - \omega A_I = D_b \frac{\partial A_{II}}{\partial x} - \omega A_{II} \tag{A24}$$

at $x = L_2$
$$C_{II} = C_{III} \tag{A25}$$

$$G_{II} = G_{III} \tag{A26}$$

$$M_{II} = M_{III} \tag{A27}$$

$$A_{II} = A_{III} \tag{A28}$$

$$[D_b + D_s]\frac{\partial C_{II}}{\partial x} - \omega C_{II} = D_s \frac{\partial C_{III}}{\partial x} - \omega C_{III} \tag{A29}$$

$$D_b \frac{\partial G_{II}}{\partial x} - \omega G_{II} = -\omega G_{III} \tag{A30}$$

$$D_b \frac{\partial M_{II}}{\partial x} - \omega M_{II} = -\omega M_{III} \tag{A31}$$

$$D_b \frac{\partial A_{II}}{\partial x} - \omega A_{II} = -\omega A_{III} \tag{A32}$$

when $x \to \infty$

$$C_{III} \to C_a \tag{A33}$$

$$G_{III} \to G_\infty \tag{A34}$$

$$M_{III} \to M_\infty \tag{A35}$$

The solutions to the equations and the Excel worksheet containing the model can be obtained from the first author upon request.

Summary

Most of the organic material in the oceans that reaches the sea floor is deposited on continental margins and not in the deep sea. This organic matter is the principal carrier of phosphorus (P) to sediments. A part of the organic material is buried definitely. The other part decomposes, resulting in a release of dissolved HPO_4^{2-} to the pore water. This HPO_4^{2-} either returns to the overlying water and becomes available for uptake by phytoplankton, or is retained in the sediment in an organic or inorganic form.

Quantification of the P release from and P retention in sediments on relatively short time scales of days to years is necessary for a correct understanding of the nutrient dynamics in regional seas such as, for example, the North Sea. An accurate assessment of the modern global ocean burial flux of reactive P (i.e potentially bioavailable P) and the burial flux in the geological past is important for understanding the global oceanic P cycle. This, in turn, can provide insight in possible controls on organic C burial and atmospheric concentrations of CO_2 and O_2, because P may limit oceanic primary production and thus determine the amount of organic material in the oceans on geological time scales.

The research presented in this thesis concentrates on the short-term processes controlling sediment P release and retention in temperate, non-upwelling, continental margin environments. The research commenced with a laboratory study on the effect of organic matter deposition and macrofauna on sediment-water exchange and retention of P in Fe oxide-poor, sandy sediments (Chapter 2). A suspension of dead algal cells (*Phaeocystis sp.*) was applied to sediment in experimental systems (boxcosms), either once or every week during 19 weeks. The results demonstrate that deposition of organic matter on this type of sediment enhances pore water concentrations and sediment-water exchange of HPO_4^{2-}. The enhanced HPO_4^{2-} release was due to microbially mediated mineralization of the organic material and due to direct release of HPO_4^{2-} from the algal cells (lysis). A major portion of the algal material remained at the sediment-water interface and this organic layer probably regulated the sediment-water exchange of HPO_4^{2-} directly. The activity of the macrofauna was mainly limited to reworking of the sediment. The effect of the macrofauna on the sediment-water exchange of HPO_4^{2-} was negligible. In the boxcosms to which organic material was added only once, the concentration of NaOH-extractable sediment P increased following the addition, especially in the presence of macrofauna.

Sorption of P to Fe oxides is the most important short-term process responsible for the retention of P in sediments. Using a combination of differential X-ray diffraction (DXRD) and extraction procedures, the character of the Fe oxides that bind P in 4 North Sea sediments was studied (Chapter 3). The results indicate that poorly crystalline ferrihydrite and akageneite were present in the fine sediment fraction (< 10 μm) of surface samples

from all locations. Combination of these results with bulk sediment extractions of Fe and P and sorption characteristics for P provides evidence for the dominant role of poorly crystalline Fe oxides for the binding of P in these North Sea sediments. These poorly crystalline Fe oxides are suggested to act as both a temporary and permanent sink for P.

The redox conditions in continental margin sediments can vary both seasonally and spatially. To obtain more insight in the redox conditions in North Sea sediments, the Mn and Fe cycle at 15 locations in 4 different sedimentary environments was studied in 2 contrasting seasons (Chapter 4). The quality and quantity of the organic matter deposited in each environment was found to determine whether sediments become sufficiently depleted of O_2 and NO_3^- to allow for (1) Fe and Mn reduction and (2) escape of dissolved Fe^{2+} and Mn^{2+} to the overlying water. A steady-state diagenetic model describing solid phase and pore water metal profiles was developed and applied to Mn and Fe data for 11 and 3 stations, respectively. The model results demonstrate that (1) reversible sorption in combination with sediment mixing can enhance diffusive transport of dissolved metals; (2) precipitation of Fe^{2+} and Mn^{2+} in the form of reduced authigenic minerals can explain the reversal of the pore water Fe^{2+} and Mn^{2+} gradients at depth at many stations, and (3) in most North Sea sediments, Fe and Mn oxides do not play an important role as redox intermediates in organic C oxidation (accounting for $< 4 \%$); only in the depositional environment of the Skagerrak, metal oxide reduction may contribute substantially to organic C oxidation (~20%).

Reversible sorptive reactions can both constrain and enhance the flux of HPO_4^{2-} from the sediment to the overlying water. The role of sorption in sediment-water exchange of HPO_4^{2-} in North Sea sediments was investigated for 15 locations in 2 seasons (Chapter 5). P sorption data, pore water HPO_4^{2-} profiles, solid phase results and measured and calculated rates of sediment-water exchange of HPO_4^{2-} were combined. Sorption was found to play an important role in controlling sediment-water exchange of HPO_4^{2-} during at least part of the year in 3 of the 4 North Sea environments. At most stations, adsorption limits the flux of HPO_4^{2-} to the overlying water. At one station in the Skagerrak, however, desorption is responsible for the maintenance of a flux of HPO_4^{2-} to the overlying water. A one-dimensional reaction-diffusion model describing the sedimentary P cycle was developed and applied to the results for 2 stations. The model results show that both enhanced retention and enhanced release due to sorption can be adequately described when simultaneous equilibrium and first-order reversible sorptive reactions are assumed.

P bound in authigenic minerals may not be solubilized again, whereas Fe-bound and organic P can still be released upon deep burial. Therefore, more insight in the extent of authigenic P mineral formation in continental margin sediments is important. A combination of pore water and solid phase analysis was used to determine whether

authigenic carbonate fluorapatite (CFA) is currently forming at two locations on a North Atlantic continental platform (Chapter 6). Results of selective extractions suggest that an authigenic P phase is forming at the expense of Fe-bound P at both stations. A steady-state diagenetic model for the P cycle was developed and applied to the data of 1 station. The model results indicate that CFA formation can account for the observed increase of authigenic P with depth at this station. Furthermore, the results show that an intense cycling of P between Fe-bound P and pore water HPO_4^{2-} at the redox interface can create conditions beneficial for CFA formation. This internal P cycle is driven by downward, bioturbational transport of mainly in-situ formed Fe-bound P into the reduced sediment zone. Losses from the internal P cycle due to CFA formation and HPO_4^{2-} diffusion are compensated for by sorption of HPO_4^{2-} released from organic matter to Fe oxides. Fe-bound P thus acts as an intermediate between organic P and CFA. Burial of CFA can account for between 25 and 70% of the total burial flux of reactive P and thus may act as an important sink for P in this low sedimentation, continental margin environment.

Samenvatting

Het grootste deel van het organisch materiaal in de oceanen dat de zeebodem bereikt, komt terecht op het continentale plat en de continentale helling (samen de *continental margin*) en niet in de diepzee. Voor het sediment is dit organisch materiaal de belangrijkste bron van reactief, d.w.z. potentieel voor mariene organismen beschikbaar fosfaat. Een deel van dit organisch materiaal wordt definitief begraven. Het overige gedeelte breekt af, wat resulteert in het vrijkomen van opgelost fosfaat in het poriewater. Dit fosfaat keert òf terug naar het bovenstaande water, en komt daarbij weer beschikbaar voor opname door fytoplankton, òf wordt in het sediment vastgelegd in organische of anorganische vorm.

Kwantitiatief inzicht in de rol van sedimenten als een bron en opslagplaats voor fosfaat, op tijdschalen van dagen tot jaren, is van belang voor een goed begrip van de dynamiek van nutriënten in randzeeën, zoals bijvoorbeeld de Noordzee. Voor een juist begrip van de fosforcyclus in de oceanen als geheel is het belangrijk te weten met welke snelheid fosfaat op mondiale schaal definitief in sedimenten wordt opgeslagen. Dit is vooral interessant omdat fosfaat mogelijk de limiterende factor voor de totale primaire productie in de oceanen op geologische tijdschalen is. De hoeveelheid beschikbaar fosfaat kan dus bepalen hoeveel organisch materiaal er in de oceanen gevormd en begraven wordt en daarmee de atmosferische concentraties van kooldioxide en zuurstof beïnvloeden.

Het onderzoek dat in dit proefschrift beschreven is, beperkte zich tot het bestuderen van de korte termijn-processen die verantwoordelijk zijn voor de vastlegging en afgifte van fosfaat door sedimenten van *continental margins* in gematigde gebieden waar geen opwelling plaatsvindt. Het onderzoek begon met een laboratoriumstudie naar het effect van de depositie van organisch materiaal en de aanwezigheid van macrofauna op de sediment-wateruitwisseling en retentie van fosfaat in zandige, ijzer-arme sedimenten (Hoofdstuk 2). Een suspensie van dode algencellen (*Phaeocystis sp.*) werd, eenmalig of iedere week gedurende 19 weken, op sediment in experimentele systemen (boxcosms) aangebracht. De resultaten laten zien dat depositie van organisch materiaal op dit type sedimenten leidt tot een verhoging van de poriewaterconcentraties en sediment-wateruitwisseling van fosfaat. De verhoogde fosfaatafgifte was het gevolg van de mineralisatie van het organisch materiaal en het direct vrijkomen van opgelost fosfaat uit de algencellen. Een groot deel van het algenmateriaal bleef op het sediment liggen en deze organische laag reguleerde waarschijnlijk direct de sediment-wateruitwisseling van fosfaat. De activiteit van de macrofauna bleef grotendeels beperkt tot het omwoelen van het sediment. Het effect hiervan op de sediment-wateruitwisseling van fosfaat was verwaarloosbaar klein. In de boxcoms waaraan eenmalig organisch materiaal was toegevoegd, nam de concentratie

NaOH-extraheerbaar sediment fosfaat direct na de gift toe, vooral in de aanwezigheid van macrofauna.

Sorptie van fosfaat aan ijzeroxiden is het belangrijkste korte termijn-proces dat zorgt voor de vastlegging van fosfaat in sedimenten. Met behulp van een combinatie van differentiële röntgendiffractiemetingen (DXRD) en extractiemethoden, werd onderzocht wat voor ijzeroxiden fosfaat binden in 4 Noordzee sedimenten (Hoofdstuk 3). De resultaten geven aan dat weinig-kristallijn ferrihydriet en akaganeite aanwezig was in de fijne sediment fractie (<10 µm) van oppervlakte monsters van alle locaties. Combinatie van deze gegevens met bulk-sedimentextracties voor ijzer en fosfaat en sorptiegegevens voor fosfaat, wijzen op een belangrijke rol van deze ijzeroxiden voor de binding van fosfaat in Noordzee sedimenten. Deze ijzeroxiden zorgen waarschijnlijk voor een tijdelijke en een permanente opslag van fosfaat in het sediment.

De redoxcondities in sedimenten van *continental margins* kunnen zowel in de ruimte als in de tijd sterk variëren. Om meer inzicht te verkrijgen in de redoxcondities in Noordzee sedimenten, werd de mangaan- en ijzercyclus op 15 locaties in 4 verschillende sedimentatiemilieus in 2 contrasterende seizoenen bestudeerd (Hoofdstuk 4). De resultaten laten zien dat de kwaliteit en kwantiteit van het organisch materiaal dat in ieder milieu gedeponeerd wordt bepaalt of het sediment voldoende arm is aan zuurstof en nitraat om (1) de reductie van ijzer- en mangaanoxiden mogelijk te maken en (2) opgelost gereduceerd ijzer en mangaan naar het bovenstaande water te laten ontsnappen. Er werd een reactie-diffusiemodel ontwikkeld om de vaste fase- en poriewaterprofielen voor ijzer en mangaan te beschrijven. Dit model werd vervolgens toegepast op de gegevens voor ijzer en mangaan voor, respectievelijk, 4 en 11 stations. De modelresultaten laten zien dat (1) reversibele sorptie in combinatie met menging van het sediment het diffusieve transport van opgeloste metalen kan versnellen; (2) precipitatie de afname van de opgelost ijzer- en mangaanconcentraties met de diepte in de gereduceerde sediment zone kan verklaren; (3) in de meeste Noordzee sedimenten ijzer- en mangaanoxiden geen belangrijke rol spelen als oxidator bij de afbraak van organisch materiaal (<4% bijdrage); alleen in het Skagerrak kunnen deze metaaloxiden een substantiële bijdrage leveren (~20%).

Reversibele sorptie van fosfaat aan ijzeroxiden kan de fosfaatflux van het sediment naar het bovenstaande water niet alleen beperken maar ook versterken. Het effect van sorptie op de sediment-wateruitwisseling van fosfaat in Noordzee sedimenten werd bestudeerd voor 15 locaties in 2 seizoenen (Hoofdstuk 5). Sorptiegegevens, poriewaterprofielen en gemeten en berekende sediment-water fluxen voor fosfaat werden gecombineerd met vaste-fasegegevens. Sorptie bleek een belangrijke controlerende factor te zijn voor de sediment-wateruitwisseling van fosfaat gedurende een deel van het jaar in 3 van de 4 bezochte Noordzee gebieden. Op de meeste locaties beperkte adsorptie de fosfaatafgifte van het

sediment naar het bovenstaande water. Op een locatie in het Skagerrak was desorptie daarentegen verantwoordelijk voor de instandhouding van de flux van fosfaat naar het bovenstaande water. Er werd een reactie-diffusiemodel voor de sedimentaire fosforcyclus ontwikkeld en toegepast op de resultaten voor 2 stations, waaronder die in het Skagerrak. De modelresultaten laten zien dat zowel een door sorptie verhoogde retentie van fosfaat als een verhoogde afgifte adequaat met het model beschreven kan worden, indien gelijktijdige evenwichts en eerste-orde reversibele sorptieprocessen worden aangenomen.

Fosfaat dat in het mariene milieu in minerale vorm precipiteert komt waarschijnlijk niet meer in oplossing, dit in tegenstelling tot fosfaat dat gebonden is aan ijzeroxiden of in organisch materiaal. Het is daarom van belang te weten in welke mate deze zogenaamde authigene mineralen in sedimenten van *continental margins* worden gevormd. In dit onderzoek (Hoofdstuk 6) werden poriewater- en vaste-fasegegevens gecombineerd om te bepalen of authigene carbonaatfluorapatite (CFA) gevormd wordt op twee locaties op een Noord-Atlantisch continentaal platform. Resultaten van selectieve extracties wijzen op de vorming van een authigene fosfaatfase ten koste van ijzergebonden fosfaat op beide locaties. Er werd een reactie-diffusiemodel voor de sedimentaire fosforcyclus ontwikkeld en toegepast op de resultaten voor een van de twee locaties. De modelresultaten laten zien dat de vorming van CFA de toename van de authigene fosfaatfase met de diepte op deze locatie kan verklaren. Bovendien wijzen de modelresultaten op een intensieve cyclus van fosfaat tussen ijzergebonden fosfaat en poriewaterfosfaat bij het grensvlak tussen het geoxideerde en gereduceerde deel van het sediment. Deze interne cyclus van fosfaat wordt gedreven door een neerwaarts transport door menging van vooral *in-situ* gevormd ijzergebonden fosfaat van de geoxideerde zone naar de gereduceerde zone. Het verlies van fosfaat door CFA vorming en door diffusie wordt gecompenseerd door sorptie van fosfaat aan ijzeroxiden in de geoxideerde zone. Dit fosfaat is afkomstig van organisch materiaal. IJzergebonden fosfaat fungeert dus als een intermediair tussen organisch fosfaat en CFA. Deze authigene fosfaatfase kan verantwoordelijk zijn voor 25 tot 70% van de totale hoeveelheid van het fosfaat dat begraven wordt in deze sedimenten en kan dus een belangrijke bijdrage leveren aan de definitieve opslag van fosfaat in dit laag-sedimentatie *continental margin* gebied.

Curriculum vitae

Caroline Petra Slomp werd geboren op 17 juli 1967 te Khairagali (Pakistan) en verhuisde in 1976 naar Nederland. Na het behalen van het gymnasium-β diploma aan het Corderius College te Amersfoort, begon zij in september 1985 met de studie Bodemkunde aan de Landbouwuniversiteit te Wageningen. Zij verrichtte drie doctoraalonderzoeken op het gebied van de Microbiologie, Geologie en Mineralogie, en Bodemvorming en Ecopedologie/Theoretische Produktie Ecologie. In het kader van een stage Bodemkunde werkte zij van juni t/m december 1989 bij de Department of Civil and Environmental Engineering aan de universiteit van Syracuse (New York, Verenigde Staten). In juni 1991 studeerde zij af. In mei 1991 trad zij in dienst bij het Nederlands Instituut voor Onderzoek der Zee (NIOZ) te Texel, waar zij als onderzoeker-in-opleiding het in dit proefschrift beschreven onderzoek verrichtte. Sinds juni 1996 werkt zij als post-doc bij de vakgroep Fytopathologie van de Landbouwuniversiteit te Wageningen aan de modellering van de afbraak van organisch materiaal en diffusie in bodems.

Nawoord

Het in dit proefschrift beschreven onderzoek is uitgevoerd bij de afdelingen Beleidsgericht Wetenschappelijk Onderzoek (BEWON) en Chemische Oceanografie en Zeeverontreiniging (thans Mariene Chemie en Geologie) van het Nederlands Instituut voor Onderzoek der Zee (NIOZ) te Texel. Vele medewerkers van het NIOZ hebben direct of indirect een bijdrage aan het werk geleverd. Ik ben met name Wim van Raaphorst dankbaar voor de belangstelling en de goede adviezen gedurende het gehele onderzoek. Hans Malschaert leverde waardevolle assistentie op het lab, zowel op zee als op het NIOZ. Lutz Lohse was een goede discussiepartner en prettige kamergenoot. Daarnaast was zijn werk aan stikstof en zuurstof in Noordzee sedimenten van grote waarde voor hoofdstuk 4. Sjerry van der Gaast ben ik erkentelijk voor de DXRD metingen en interpretatie voor hoofdstuk 3. Eric Epping en Wim Helder verrichtten het veldwerk in het Goban Spur gebied voor hoofdstuk 6. De bemanning van het onderzoeksschip de Pelagia verleende onmisbare steun tijdens de BELS- en OMEX-vaartochten. Ik ben alle deelnemers aan de Mesocosm, BELS en OMEX projecten dankbaar voor de prettige samenwerking.